Fall 2012

A pharmacokinetic receptor-based recirculation model for target-mediated disposition drugs

Mohammed Hassan Mohammed Ewis El-Komy
University of Iowa

A PHARMACOKINETIC RECEPTOR-BASED RECIRCULATION MODEL FOR TARGET-MEDIATED DISPOSITION DRUGS

by

Mohammed Hassan Mohammed Ewis El-Komy

An Abstract

Of a thesis submitted in partial fulfillment
of the requirements for the Doctor of
Philosophy degree in Pharmacy
in the Graduate College of
The University of Iowa

December 2012

Thesis Supervisor: Professor Peter Veng-Pedersen

ABSTRACT

Physiologically based pharmacokinetic (PBPK) models, also known as recirculation models, consist of a series of tissue and organ blocks linked together by blood circulation, mimicking the anatomical structure of mammalian body. Each tissue is divided into vascular, interstitial, and intracellular sub-compartments. Linear system analysis (LSA)-recirculation models differ from the classical PBPK model in that they characterize each organ or tissue with a unit impulse response in the framework of input-output convolution relationship rather than systems of differential equations. Target-mediated disposition (TMD) is a phenomenon where drug disposition is influenced by capacity-limited binding to a target, resulting in dose-dependent events, such as a decrease in drug clearance with increasing dose level. Erythropoiesis stimulating agents such as recombinant human erythropoietin (EPO) and Continuous Erythropoietin Receptor Activator (C.E.R.A.) exhibit TMD where their disposition and anti-anemic activity are mediated by their interaction with EPO receptor (EPOR).

The objectives of this work were: 1) to develop a minimal, receptor-based LSA-recirculation model, 2) to apply the developed model in analyzing the effect of bone marrow (BM) ablation on C.E.R.A. elimination kinetics, and comparing EPO and C.E.R.A. interaction with EPOR *in vivo*, 3) to investigate the efficiency of the experimental design used to achieve the previous objective for estimation of the developed model parameters, and 4) To identify the physiological conditions at which TMD-compartmental models approximate TMD-recirculation models.

A literature review of LSA- recirculation models is provided in Chapter 2. In Chapter 3, receptor-based, LSA-recirculation model was mathematically formulated, and

applied to analyze C.E.R.A. pharmacokinetics studied in adult sheep with normal and ablated BM using a tracer interaction method (TIM). In Chapter 4, the model developed in Chapter 3 was further applied to analyze EPO and C.E.R.A. TIM data collected in adult sheep. A comprehensive, sensitivity analysis was performed in Chapter 5. In Chapter 6, statistical moments of linearized receptor-based compartmental and recirculation models were computed; and simulation of plasma drug concentrations, and receptor profiles in both structures were presented.

The developed model, together with the TIM, was able to quantitatively assess the interaction of C.E.R.A. with hematopoietic and non-hematopoietic EPOR population and provide a mechanism based explanation for C.E.R.A.'s slower elimination and greater erythropoietic activity *in vivo* compared to EPO, despite its lower affinity to EPOR. The TIM detected a saturable interaction between C.E.R.A. and non-hematopoietic EPOR which contradicts the behavior of EPO. The TIM experimental setting is adequate for estimation of the developed model parameters. TMD-recirculation models reduce to TMD-compartmental models under conditions of well-perfused target tissue, comparable drug initial distribution volume and target tissue extracellular volume, negligible non-receptor mediated clearance, and rapid equilibrium between venous and arterial blood drug concentrations, small extracellular volume, reduced cardiac output, low receptor pool concentration, and high drug-receptor equilibrium dissociation constant.

Abstract Approved:_____
Thesis Supervisor

_____
Title and Department

_____
Date

A PHARMACOKINETIC RECEPTOR-BASED RECIRCULATION MODEL FOR TARGET-MEDIATED DISPOSITION DRUGS

by

Mohammed Hassan Mohammed Ewis El-Komy

A thesis submitted in partial fulfillment
of the requirements for the Doctor of
Philosophy degree in Pharmacy
in the Graduate College of
The University of Iowa

December 2012

Thesis Supervisor: Professor Peter Veng-Pedersen

Graduate College
The University of Iowa
Iowa City, Iowa

CERTIFICATE OF APPROVAL

_____

PH.D. THESIS

_____

This is to certify that the Ph.D. thesis of

Mohammed Hassan Mohammed Ewis El-Komy

has been approved by the Examining Committee
for the thesis requirement for the Doctor of Philosophy
degree in Pharmacy at the December 2012 graduation.

Thesis Committee: _____
Peter Veng-Pedersen, Thesis Supervisor

_____
Lawrence Fleckenstein

_____
David G. Rethwisch

_____
Daryl J. Murry

_____
Gary Milavetz

To my parents, Hassan and Amani, my beloved wife, Asmaa, my daughter, Jana, my son, Walid, my brother, Ahmed, and friends

ACKNOWLEDGMENTS

My sincere gratitude to the one above all of us, the mighty GOD, for answering my prayers for giving me the strength not to give up, thank you so much Dear Lord.

This dissertation would not have been possible without the generous guidance and support of several individuals who in one way or another participated in this work by providing their valuable assistance and feedback. First and foremost, I owe my deepest gratitude to my advisor Professor Peter Veng-Pedersen for giving me the opportunity to work on this project. Throughout my graduate studies, he was a dedicated teacher who helped me develop my potentials as a research scientist in the field of Pharmacokinetic/Pharmacodynamic Modeling and Simulation. Words would never be enough to express my deepest thanks for his wholehearted guidance, infinite support, patience, and continuous encouragement since his proposal of the subject of this thesis and throughout the progress of the study.

Secondly, my sincere appreciation, everlasting thanks and particular gratitude to Professor John A. Widness for his valuable instructions that helped me improve my skills as a scientific writer. Also, I would like to thank our laboratory technicians, Robert Schmidt, Earl Gingerich, Demet Nalbant, and Jessica Goehring for their dedicated laboratory work that made conducting the pharmacokinetic analysis in this thesis possible.

I must extend my appreciation to all of my faculties, especially the committee members of my comprehensive exam and dissertation defense, Dr. Flanagan, Dr. Fleckenstein, Dr. Rethwisch, Dr. Murry, and Dr. Milavetz, for sharing valuable insights in the pharmacokinetic analysis developed and implemented in this thesis. Also, I want to

thank all former and current students in Dr. Veng-Pedersen's lab including Kevin Freise, Chih-Wei Lin, Lanyi Xie, Mohammad Saleh, Matthew Rosebraugh, and Denison Kuruvilla.

I need to thank the Ministry of Higher Education and Scientific Research of Egypt and the Department of Pharmaceutics at the University of Iowa for their financial support of my education. Also, I am grateful to Hoffman-La-Roche, Penzberg, Germany and the National Institutes of Health for sponsoring my research.

Last but not least, I want to thank my parents, wife, children, and all of my friends for their support.

ABSTRACT

Physiologically based pharmacokinetic (PBPK) models, also known as recirculation models, consist of a series of tissue and organ blocks linked together by blood circulation, mimicking the anatomical structure of mammalian body. Each tissue is divided into vascular, interstitial, and intracellular sub-compartments. Linear system analysis (LSA)-recirculation models differ from the classical PBPK model in that they characterize each organ or tissue with a unit impulse response in the framework of input-output convolution relationship rather than systems of differential equations. Target-mediated disposition (TMD) is a phenomenon where drug disposition is influenced by capacity-limited binding to a target, resulting in dose-dependent events, such as a decrease in drug clearance with increasing dose level. Erythropoiesis stimulating agents such as recombinant human erythropoietin (EPO) and Continuous Erythropoietin Receptor Activator (C.E.R.A.) exhibit TMD where their disposition and anti-anemic activity are mediated by their interaction with EPO receptor (EPOR).

The objectives of this work were: 1) to develop a minimal, receptor-based LSA-recirculation model, 2) to apply the developed model in analyzing the effect of bone marrow (BM) ablation on C.E.R.A. elimination kinetics, and comparing EPO and C.E.R.A. interaction with EPOR *in vivo*, 3) to investigate the efficiency of the experimental design used to achieve the previous objective for estimation of the developed model parameters, and 4) To identify the physiological conditions at which TMD-compartmental models approximate TMD-recirculation models.

A literature review of LSA- recirculation models is provided in Chapter 2. In Chapter 3, receptor-based, LSA-recirculation model was mathematically formulated, and

applied to analyze C.E.R.A. pharmacokinetics studied in adult sheep with normal and ablated BM using a tracer interaction method (TIM). In Chapter 4, the model developed in Chapter 3 was further applied to analyze EPO and C.E.R.A. TIM data collected in adult sheep. A comprehensive, sensitivity analysis was performed in Chapter 5. In Chapter 6, statistical moments of linearized receptor-based compartmental and recirculation models were computed; and simulation of plasma drug concentrations, and receptor profiles in both structures were presented.

The developed model, together with the TIM, was able to quantitatively assess the interaction of C.E.R.A. with hematopoietic and non-hematopoietic EPOR population and provide a mechanism based explanation for C.E.R.A.'s slower elimination and greater erythropoietic activity *in vivo* compared to EPO, despite its lower affinity to EPOR. The TIM detected a saturable interaction between C.E.R.A. and non-hematopoietic EPOR which contradicts the behavior of EPO. The TIM experimental setting is adequate for estimation of the developed model parameters. TMD-recirculation models reduce to TMD-compartmental models under conditions of well-perfused target tissue, comparable drug initial distribution volume and target tissue extracellular volume, negligible non-receptor mediated clearance, and rapid equilibrium between venous and arterial blood drug concentrations, small extracellular volume, reduced cardiac output, low receptor pool concentration, and high drug-receptor equilibrium dissociation constant.

TABLE OF CONTENTS

LIST OF TABLES

LIST OF FIGURES

LIST OF SYMBOLS AND ABBREVIATIONS

$*$	Convolution operator
A_T	Drug amount in tissue compartment
AIC	Akaike Information Criterion
α, β	Rate parameters of transit time density function
BM	Bone marrow
C_{input}	Input concentration of free drug to receptor interaction site
COMP-TMD	Compartmental target-mediated disposition model
$C_{in}^{TM}(t)$	Input concentration to TM tissues
$C_{out}^{TM}(t)$	Output concentration from TM tissues
$C_{out}^{tot}(t)$	Total output concentration
$C_{cold}(t)$	Unlabeled drug plasma concentrations
C	Drug concentration in the central compartment
$C_{out}^{tot}(\theta_i, t)$	Model output calculated at time t and parameter value θ
CL	Total plasma clearance
CV%	Coefficient of variation
C.E.R.A.	Continuous Erythropoietin Receptor Activator
$\delta(t)$	Dirac-delta function
Δt	Time interval
D_{iv}	IV bolus dose
E	Extraction ratio of a tissue
$E_{TM}(t)$	Receptor-dependent extraction function
EPO	Erythropoietin
EPOR	Erythropoietin receptors
ESA	Erythropoiesis Stimulating Agent

$f_{out}(t)$	Output rate from a tissue
$g(t)$	Transit time density function
HLS	Heart-lung segment
$In(t)$	External input rate function
$Inf(t)$	Constant infusion rate of the tracer
^{125}I-C.E.R.A.	Radiolabeled C.E.R.A.
^{125}I-EPO	Radiolabeled EPO
IV	Intravenous
K_D	Drug/receptor equilibrium dissociation constant
k_{deg}	First-order receptor degradation rate constant
k_{el}	First-order elimination rate constant
k_{int}	First-order drug/receptor internalization rate constant
k_{off}	First-order drug/receptor dissociation rate constant
k_{on}	Second-order drug/receptor association rate constant
k_{pt}	First-order plasma-to-tissue distribution rate constant
k_{syn}	Zero-order receptor synthesis rate constant
k_{tp}	First-order tissue-to-plasma distribution rate constant
λ	Mixing parameter of transit time density function
LSA	Linear system analysis
MRT	Mean residence time
MSE%	Mean percent standard error
NESP	Novel Erythropoiesis Stimulating Protein
NLI	Nonlinearity index
$NS(t)$	Normalized sensitivity function
NTM	Non-target mediated
P	Fraction of blood flow to a tissue
PBPK	Physiologically based pharmacokinetic

PD	Pharmacodynamic(s)
PEG	Polyethylene glycol
PK	Pharmacokinetic(s)
Q	Cardiac output
QE	Quasi-equilibrium
QSS	Quasi-steady state
RBC	Red blood cell
REC-TMD	Recirculation target-mediated disposition model
RIA	Radioimmunoassay
R	Free receptor concentration
R^*	Bound receptor concentration
R_{tot}	Total receptor concentration
R_0	Initial receptor concentration
R_{ss}	Steady-state receptor concentration
$S(t)$	Sensitivity function
θ	Model parameter vector
$t_{1/2}(\alpha)$	Distribution half-life
$t_{1/2}(\beta)$	Elimination half-life
$t_{1/2}(kdeg)$	Receptor degradation half-life
$t_{1/2}(k_{int})$	Drug/receptor internalization half-life
t_{cold}	Time of injection of unlabeled drug
TIM	Tracer interaction method
TM	Target mediated
TMD	Target mediated disposition
$UIR(t)$	Unit impulse response function
y	Dummy variables
V	Volume of the central compartment

V_d	Initial volume of distribution
V_{EC}	Volume of extracellular space of TM tissues

CHAPTER 1. INTRODUCTION

1.1. Background

In 1937, Teorell introduced the first physiological model for the distribution of a substance in the body. The model consisted of four compartments representing sites of drug administration, elimination, and inactivation connected through a blood circulation compartment (Figure 1.1) [1]. Bellman, Jacquez, and Kalaba, in 1960, derived mathematical expressions for drug distribution in a tissue with vascular, interstitial and cellular components [2], as well as in the whole body [3]. In the late 1960's, Bischoff and Brown [4] were the first to apply a whole-body physiologically based pharmacokinetic (PBPK) model (Figure 1.2) to describe drug distribution in mammals. Since the 1970's, PBPK modeling has been applied to the prediction of disposition of several anticancer agents [5-11], individual toxicants, and chemical mixtures [12-15]; and in human health risk assessment [16-19].

1.2. Physiologically based pharmacokinetic model development

The procedure of developing a whole-body PBPK model essentially consists of the following four stages [20, 21]: 1) model structure specification, 2) tissue model specification, 3) equation writing and coding, and 4) parameter specification and/or estimation.

1.2.1. Model structure specification

The overall structure of a whole-body PBPK model is a series of tissue and organ blocks linked together by blood circulation (Figure 3), mimicking the anatomical structure of mammalian body. Although there are no rules available regarding which tissues should be included or excluded, a typical whole-body PBPK model consists of

core, special, and reservoir tissues [21]. The core tissues comprise blood, heart-lung segment, liver (for metabolized drugs), kidneys (for urinary excreted drugs), and adipose tissue (for lipophilic drugs). The special tissues include sites of drug administration, sites of drug action, tissues with atypical (e.g., nonlinear) kinetics, and tissues for which experimental data is available. Tissues that constitute a considerable mass of the mammalian body such as muscles, skin, adipose, and bone may be included as reservoir tissues. Examples of minimal PBPK models for particular applications have been presented in literature [22-26]. A lumping principle stating that only dynamically similar tissues should be lumped together was derived [27]. In the field of toxicokinetics, the PBPK model structures mainly include the core tissues and the rest is lumped into "rapidly equilibrating" and "slowly equilibrated", or "highly perfused" and "poorly perfused" [28-31].

1.2.2. Tissue model specification

After the whole-body PBPK model is determined, the model structure for each tissue block needs to be specified. Each tissue block is divided into sub-compartments that represent the vascular space, interstitial space, and intracellular space (Figure 1.4). Based on the available physicochemical and biochemical information of the drug, such as molecular size, lipophilicity, tissue membrane permeability, tissue protein binding, and tissue metabolism, the tissue blocks are categorized into flow (perfusion) rate-limited or permeability rate-limited.

Flow rate-limited models represent the simplest and the most widely used case. They are based on the assumption of a well-mixed model, where drug partioning across tissue membranes is instantaneous and homogenous [21, 32]. Thus, the rate limiting step

is blood flow and the sub-compartments in Figure 1.4 can be combined into a single compartment. Flow models are normally assumed when the drug has a small molecular weight or when the tissue has a relatively small volume [21, 33-35].

In cases where drug diffusion across membranes is the rate limiting step, a permeability rate-limited model should be prescribed. The sub-compartments in Figure 1.4 can be combined into vascular and extravascular spaces, depending on whether the rate limitation is at the capillary membrane or at both the capillary and cellular membranes [21, 36-38]. Permeability models are usually used for high molecular weight drugs that are polar (e.g., peptides and proteins) or when the tissue has a relatively large volume (e.g., adipose) or a protective barrier (e.g., brain) [35].

1.2.3. Equation writing and coding

Once the structure of the whole-body PBPK model and the rate-limiting features of the tissue blocks have been defined, the model is mathematically represented by a series of mass balance differential equations (or algebraic equations for processes that equilibrate instantly) [21]. For a non-eliminating tissue with flow limited mass transport (Figure 1.5A), this equation is:

$$V \cdot \frac{dC}{dt} = Q \cdot (C_{ART} - C/K_P) \tag{1.1}$$

where Q, V, and C are the blood flow, anatomic volume, and concentration of the drug in the tissue, respectively. C_{ART} is the drug concentration in the arterial blood, K_P is the tissue-to-blood partition coefficient. For the liver (LV), Eq. 1.1 is modified to include an input from the gut (GU) and spleen (SP), as well as to include an elimination pathway *via* metabolism (Figure 1.3):

$$V_{LV} \cdot \frac{d\,C_{LV}}{dt} = (Q_{LV} - Q_{GU} - Q_{SP}) \cdot C_{ART} + Q_{GU} \cdot C_{GU} / K_{P,GU} + Q_{SP} \cdot C_{SP} / K_{P,SP} - Q_{LV} \cdot C_{LV} / K_{P,LV} - CL_{LV} \cdot C_{LV} \quad (1.2)$$

where CL_{LV} is the hepatic metabolic clearance that can be expressed as [39]:

$$CL_{LV} = CL_{\text{int}} \cdot f_u \quad (1.3)$$

where f_u is the fraction unbound in the plasma, and $Cl_{int,}$ is the hepatic intrinsic clearance that is related to the hepatic extraction ratio, E_{LV}, by the "well-stirred" model [40]:

$$E_{LV} = \frac{Cl_{\text{int}} \cdot f_u}{Q_{LV} + Cl_{\text{int}} \cdot f_u} \quad (1.4)$$

, or the "parallel tube" model [40]:

$$E_{LV} = 1 - \exp[Cl_{\text{int}} \cdot f_u / Q_{LV}] \quad (1.5)$$

The hepatic intrinsic clearance is described by the Michaelis-Menten equation [41]:

$$CL_{\text{int}} = \frac{V_{\max}}{f_c \cdot (K_m + C_{LV})} \quad (1.6)$$

that reduces under linear, non-saturable elimination to:

$$CL_{\text{int}} = \frac{V_{\max}}{f_c \cdot K_m} \quad (1.7)$$

where V_{max} and K_m are the maximum reaction velocity and the equilibrium dissociation constant, respectively, and f_c is the fraction unbound in the hepatocytes.

For the kidneys (KD), Eq. 1.1 is modified to include the renal clearance, CL_{KD} (Figure 1.3):

$$V_{KD} \cdot \frac{d\,C_{KD}}{dt} = Q_{KD} \cdot (C_{ART} - C_{KD} / K_{P,KD}) - CL_{KD} \cdot C_{KD} \quad (1.8)$$

CL_{KD} can be modeled by [42]:

$$CL_{KD} = f_u \cdot GFR \cdot (1 - F_r) \quad (1.9)$$

where *GFR* is the glomerular filteration rate, and F_r is the fraction reabsorbed.

The basic equations for a permeability rate-limited, non-eliminating tissue, where vascular space is assumed to be in equilibrium with extravascular space (Figure 1.5B), are defined as:

$$V_V \cdot \frac{d\,C_V}{dt} = Q \cdot (C_{ART} - C_V) - PS \cdot (C_V - C_{EV}/K_P) \tag{1.9}$$

$$V_{EV} \cdot \frac{d\,C_{EV}}{dt} = PS \cdot (C_V - C_{EV}/K_P) \tag{1.10}$$

where V_V and V_{EV} are the volumes of the vascular and extra-vascular spaces of the tissue, respectively. C_V and C_{EV} are drug concentrations in the vascular and extra-vascular spaces of the tissue, respectively. *PS* is the tissue permeability surface area coefficient. For an eliminating tissue, Eq. 1.10 is modified by inclusion of clearance elements similar to the flow-rate models.

The final step in writing the mathematical model is to provide the equations for the heart-lung segment (HLS), venous (VEN), and arterial (ART) blood to establish the mass balance for the closed system (Figure 1.3):

$$V_{HLS} \cdot \frac{d\,C_{HLS}}{dt} = Q_{HLS} \cdot (C_{VEN} - C_{HLS}/K_{P,HLS}) \tag{1.11}$$

$$V_{VEN} \cdot \frac{d\,C_{VEN}}{dt} = \sum_{i=1}^{n} Q_i \cdot C_i/K_{P,i} - Q_{HLS} \cdot C_{VEN} \tag{1.12}$$

$$V_{ART} \cdot \frac{d\,C_{ART}}{dt} = Q_{HLS} \cdot (C_{HLS}/K_{P,HLS} - C_{ART}) \tag{1.13}$$

where Q_{HLS} is the cardiac output, Q_i, C_i, and $K_{P,i}$ are the flow rate, the concentration, and the tissue-to-blood partition coefficients for the ith tissue.

For drugs exhibiting non-linear plasma and/or tissue protein binding, Bischoff and Dedrick [43] proposed a modification for the PBPK model equations that involved partitioning of drug concentrations in the blood and tissue regions, *C*, according to the equation:

$$C = w \cdot C_u + p \cdot C_b \tag{1.14}$$

where *w* and *p* are the volume fractions of water and protein, respectively. C_u and C_b are the unbound and bound drug concentrations, respectively, that were assumed to be related by the Langmuir isotherm:

$$C_b = \sum_{i=1}^{n} \frac{B_i \cdot K_i \cdot C_u}{1 + K_i \cdot C_u} \tag{1.15}$$

where B_i and K_i are the concentration and equilibrium dissociation constant of the ith binding site.

After the PBPK model has been defined mathematically, it must be coded in particular software for estimation and simulation purposes. Software packages like ACSL® [44, 45], MATLAB® with its graphic interface SIMULINK® (The Math Works, Inc.), SAAM II® (SAAM Institute, Inc.), CMTRIX [46], PK-Sim (Bayer Technology Services GmbH, Leverkusen, Germany), GastroPlus® (Simulations Plus, Inc., Lancaster, CA), SimCYP® (SimCYP Ltd., Sheffield, UK), and PKQuest [47] can serve for such purposes.

1.2.4. Parameter specification and/or estimation

PBPK models comprise drug-independent (physiological) and drug-dependent (physicochemical and biochemical) parameters. The drug-independent parameters include body weight, tissue volumes, cardiac output, and regional blood flow rates. These

parameters are normally taken from the literature for the species of interest [48-51]. The drug-dependent parameters include partitioning and permeability coefficients, protein and enzyme binding, and intrinsic clearance. These parameters are either (1) obtained from literature, (2) estimated by fitting the PBPK model to concentration-time data [33, 52], (3) predicted using *in vitro-in vivo* extrapolation and allometric scaling techniques (e.g., scaling of hepatic metabolic clearance [53-57]), or (4) predicted using *in silico* techniques that depend on drug molecule descriptors and tissue composition (e.g., prediction of tissue partition coefficients [58-61]).

1.3. Classical compartmental versus physiological pharmacokinetic models

In the conventional pharmacokinetic (PK) modeling approach, the behavior of the system is described as a series of kinetically similar compartments, whose number is determined based on the best fit to the observed PK data. The physiological modeling approach, on the other hand, uses well-defined tissues in a heterogenous structure that follows the mammalian anatomy and physiology. Thus, unlike the classical compartmental models, where structure is defined after collection of plasma time-concentration data and in terms of drug-dependent parameters only, the PBPK model structure is determined before any PK experiment is conducted and in terms of both drug-dependent and independent parameters.

A first-order process describes the drug transfer between compartments in the classical approach, while a convection process *via* the vascular network characterizes the transfer between tissue blocks in the physiological approach. Conventional models assume that drug molecules are distributed instantly and homogenously after entering a

compartment. PBPK models allow selection between one- and multi-compartment tissue structure, depending on the drug properties and the nature of a given tissue.

1.4. Advantages and limitations of physiologically based pharmacokinetic models

The main advantage of PBPK models over the classical compartmental models is its physiologically predictive nature [62]. Such multi-organ models can predict the time course of drug concentration in venous and arterial blood, as well as in particular organs or tissues by the virtue of their heterogeneity. Additionally, they can predict the influence of initial distribution from the injection to the target site on drug pharmacodynamics. This is of importance for the onset of action when drugs have a very short effect site equilibration time (e.g., general anesthetics) [63]. PBPK models can predict alterations in drug disposition kinetics due to physiological or pathological perturbations in organ functions by the virtue of comprising parameters that correspond to the anatomy and the physiology. Physiological parameters can show sensitivity to changes in hydrodynamics [64-66], rest and physical exercise [67-69], age [70-80], gender [72, 77, 81], pregnancy [82, 83], disease development (e.g., liver cirrhosis [84, 85],and kidney diseases [86]), and medical intervention (e.g., surgery [87]) . Thus, PBPK modeling, like population modeling, can be very useful in explaining the sources of PK variability. Impact of drug-drug interactions on disposition kinetics can be mechanistically predicted using PBPK modeling [88-92]. The unified structure of PBPK model between mammalian species allows for the inter-species scaling of anatomical and physiological parameters. Therefore, PBPK modeling provides a mechanistic approach to predict drug disposition

profiles in humans based on data from other species (rather than using empirical formulae based on body weight as in the allometric scaling of the compartmental models) [93].

PBPK models can only be identified by literature resources, separate experiments, and concentrations measured in several tissues (using invasive or destructive sampling) but not on the basis of routine clinical pharmacokinetic data [63]. Therefore, these models require extensive literature mining and experimentation. The accuracy of predictions using a PBPK model depends on the accuracy of the parameters defined in the mass balance equations. The uncertainty introduced into PBPK model parameters, due to its dependence on literature and separate experiments or due to unidentifiability of parameters estimated from the PK data, may result in a final model that fails to reflect true *in vivo* drug concentrations [94, 95].

1.5. Systems analysis and physiological models

A modern approach based on implementation of linear system analysis (LSA) principles in physiological models has been applied to describe the disposition of several therapeutic agents [25, 26, 96-100]. This approach aims at reducing the complexity of the classical PBPK models by keeping restrictive assumptions to the minimum. The difference between classical and LSA-recirculation models is that the latter is based on a general “building block” that is characterized by a unit impulse response (UIR) function that encapsulates the essential two fundamental disposition components, namely distribution and elimination [39, 101]. The other difference is that the rate of transfer of a drug out from a block in a LSA-based system depends linearly on the input rate to the block and the UIR of that block by a convolution operator [101], rather than by systems

of ordinary differential equations. Literature review of LSA implementation in PBPK models is presented in Chapter 2.

1.6. Target-mediated disposition

Target-mediated disposition (TMD) is a phenomenon where drug distribution and/or elimination are influenced by capacity-limited binding to a target (receptor or enzyme) [102]. This binding results in dose-dependent events, including a decrease in the volume of distribution at steady state and/or target-mediated clearance with increasing dose level [102, 103]. A general mechanism-based pharmacokinetic (PK) model of TMD was developed to describe the behavior of such systems [103]. The model comprises elements for target turnover, drug–target binding, and drug–target complex endocytosis. The model in its simplest form does not account for a possible feedback up-regulation or down-regulation of the target due to interaction with the drug. Additionally, the model does not assume recycling of the drug or its target subsequent to the endocytosis process. The model is presented in detail in Chapter 6.

The TMD model in the framework of a 2- or 3-compartment mammillary model has been applied to analyze the disposition of various small molecules, peptides, proteins, hormones, and monoclonal antibodies, using plasma concentration–time data obtained from individual or population pharmacokinetic studies in different mammalian species [104-106]. This traditional paradigm of TMD system analysis does not specify a particular organ or tissue expressing the target based on the assumption that the biophase is well perfused by the circulating blood. Unfortunately, this assumption is not valid for some drugs experiencing TMD, for example recombinant human erythropoietin (EPO),

where a lag has been reported between its peak serum and bone marrow (BM) concentrations [107].

1.7. Erythropoiesis stimulating agents as examples of target-mediated disposition drugs

Erythropoietin (EPO) is a 34-kD glycoprotein hormone that regulates erythropoiesis. It binds to a cell surface receptor (EPOR) on bone marrow (BM) erythroid progenitor cells (burst-forming unit-erythroids and colony-forming unit-erythroids), promoting their proliferation and differentiation into mature red blood cells (RBC) and protecting them from apoptosis [108]. Simultaneously, activation of EPOR by EPO binding promotes degradation of the formed complex *via* internalization followed by targeting to lysosomes [109]. Continuous Erythropoiesis Stimulating Agent, C.E.R.A., is a methoxy pegylated EPO analogue weighing approximately 60 kD. C.E.R.A. has unique binding characteristics to EPOR that involve slow association, but slightly faster dissociation compared to EPO [110]. C.E.R.A. has slower systemic clearance, longer elimination half-life, and higher *in vivo* erythropoietic activity than EPO [96, 111].

Previous studies provided several evidences that EPOR-mediated pathways play a major role in elimination of EPO and its long acting analogues. Patients with aplastic anemia (i.e., anemia caused by damage of BM stem cells) demonstrated much higher EPO levels than in patients with beta-thalassemia (i.e., anemia caused by reduced or absent synthesis of the beta chains of hemoglobin) at the same hemoglobin concentration [112]. Receptor-mediated elimination of EPO as a result of lysosomal degradation was reported in erythroid progenitor cells extracted from spleens of mice infected with anemia inducing virus [109]. *In vitro* cellular trafficking of EPO and darbepoetin alfa, a

hyperglycosylated EPO analogue, showed that only cells expressing surface EPOR were able to degrade both compounds [113]. Busulfan-induced BM ablation resulted in significant reduction of EPO clearance in adult sheep [114, 115]. EPO clearance in sheep was not affected by hepatectomy or nephrectomy [116]. Given the lack of differences in C.E.R.A. PK properties among healthy humans, chronic kidney disease patients, and patients with impaired hepatic function; it appears that kidneys and liver are also unimportant in C.E.R.A. elimination [117-119]. Recently, a significant positive linear correlation was found between EPOR mRNA level in the bone marrow and EPO clearance in phlebotomized sheep [120].

EPO exhibits TMD in several animals and in humans as evidenced by a decrease in clearance with increasing dose [121, 122]. The disappearance of EPO non-linear disposition by BM ablation in sheep [115, 123] provides strong evidence that the EPO TMD is due to its saturable interaction with EPOR in the BM. Non-linear kinetics of EPO was previously studied using several PK models that assume Michaelis-Menten type of elimination. The proposed models were either: open two-compartment with central elimination [121], disposition decomposition analysis [115, 123], or recirculation two-compartment with tissue-specific elimination [96]. Recently, a two-compartment TMD model was used to study EPO pharmacokinetics in rats, monkeys, and humans. The model was integrated to a cellular life-span model for simultaneous analysis of PK and pharmacodynamic data [124]. The PK TMD model is presented in detail in Chapter 6.

1.8. Objectives and specific aims

The primary objective was to develop a mechanistic modeling platform that integrates a minimal, linear system analysis based recirculation model and a receptor

based model to characterize the PK properties of drugs experiencing target mediated disposition. Under that overall objective, the specific aims were:

1. To formulate a receptor-based recirculation model.
2. To apply the formulated model in analyzing the effect of bone marrow ablation on C.E.R.A. elimination kinetics.
3. To apply the formulated model in comparing EPO and C.E.R.A. interaction with EPOR *in vivo.*
4. To investigate the efficiency of the experimental design used to achieve aims 2 and aim 3 for estimation of the developed model parameters.
5. To identify the physiological conditions at which TMD-compartmental models approximate TMD-recirculation models.

1.9. Hypothesis

The overall hypothesis of this work is that physiologically based pharmacokinetic modeling is a more appropriate approach to characterize the pharmacokinetics of target mediated disposition drugs than the abstract classical compartmental approach and can extend the applications of the receptor-based models.

Hypothesis 1: It is mathematically possible to integrate a minimal, linear system analysis based recirculation model and a receptor based model.

Hypothesis 2: C.E.R.A. elimination is mediated by binding with EPO receptor (EPOR) on the surface of EPOR expressing cells, followed by endocytosis and lysosomal degradation in the intracellular space.

Hypothesis 3: EPO and C.E.R.A. different elimination rate and *in vivo* erythropoietic activity is driven by different interaction properties with EPOR.

Hypothesis 4: The formulated model parameters are reliably estimated from the experimental design implemented in Chapter 3 and Chapter 4.

Hypothesis 5: The nature of the hosting structure impacts the drug and receptor time-concentration profiles and influences the performance of target-mediated disposition models.

1.10. Outline of the thesis

A literature review of linear systems analysis (LSA)-recirculation models is provided in Chapter 2. This review: 1) presents a "unified" methodology for building LSA-recirculation models, 2) addresses the mean time and clearance concepts in those models, 3) discusses the various mechanistic models of organ disposition, and 4) introduces a recirculation model for drugs exhibiting non-linear elimination.

In Chapter 3, a receptor-based recirculation model was mathematically formulated, and C.E.R.A. pharmacokinetics (PK) was studied in adult sheep with normal and ablated bone marrow (BM) using a sensitive and specific technique, the tracer interaction method (TIM) [125]. To quantitatively assess the interaction of C.E.R.A. with EPO receptor (EPOR) populations located inside and outside the BM in adult sheep, the developed model was fitted to the tracer component of the TIM with the non-tracer component being represented as a forcing function. Besides the model-based analysis of the TIM data, a non-compartmental analysis was conducted using the non-tracer component of the TIM. The information obtained from this analysis enabled direct assessment of the effect of BM ablation on C.E.R.A. macro-parameters (e.g., clearance, half-life, volume of distribution at steady state, etc.) which were explained in terms of the receptor-based processes incorporated in the developed model.

In Chapter 4, the model developed in Chapter 3 was further applied to provide a mechanism based explanation for C.E.R.A.'s slower elimination and greater erythropoietic activity *in vivo* compared to EPO. This was achieved by analyzing EPO and C.E.R.A. TIM data collected in adult sheep.

To investigate the suitability of the TIM experimental design used in Chapters 3 and 4 for estimation of the developed model parameters, a comprehensive, partial-derivative sensitivity analysis was performed in Chapter 5.

In Chapter 6, the physiological conditions at which a target-mediated disposition (TMD)-two compartment model approximates a minimal, linear systems analysis, TMD-recirculation model were identified by: 1) Comparing the statistical moments of the linearized forms of both models; and 2) Simulation of drug and receptor profiles at different IV bolus doses based on EPO/EPOR parameter values reported in literature for humans and perturbing these parameter values. Additionally, the influence of the host structure on parameter estimation efficiency was evaluated by simulation of 1,000 datasets for each model at D-optimized sampling times in a dose-escalation design followed by re-estimation of the parameters and calculation of estimation metrics.

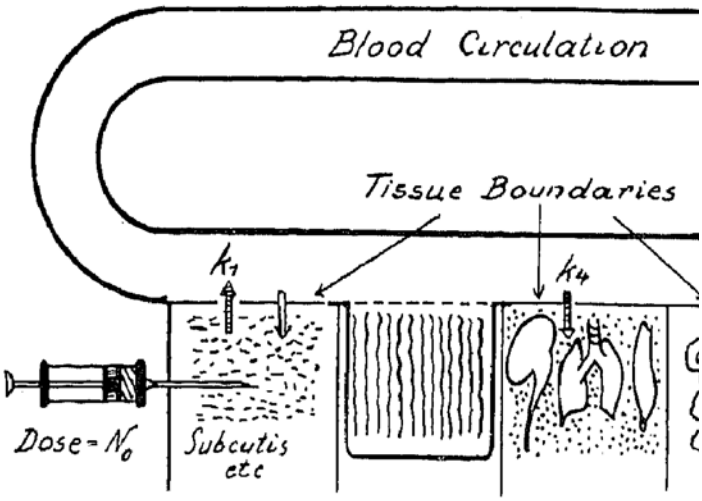

Figure 1.1. The first physiological model proposed by Teorell in 1937. The *k*'s are first-order transfer, excretion, and inactivation rate constants.

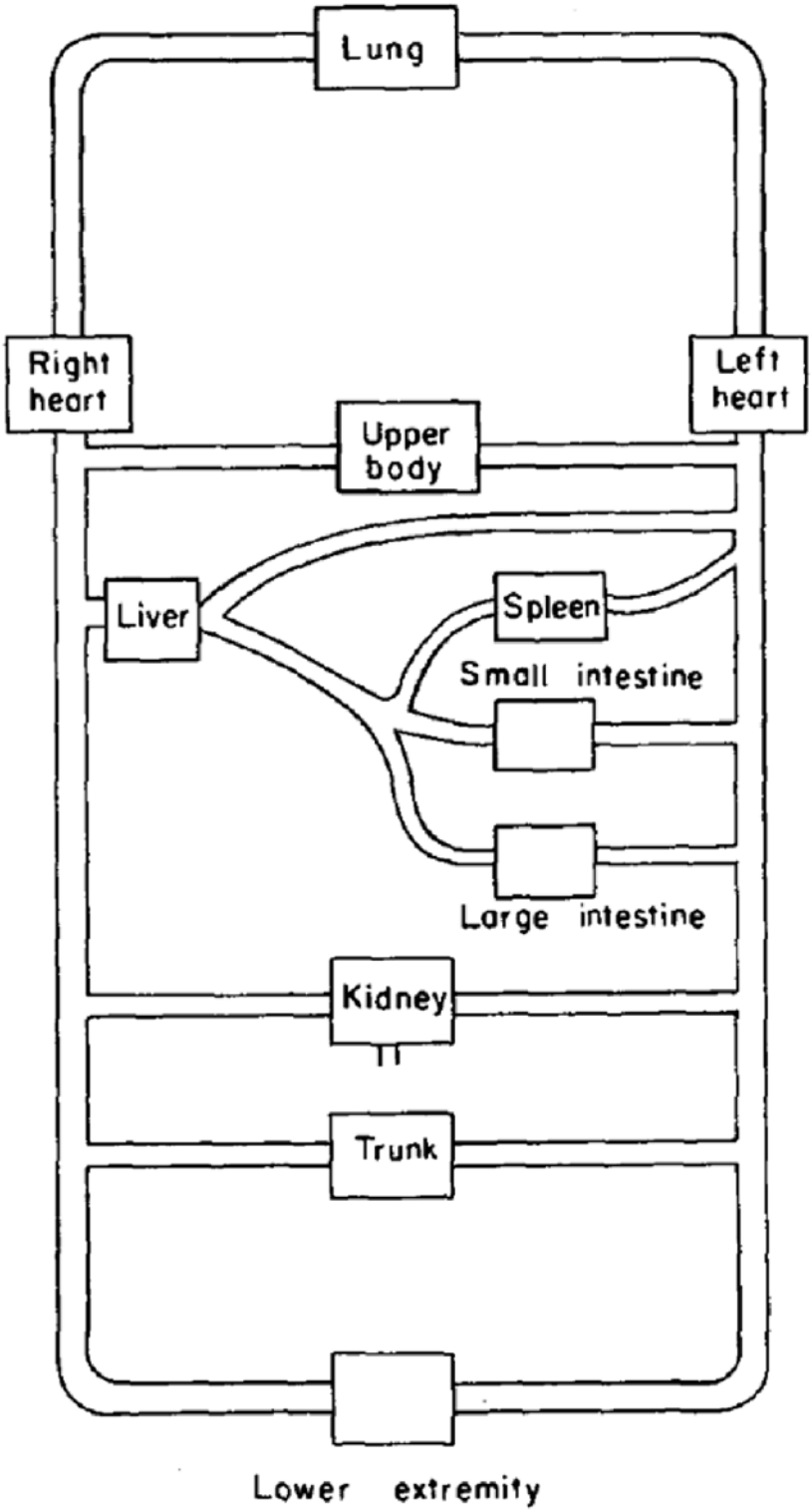

Figure 1.2. The physiological model proposed by Jacquez et al in 1960 and applied in mammals by Bischoff and Brown in 1967.

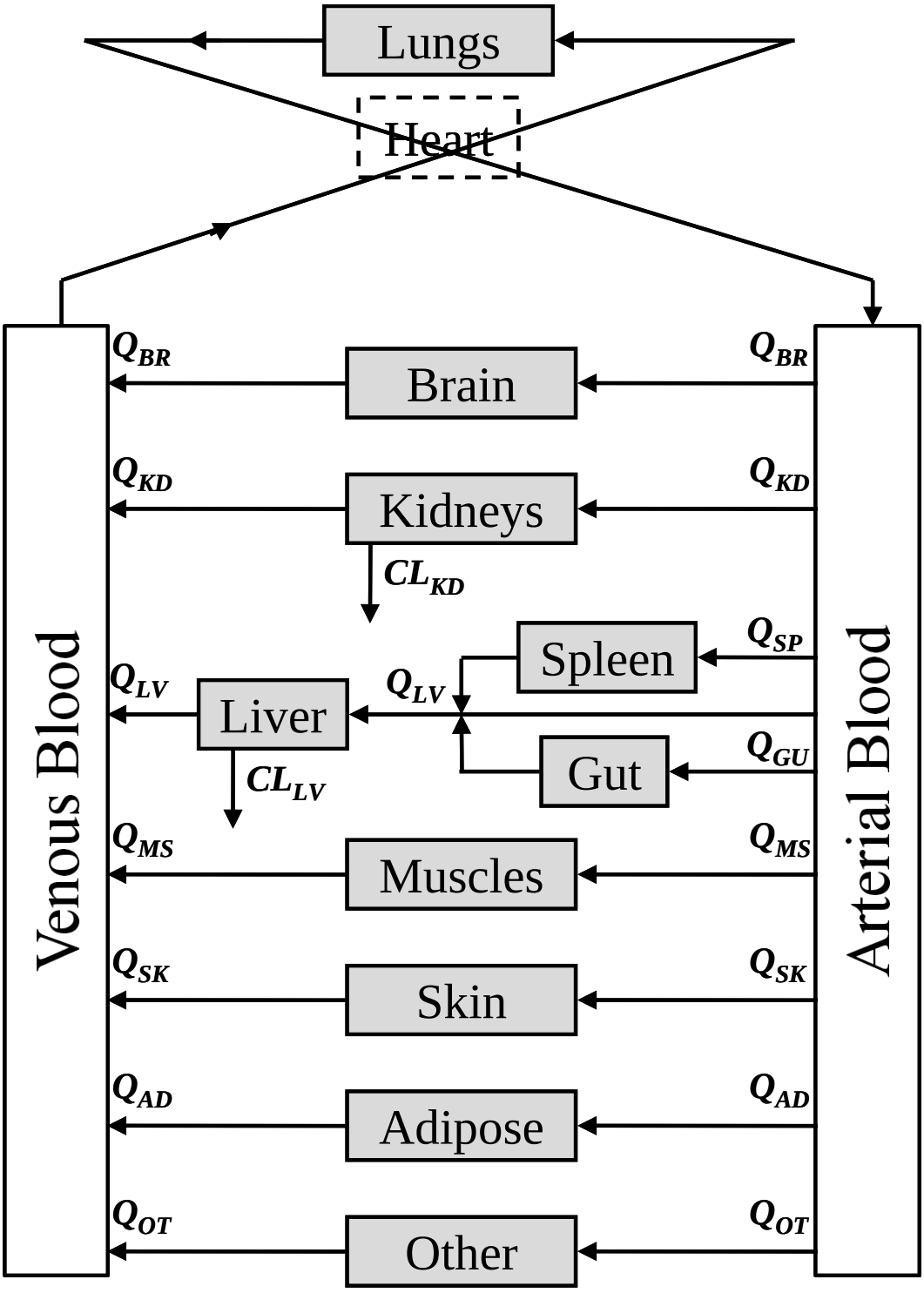

Figure 1.3. Schematic representation of a generic whole-body physiologically based pharmacokinetic model. The *Q*'s are the blood flow rates. The *CL*'s are the clearances.

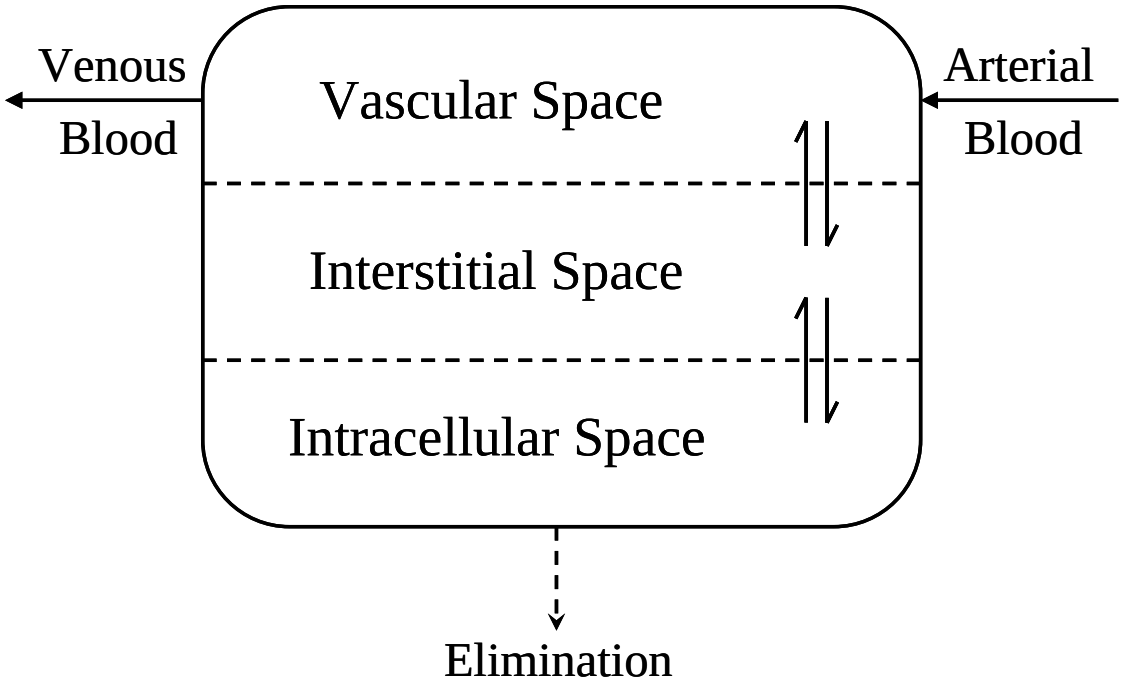

Figure 1.4. Schematic representation of a complex tissue block.

(A)

(B)

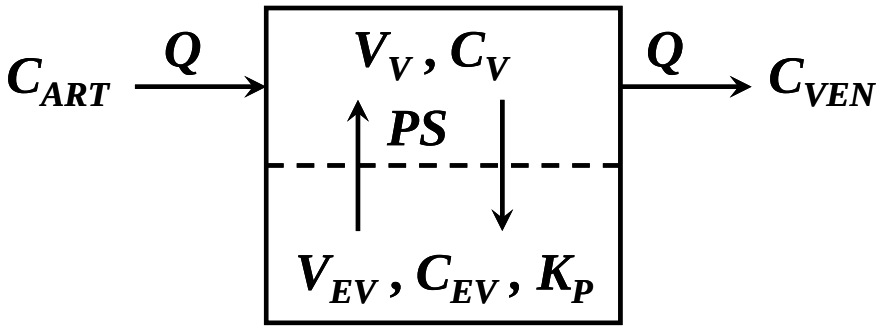

Figure 1.5. Schematic representation of blood flow rate-limited (A) and capillary membrane permeability rate-limited (B) tissue model. Symbols are defined in the text.

CHAPTER 2. SYSTEM ANALYSIS IN PHYSIOLOGICAL MODELING

2.1. Background

Linear system analysis (LSA) is a PK modeling approach that, unlike classical compartmental modeling used in a physiological or non-physiological context, is characterized by the following [126, 127]: 1) its applicability is independent of a particular structural model, 2) its dependence on convolution and deconvolution rather than on ordinary differential equations, and 3) the pharmacokinetic processes are regarded as stochastic at the level of a single molecule. Furthermore, the applicability of LSA is based on the assumption that movements of single molecules are mutually independent which implies the validity of the superposition principle [126, 127]. Therefore, linearity of the recirculatory system is a prerequisite for the physiological approach presented in this section. Recirculation models implementing LSA principles have been applied to describe the disposition of several therapeutic agents [25, 26, 96-100].

2.2. Building system analysis recirculation models

The difference between classical and LSA-recirculation models is that the latter views the organ as a general “building block” that is characterized by a unit impulse response (UIR) function, also known as a transfer function, which defines the basic disposition kinetics of the organ block [39, 101]. The other difference is that the rate of transfer of a drug out from an organ block in a LSA-based system depends linearly on the input rate to the organ and the UIR of that organ according to the general convolution equation [96, 101, 128-130]:

$$Output\ rate = Input\ rate * UIR(t) \quad , (*)\ denotes\ convolution \tag{2.1}$$

The UIR encapsulates the essential two fundamental disposition components, namely distribution and elimination [39, 96, 128, 129]. Accordingly, the UIR function may be reparametrized in terms of [39, 96]: 1) an extraction fraction, *E*, which represents the probability that a drug molecule which enters the organ will be eliminated, i.e. does not appear as a part of the output; and 2) a transit time density function, *g(t)*, which represents the distribution component:

$$UIR(t) = (1 - E) \cdot g(t) \tag{2.2}$$

The body may be considered kinetically as composed of a number of organ blocks connected partly in series and partly in parallel in such a way that the drug transfer can be recycled through the system. Mathematically, such systems (e.g., Figure 2.1A) can suitably be treated in a two step derivation, namely by first deriving the 'open loop' characteristics of the system, and secondly by closing the loop.

2.2.1. Open-loop system

To describe the physiological model shown in Figure 2.1A, a simpler single-pass system (Figure 2.1B) is obtained by cutting open the vascular system at plane P (Figure 2.1A). The system can be "broken down" into a set of pathways with serial and parallel connections, as shown in Figure 2.2. In serially connected blocks (Figure 2.2A), the transfer function of the pathway, $UIR_{12}(t)$:

$$UIR_{12}(t) = UIR_1(t) * UIR_2(t) = (1 - E_{12}) \cdot g_{12}(t) \tag{2.3}$$

where:

$$g_{12}(t) = g_1(t) * g_2(t) \tag{2.4}$$

$$E_{12} = 1 - (1 - E_1) \cdot (1 - E_2) \tag{2.5}$$

In parallel connected blocks with fraction of blood flow to the ith block, P_i (Figure 2.2B), the transfer function of the pathway, $UIR_{12}(t)$:

$$UIR_{12}(t) = P_1 \cdot UIR_1(t) + P_2 \cdot UIR_2(t) = (1 - E_{12}) \cdot g_{12}(t) \tag{2.6}$$

where:

$$g_{12}(t) = P_1 \cdot g_1(t) + P_2 \cdot g_2(t) \tag{2.7}$$

$$E_{12} = P_1 \cdot E_1 + P_2 \cdot E_2 \tag{2.8}$$

From above it can be concluded that, under linear conditions, irrespectively of the complexity of the connections of the individual organ blocks, an "open-loop" system (Figure 2.1B) can be reduced or 'lumped together' exactly to form a single organ block (Figure 2.1C). This is a very useful property because it provides a 'unified' way of considering the recirculation system.

In this conceptual "open-loop" analysis, the recirculation system is regarded as a black-box (Figure 2.1C) that can be described by a unit response function, $UIR_{SP}(t)$:

$$UIR_{SP}(t) = UIR_{HLS}(t) * \sum_{i=1}^{N} (Q_i/Q) \cdot UIR_i(t) = (1 - E_{SP}) \cdot g_{SP}(t) \tag{2.9}$$

where $UIR_{HLS}(t)$ is the transfer function of the heart-lung segment (with cardiac output Q), and the transfer function of different organs of systemic circulation (with blood flow rates Q_i) are denoted by UIR_i (i= 1,2,---,N). The transit time density function of the "open-loop" system, $g_{sp}(t)$ is given by:

$$g_{SP}(t) = g_{HLS}(t) * \sum_{i=1}^{N} (Q_i/Q) \cdot g_i(t) \tag{2.10}$$

, and the extraction ratio of the single-pass, E_{SP}, is given by:

$$E_{SP} = 1 - (1 - E_{HLS}) \cdot (1 - \sum_{i=1}^{N} (Q_i/Q) \cdot E_i) \tag{2.11}$$

Working with Laplace transform facilitates dealing with complex mathematical formulae because it converts the convolution operator into multiplication. In the Laplace domain, after inclusion of Eqs. 2.10 and 2.11, Eq. 2.9 becomes:

$$UIR_{SP}(s) = UIR_{HLS}(s) \cdot \sum_{i=1}^{N} \left(Q_i/Q\right) \cdot UIR_i(s) = (1 - E_{HLS}) \cdot (1 - \sum_{i=1}^{N} \left(Q_i/Q\right) \cdot E_i) \cdot g_{HLS}(s) \cdot \sum_{i=1}^{N} \left(Q_i/Q\right) \cdot g_i(s) \quad (2.12)$$

2.2.2. Closed-loop system

Closing the loop of the single-pass system (Figure 2.1D), results in an output from the system that contains recycled drug due to the additive feed-back on the input. The result is an output that is consistently larger than seen for the “open-loop” system. The input, $f_{in}(t)$, and output, $f_{out}(t)$, for a “closed-loop” system, similar to the “open-loop” system, are related by a convolution expression:

$$f_{out}(t) = UIR_{CIRC}(t) * f_{in}(t) \quad (2.13)$$

where $UIR_{CIRC}(t)$ is the transfer function of the “closed-loop” system. If the point of sampling is directly from the input site (e.g., intravenous administration and sampling), $UIR_{CIRC}(t)$ is related to the single-pass transfer function, $UIR_{SP}(t)$, in the Laplace domain:

$$UIR_{CIRC}(s) = \frac{UIR_{SP}(s)}{1 - UIR_{SP}(s)} \quad (2.14)$$

If the point of sampling is not directly from the input site, the rate must be propagated to the point of sampling. For instance, in case of intravenous administration and arterial sampling, the Laplace transform of $UIR_{CIRC}(t)$ is given by:

$$UIR_{CIRC}(s) = \frac{UIR_{SP}(s) \cdot UIR_{HLS}(s)}{1 - UIR_{SP}(s)} \quad (2.15)$$

The drug time-concentration disposition curve (*C(t)*) in LSA-based recirculation systems can be obtained only in Laplace-transformed form according to the relationship:

$$C(s) = \frac{f_{in}(s)}{Q} \cdot UIR_{CIRC}(s) \tag{2.16}$$

where $f_{in}(s)$ is the Laplace transform of the external drug input rate function. Software packages like MULTI (FILT) [131], MINIM [132], SCIENTIST (Micromath, Inc.), and ADAPT II (with Talbot's method) [133] can fit models specified in the Laplace domain based on numerical inverse Laplace transform.

2.3. Mean time and clearance concepts

The transit time density function, *g(t)*, in Eq. 2.2 provides the mean transit time through an organ block, *MTT*:

$$MTT = \int_0^\infty t \cdot g(t)\, dt = -\lim_{s \to 0} (dg(s)/ds) \tag{2.17}$$

Accordingly, if the *MTT* is large it means that the 'affinity' of the drug to stay in the organ is large. The degree of 'accumulation' of drug in the organ is therefore related to the *MTT*, which depends only on *g(t)*. Thus, *g(t)* determines the distribution properties for the organ block. Additionally, the *MTT* can be obtained by the moment ratio of the transfer function through the organ block, *UIR(t)*:

$$MTT = \frac{\int_0^\infty t \cdot UIR(t)\, dt}{\int_0^\infty UIR(t)\, dt} = \frac{-\lim_{s \to 0} (dUIR(s)/ds)}{\lim_{s \to 0} UIR(s)} \tag{2.18}$$

In serially connected blocks (Figure 2.2A), the *MTT* is given by:

$$MTT_{12} = MTT_1 + MTT_2 \tag{2.19}$$

, while in parallel connected blocks (Figure 2.2B), the *MTT* is given by:

$$MTT_{12} = P_1 \cdot MTT_1 + P_2 \cdot MTT_2 \tag{2.20}$$

Extending the above concepts to the recirculation system shown in Figure 2.1A, the mean transit time of the single-pass, MTT_{SP} is given by:

$$MTT_{SP} = MTT_{HLS} + \sum_{i=1}^{N} (Q_i/Q) \cdot MTT_i \tag{2.21}$$

where $MTT_{HLS}(t)$ is the mean transit time of the heart-lung segment (with cardiac output Q), and the mean transit time of different organs of systemic circulation (with blood flow rates Q_i) are denoted by MTT_i ($i = 1,2,---,N$). MTT_{SP} gives the volume of distribution at steady state, V_{ss}:

$$V_{ss} = MTT_{SP} \cdot Q \tag{2.22}$$

The extraction ratio of an organ block, E, represents the probability that a drug molecule which enters the tissue once will be eliminated, i.e. does not appear as part of the output. Thus, E can be obtained only in the context of an "open-loop" system. E is calculated from the zero-moment of the transfer function, $UIR(t)$:

$$E = 1 - \int_0^{\infty} UIR(t)\,dt = 1 - \lim_{s \to 0} UIR(s) \tag{2.23}$$

or, by measuring the steady-state input, $A_{in,ss}$, and output, $A_{out,ss}$ amounts:

$$E = \frac{A_{in,ss} - A_{out,ss}}{A_{in,ss}} \tag{2.24}$$

The average time the drug spends in the "closed-loop" system before it is completely eliminated is known as the mean residence time (*MRT*). In contrast to the *MTT*, the *MRT* can be defined only in the context of a "closed-loop" system as the moment ratio of the recirculation transfer function, $UIR_{CIRC}(t)$:

$$MRT = \frac{\int_0^\infty t \cdot UIR_{CIRC}(t)\,dt}{\int_0^\infty UIR_{CIRC}(t)\,dt} = \frac{-\lim_{s\to 0}(d\,UIR_{CIRC}(s)/ds)}{\lim_{s\to 0} UIR_{CIRC}(s)} \tag{2.25}$$

For a system with identical input and sampling points, the *MRT* depends on both the mean transit time, MTT_{SP} (Eq. 2.22), and the extraction ratio, E_{SP} (Eq. 2.11), of the single-pass:

$$MRT = \frac{MTT_{SP}}{E_{SP}} \tag{2.26}$$

Two types of clearance can be defined within the framework of LSA-based recirculation models, the extraction clearance, CL_E, and the response clearance, CL_R. The extraction clearance can only be defined in the sense of a single pass system and it depends on the extraction-ratio of the single-pass, E_{SP} (Eq. 2.11), and the total blood flow, Q:

$$CL_E = E_{SP} \cdot Q \tag{2.27}$$

In contrast to this, one can always define a response-type clearance, CL_R, that is equivalent to the general definition of the clearance in classical compartmental and non-compartmental models, the ratio of the input dose to the produced area under the time-concentration curve:

$$CL_R = Q / \int_0^\infty UIR_{CIRC}(t)\,dt = Q / \lim_{s\to 0} UIR_{CIRC}(s) \tag{2.28}$$

For a system with identical input and sampling points, the CL_R depends on the extraction ratio of the single-pass, E_{SP} (Eq. 2.11):

$$CL_R = E_{SP} \cdot Q / (1 - E_{SP}) \tag{2.29}$$

2.4. Organ transfer and distribution models

Although the organ transfer function, *UIR(t)* (Eq. 2.1), and transit time density function, *g(t)* (Eq. 2.2), can be always specified on an empirical basis [39, 96, 134-137], attempts to derive functions based on mechanistic models for drug disposition and distribution through the organ have been published. In this section, the widely used mechanistic models with their derived transfer and/or distribution functions are presented. The kinetic parameters based on moment analysis of such functions, namely the extraction ratio and the mean transit time, are also shown.

2.4.1. Flow limited mass transfer model

In 1982, Weiss [39] derived the transfer function of an organ consisting of homogenous blood (B) and tissue (T) regions separated by a capillary membrane (Figure 2.3A). Denoting the input and output concentrations of the organ by C_{in} and C_{out}, the mass balance equation was written as:

$$Q \cdot (C_{in} - C_{out}) = V_T \cdot (d\,C_T/dt) + V_B \cdot (d\,C_B/dt) + CL_{\text{int}} \cdot f_u \cdot C_B \qquad (2.30)$$

where Q is the blood flow, V_T and V_B are the volumes of the organ blood and tissue regions, C_T and C_B are the concentrations in the organ blood and tissue regions, and Cl_{int} is the intrinsic clearance describing the elimination of the drug from the organ that was assumed to occur from the blood space. Cl_{int} was related to the free drug molecules in the organ by f_u that denotes the fraction of drug unbound in the blood. Assuming: 1) a flow rate limited transport, 2) the concentration of the drug in the blood and tissue regions are in equilibrium (i.e., $C_T = K_P \cdot C_B$, where K_P is the tissue-to-blood partition coefficient), and 3) $V_B << V_T$ (i.e., the organ volume, $V \approx V_T$), the effect of the tissue membrane

(Figure 2.3A) becomes negligible and the organ behaves as a one-compartment structure (Figure 2.3B). In this case Eq. 2.30 reduces to:

$$Q \cdot (C_{in} - C_{out}) = K_P \cdot V \cdot (d\,C_B/dt) + CL_{\text{int}} \cdot f_u \cdot C_B \tag{2.31}$$

For simplicity, it was assumed that the organ behaves as a "well-stirred" structure [40], where the effluent blood is in equilibrium with the blood in the organ (i.e., $C_{out} = C_B$). Thus, Eq. 2.31 becomes:

$$Q \cdot (C_{in} - C_{out}) = K_P \cdot V \cdot (d\,C_{out}/dt) + CL_{\text{int}} \cdot f_u \cdot C_{out} \tag{2.32}$$

After taking Laplace transform for Eq. 2.32 and using the definition $UIR(s) = C_{out}(s)/C_{in}(s)$, Eq. 2.32 yields:

$$UIR(s) = \frac{Q/(K_P \cdot V)}{s + (Q + CL_{\text{int}} \cdot f_u)/(K_P \cdot V)} \tag{2.33}$$

with inverse Laplace transform:

$$UIR(t) = \frac{Q}{K_P \cdot V} \cdot \exp\left[-\frac{Q + CL_{\text{int}} \cdot f_u}{K_P \cdot V} \cdot t \right] \tag{2.34}$$

Utilizing Eqs. 2.23 and 2.18, the kinetic parameters characterizing the transfer function in Eq. 2.33 or 2.34, namely the extraction ratio, E, and mean transit time, MTT, are given by:

$$E = 1 - \frac{Q}{Q + CL_{\text{int}} \cdot f_u} \tag{2.35}$$

, and:

$$MTT = \frac{K_P \cdot V}{Q + CL_{\text{int}} \cdot f_u} \tag{2.36}$$

2.4.2. Finite mass transfer resistance model

Extending the derivations to an organ structure with tissue membrane resistance, Weiss [39] defined the mass balance for the blood and tissue regions in Figure 2.3C by:

$$V_T \cdot (d\,C_T/dt) = PS \cdot (C_B - C_T/K_P) \quad (2.37)$$

$$V_B \cdot (d\,C_B/dt) = Q \cdot (C_{in} - C_{out}) - PS \cdot (C_B - C_T/K_P) - CL_{\text{int}} \cdot f_u \cdot C_B \quad (2.38)$$

where *PS* is membrane permeability-surface area coefficient. Again, using the 'well-stirred" assumption Eqs. 2.37 and 2.38 become:

$$V_T \cdot (d\,C_T/dt) = PS \cdot (C_{out} - C_T/K_P) \quad (2.39)$$

$$V_B \cdot (d\,C_{out}/dt) = Q \cdot (C_{in} - C_{out}) - PS \cdot (C_{out} - C_T/K_P) - CL_{\text{int}} \cdot f_u \cdot C_{out} \quad (2.40)$$

, and the transfer function is defined as:

$$UIR(s) = \frac{Q}{V_B} \cdot \frac{s + X}{(s + a) \cdot (s + b)} \quad (2.41)$$

with inverse Laplace transform:

$$UIR(t) = \frac{Q}{V_B \cdot (b - a)} \cdot \left[(X - a) \cdot \exp(-a \cdot t) - (X - b) \cdot \exp(-b \cdot t)\right] \quad (2.42)$$

where:

$$a, b = (X + Y)/2 \pm \left[(X + Y)^2/4 + PS^2/(V_T \cdot V_B \cdot K_P) - X \cdot Y\right]^{1/2} \quad (2.43)$$

$$X = Q/(K_P \cdot V_T) \quad (2.44)$$

$$Y = (Q + PS + CL_{\text{int}} \cdot f_u)/V_B \quad (2.45)$$

, and:

$$E = 1 - \frac{X}{a + b} = 1 - \frac{Q}{Q + CL_{\text{int}} \cdot f_u} \quad (2.46)$$

$$MTT = \frac{1}{a} + \frac{1}{b} + \frac{1}{X} = \frac{V_B + K_P \cdot V_T}{Q + CL_{\text{int}} \cdot f_u} \tag{2.47}$$

2.4.3. Dispersion models

In the theory of chromatography, two mathematical models were proposed to describe the elution of a non-degradable [138] and a degradable [139] solute from a chromatographic column taking into consideration the axial dispersion of the solute. The first model, referred to as the one-compartment dispersion model, assumes instant equilibrium of the solute between the mobile and the stationary phases. The second one, termed as the two-compartment dispersion model, assumes finite mass partitioning between the phases.

2.4.3.1. One-compartment model

The model was introduced to the field of pharmacokinetics by Roberts and Rowland [140, 141] who used it to analyze the outflow curves of liver perfusion experiments. The key assumption of the model is that the transit time distribution of the solute as it moves through the organ is principally due to the process of longitudinal or axial dispersion (Figure 2.4A). This means that the transverse or radial diffusion is many orders of magnitude more rapid than the transit through the organ, so it can be neglected. The axial dispersion may be caused by: 1) variations in flow velocity and or variations in solute path lengths; 2) mixing of blood at the branch points of interconnected capillaries; and/or 3) molecular diffusion. Under the assumption of rapid equilibrium between the organ blood and tissue spaces (Figure 2.4B), the solute concentration in the organ was described by the partial differential equation:

$$V_{ss} \cdot \frac{dC(t,z)}{dt} + V \cdot \nu \cdot \frac{dC(t,z)}{dz} = V \cdot D_{disp} \cdot \frac{d^2C(t,z)}{dz^2} - CL_{\text{int}} \cdot f_u \cdot C(t,z) \tag{2.48}$$

where *C(t,z)* is the concentration at time *t* and distance *z*, *v* is the linear flow velocity of blood through the organ, and D_{disp} is the axial dispersion coefficient that characterizes the degree of mixing of the injected solute with the organ. Cl_{int} is the intrinsic clearance, and f_u is the fraction unbound in the plasma. *V* denotes the organ volume, and V_{ss} denotes the steady-state volume of distribution that can be calculated by:

$$V_{ss} = V_B + K_p \cdot V_T \cdot \frac{f_u}{f_{u,t}} \tag{2.49}$$

where V_B is the volume of the blood space, V_T is the volume of the tissue space, K_P is the tissue-to-blood partition coefficient, and $f_{u,t}$ is the fraction unbound in the tissue. If $V_T >> V_B$, V_{ss} can be approximated by:

$$V_{ss} = K_p \cdot V \cdot \frac{f_u}{f_{u,t}} = K_p \cdot V_W \tag{2.50}$$

, V_W denotes the organ total water volume.

Using Laplace transform to solve Eq. 2.48 at the initial and boundary conditions:

$$C(0,z) = 0 \ , \ C(t,0) = 1/Q \cdot \delta(t) \ , \ C(t,\infty) = 0 \tag{2.51}$$

where *Q* is the blood flow, *δ(t)* is dirac-delta function, and *C(t,0)* is equivalent to a unit bolus input, yielded the following transfer function:

$$UIR(s) = \exp\left[\frac{1}{2D_N} - \sqrt{\left(\frac{1}{2D_N}\right)^2 + \frac{R_N \cdot Q + V_{ss} \cdot s}{D_N \cdot Q}}\right] \tag{2.52}$$

with inverse Laplace transform:

$$UIR(t) = \frac{V \cdot \sqrt{X}}{Q \cdot 2t \cdot \sqrt{\pi \cdot t}} \exp\left[\frac{1}{2D_N} - \frac{Y}{X} \cdot t - \frac{X}{4t} \cdot V^2\right] \tag{2.53}$$

where:

$$X = \frac{V_{ss}}{D_N \cdot Q \cdot V^2} \tag{2.54}$$

$$Y = \left(\frac{1}{2D_N \cdot V} \right)^2 + \frac{R_N}{D_N \cdot V^2} \tag{2.55}$$

, and:

D_N is the dispersion number that is given by:

$$D_N = D_{disp} / (v \cdot L) \tag{2.56}$$

where L is the organ length. R_N is the efficiency number that is given by:

$$R_N = CL_{\text{int}} \cdot f_u / Q \tag{2.57}$$

D_N measures the relative importance of the dispersion to the convective movement of the solute through the organ, while R_N is a measure for the removal rate of the solute by the organ.

The moment-based parameters characterizing the transfer function in Eq. 2.52 or 2.53 are:

$$E = 1 - \exp\left[\frac{1}{2D_N} - \sqrt{\left(\frac{1}{2D_N} \right)^2 + \frac{R_N}{D_N}} \right] \tag{2.58}$$

$$MTT = \frac{V_{ss}}{Q} \cdot \frac{1}{\sqrt{1 + 4 D_N \cdot R_N}} \tag{2.59}$$

2.4.3.2. Two-compartment model

In 1989, Yano et al [142] introduced the two-compartment dispersion model and used it to analyze the outflow curves of liver perfusion experiments. In addition to the assumptions made by the one-compartment dispersion model, the two-compartment model assumes a finite mass transfer occurring between the blood (B) and tissue (T)

spaces of the organ (Figure 2.4C). Accordingly, the model is a hybrid of the one-compartment dispersion model supported by Roberts and Rowland [140, 141] and the finite mass transfer resistance model supported by Weiss [39]. The model was described by the equations:

$$V_B \cdot \frac{dC_B(t,z)}{dt} + V_B \cdot \nu \cdot \frac{dC_B(t,z)}{dz} = V_B \cdot D_{disp} \cdot \frac{d^2 C_B(t,z)}{dz^2} - V_B \cdot k_{BT} \cdot C_B(t,z) + V_T \cdot k_{TB} \cdot C_T(t,z) - CL_{\text{int}} \cdot f_u \cdot C_B(t,z) \quad (2.60)$$

$$V_T \cdot \frac{dC_T(t,z)}{dt} = V_B \cdot k_{BT} \cdot C_B(t,z) - V_T \cdot k_{TB} \cdot C_T(t,z) \quad (2.61)$$

where $C_B(t,z)$ and $C_T(t,z)$ are the concentrations in the blood and tissue phases at time t and distance z. V_B and V_T are the volumes of the blood and tissue spaces. k_{BT} and k_{TB} denote the forward and backward partition rate constants between blood and tissue. Using the initial and boundary conditions:

$$C_B(0,z) = 0 \ , \ C_B(t,0) = 1/Q \cdot \delta(t) \ , \ C_B(t,\infty) = 0 \quad (2.62)$$

$$C_T(0,z) = 0 \ , \ C_T(t,0) = 0 \quad (2.63)$$

and solving using Laplace transform, the transfer function was:

$$UIR(s) = \exp\left[\frac{1}{2D_N} - \sqrt{\left(\frac{1}{2D_N}\right)^2 + \frac{V_B}{D_N \cdot Q} \cdot \left(s + \frac{R_N \cdot Q}{V_B} + k_{BT} - \frac{k_{BT} \cdot k_{TB}}{s + k_{TB}}\right)}\right] \quad (2.64)$$

where D_N and R_N are the dispersion and efficiency numbers, respectively, and they were defined as in the one-compartment model (Eqs. 2.56 and 2.57). k_{BT} and k_{TB} were correlated with the tissue-to-blood partition coefficient, K_P and the permeability surface area coefficient, PS, that were proposed by Weiss [39] in the finite mass transfer resistance model:

$$k_{BT} = PS/V_B \quad (2.65)$$

$$k_{TB} = PS/(V_T \cdot K_P) \tag{2.66}$$

Unlike the one-compartment dispersion model, an analytical solution for the inverse of the Laplace transform of the two-compartment model (Eq. 2.64) does not exist. The extraction ratio calculated from the zero-moment of Eq. 2.64 is the same as that of the one-comp model (Eq. 2.58), while the mean transit time is:

$$MTT = \frac{V_B}{Q} \cdot \left(1 + \frac{k_{BT}}{k_{TB}}\right) \cdot \frac{1}{\sqrt{1 + 4 D_N \cdot R_N}} \tag{2.67}$$

2.4.4. Extended dispersion models

The one-compartment dispersion model assumes well-mixed organ compartment, while the two-compartment dispersion model assumes instant radial equilibrium within the tissue space. In other words, the former model is suitable to capture the PK of a non-permeable solute, while the later model is well-suited for a permeating, but non-diffusing solute. Weiss and Roberts [143], and Weiss [144] presented a stochastic approach to extend the one-compartment dispersion model to account for the distribution of a permeating solute under the assumptions of 1) slow intra-tissue distribution "the dispersion-diffusion model", or 2) slow intra-tissue binding " the dispersion-binding model". The approach considers the transit time of a permeating solute molecule as a random variable, *W*, that is equivalent to the sum of the random transit time of intravascular marker, *X*, and the sojourn times, Y_i, of *N* excursions from the blood to the tissue space [143]:

$$W = X + Y_1 + Y_2 + \cdots\cdots + Y_N \tag{2.68}$$

In this analysis, it was assumed that each molecule distributes radially in the tissue space and returns to the same point in the blood space which implies that axial distribution was

neglected. Assuming: 1) independent, identically distributed random variables, Y_1, Y_2, …,Y_N, with density function in the Laplace domain $g_y(s)$ (sojourn time density), and 2) the number of excursions, N, can be modeled as a Poisson renewal process, the organ transit time density function of the permeating molecule in the Laplace domain, $g_w(s)$ was given by:

$$g_w(s) = g_x[s + k_{in} \cdot (1 - g_y(s))] \tag{2.69}$$

where $g_x(s)$ denotes the Laplace transform of the transit time density function of a non-permeating solute (i.e. an intravascular marker), while $g_y(s)$ denotes the Laplace transform of the residence time distribution for a single excursion to the extra-vascular space (i.e. sojourn time density). k_{in} is the influx rate from the vascular to the extra-vascular space. An inverse Gaussian density function parametrized in terms of blood flow, Q, blood volume, V_B, and distribution coefficient of variation, CV, was empirically used to model $g_x(s)$:

$$g_x(s) = \exp\left[\frac{1}{CV^2} - \sqrt{\frac{V_B/Q}{CV^2/2} \cdot \left(s + \frac{1}{2(V_B/Q) \cdot CV^2}\right)}\right] \tag{2.70}$$

The use of inverse Gaussian distribution was proven to be equivalent to the one-compartment dispersion model for a non-eliminated solute [137]. Modeling of $g_y(s)$ was done using the distribution function of the diffusion or the binding model (derivations are shown in the following sections). The resulting density function, $g_w(s)$ (Eq. 2.69), can be presented in the Laplace domain only (i.e. the analytical solution in the time domain does not exist).

The same approach was used to model solute cellular distribution by assuming an organ structure with cellular and extracellular spaces rather than tissue (extra-vascular)

and blood (vascular) spaces [144]. In contrast to the dispersion model whose parameters can be determined using standard organ perfusion experiments [141, 142, 145-153], the extended dispersion model parameters require specific experimental setting known as the multiple indicator dilution method [25, 98, 134, 154-159]. The method involves simultaneous administration of the drug with an intravascular marker (e.g., indocyanine green) or an extracellular marker (e.g., sucrose or inulin) and a marker for the total body water (e.g., antipyrine or hydrogenated water). Fitting to the time-concentration data of such markers allows estimation of several physiological parameters (e.g., blood flow, blood volume, extra-vascular water volume, cellular water volume, etc.) which ensures accurate estimation of drug-dependent parameters (e.g., dispersion and distribution parameters, cellular binding parameters, partition coefficient, membrane permeability, etc.).

2.4.4.1. Dispersion-diffusion model

The model was derived by Wiess and Roberts in 1996 [143]. The model consists of blood (B) and tissue (T) spaces separated by a capillary membrane (Figure 2.5A). Q is the blood flow. k_{in} and k_{out} are the influx and outflux rate constants:

$$k_{in} = PS \cdot f_u / V_B \tag{2.71}$$

$$k_{out} = PS \cdot f_{u,t} / V_T \tag{2.72}$$

where PS is the permeability surface area coefficients. V_B and V_T are the volumes of the blood and tissue spaces. f_u and $f_{u,t}$ are the fractions unbound in plasma and tissue. The model assumes that the solute distributes within the tissue space by radial diffusion neglecting the effect of axial diffusion (Figure 2.5A). Transport in the tissue space was defined by a one-dimensional diffusion process:

$$\frac{dC_T(t,z)}{dt} = D_{diff} \cdot \frac{d^2 C_T(t,z)}{dz^2} \quad , \quad 0 \le z \le L \tag{2.73}$$

where $C_T(t,z)$ is the concentration in the tissue space at time t and distance z. D_{diff} is the radial diffusion coefficient, and L is the depth of the tissue space. The boundary conditions describing the transfer between the blood and tissue regions across the capillary membrane with permeability P:

$$-D_{diff} \cdot \frac{dC_T(t,0)}{dz} = P \cdot [f_u \cdot C_B(t) - f_{u,t} \cdot C_T(t,0)] \tag{2.74}$$

, and outer boundary conditions:

$$\frac{dC_T(t,L)}{dz} = 0 \tag{2.75}$$

where $C_B(t)$ is the concentration in the blood space. The mass balance of the solute in the blood:

$$V_B \cdot \frac{dC_B(t)}{dt} = -Q \cdot C_B(t) - V_B \cdot k_{in} \cdot C_B(t) + V_T \cdot k_{out} \cdot C_T(t,0) \tag{2.76}$$

with initial condition that reflects a unit bolus input:

$$C_B(0) = 1/Q \cdot \delta(t) \tag{2.77}$$

Solving the model (Eqs. 2.73-2.77) for $C_B(t)$ using Laplace transform yielded the organ density function for a permeable solute, $g_w(s)$. Assuming a single exponential distribution for the vascular marker, $g_x(s)$:

$$g_x(s) = \frac{Q/V_B}{s + (Q/V_B)} \tag{2.78}$$

substitution in Eq. 2.69 yielded the Laplace transform of the sojourn time density in the extra-vascular space, $g_y(s)$:

$$g_y(s) = \frac{1}{1 + \frac{V_T}{k_{in} \cdot V_B \cdot d} \cdot \sqrt{d \cdot s} \cdot \tanh(\sqrt{d \cdot s})} \tag{2.79}$$

where d is the time constant for the intra-tissue diffusion process ($d = L^2/D_{diff}$).

2.4.4.2. Dispersion-binding model

The model was derived for the liver by Weiss [144] and Weiss et al [160]. The model assumes that during the radial distribution through the tissue space, the solute binds with a receptor, R, in the cellular phase with a rate constant k_{on} to form a solute-receptor complex, R^*, that dissociates to free solute and free receptor with rate constant k_{off} (Figure 2.5B). The model was described by the following ordinary differential equations:

$$\frac{dC_{EC}(t)}{dt} = -\frac{Q}{V_{EC}} \cdot C_{EC}(t) - k_{in} \cdot C_{EC}(t) + \frac{V_C}{V_{EC}} \cdot k_{out} \cdot C_C(t) \tag{2.80}$$

$$\begin{aligned} \frac{dC_C(t)}{dt} = {} & \frac{V_{EC}}{V_C} \cdot k_{in} \cdot C_{EC}(t) + k_{off} \cdot R^*(t) - k_{out} \cdot C_C(t) \\ & - k_{on} \cdot [R_{tot} - R^*(t)] \cdot C_C(t) \end{aligned} \tag{2.81}$$

$$\frac{dR^*(t)}{dt} = -k_{off} \cdot R^*(t) + k_{on} \cdot [R_{tot} - R^*(t)] \cdot C_C(t) \tag{2.82}$$

where $C_C(t)$ and $C_{EC}(t)$ are the concentrations in the organ cellular and extracellular regions, V_C and V_{EC} are the volumes of the organ cellular and extracellular regions, Q is the blood flow, k_{in} and k_{out} are the influx and outflux rate constants, and R_{tot} is the total receptor. For relatively small occupancies (i.e. $R^* << R_{tot}$), Eqs. 2.81 and 2.82 simplify to that of a linear, non-saturable binding:

$$\frac{dC_C(t)}{dt} = \frac{V_{EC}}{V_C} \cdot k_{in} \cdot C_{EC}(t) + k_{off} \cdot R^*(t) - k_{out} \cdot C_C(t) - k_{on} \cdot R_{tot} \cdot C_C(t) \tag{2.83}$$

$$\frac{dR^*(t)}{dt} = -k_{off} \cdot R^*(t) + k_{on} \cdot R_{tot} \cdot C_C(t) \quad (2.84)$$

Solving Eqs. 2.80, 2.83, and 2.84 for $C_B(t)$ using the same approach in the dispersion-diffusion model, the Laplace transform of the residence time distribution for a single excursion to the cellular space, $g_y(s)$ is given by:

$$g_y(s) = \frac{k_{out} \cdot (s + k_{off})}{(s + \lambda_1) \cdot (s + \lambda_2)} \quad (2.85)$$

where:

$$\lambda_1, \lambda_2 = \frac{1}{2}\left(k_{on}{}^* + k_{off} + k_{out} \pm \sqrt{(k_{on}{}^* + k_{off} + k_{out})^2 - 4\, k_{off} \cdot k_{out}} \right) \quad (2.86)$$

, and $k_{on}{}^* = k_{on} \cdot R_{tot}$.

The model assumes slow tissue binding. Later [97, 161], the model was extended to include quasi-instant binding to cell constituents characterized by an equilibrium amount ratio K_R (Figure 2.5C). $g_y(s)$ was modified to:

$$g_y(s) = \frac{k_{in} \cdot (s + k_{off})}{s^2 \cdot K_{dist} \cdot (1 + K_R) + s \cdot \left[K_{dist} \cdot (k_{on}{}^* + K_R \cdot k_{off} + k_{off}) + k_{in} \right] + k_{in} \cdot k_{off}} \quad (2.87)$$

, and $K_{dist} = k_{in}/k_{out}$.

2.5. Extension to non-linear elimination

In 2008, Veng-Pedersen et al [96] was the first to extend the LSA-based recirculation model to account for non-linear elimination. The initial proposed model was a complex system (Figure 2.6A) consisting of a pulmonary circulation in serial connection with two parallel connected sub-systems, S1 and S2. The arterial blood is pumped with a cardiac output that was proportional to a constant K_{out}. The sub-systems, S1 and S2, receive blood flow rates with fractions w_1, and w_2, respectively. Following the simplifying lumping rules of serial (Eqs. 2.3-2.5), and parallel (Eqs. 2.6-2.8) connected

sub-systems, the pulmonary circulation was reduced to heart-lung (HL) segment (Figure 2.6B) that was lumped with the sub-systems, S1 and S2, resulting in a final model with two parallel connected subsystems, HLS1 and HLS2 (Figure 2.6C). Figure 2.6D illustrates the implementation of non-linearity in the model where it was assumed that saturable elimination occurs from the sub-system HLS1, resulting in a heterogenous final model. A Front-End-Back-End approach was used to model the non-linear elimination where it was assumed that the extraction ratio, *E* depends on the input rate, $f_{in}(t)$, and the output rate, $f_{out}(t)$. Accordingly, the output rate from the sub-system HLS1, $f_{out1}(t)$ was given by:

$$f_{out1}(t) = N(E_1, K_{N1}, w_1 \cdot (f_{in}(t) + N(E_1, K_{N1}, f_{out1}(t)) + f_{out2}(t))) * g(t) \qquad (2.88)$$

where *N(.)* is a non-linearity function that was modeled as a Michaelis-Menten equation:

$$N(E_1, K_{N1}, X) = (1 - E_1 \cdot K_{N1}/(K_{N1} + X) \cdot X \qquad (2.89)$$

At the linear operating range when the input rate and output rate are much smaller than the non-linearity constant, K_N, Eq. 2.89 reduces to $(1\text{-}E_1)*X$, and Eq. 2.88 becomes:

$$f_{out1}(t) = (1 - E_1) \cdot (f_{in}(t) + f_{out1}(t) + f_{out2}(t)) * g(t) \qquad (2.90)$$

The disposition through the sub-system HLS2 was assumed to be linear and does not involve drug extraction. Accordingly, the output rate from HLS2, $f_{out2}(t)$ was given by:

$$f_{out2}(t) = w_2 \cdot (f_{in}(t) + N(E_1, K_{N1}, f_{out1}(t)) + f_{out2}(t)) * g(t) \qquad (2.91)$$

Using a bi-exponential transit time density function, *g(t)*:

$$g(t) = \alpha \cdot \beta \cdot (\exp(-\alpha \cdot t) - \exp(-\beta \cdot t))/(\beta - \alpha) \qquad (2.92)$$

the convolution equations (Eqs. 2.88 and 2.91) were converted to the following ordinary differential equations:

$$d\,y_1/dt = N(E_1, K_{N1}, w_1 \cdot (f_{in}(t) + N(E_1, K_{N1}, f_{out1}(t)) + f_{out2}(t))) - \alpha \cdot y_1 \qquad (2.93)$$

$$d\ f_{out1}(t)/dt = \alpha \cdot \beta \cdot y_1 - \beta \cdot f_{out1}(t) \quad (2.94)$$

$$d\ y_2/dt = w_2 \cdot (f_{in}(t) + N(E_1, K_{N1}, f_{out1}(t)) + f_{out2}(t)) - \alpha \cdot y_2 \quad (2.95)$$

$$d\ f_{out2}(t)/dt = \alpha \cdot \beta \cdot y_2 - \beta \cdot f_{out2}(t) \quad (2.96)$$

The output drug concentration that was measured in the venous blood, $C_{out}(t)$ was given by:

$$C_{out}(t) = K_{out} \cdot (f_{out1}(t) + f_{out2}(t)) \quad (2.97)$$

2.6. Summary

The mechanistic nature and universality of physiologically based pharmacokinetic (PBPK) model structure between mammalian species make them uniquely suited to 1) predict drug pharmacokinetics in humans from *in vitro* and preclinical data, 2) characterize the physiological and biochemical basis for drug altered pharmacokinetics and toxicokinetics, and 3) recognize the underlying reasons for variability in drug response which contributes to optimized or even individualized drug dosing for patients. Although some advanced PBPK models have been developed and successfully applied in environmental and toxicological research, PBPK modeling has not received the proper attention in drug development. Generally, this is attributed to the complexity of model development process and the uncertainty introduced into model parameters that negatively influence the accuracy of model predictions. Those drawbacks necessitated the use of minimal PBPK models and the search for alternative means to mathematically represent the processes of drug transport within a physiological structure. Linear systems analysis (LSA) principles applied to physiological modeling is an approach that simplifies PBPK model development by characterizing the organ with a unit impulse response (UIR) function in the framework of input-output convolution relationship. The

organ UIR can be specified on an empirical basis avoiding assumptions about mechanism of drug distribution and elimination or it can reflect rigorous, mechanism-based processes on the sub-organ or even the cellular level. This review: 1) presents a “unified” methodology for building LSA-recirculation models, 2) addresses the mean time and clearance concepts in those models, 3) discusses the various mechanistic models of organ disposition, and 4) introduces a recirculation model for drugs exhibiting non-linear elimination. This review is important for the readers in order to understand 1) the rationale for adopting the LSA-physiological paradigm in this thesis, and 2) the principles of the physiological model developed in Chapter 3 and applied in Chapter 3 and Chapter 4.

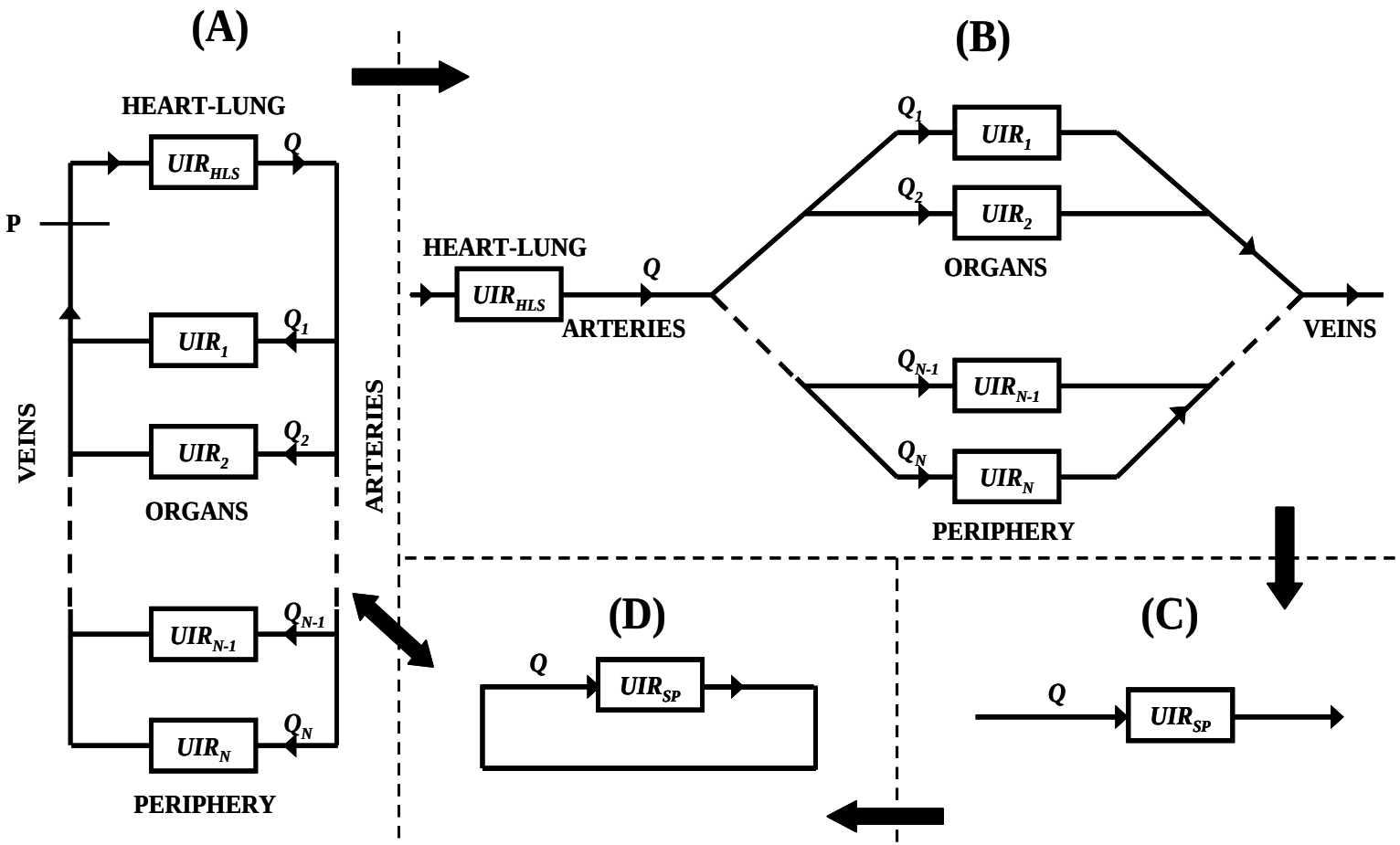

Figure 2.1. Schematic representation of a linear recirculation model development showing closed-loop system (A), open-loop system (B), lumped open-loop system (C), and lumped closed-loop system (D). Symbols are defined in the text.

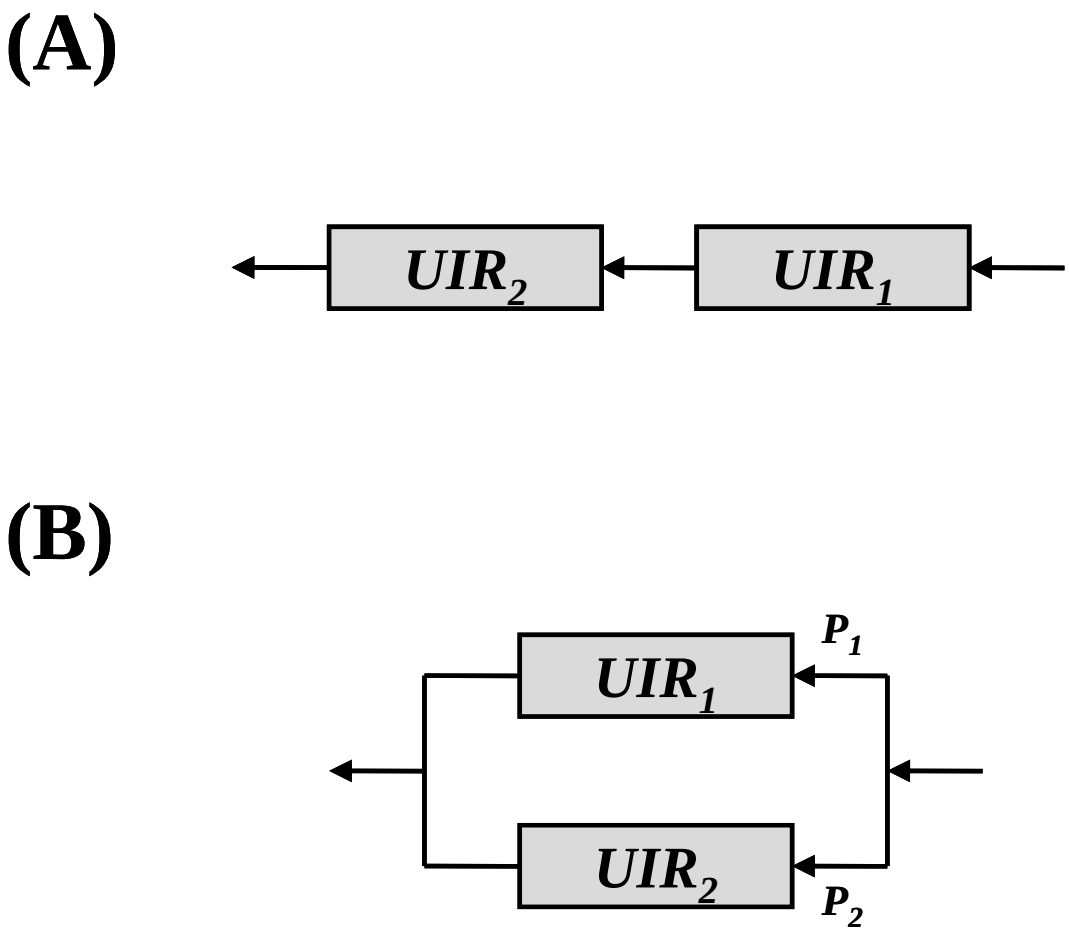

Figure 2.2. Schematic representation of organ blocks in serial connection (A), and in parallel connection (B). Symbols are defined in the text.

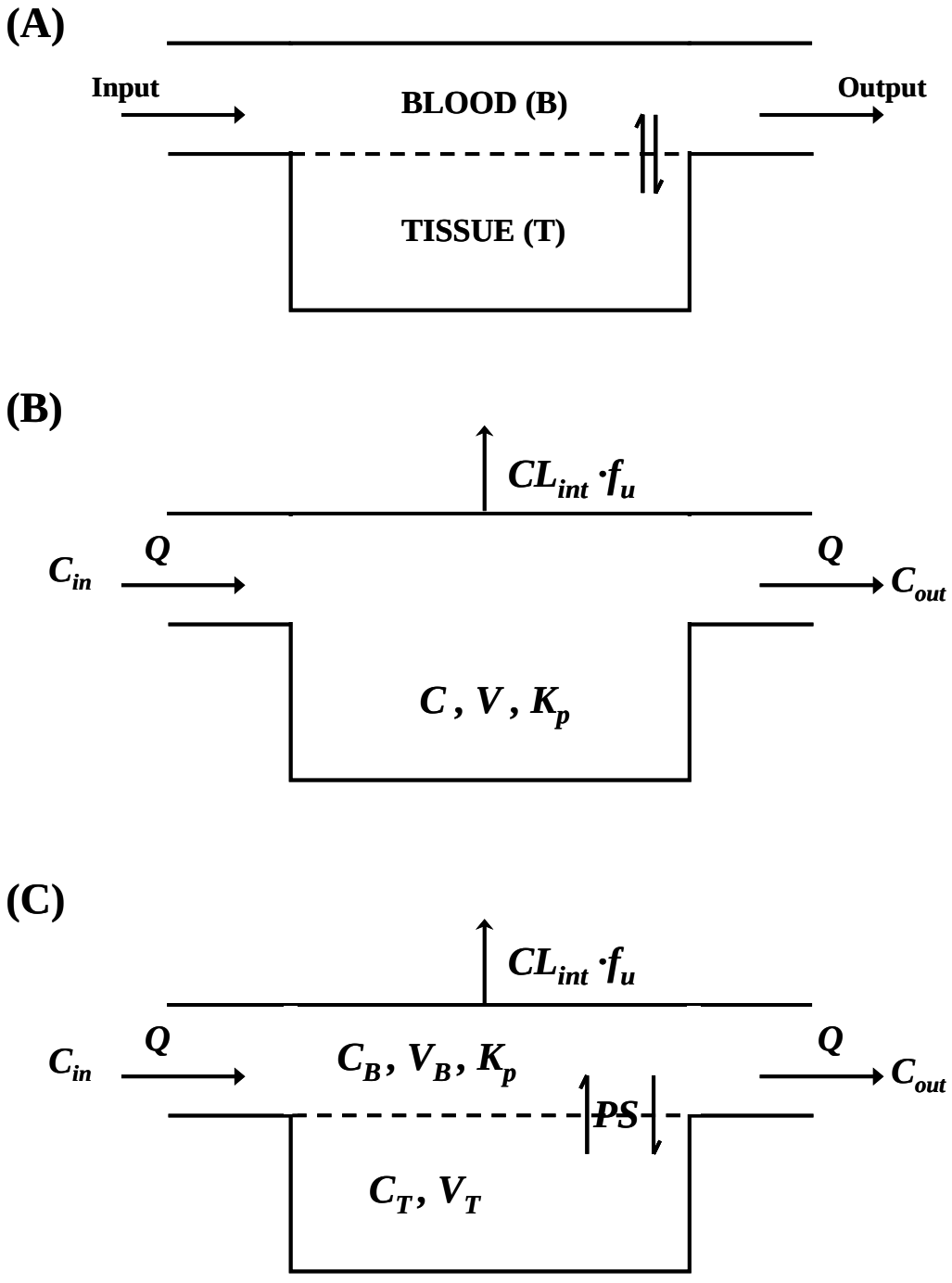

Figure 2.3. Schematic representation of organ structure (A) used for the derivation of the flow limited mass transfer model (B), and finite mass transfer resistance model (C). Symbols are defined in the text.

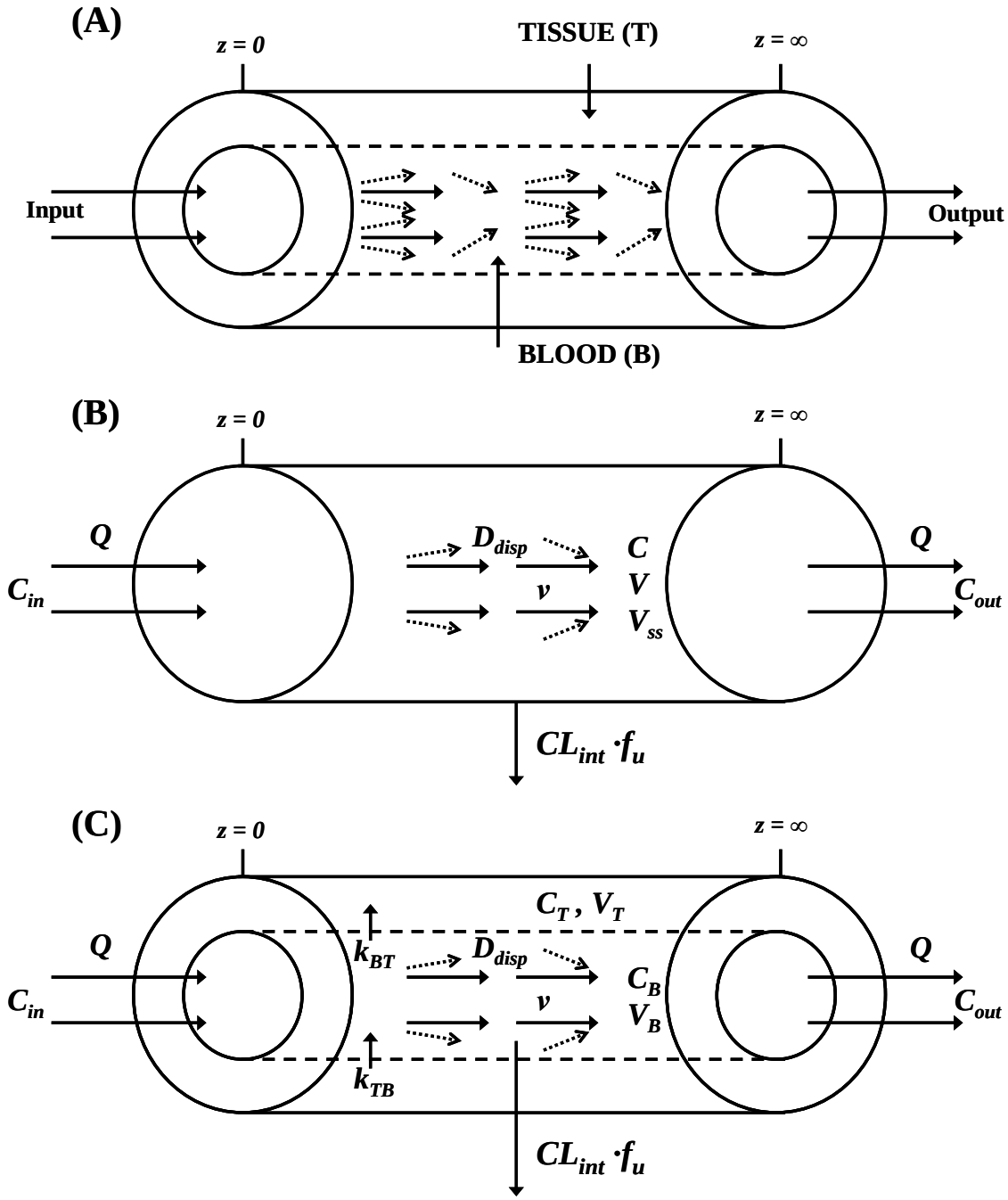

Figure 2.4. Schematic representation of organ structure (A) used for the derivation of the one-compartment dispersion model (B), and the two-compartment dispersion model (C). Symbols are defined in the text.

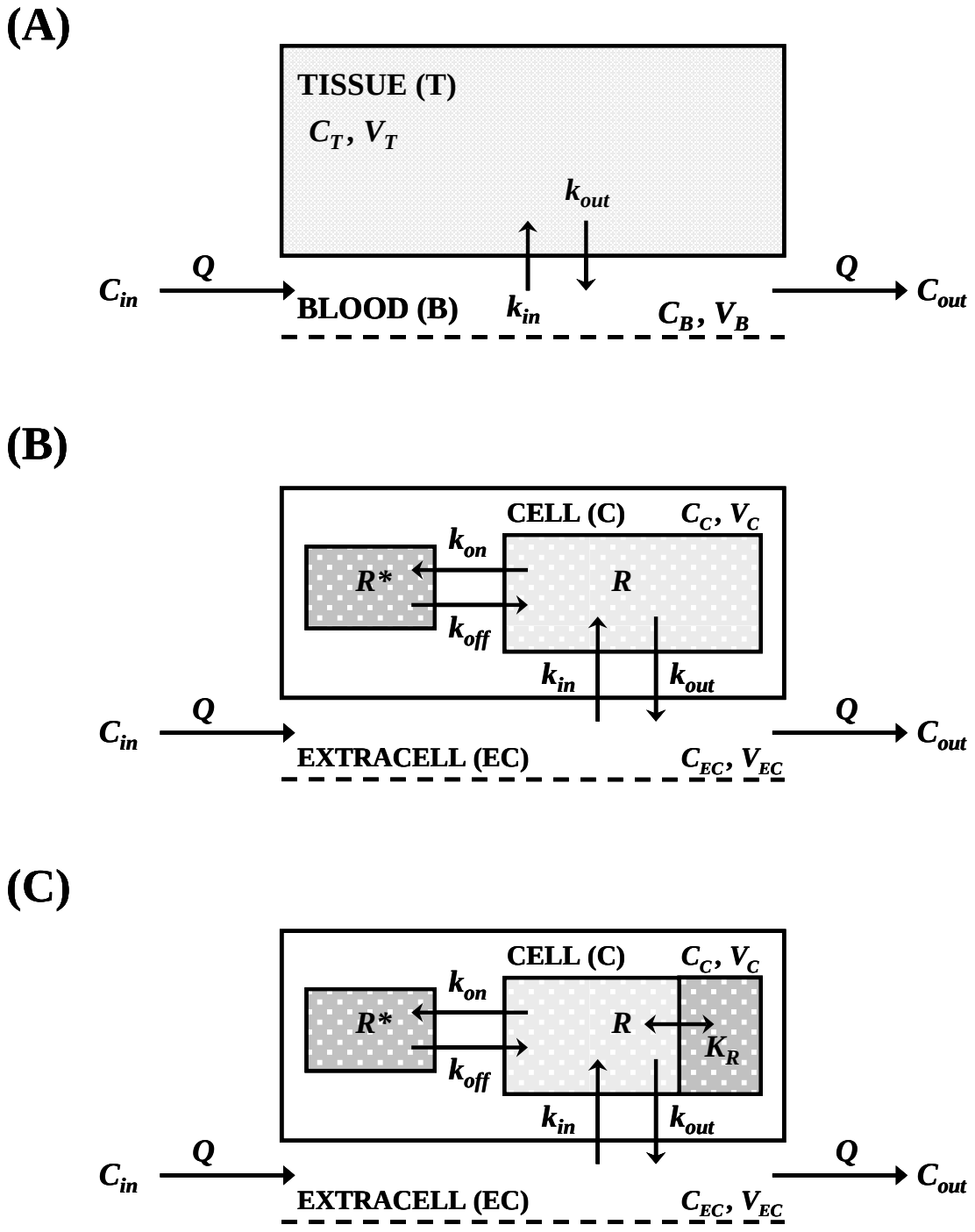

Figure 2.5. Schematic representation of the extended dispersion model showing dispersion-diffusion model (A), the dispersion-binding model (B), and the dispersion-binding model accounting for non-specific binding (C). Symbols are defined in the text.

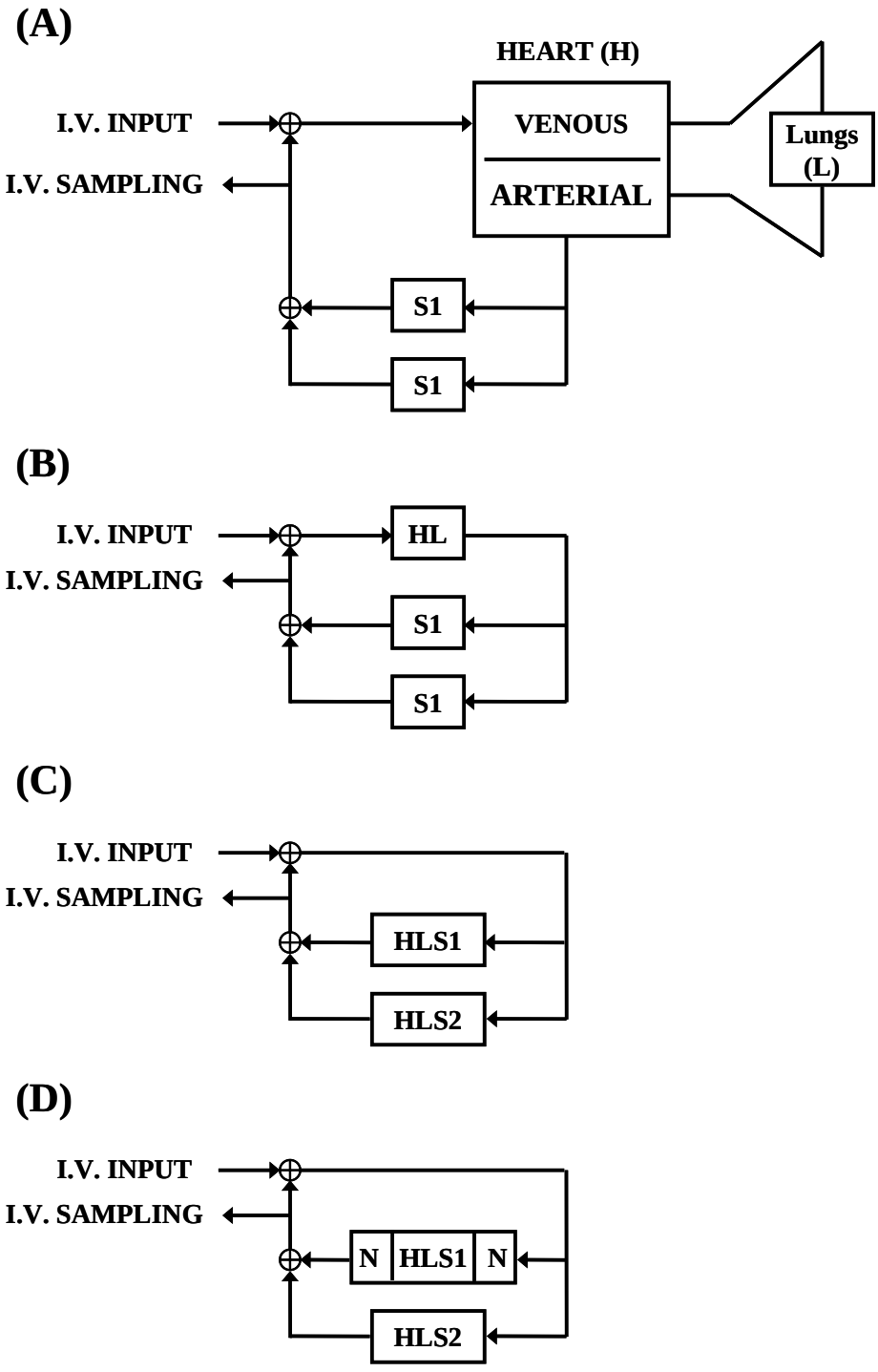

Figure 2.6. Schematic representation of a non-linear recirculation model development showing complex initial model (A), reduced model (B), final model in the linear operation range (C), final model in the non-linear operation range (D). Symbols are defined in the text.

CHAPTER 3. PHARMACOKINETIC ANALYSIS OF CONTINUOUS ERYTHROPOIETIN RECEPTOR ACTIVATOR (C.E.R.A.) IN ADULT SHEEP WITH NORMAL AND ABLATED BONE MARROW

3.1. Introduction

Continuous Erythropoietin Receptor Activator (C.E.R.A.) is a novel erythropoiesis stimulating agent (ESA) that differs from epoetin β by the integration of amide bonds between amino groups and methoxy polyethylene glycol-succinimidyl butanoic acid, resulting in a molecule weighing approximately 60 kD [162]. C.E.R.A. has unique binding characteristics to erythropoietin receptors (EPOR) that involve slow association, but slightly faster dissociation compared to EPO, resulting in reduced internalization and degradation [110, 162, 163] . Studies in animals, healthy humans and patients with chronic kidney disease show that C.E.R.A. has a slow systemic clearance and an extended elimination half-life [96, 117, 118]. The pharmacokinetic (PK) properties of C.E.R.A., together with its receptor binding properties are responsible for improved pharmacodynamics reflected in increased reticulocyte count and stable hemoglobin level *in vivo* [111, 164].

In contrast to Michaelis-Menten kinetics, which is the frequently used empirical model to address saturation kinetics, the target-mediated disposition (TMD) model can adequately describe several molecular processes such as drug-receptor binding, drug-receptor complex internalization, receptor production and degradation [103]. The TMD model can be simplified to its quasi-equilibrium (QE) form, if drug-receptor binding is assumed to be fast [165], or to its quasi-steady state (QSS) form, if both binding of drug

to its receptor and internalization of drug-receptor complex are assumed to be rapid [166].

Since its publication, the TMD model synthesized in the context of a two- or three-compartment model for drug disposition has been extensively used to study the PK of several drugs exhibiting receptor-mediated endocytosis, including: interferon-β [167], thrombopoietin [168], and recombinant human erythropoietin (EPO) [124]. However, physiologically-based PK (PBPK) models have become a powerful alternative to classical compartmental models because they provide a mechanistic approach that: 1) relates drug disposition to various physiological, anatomical and physico-chemical factors [62]; and 2) offers a strong basis for inter-species, tissue, route, and drug extrapolations [21].

A major obstacle to the wide spread implementation of the physiological approach is the high dimensionality of PBPK models that often times makes them far too complex to be fitted to plasma concentration-time data. Accordingly, lumping dynamically similar tissues to form dimensionally smaller but still PBPK models and focusing on target tissue(s) has been considered a successful strategy [27].

The classical PBPK models are based on organ/tissue models that assume perfusion or permeability rate limited structure (described using systems of differential equations) [21]. An improvement that keeps any restrictive assumptions to the minimum is characterization of organ or tissue regions by model-independent transit time distributions in the framework of linear systems principles (i.e., input-output convolution relationship). This approach has been termed “stochastic modeling” [96, 143].

The tracer interaction method (TIM) is a tracer/non-tracer based methodology for analyzing non-linear, saturation kinetics under dynamic conditions, by monitoring perturbations in the level of a tracer form of the drug following the introduction of the parent drug [125]. The TIM approach provides not only a sensitive and an accurate method to assess drug-receptor *in vivo* binding characteristics, but also a way to differentiate between receptor populations in distinct tissues [115, 123].

It has been hypothesized that elimination of C.E.R.A. in sheep is capacity-limited and greater non-linearity was observed for C.E.R.A. than for EPO [96]. The aim of this work is to get a greater insight into C.E.R.A.'s complex, non-linear disposition, and to get a better understanding of the interaction between C.E.R.A. and EPOR in BM and non-BM tissue. This is done by a minimal stochastic receptor-based, recirculation model used for analyzing data from TIM experiments in adult sheep before and after chemical ablation of EPOR in the bone marrow (BM). The use of a sheep model allows the comparison of C.E.R.A. TIM behavior with that reported for EPO [115].

3.2. Materials and methods

3.2.1. Animals

All animal care and experimental procedures were approved by the University of Iowa Institutional Animal Care and Use Committee and adhere to the 'Principles of Laboratory Animal Care' (NIH publication #85-23, revised in 1985). A total of sixteen healthy young adult sheep (weight mean±SD = 27±2.6 kg) were selected for the study. Four sheep were chosen for comparing the PK of labeled and unlabeled C.E.R.A.. Two sheep were used in TIM control studies. Ten sheep were used for the TIM experiments conducted under normal BM conditions, and after BM ablation (five animals for each

case). The animals were housed in an indoor, light- and temperature-controlled environment, with *ad lib* access to feed and water. Prior to study initiation, jugular venous catheters were aseptically placed under pentobarbital anesthesia. Intravenous ampicillin (1 g) was administered daily for 3 days following catheter placement. The long-term infusion of C.E.R.A. required in the TIM experiments were done with a portable infusion pump (Pegasus infusion pump, Instech/Solomon Laboratories Plymouth Meeting, PA, USA) mounted on a specially designed sheep jacket.

3.2.2. Ablation protocol

Busulfan was administered orally twice a day in a dose of 11 mg/kg/day for three consecutive days. Ampicillin (1 g b.i.d.) was administered daily for the first 3 days prior to the busulfan treatment, and again daily after the start of the treatment. Animals were clinically monitored for adverse effects of the chemotherapy such as weight loss, hair loss, blood in urine or stools, fever, unusual bleeding or bruising, and loss of appetite.

3.2.3. Study protocol

3.2.3.1. ^{125}I-Labeled vs. unlabeled C.E.R.A. PK study

Identical or near-identical disposition of the tracer and the non-tracer forms of a drug is a pre-requisite for TIM methodology. Accordingly, a 200 mU/kg intravenous (IV) bolus dose of ^{125}I- C.E.R.A. and a 109 U/kg IV bolus dose of unlabeled C.E.R.A. were simultaneously administered to three subjects, and plasma concentrations of both forms were followed for about 86 hours. The initial concentration normalized plasma profiles of unlabeled and ^{125}I-C.E.R.A. (Figure 3.4) were compared using nonparametric measures, namely, AUC [0-last] (calculated by linear trapezoidal rule), and concentrations at the

10^{th}, 25^{th}, 50^{th}, 75^{th}, and 90^{th} time percentile (calculated by linear interpolation). Wilcoxon signed rank test was used to test for significance.

3.2.3.2. TIM experiments

A detailed description of the theory and principles of the TIM was previously published [125] and a schematic representation of the TIM procedure is shown in Figure 3.1. In the current study, each animal underwent a single TIM PK experiment. A 50 mU/kg IV bolus dose of ^{125}I-C.E.R.A. was initially administered, then immediately followed by an IV infusion at 1.7 mU/h/kg of the tracer to the end of the experiment. An IV bolus injection (113 U/kg) of unlabeled C.E.R.A. was administered when the plasma ^{125}I-C.E.R.A. level approached steady state (i.e., at approximately 24 hours). An average of 53 blood samples (~0.5 mL per sample) were collected for plasma ^{125}I-C.E.R.A. from zero to 130 hours, while about 50 samples for plasma unlabeled C.E.R.A., were collected from 24 to 360 hours. To minimize hemoglobin and red cell loss due to frequent blood sampling, blood was centrifuged, the plasma removed, and the red cells re-infused.

3.2.3.3. TIM control experiments

The TIM experiment assumes that the drug disposition kinetics is time-invariant. To investigate the validity of this assumption in C.E.R.A. kinetics, a ‘half’ TIM experiment was conducted. The plasma level of ^{125}I-C.E.R.A. was followed over a period of 300 hours after a single IV bolus (66 mU/kg) and a constant rate infusion (2 mU/h/kg) administered to a normal BM and a BM ablated subjects. No unlabeled drug was given.

3.2.4. Assay

3.2.4.1. Radiolabeled C.E.R.A.

^{125}I-C.E.R.A. was prepared by iodination of 1 μg of C.E.R.A. with 1 mCi of ^{125}I-Na (Perkin Elmer, Billerica, MA, USA) using 8 μg chloramine-T. The ^{125}I-C.E.R.A. plasma concentrations and in infusion solutions were determined by non-specific protein precipitation followed by separation by centrifugation. Specifically, 1 mL duplicate aliquots of plasma sample or infusion solution were added to 12 x 75 glass test tubes, 1 mL 10% w/v trichloroacetic acid was added, then the precipitated proteins were pelleted by a 30 minute centrifugation, and the supernatant was decanted and the pellet was counted for radioactivity.

3.2.4.2. Unlabeled C.E.R.A.

C.E.R.A. was provided as 5.9 mg of protein/mL solution (Lot No. R78238600, Hoffmann-LaRoche Inc.), and was stored at -70˚ C. This stock was used to prepare working stocks (in 50 mM sodium phosphate with 0.02% sodium azide and 5% BSA, pH 7.4) at a concentration of 0.14 mg of protein/mL. Preparation and analysis of the unknown C.E.R.A. plasma, standard curve, non-specific binding, and zero standard samples were done using a double-antibody radioimmunoassay (RIA) procedure (lower limit of quantitation 1 mU EPO/mL) [169]. All plasma samples from the same animal were measured in the same assay to reduce variability.

The unknown C.E.R.A. concentrations were determined using the EPO standard curve between the EPO EC_{80} and EC_{20} as mU EPO equivalents/mL. The EPO standard curve was used instead of C.E.R.A. standard curve for convenience and because of our extensive experience with the EPO RIA [169]. The use of the EPO standard curve to

measure C.E.R.A. was validated by performing 1:2 dilutions of the C.E.R.A. stock solution until the response was between the EC_{80} and EC_{20} on the EPO standard curve. The dilution corrected responses were determined and had a C.V. of 8.3% across the linear range of the EPO standard curve, demonstrating a 1-to-1 relationship between the determined mU EPO equivalents/mL and the ng/mL of C.E.R.A. within this range. These validations resulted in a C.E.R.A. conversion constant of 71,300 mU/μg of protein (n=13). All unknown C.E.R.A. samples were measured in duplicate or triplicate and diluted between the EC_{80} and EC_{20} on the EPO standard curve, which corresponds to a linear C.E.R.A. range of 65.5-647 pg of protein/mL.

The RIA cannot distinguish between endogenously produced erythropoietin and exogenously administered C.E.R.A. in the same plasma sample. To minimize the contribution of endogenous EPO in the measured C.E.R.A. concentration, only C.E.R.A. plasma samples with concentrations greater than 300 mU EPO equivalents/mL were reported. Endogenous EPO contribution for all reported C.E.R.A. plasma samples should therefore be <10%, since baseline EPO concentrations in sheep typically range from 10-30 mU/mL [170, 171].

3.2.5. Pharmacokinetic model

A physiologically based PK model was used to analyze C.E.R.A. TIM tracer data. The proposed model consists of 3 tissues: heart–lung segment (HLS), non-target-mediated (NTM), and target-mediated (TM) disposition, which are interconnected by arteries and veins (Figure 3.2). The cardiac output is given by Q, and P_i is the fraction of blood flow to ith tissue for i=TM or NTM ($P_{TM} + P_{NTM} = 1$). Based on the assumption that drug disposition in the HLS and NTM tissues is linear, the output rates from both

tissues ($f^{i}_{out}(t)$, for *i* = HLS or NTM) were described by the following convolution equations:

$$f^{HLS}_{out}(t) = [\, D_{iv} \cdot \delta(t) + Inf(t) + f^{NTM}_{out}(t) + f^{TM}_{out}(t)] * UIR(t) \quad (3.1)$$

$$f^{NTM}_{out}(t) = P_{NTM} \cdot f^{HLS}_{out}(t) * UIR_{NTM}(t) \quad (3.2)$$

and:

$$UIR_i(t) = (1 - E_i) \cdot g_i(t) \quad , \; for\, i = HLS \; or \; NTM \quad (3.3)$$

where D_{iv} and $Inf(t)$ are IV bolus dose and constant rate infusion of the tracer, respectively. $\delta(t)$ denotes Dirac delta function, (*) denotes convolution, *UIR(t)* is the unit impulse response function, *E* is the extraction ratio and *g(t)* is a transit time density function. Under the assumption that HLS and NTM tissues are non-extracting and that the drug exhibits identical bi-exponential distribution in both tissues, Eqs. 3.1-3.3 reduce to:

$$f^{HLS}_{out}(t) = [\, D_{iv} \delta(t) + Inf(t) + f^{NTM}_{out}(t) + f^{TM}_{out}(t)] * g(t) \quad (3.4)$$

$$f^{NTM}_{out}(t) = P_{NTM} \cdot f^{HLS}_{out}(t) * g(t) \quad (3.5)$$

and:

$$g(t) = \lambda \cdot \alpha \cdot \exp(-\alpha \cdot t) + (1 - \lambda) \cdot \beta \cdot \exp(-\beta \cdot t) \quad , 0 \le \lambda \le 1 \quad (3.6)$$

where α and β are rate parameters and λ is a mixing parameter.

The convolution equations, 3.4–3.6, can be conveniently converted to a set of algebraic and first-order differential equations, which are simpler to manipulate numerically and computationally. Introducing the dummy variables y_1 and y_2 where:

$$y_1 = [\, D_{iv} \cdot \delta(t) + Inf(t) + f^{NTM}_{out}(t) + f^{TM}_{out}(t)] * \lambda \cdot \alpha \cdot \exp(-\alpha \cdot t) \quad (3.7)$$

$$y_2 = [\, D_{iv} \cdot \delta(t) + Inf(t) + f_{out}^{NTM}(t) + f_{out}^{TM}(t)] * (1-\lambda) \cdot \beta \cdot \exp(-\beta \cdot t) \tag{3.8}$$

and:

$$f_{out}^{HLS}(t) = y_1 + y_2 \tag{3.9}$$

similarly, introducing the dummy variables y_3 and y_4 where:

$$y_3 = P_{NTM} \cdot f_{out}^{HLS}(t) * \lambda \cdot \alpha \cdot \exp(-\alpha \cdot t) \tag{3.10}$$

$$y_4 = P_{NTM} \cdot f_{out}^{HLS}(t) * (1-\lambda) \cdot \beta \cdot \exp(-\beta \cdot t) \tag{3.11}$$

and:

$$f_{out}^{NTM}(t) = y_3 + y_4 \tag{3.12}$$

differentiating the convolution equations 3.7, 3.8, 3.10, and 3.11 with respect to time gives:

$$d\, y_1/dt = -\alpha\, y_1 + \lambda \cdot \alpha \cdot (Inf(t) + f_{out}^{NTM}(t) + f_{out}^{TM}(t)) \quad , \quad y_1(0) = D_{iv} \cdot \lambda \cdot \alpha \tag{3.13}$$

$$d\, y_2/dt = -\beta \cdot y_2 + (1-\lambda) \cdot \beta \cdot (Inf(t) + f_{out}^{NTM}(t) + f_{out}^{TM}(t)) \quad , \quad y_2(0) = D_{iv} \cdot (1-\lambda) \cdot \beta \tag{3.14}$$

$$d\, y_3/dt = -\alpha \cdot y_3 + P_{NTM} \cdot \lambda \cdot \alpha \cdot f_{out}^{HLS}(t) \quad , \quad y_3(0) = 0 \tag{3.15}$$

$$d\, y_4/dt = -\beta \cdot y_4 + P_{NTM} \cdot (1-\lambda) \cdot \beta \cdot f_{out}^{HLS}(t) \quad , \quad y_4(0) = 0 \tag{3.16}$$

Nonlinear drug disposition through TM tissues is considered by a receptor-based model (Figure 3.3) that follows the generalized target mediated drug disposition model [103]. Accordingly, the reversible interaction between drug tracer input concentration ($C_{in}^{TM}(t)$) and free EPOR in the extracellular space (*R*), occurs with a second-order rate constant (k_{on}), to form drug-EPOR complex (*R**), which dissociates at a first-order rate constant (k_{off}), is internalized into the intracellular space with a first-order rate constant

(k_{int}), and subsequently degraded by lysosomes. The EPOR is produced at a zero-order rate constant (k_{syn}) and degraded at a first-order rate constant (k_{deg}). The changes in *R* and *R** were described by:

$$dR/dt = k_{syn} + k_{off} \cdot R^* - k_{on} \cdot R \cdot C_{in}^{TM}(t) - k_{\deg} \cdot R \tag{3.17}$$

$$dR^*/dt = -(k_{off} + k_{\text{int}}) \cdot R^* + k_{on} \cdot R \cdot C_{in}^{TM}(t) \tag{3.18}$$

Based on the assumption that the TM tissues behave as a "well-stirred compartment" where distribution equilibrium is achieved rapidly between free drug concentration in the tissues and in the emerging venous blood such that the amount eliminated in the TM tissue in a time interval Δt is proportional to *R** while the amount entering the TM tissue over this interval is proportional to $C_{in}^{TM}(t)$, a receptor-dependent extraction function, $E_{TM}(t)$, was defined as:

$$E_{TM}(t) = \frac{R^*}{C_{in}^{TM}(t)} \quad , \quad 0 \le E_{TM}(t) \le 1 \tag{3.19}$$

where $C_{in}^{TM}(t)$ is given by:

$$C_{in}^{TM}(t) = \frac{P_{TM} \cdot f_{out}^{HLS}(t)}{P_{TM} \cdot Q} = \frac{f_{out}^{HLS}(t)}{Q} \tag{3.20}$$

and the output rate from the TM tissues is given by:

$$f_{out}^{TM}(t) = P_{TM} \cdot (1 - E_{TM}(t)) \cdot f_{out}^{HLS}(t) \tag{3.21}$$

At quasi-equilibrium conditions, it is assumed that binding and de-binding of the drug with receptor are much faster than the other processes of the system [165] resulting in:

$$\frac{R \cdot C_{in}^{TM}(t)}{R^*} = \frac{(R_{tot} - R^*) \cdot C_{in}^{TM}(t)}{R^*} = K_D \tag{3.22}$$

where R_{tot} is total receptor ($R_{tot} = R + R^*$), K_D is drug/EPOR equilibrium dissociation constant ($K_D = k_{off} / k_{on}$).

Rearranging Eq. 3.22 for R^*:

$$R^* = \frac{R_{tot} \cdot C_{in}^{TM}(t)}{K_D + C_{in}^{TM}(t)} \tag{3.23}$$

where the change in R_{tot} was obtained by adding Eqs. 3.17 and 3.18:

$$\frac{d\,R_{tot}}{dt} = k_{syn} - k_{deg} \cdot R_{tot} + (k_{deg} - k_{int}) \cdot R^* \quad , \quad R_{tot}(0) = R_0 \tag{3.24}$$

where R_0 is the initial EPOR concentration.

The initial receptor concentration (R_0) cannot be numerically estimated from drug plasma concentrations. To solve this problem, Eqs. 3.23 and 3.24 were normalized by R_0:

$$R^*/R_0 = \frac{R_{tot}/R_0 \cdot C_{in}^{TM}(t)}{K_D + C_{in}^{TM}(t)} \tag{3.25}$$

$$\frac{d\,R_{tot}}{dt} \Big/ R_0 = k_{syn}/R_0 - k_{deg} \cdot R_{tot}/R_0 + (k_{deg} - k_{int}) \cdot R^*/R_0 \quad , \quad R_{tot}(0)/R_0 = 1 \tag{3.26}$$

, and the receptor dependent extraction function, $E_{TM}(t)$, is considered to be proportional to R^*/R_0 rather than R^*. Accordingly Eq. 3.19 becomes:

$$E_{TM}(t) = \frac{R^*/R_0}{C_{in}^{TM}(t)} \quad , \quad 0 \le E_{TM}(t) \le 1 \tag{3.27}$$

Equation 3.25 was modified to account for the TIM procedure:

$$R^*/R_0 = \begin{cases} \dfrac{R_{tot}/R_0 \cdot C_{in}^{TM}(t)}{K_D + C_{in}^{TM}(t)} & for \quad 0 < t \le t_{cold} \\ \dfrac{R_{tot}/R_0 \cdot C_{in}^{TM}(t)}{K_D + C_{cold}(t)} & for \quad t > t_{cold} \end{cases} \tag{3.28}$$

where $C_{cold}(t)$ is plasma non-tracer concentrations and t_{cold} is time of injection of the non-tracer.

The total plasma concentration that is measured in venous blood ($C_{out}^{tot}(t)$) (Figure 3.2) was given by:

$$C_{out}^{tot}(t) = (f_{out}^{NTM}(t) + f_{out}^{TM}(t))/Q \tag{3.29}$$

The final model equations were 3.9, 3.12, 3.13-3.16, 3.20, and 3.26-3.29. The selection of the final model was based on comparing the Akaike information criterion (AIC) of several competing nested models. In a preliminary analysis, it became evident that the rapid binding was more favorable than the full TMD model. Sharing the transit time density function parameters between HLS and NTM tissues reduced the number of rate parameters, Alpha's and Beta's, and the mixing parameter, Lambda's, from six to three and resulted in lower AIC value. Another interesting finding in the search for the optimal model was that the data doesn't support the identification of extra-TM tissue elimination parameters. Thus, the extraction ratio of HLS and NTM tissues was set to zero.

To improve the estimation of the parameters, the sheep physiological parameters, Q and P_{TM}, were fixed to values drawn from literature [51], with Q = 7122.7 ml/h/kg, and P_{TM} was assumed to be equal to the fraction of blood flow to the bone marrow (0.0597).

3.2.6. Non-compartmental analysis

To assess the effect of bone marrow ablation on C.E.R.A. total plasma clearance (*CL*), initial volume of distribution (V_d), steady-state volume of distribution (V_{ss}), distribution half-life ($t_{1/2}(\alpha)$), elimination half-life ($t_{1/2}(\beta)$), and mean residence time (*MRT*), a non-compartmental analysis was performed by fitting a biexponential equation ($C_p(t) = C_1 \cdot \exp(-P_1 \cdot t) + C_2 \cdot \exp(-P_2 \cdot t) \quad , \; P_1 > P_2 > 0$) to unlabeled C.E.R.A. plasma concentrations.

3.2.7. Computational details

Pharmacokinetic modeling and non-compartmental analysis were conducted using WINFUNFIT, an interactive Microsoft Windows program evolved from the general non-linear regression program FUNFIT [172]. The numerical solution for the final model (Eqs. 3.9, 3.12, 3.13-3.16, 3.20, and 3.26-3.29) was fitted to tracer data for the pre- ($t < t_{cold}$) and post- ($t > t_{cold}$) unlabeled drug administration phases with the plasma non-tracer concentrations represented as a cross-validation cubic spline [173]. The best fit was accepted only if simulated $E_{TM}(t)$ (Eq. 3.27) values were ≤ 1 at all time points.

To summarize the uncertainty in the individual subject receptor-related parameter estimates, the mean percent standard error (MSE%) of the estimate was calculated for each parameter as:

$$\mathrm{MSE\%} = \frac{1}{\mathrm{n}} \times \sum_{\mathrm{i}=1}^{\mathrm{n}} \frac{\mathrm{SE_i}}{\left|\mathrm{P_i}\right|} 100/\mathrm{n} \tag{3.30}$$

where SE_i and P_i are the standard error of the parameter and the estimate of the parameter for the ith subject, respectively, and n is the number of subjects.

Statistical comparisons of mean values for the receptor-related (Table 3.1) and non-compartmental PK parameters (Table 3.2) between normal and ablated BM sheep populations were done using a one- or two-tailed Student's t-test with correction for non-equal variance, if needed. P-values of 0.05 and 0.01 were taken as the levels of significance for the type I null hypotheses error.

3.3. Results

3.3.1. Checking TIM assumptions

TIM experiment is based on the assumption that the tracer behaves in the same kinetic manner as the parent drug [125]. Figure 3.4 indicates that ^{125}I-C.E.R.A. can be considered a proper tracer by having very similar disposition curve to unlabeled C.E.R.A., when both forms are mixed together. This finding was confirmed by a non-significant difference ($p > 0.05$) in AUC [0-last] and concentrations at various time percentiles. Additionally, TIM experiment assumes that the drug disposition kinetics is time-invariant [125]. This assumption is not likely to be violated for the EPO TIM experiments due to their relatively short duration. However, for C.E.R.A., due to the much slower elimination kinetics requiring approximately 10 times longer TIM experiments, a violation of this assumption is a possibility and needs to be tested. This was done by performing a TIM experiment in which no parent drug was given. In that case, if it is assumed that the kinetics is time-invariant, then the tracer level should approach an asymptote in the continued constant rate IV infusion of the tracer. This was indeed observed for C.E.R.A. not only before but also after BM ablation (Figure 3.5).

3.3.2. Model adequacy

The average correlation coefficient between predicted (3.9, 3.12, 3.13-3.16, 3.20, and 3.26-3.29) and observed ^{125}I-C.E.R.A. plasma concentrations was 0.993 for both normal and ablated animal subjects. This finding indicates that the proposed PK model is well suited for capturing the behavior of the observed data. From Table 3.1, the receptor-related parameters were well estimated with mean percent standard error, MSE%, of less than 30% for all parameters, with most of them less than 15%. The relatively high MSE% for C.E.R.A.-EPOR complex internalization rate constant, k_{int}, is due to two subjects having a high relative standard error of 69 and 85%, respectively. Calculation of the MSE% for k_{int} without those subjects results in a MSE% of less than 17%. A relatively small amount of subject to subject variability was observed in all parameters with maximum coefficient of variation, CV%, less than 60% and a larger variability was found between ablated subjects compared to normal subjects (Table 3.1).

3.3.3. Effect of busulfan ablation on elimination kinetics

TIM data before ablation (Figure 3.6, upper panel) shows a significant perturbation in the ^{125}I-C.E.R.A. plasma level (square symbols) caused by the bolus injection of unlabeled C.E.R.A. (triangle symbols) at about 24 hours. The pronounced perturbation, which is a characteristic of non-linear elimination pathway [125], is persistent after busulfan treatment (Figure 3.6, lower panel). This pronounced phenomenon was consistently observed in all of the animals with ablated BM. This behavior of C.E.R.A. differs from what has been reported for EPO, whose elimination is completely linearized by BM ablation [115].

3.3.4. Effect of busulfan ablation on PK parameters

The estimated receptor-related micro-parameters obtained from the physiological modeling of the tracer component of the TIM are displayed in Table 3.1. The macro-parameters estimated from the non-compartmental analysis performed on the non-tracer component of the TIM are depicted in Table 3.2. The ablation resulted in a highly significant reduction ($p < 0.01$) in the EPOR normalized production rate constant, k_{syn} / R_0, EPOR degradation rate constant, k_{deg}, and C.E.R.A.-EPOR complex internalization rate constant, k_{int}, and C.E.R.A. total clearance, *CL*, to about 44, 28, 0.4, and 60 percentage of the normal subjects mean values, respectively. A pronounced increase ($p < 0.01$) in C.E.R.A. elimination half-life, $t_{1/2(\beta)}$, and mean residence time, *MRT*, by approximately 2.4-folds, was detected. No significant change ($p > 0.05$) was observed in C.E.R.A./EPOR equilibrium dissociation constant, K_D, C.E.R.A. initial volume of distribution, V_d, steady-state volume of distribution, V_{ss}, or distribution half-life, $t_{1/2(\alpha)}$.

3.4. Discussion

3.4.1. Role of EPOR in C.E.R.A.'s elimination

The main assumption of our model is that C.E.R.A. is degraded only by cells expressing EPOR through binding to those receptors, followed by internalization via endocytosis, and subsequent degradation in the lysosomes. Although no specific sites and mechanisms of C.E.R.A. metabolism have been identified yet, several lines of evidence support our key assumption. *In vitro* cellular trafficking of EPO and NESP, a hyperglycosylated EPO analogue, showed that only cells expressing surface EPOR were able to degrade both compounds [113]. Under the assumption that hyperglycosylation

and PEGylation exert similar effects on EPO molecule, the role of EPOR in C.E.R.A. elimination must be considered.

C.E.R.A. PK parameters were similar in patients with severe hepatic impairment and healthy subjects after single IV bolus dose [119]. The same observation can be made when comparing the bioavailability normalized clearance (0.66 vs. 0.90 mL/h/kg), and terminal half-life (160 vs. 139 h) of C.E.R.A. in healthy volunteers and patients with chronic kidney diseases following subcutaneous (SC) administration of a single dose [117, 118]. In accordance with EPO whose clearance in sheep is not affected by hepatectomy and nephrectomy [116], C.E.R.A. *in vivo* elimination seems to be independent of liver and kidneys. C.E.R.A. polyethylene glycol (PEG) chains stabilize the core glycoprotein against the action of proteases, reducing the probability of biotransformation taking place in blood.

3.4.2. Busulfan ablation and EPOR distribution

It is proposed, but is still a controversial issue [174] that EPOR is expressed not only on erythroid progenitor cells found mainly in the BM but also on non-hematopoietic cells present outside the BM, e.g., capillary endothelial cells, myocardiocytes, liver parenchyma cells, kidney interstitial cells, retinal cells, myoblasts, neural cells, glia and astrocytes [175-178]. Busulfan is a potent and selective inhibitor of myeloid hematopoietic stem cells [179], the cells that give rise to the erythroid progenitor cells. Thus, it does not seem very likely that non-hematopoietic EPOR expressing cells outside the BM will be much affected by busulfan treatment. From our previous work with chemical ablation by busulfan [114, 115, 123], no colony-forming unit erythroids, and only extremely few burst-forming unit erythroids colonies were found after 6 days of

incubation of BM aspirates drawn at day 8 and day 13 following busulfan treatment of sheep. Thus, the ablation protocol effectively eradicates BM progenitor cells within 8 days post-treatment without possibility of future cellular regeneration. In the current study, all C.E.R.A. PKs in BM ablated sheep were performed 8 days after the ablation procedure ruling out the probability of interaction with regenerated BM progenitors.

3.4.3. Effect of busulfan ablation on EPO and C.E.R.A. behavior

Previous TIM studies showed that EPO elimination kinetics changed from non-linear to purely linear after ablation of the BM, suggesting that EPOR expressed outside BM may contribute to non-saturable clearance of EPO [115]. Contrary to EPO, persistence of a significant perturbation in ^{125}I-C.E.R.A. plasma level after introducing a high bolus dose of non-tracer in BM ablated sheep indicates a different molecular elimination mechanism for C.E.R.A. outside BM. The suggested mechanism is believed to be mediated through saturable interaction of C.E.R.A. with “classical EPOR”, and/or other receptor populations located outside BM. The reason for this qualitative difference in the behavior of EPO and C.E.R.A., as well as the extra-BM location(s) responsible for the persistent C.E.R.A. non-linearity in ablated sheep is not clear.

3.4.4. Differentiation of C.E.R.A.’s interaction characteristics with hematopoietic and non-hematopoietic EPOR populations

Combining the receptor-based modeling with TIM experiments conducted before and after BM ablation permits the differentiation of erythropoietic and non-erythropoietic receptor populations’ characteristics. This differentiation assumes that the receptor-related PK parameters of non-ablated animals are representative of EPOR inside and outside the BM, while those of ablated animals are representative of EPOR only outside

the BM. From Table 3.1, the ratio of EPOR synthesis rate constant, k_{syn} to initial total EPOR concentration, R_0 was significantly reduced by busulfan treatment. This change is obtained as a result of a significant reduction in k_{syn} and/or a significant increase in R_0. Assuming that R_0 was not affected by the ablation, the change in k_{syn} / R_0 can be attributed to a difference in k_{syn} but not in R_0, although both parameters appear to be important. Thus, in comparing erythropoietic and non-erythropoietic receptors; the latter seem to be formed at a slower rate. The same seems to be the case for both receptor populations' degradation rates, as suggested by the significant reduction in k_{deg} after BM ablation (Table 3.1).

The internalization and lysosomal degradation processes in our model were presented by k_{int}. Study of the fate of ^{125}I-EPO and EPOR in human EPOR expressing UT-7 cells, demonstrated that EPO was completely degraded after endocytosis, while few of EPORs were recycled back to the surface of the cells [109, 180]. In a different study in cultured Ba/F3 and UT-7/EPO cells, 60% of internalized EPO or NESP was re-secreted intact. In spite of this, however, the absence of differences in the proportions of EPO and NESP subject to degradation or recycling, as well as, the identical internalization rate of both compounds ruled out the importance of the fate of the ESAs after binding with surface EPOR in influencing their half-lives [113]. In the current model, fractions of recycled C.E.R.A. or EPOR were not considered due to our desire to keep the model simple. The interesting finding that C.E.R.A.-EPOR complex internalization rate constant, but not the dissociation constant, was significantly reduced by busulfan treatment (Table 3.1) suggests that despite erythropoietic and non-erythropoietic

populations have the same affinity to C.E.R.A. molecules, the former contribute more effectively to C.E.R.A. *in vivo* elimination.

3.4.5. Effect of busulfan ablation on C.E.R.A.'s macro-parameters

Our finding that some of C.E.R.A. PK parameters determined by non-compartmental analysis were significantly affected by busulfan-induced BM ablation (Table 3.2) provides a strong evidence for the importance of BM in C.E.R.A. disposition. Substantial changes in C.E.R.A. total plasma clearance, *CL*, elimination half-life, $t_{1/2}(\beta)$, and mean residence time, *MRT*, but not in initial volume of distribution, V_d, steady-state volume of distribution, V_{ss}, or distribution half-life, $t_{1/2}(\alpha)$, indicate that busulfan treatment affects the elimination phase (β phase) of C.E.R.A., and is consistent with the finding of the physiological model that BM plays a major role in C.E.R.A. elimination. Similar changes in EPO *CL*, $t_{1/2}(\beta)$, *MRT*, V_d, and $t_{1/2}(\alpha)$ were previously reported from PK studies performed in pre- and post-BM ablated sheep [114], suggesting that ESAs have a common elimination pathway that depends on hematopoietic EPOR.

The substantial reduction in C.E.R.A. internalization rate constant, k_{int}, after busulfan treatment can explain the significant decrease in *CL*, as well as the significant increase in $t_{1/2}(\beta)$, and *MRT*. However, the C.E.R.A. elimination after the ablation of the BM could be mediated by EPOR located outside the BM, or other EPOR independent elimination pathway(s). However, questions regarding location and nature of such pathway(s) require additional investigations.

3.5. Conclusion

A receptor-based recirculation model was successfully developed. Similar to the classical receptor based compartmental model [103, 165], the developed model accounts

for drug-receptor binding, receptor turnover, and drug/receptor complex endocytosis and lysosomal degradation. However, the developed model differs from the classical approach in retaining the key features of mammalian anatomy, namely, the heterogeneity of the tissue building blocks and the connection *via* the vascular network. Additionally, the developed model keeps restrictive assumptions to the minimum through characterization of the tissue blocks by model-independent transit time distributions in the framework of linear systems principles (i.e., input-output convolution relationship).

The developed model, together with the TIM, was able to quantitatively assess the interaction of C.E.R.A. with hematopoietic and non-hematopoietic EPOR population in adult sheep. As predicted by the model, the hematopoietic EPOR has higher production and degradation rates, similar affinity to C.E.R.A., and it is more involved in C.E.R.A's *in vivo* elimination, compared to the non-hematopoietic population. In agreement with the physiologic model, the non-compartmental analysis provided clear evidence that BM plays a major role in the *in vivo* elimination of C.E.R.A.

The TIM detected a saturable interaction between C.E.R.A. and non-hematopoietic EPOR. The saturable nature of the non-erythropoietic, non-BM pathway(s) for C.E.R.A in contrast to EPO predicts two fundamental differences : 1. An increasing fraction of C.E.R.A is utilized for erythropoiesis for increasing concentrations, and 2. The clearance of C.E.R.A becomes more limited for increasing concentrations. Taken together these differences favor a more efficacious and prolonged action for C.E.R.A.

Table 3.1. Receptor-related parameter estimates obtained from the tracer component of the C.E.R.A. TIM study in normal and BM ablated sheep using the physiological model.

Parameter (units)	Definition	Normal (n = 5)	Ablated (n = 5)	*p*-value	MSE% (n = 10)
		Mean (CV%)	Mean (CV%)		
k_{syn} / R_0 (1/h)	Initial EPOR normalized synthesis rate constant	164.3 (31.3)	71.5 (48.1)	< 0.01	8.7
k_{deg} (1/h)	EPOR degradation rate constant	42.5 (32.4)	11.7 (57.9)	< 0.01	8.7
K_D (pmol)	C.E.R.A./EPOR equilibrium dissociation constant	88.4 (18.3)	62.1 (44.8)	> 0.05	12.3
k_{int} (1/h)	C.E.R.A./EPOR internalization rate constant	2.41 (17.7)	0.009 (44.9)	< 0.01	29
CV%, Coefficient of Variation. MSE%, Mean Percent Standard Error.					

Table 3.2. Parameter estimates obtained from the non-tracer component of the C.E.R.A. TIM study in normal and BM ablated sheep using non-compartmental analysis.

Parameter (units)	Definition	Normal (n = 5)	Ablated (n = 5)	*p*-value
		Mean (CV%)	Mean (CV%)	
CL (mL/h/kg)	Total plasma clearance	0.74 (20.9)	0.44 (15.5)	< 0.01
V_d (mL/kg)	Initial volume of distribution	19.2 (27.2)	24.6 (20.2)	> 0.05
V_{ss} (mL/kg)	Steady-state distribution volume	42.0 (29.2)	59.3 (20.0)	> 0.05
MRT (h)	Mean residence time	56.6 (13.7)	135.9 (12.7)	< 0.01
$t_{1/2}(\alpha)$ (h)	Distribution half-life	0.65 (0.49)	0.66 (0.53)	> 0.05
$t_{1/2}(\beta)$ (h)	Elimination half-life	40.0 (13.5)	95.1 (12.6)	< 0.01
CV%, Coefficient of Variation.				

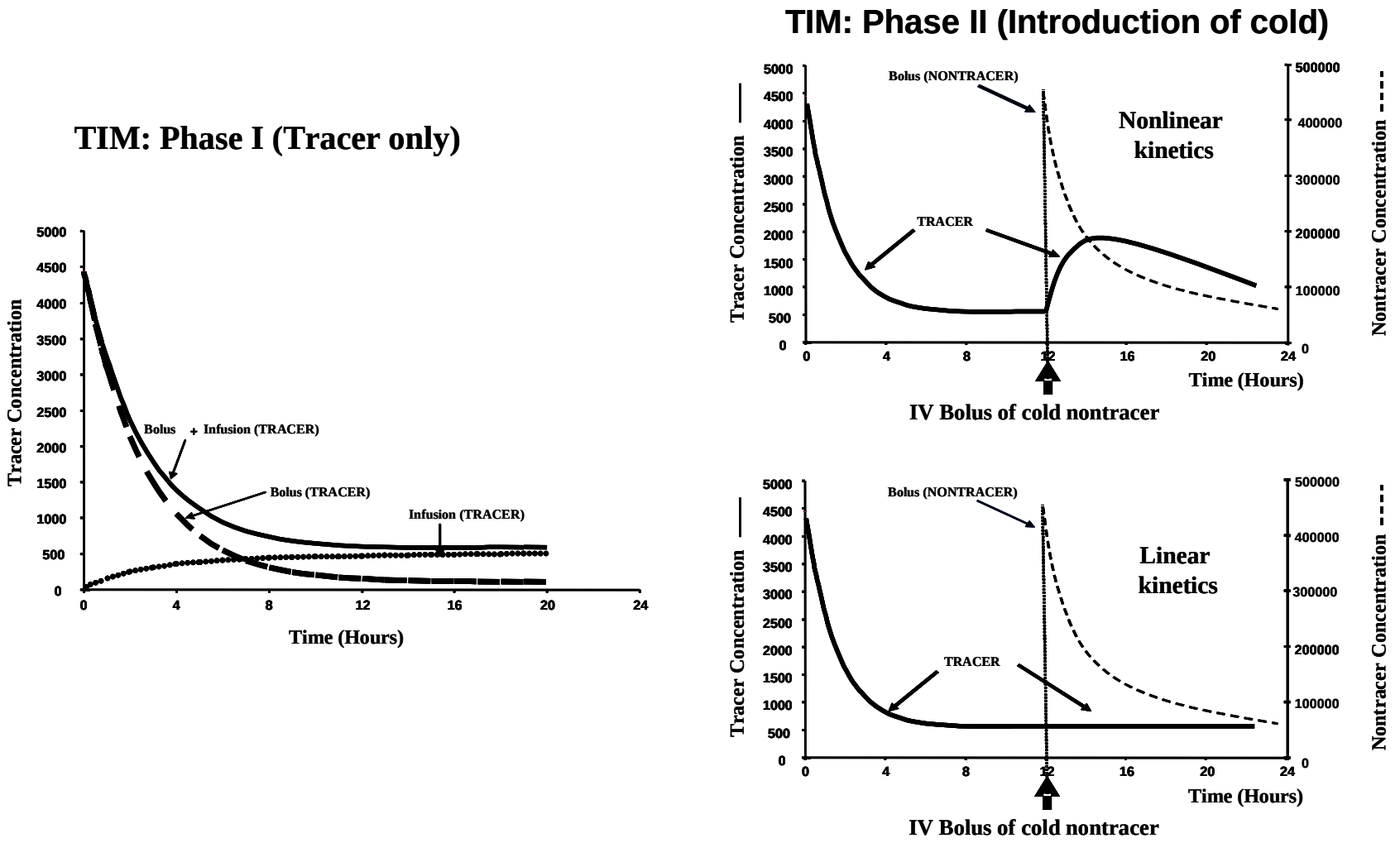

Figure 3.1. Scheme of the tracer interaction method (TIM)

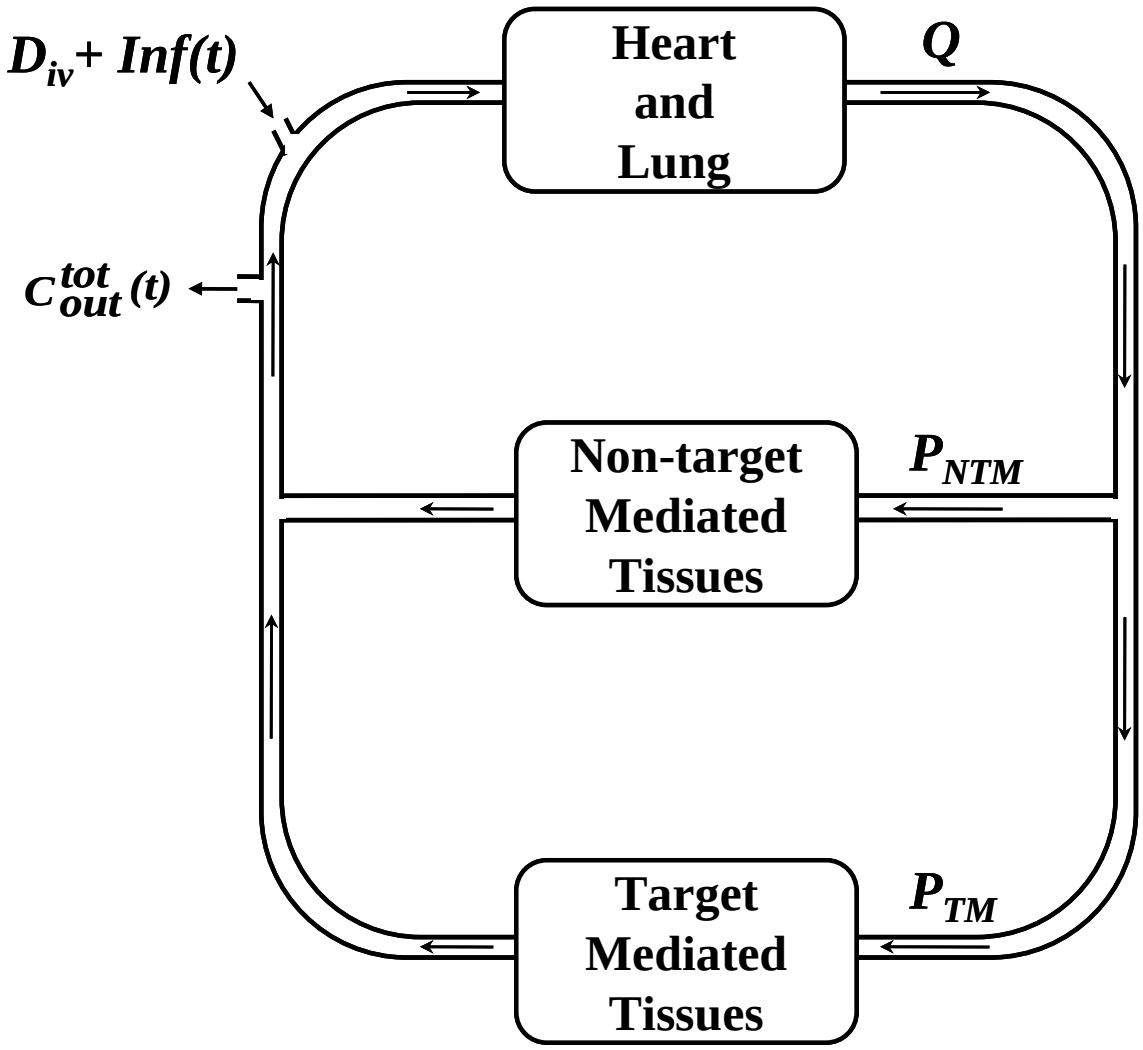

Figure 3.2. Scheme of the developed physiologic model. Symbols are defined in the text.

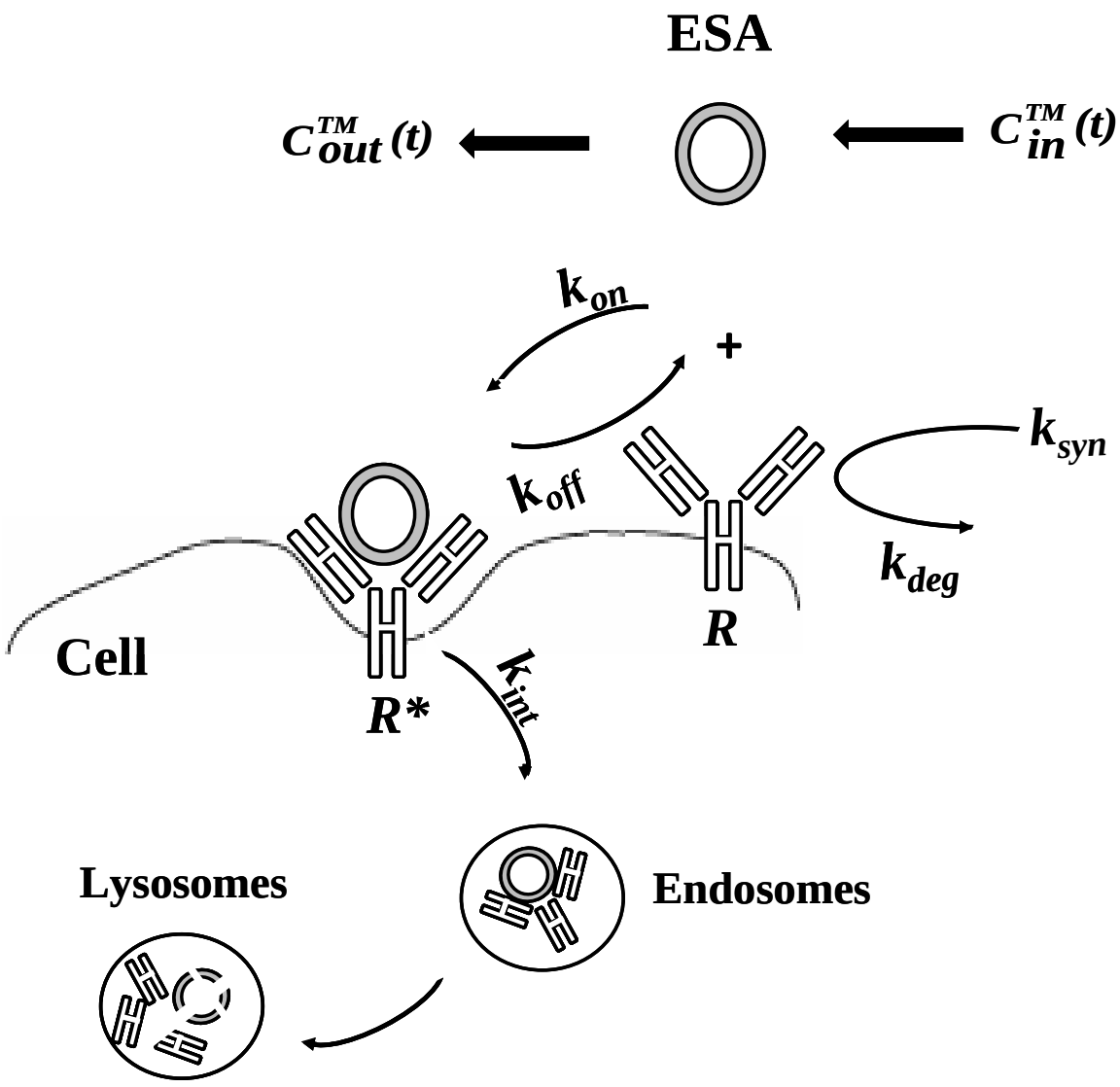

Figure 3.3. Scheme of the receptor-based model in target mediated disposition tissues. Symbols are defined in the text.

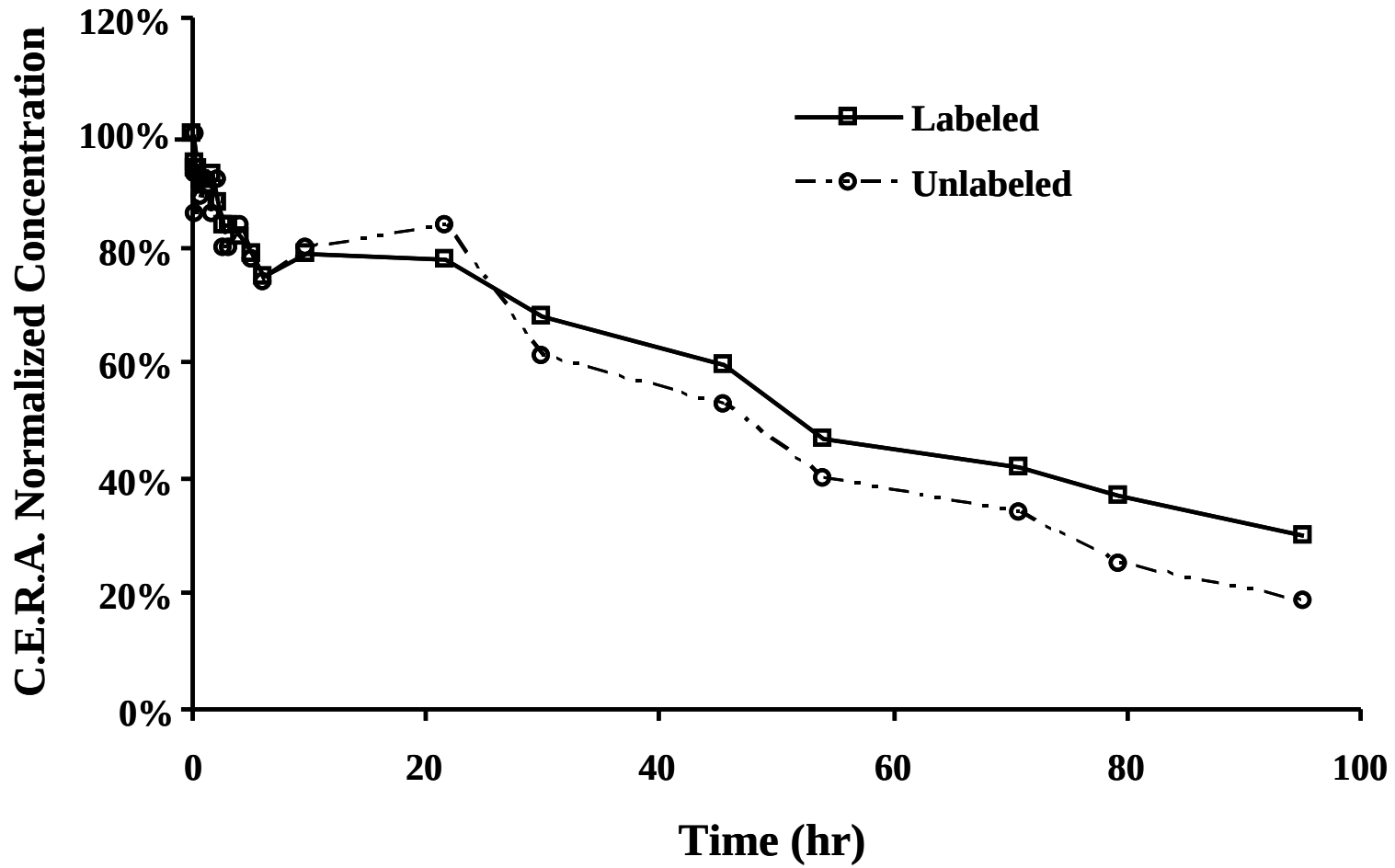

Figure 3.4. C.E.R.A. concentration-time profiles normalized to the initial measured concentration following simultaneous bolus administration of ^{125}I-labeled and unlabeled C.E.R.A.

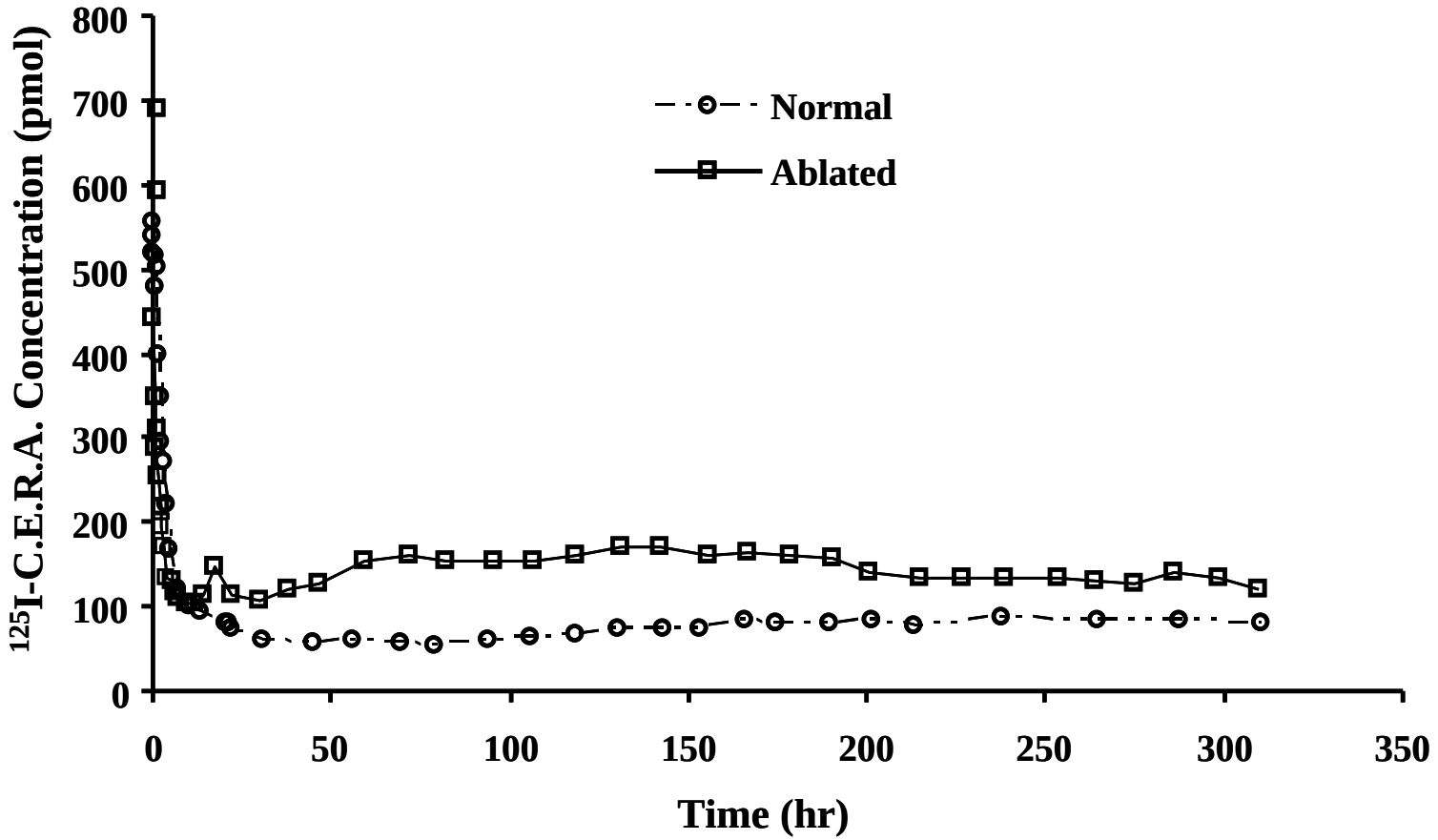

Figure 3.5. TIM concentration-time profiles for control animals (unlabeled bolus dose not administered) in both normal and BM ablated animals.

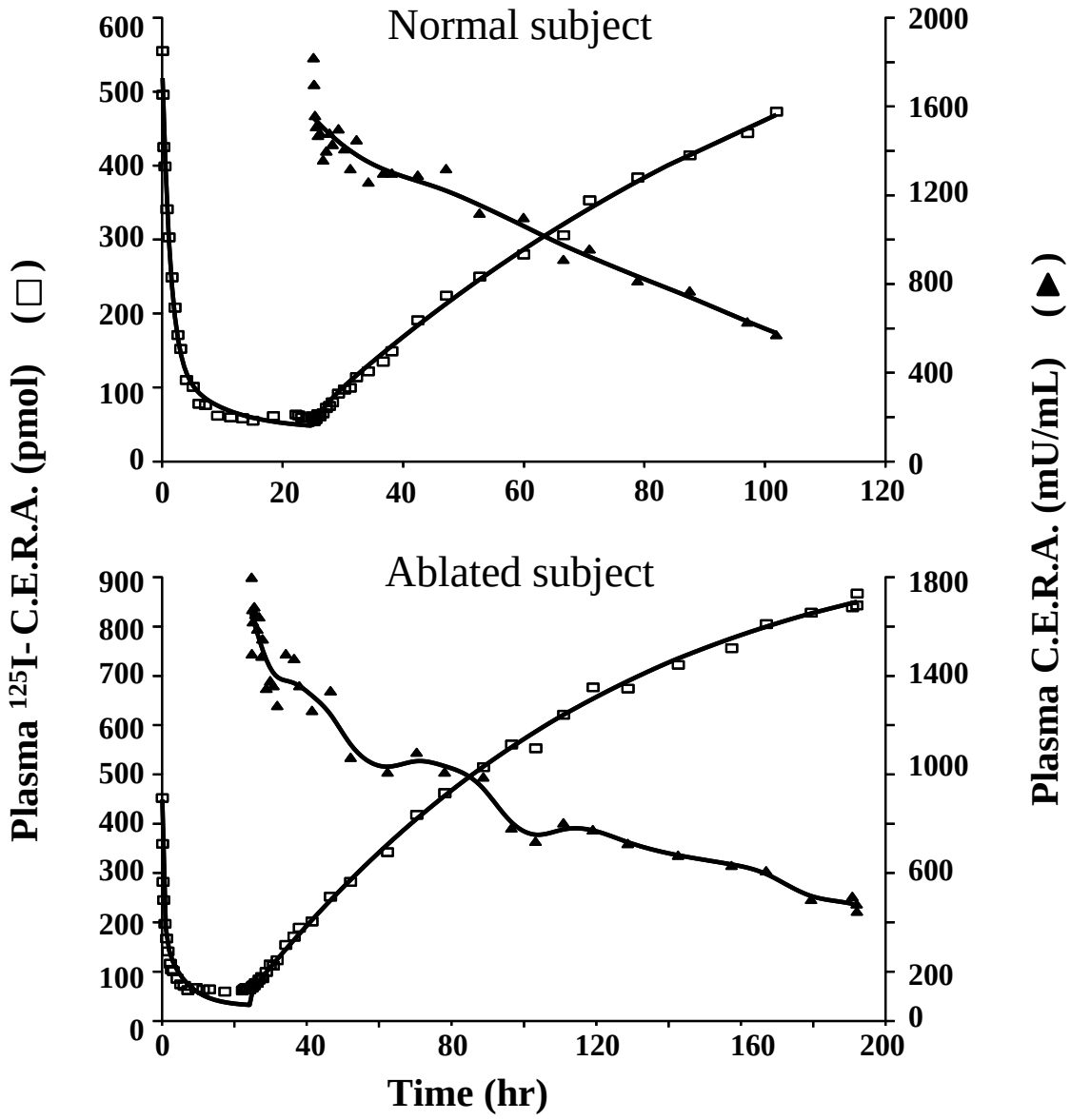

Figure 3.6. Representative fits of the receptor-based recirculation model to the ^{125}I-C.E.R.A. tracer data (squares) in adult sheep with normal and ablated BM (top and bottom panels). The non-tracer C.E.R.A. data (triangles) are fitted to a general cross validation cubic spline function.

CHAPTER 4. DIFFERENTIAL PHARMACOKINETIC ANALYSIS OF *IN VIVO* ERYTHROPOIETIN RECEPTOR INTERACTION WITH RECOMBINANT HUMAN ERYTHROPOIETIN (EPO) AND CONTINUOUS ERYTHROPOIETIN RECEPTOR ACTIVATOR (C.E.R.A.) IN ADULT SHEEP

4.1. Introduction

Erythropoietin (EPO) is a 34-kD glycoprotein hormone that regulates erythropoiesis. It binds to cell surface receptors (EPOR) on bone marrow erythroid progenitor cells (burst-forming unit-erythroids and colony-forming unit-erythroids), promoting their proliferation and differentiation into mature red blood cells (RBC) and protecting them from apoptosis [108, 181]. Binding of EPO to the cell surface induces dimerization of two EPOR molecules, which, in turn, initiates the Janus kinase intracellular signal transduction required for erythropoiesis [182]. Simultaneously, activation of EPOR by EPO binding promotes degradation of the formed complex *via* internalization followed by targeting to lysosomes [109]. On a macroscopic level, receptor-mediated elimination is responsible for the nonlinear clearance of EPO that is observed in various animal species [121, 183-185], including humans [122].

Continuous Erythropoietin Receptor Activator (C.E.R.A.) is a novel erythropoiesis stimulating agent (ESA). Unlike EPO, C.E.R.A. contains methoxy polyethylene glycol chains linked to amino groups *via* amide bonds, resulting in a molecule weighing approximately 60 kD [162]. Studies in humans have shown that C.E.R.A. has a long half-life (approximately 130 hours) [117] and is able to correct anemia and maintain a stable hemoglobin level for extended intervals. These features

allow the direct conversion of patients with chronic kidney disease from shorter frequencies (three times a week to one time every second week) EPO treatment to once a month C.E.R.A. administration [164, 186].

Preclinical studies in animal models demonstrated that C.E.R.A. has slower systemic clearance, longer elimination half-life, and higher *in vivo* erythropoietic activity than EPO [96, 111]. The differences in pharmacokinetic (PK) and pharmacodynamic (PD) properties of EPO and C.E.R.A. have been hypothesized to be attributed to a unique interaction between C.E.R.A. and EPOR, which involves a slower association, but a slightly faster dissociation, than those observed between EPOR and EPO. However, this hypothesis was based solely on *in vitro* binding studies that reported 50 to 100-fold lower affinity of C.E.R.A. for EPOR binding sites [110].

In order to elucidate the mechanism behind the significantly slower elimination and prolonged activity of C.E.R.A. *in vivo*, we studied the interactions between EPOR and both EPO and C.E.R.A. in adult sheep using a sensitive PK methodology, the tracer interaction method (TIM) [125], and a receptor-based physiological recirculation model. The model incorporates parameters for drug-receptor binding, receptor turnover, and drug-receptor complex endocytosis. The modeling is done within a physiological modeling framework that considers heterogeneous tissues connected through a recirculatory vascular network.

4.2. Materials and methods

4.2.1. Animals

All animal care and experimental procedures were approved by the University of Iowa Institutional Animal Care and Use Committee and adhere to the ‘Principles of

Laboratory Animal Care' (NIH publication #85-23, revised in 1985). Seven healthy young adult sheep, 2-4 months old, 24.9±3.5 kg (mean±SD), were selected for the EPO experiments, and five sheep, 2-4 months old, 28.4±2.44 kg, were used for the C.E.R.A. experiments. The animals were housed in an indoor, light- and temperature-controlled environment, with *ad lib* access to feed and water. Prior to study initiation, jugular venous catheters were aseptically placed under pentobarbital anesthesia. Intravenous ampicillin (1 g) was administered daily for 3 days following catheter placement. The long-term infusion of C.E.R.A. required in the TIM experiments were done with a portable infusion pump (Pegasus infusion pump, Instech/Solomon Laboratories Plymouth Meeting, PA, USA) mounted on a specially designed sheep jacket.

4.2.2. Study protocol

A detailed description of the theory and principles of the TIM was previously published [125]. In the current study, each animal underwent a single TIM PK experiment. A single IV bolus dose of ^{125}I- labeled drug (465 mU/kg for EPO and 50 mU/kg for C.E.R.A.) was initially administered, then immediately followed by a constant rate infusion of the tracer (117 mU/h/kg for EPO and 1.6 mU/h/kg for C.E.R.A.). An IV bolus injection of the non-tracer (94.8 U/kg for EPO and 104 U/kg for C.E.R.A.) was administered when the plasma level of the tracer approached steady state (at approximately 4 hours for EPO and 20 hours for C.E.R.A.). Blood samples (0.5 mL per sample) were collected subsequent to the tracer and the non-tracer administrations for determination of plasma EPO and plasma C.E.R.A. levels. For the tracer, about 38 samples were collected for EPO from 0 to 14 hours, while about 50 samples were collected for C.E.R.A. from 0 to 85 hours. For the non-tracer, 24 samples were collected

for EPO from 4 to 14 hours, while 30 samples were collected for C.E.R.A. from 20 to 85 hours. The longer sampling period for C.E.R.A. was required due to the slower elimination of C.E.R.A.. To minimize hemoglobin and red cell loss due to frequent blood sampling, blood was centrifuged, the plasma removed, and the red cells re-infused.

4.2.3. Assay

4.2.3.1. Radiolabeled drug

Radiolabeled EPO (^{125}I-EPO) and radiolabeled C.E.R.A. (^{125}I-C.E.R.A.) were prepared by iodination of 1 μg of the drug with 1 mCi of ^{125}INa (Perkin Elmer, Billerica, MA, USA) using 8 μg chloramine-T (Sigma-Aldrich, St. Louis, MO, USA) in a 10 second reaction that is terminated with 24 μg sodium metabisulfite (Sigma-Aldrich, St. Louis, MO, USA). This reaction mixture is desalted on a Sephadex 25 column (PD10, GE Healthcare Biosciences Corp., Piscataway, NJ, USA) and stored at 4° C before final purification on a size separation column (Sephadex g100, GE Healthcare Biosciences Corp.). The radiolabeled drug was measured in plasma samples or infusion solution by non-specific protein precipitation followed by separation by centrifugation. Specifically 1 mL duplicate aliquots of plasma sample or infusion solution are added to 12 x 75 glass test tubes, 1 mL 10% w/v trichloroacetic acid (TCA) is added, the precipitated proteins are pelleted by a 30 minute centrifugation, the supernatant is decanted and the pellet is counted for radioactivity.

4.2.3.2. Unlabeled drug

Plasma EPO concentrations were measured in triplicate using a double-antibody radioimmunoassay (RIA) procedure (lower limit of quantitation 1 mU/mL) [169]. All samples from the same animal were measured in the same assay to reduce variability.

C.E.R.A. was provided as 5.9 mg of protein/mL solution (Lot No. R78238600, Hoffmann-LaRoche Inc.), and was stored at -70° C. This stock was used to prepare working stocks (in 50 mM sodium phosphate with 0.02 % sodium azide and 5% BSA, pH 7.4) at a concentration of 0.14 mg of protein/mL. Preparation and analysis of the unknown C.E.R.A. plasma, standard curve, non-specific binding, and zero standard samples was identical to the unlabeled EPO determination. The unknown C.E.R.A. concentrations were determined using the EPO standard curve between the EPO EC_{80} and EC_{20} as mU EPO equivalents/mL. The EPO standard curve was used instead of C.E.R.A. standard curve for convenience and our extensive experience with the EPO RIA. The use of the EPO standard curve to measure C.E.R.A. was validated by performing 1:2 dilutions of the C.E.R.A. stock solution until the response was between the EC_{80} and EC_{20} on the EPO standard curve. The dilution corrected responses were determined and had a C.V. of 8.3% across the linear range of the EPO standard curve, demonstrating a 1-to-1 relationship between the determined mU EPO equivalents/mL and the ng/mL of C.E.R.A. within this range. These validations resulted in a C.E.R.A. conversion constant of 71,300 mU/μg of protein (n=13). All unknown C.E.R.A. samples were measured in duplicate or triplicate and diluted between the EC_{80} and EC_{20} on the EPO standard curve, which corresponds to a linear C.E.R.A. range of 65.5-647 pg of protein/mL.

The RIA cannot distinguish between endogenously produced erythropoietin and exogenously administered EPO or C.E.R.A. in the same plasma sample. To minimize the contribution of endogenous EPO in the measured drug concentration, only plasma samples with concentrations greater than 300 mU EPO equivalents/mL were reported. Endogenous EPO contribution for all reported EPO and C.E.R.A. plasma samples should

therefore be <10%, since baseline EPO concentrations in sheep typically range from 10-30 mU/mL [170, 171].

4.2.4. Pharmacokinetic analysis

The previously introduced receptor-based recirculation PK model in Chapter 3, section 3.2.5 was adopted to analyze the kinetics of EPO and C.E.R.A. using tracer data and the TIM methodology [125]. Briefly, the model consists of three tissues, heart-lung segment (HLS), non-target mediated disposition (NTM) and target mediated disposition (TM), interconnected by arteries and veins (Figure 3.2). The cardiac output is given by Q, and P_i is the fraction of blood flow to i^{th} tissue for i=TM or NTM ($P_{TM} + P_{NTM} = 1$). Drug disposition in the HLS and NTM tissues was assumed to be linear. Therefore, the output rates from both tissues ($f^{i}_{out}(t)$, for i = HLS or NTM) are described by the following convolution equations (* denotes convolution) that relate the input and input rates for a given tissue to a unit impulse response function ($UIR(t)$):

$$f^{HLS}_{out}(t) = [D_{iv} \cdot \delta(t) + Inf(t) + f^{NTM}_{out}(t) + f^{TM}_{out}(t)] * UIR(t) \quad (4.1)$$

$$f^{NTM}_{out}(t) = P_{NTM} \cdot f^{HLS}_{out}(t) * UIR(t) \quad (4.2)$$

where $D_{iv} \cdot \delta(t)$ and $Inf(t)$ are IV bolus dose and constant rate infusion of the tracer, respectively.

Assuming both HLS and NTM tissues are non-extracting, the $UIR(t)$ function reduces to a transit time density function ($g(t)$) that was nonparametrically described as a biexponential function:

$$UIR(t) = g(t) = \lambda \cdot \alpha \cdot \exp(-\alpha \cdot t) + (1-\lambda) \cdot \beta \cdot \exp(-\beta \cdot t), \quad 0 \le \lambda \le 1 \quad (4.3)$$

Nonlinear drug disposition through TM tissues was considered by a receptor-based model (Figure 3.3) that follows the generalized target mediated drug disposition model [103] and its quasi-equilibrium approximation [165]. Accordingly, the interaction between drug input concentration ($C_{in}^{TM}(t)$) and free EPOR in the extracellular space (R), occurs with a second-order rate constant (k_{on}), to form a Drug-EPOR complex (R^*), which dissociates at a first-order rate constant (k_{off}), or is internalized into the intracellular space with a first-order rate constant (k_{int}), and then subsequently degraded by lysosomes. The EPOR is assumed to be produced at a zero-order rate constant (k_{syn}) and degraded at a first-order rate constant (k_{deg}) (Figure 3.3)

At quasi-equilibrium conditions, where binding and de-binding of the drug with receptor are much faster than the other processes of the system:

$$\frac{R \cdot C_{in}^{TM}(t)}{R^*} = \frac{(R_{tot} - R^*) \cdot C_{in}^{TM}(t)}{R^*} = K_D \tag{4.4}$$

where R_{tot} is total EPOR, ($R_{tot} = R + R^*$), K_D is drug/EPOR equilibrium dissociation constant ($K_D = k_{off} / k_{on}$).

Rearranging Equation 4.4 for R^* and normalizing the resulting equation by initial total EPOR (R_0) gives:

$$R^* / R_0 = \frac{R_{tot} / R_0 \cdot C_{in}^{TM}(t)}{K_D + C_{in}^{TM}(t)} \tag{4.5}$$

The changes in R and R^* were added to obtain the change in R_{tot} and the resulting equation was normalized by R_0:

$$\frac{d\,R_{tot}}{dt} \Big/ R_0 = K_{syn} / R_0 - K_{deg} \cdot R_{tot} / R_0 + (K_{deg} - K_{int}) \cdot R^* / R_0 \quad , \quad R_{tot}(0) / R_0 = 1 \tag{4.6}$$

The normalization in Eqs. 4.5 and 4.6 is necessary because R_0 cannot be estimated from drug plasma concentrations.

To establish a link between the receptor-based model in TM tissues and the rest of the recirculation model, a receptor-dependent extraction function, $E_{TM}(t)$, was defined as:

$$E_{TM}(t) = \frac{R^*/R_0}{C_{in}^{TM}(t)} \quad , \quad 0 \le E_{TM}(t) \le 1 \tag{4.7}$$

where $C_{in}^{TM}(t)$ is given by:

$$C_{in}^{TM}(t) = \frac{P_{TM} \cdot f_{out}^{HLS}(t)}{P_{TM} \cdot Q} = \frac{f_{out}^{HLS}(t)}{Q} \tag{4.8}$$

Assuming that distribution equilibrium is achieved rapidly between the tissues and the emerging venous blood the output rate from TM tissues is given by:

$$f_{out}^{TM}(t) = P_{TM} \cdot (1 - E_{TM}(t)) \cdot f_{out}^{HLS}(t) \tag{4.9}$$

Finally, the total plasma tracer concentration that is measured in the venous blood ($C_{out}^{tot}(t)$) is given by:

$$C_{out}^{tot}(t) = (f_{out}^{NTM}(t) + f_{out}^{TM}(t))/Q \tag{4.10}$$

Equations 4.1 to 4.3 were conveniently converted to the following equivalent equations (Eqs. 4.11-4.16). The latter six equations are simpler to deal with numerically and computationally because they include first-order differential equations and avoid the convolution operator.

$$\begin{aligned} dy_1/dt &= -\alpha y_1 + \lambda \cdot \alpha \cdot (Inf(t) + f_{out}^{NTM}(t) + f_{out}^{TM}(t)) \\ &\quad , \quad y_1(0) = D_{iv} \cdot \lambda \cdot \alpha \end{aligned} \tag{4.11}$$

$$d\,y_2/dt = -\beta \cdot y_2 + (1-\lambda)\cdot\beta\cdot(Inf(t) + f_{out}^{NTM}(t) + f_{out}^{TM}(t)) \quad , \quad y_2(0) = D_{iv}\cdot(1-\lambda)\cdot\beta \tag{4.12}$$

$$f_{out}^{HLS}(t) = y_1 + y_2 \tag{4.13}$$

$$d\,y_3/dt = -\alpha \cdot y_3 + P_{NTM}\cdot\lambda\cdot\alpha\cdot f_{out}^{HLS}(t) \quad , \quad y_3(0) = 0 \tag{4.14}$$

$$d\,y_4/dt = -\beta \cdot y_4 + P_{NTM}\cdot(1-\lambda)\cdot\beta\cdot f_{out}^{HLS}(t) \quad , \quad y_4(0) = 0 \tag{4.15}$$

$$f_{out}^{NTM}(t) = y_3 + y_4 \tag{4.16}$$

Equation (4.5) was modified to account for the TIM procedure:

$$R^*/R_0 = \begin{cases} \dfrac{R_{tot}/R_0\cdot C_{in}^{TM}(t)}{K_D + C_{in}^{TM}(t)} & for \quad 0 < t \le t_{cold} \\ \dfrac{R_{tot}/R_0\cdot C_{in}^{TM}(t)}{K_D + C_{cold}(t)} & for \quad t > t_{cold} \end{cases} \tag{4.17}$$

where $C_{cold}(t)$ is plasma non-tracer concentrations represented as a cross-validation cubic spline [173] when fitting the model to tracer data and t_{cold} is time of injection of the non-tracer.

To improve the estimation of the parameters, the sheep physiological parameters, Q and P_{TM}, were fixed to values drawn from literature [51], with Q = 7122.7 ml/h/kg, and P_{TM} was assumed to be equal to the fraction of blood flow to the bone marrow (0.0597).

4.2.5. Computational details

The numerical solution for Equation 4.10 was individually fitted to sheep tracer data for the pre- ($t < t_{cold}$) and post- ($t > t_{cold}$) unlabeled drug administration phases using WINFUNFIT, an interactive Microsoft Windows program evolved from the general non-linear regression program FUNFIT [172]. The ratio of maximum unlabeled drug

concentration to equilibrium dissociation constant, K_D , was calculated and taken as a nonlinearity index (*NLI*). Statistical comparisons of mean values for the TIM receptor-related PK parameters (Table 4.1) between EPO and C.E.R.A. were done using a one-tailed Student's t-test with correction for non-equal variance, if needed, after testing by an F-ratio test. *p*-values of 0.05 and 0.01 were taken as the levels of significance for the type I null hypotheses error. All statistical tests were done using SAS/STAT (SAS Institute Inc., Cary, NC).

4.3. Results

The elimination patterns of both EPO (Figure 4.1) and C.E.R.A. (Figure 4.2) were nonlinear, as evidenced by the significant perturbation in plasma tracer level (square symbols) caused by the injection of the non-tracer bolus (triangle symbols). This pronounced phenomenon was observed consistently in all animals. The plasma tracer concentrations were adequately described by the receptor-based recirculation model, as indicated by mean correlation coefficients of 0.984 and 0.993 for the fits of EPO and C.E.R.A. data, respectively. This conclusion was supported by strong correlations between predicted and observed plasma tracer concentrations in both EPO and C.E.R.A. treatment populations (Figure 4.3).

Receptor-related parameters obtained from the model fittings are summarized in Table 4.1. The inter-individual coefficients of variation (CV) of all parameter estimates were less than 33%, suggesting small variability between subjects. EPO and C.E.R.A. had significantly different parameter values ($p < 0.05$). The most extreme difference was observed for the equilibrium dissociation constant (K_D), where the mean value was 15-fold larger for C.E.R.A. than for EPO. The nonlinearity index (*NLI*), the initial total

EPOR-normalized production rate constant (k_{syn} / R_0), and the internalization rate constant of the drug/EPOR complex (k_{int}), were approximately 7.5-, 8-, and 10-fold higher for EPO than for C.E.R.A., respectively. The EPOR degradation rate constant (k_{deg}) was the most similar for the two compounds with a mean value that was about 1.5-fold larger for EPO than for C.E.R.A.. The EPOR underwent faster elimination in presence of EPO than in presence of C.E.R.A., as indicated by mean half-life values of both degradation ($t_{1/2}(k_{deg})$) and internalization ($t_{1/2}(k_{int})$) processes that were 1.5- and 10-fold longer for C.E.R.A., respectively.

4.4. Discussion

The present study hypothesizes that EPOR-expressing cells play a major role in ESAs elimination from the body and that this process is initiated by binding of the ESA to surface EPOR, followed by internalization and degradation by lysosomes. Thus, changes in receptor homeostasis due to EPO or C.E.R.A. administration, as well as receptor binding and endocytosis properties of both hormones, should explain their different rates of metabolism. In this work we indirectly quantify these processes using the TIM, which is an experimental procedure that specifically deals with the competition between labeled and unlabeled forms of a drug on receptor binding sites enabling the kinetic mechanism of the binding to be elucidated.

4.4.1. Receptor-based in vivo elimination of EPO and C.E.R.A.

Our previous studies provided significant evidence that EPOR-mediated pathways play a major role in the *in vivo* elimination of EPO and C.E.R.A.. Busulfan-induced bone marrow ablation resulted in pronounced reduction of EPO clearance in adult sheep [114, 115]. The same phenomenon was observed for C.E.R.A. as a consequence of busulfan

administration to adult sheep (Chapter 3). Furthermore, in phlebotomized sheep, a significant correlation was found between increases in EPOR mRNA and EPO clearance [120].

Kidneys and liver are not considered important in the *in vivo* elimination of EPO [116]. Likewise, given the lack of differences in C.E.R.A. PK properties among healthy humans, chronic kidney disease patients, and patients with impaired hepatic function, it appears that these organs are also unimportant in C.E.R.A. elimination [117-119]. Long-term stability of EPO in whole blood at room temperature indicates no significant biotransformation taking place in circulation [187].

4.4.2. EPOR turnover

For a fixed volume of target-mediated tissues, free EPOR concentration (R) is proportional to EPOR mass and therefore determines the capacity of the receptor-mediated elimination process. The larger the R, the greater the rate of elimination *via* the EPOR route. Assuming negligible variations in pre-administration receptor concentration (R_0) between animals in the EPO and C.E.R.A. treatment groups, the observed difference in k_{syn} / R_0 is mainly due to a difference in k_{syn}. The k_{syn} / R_0 ratio was eightfold larger, while k_{deg} was only about twofold larger, for EPO than for C.E.R.A. ($p < 0.01$) (Table 4.1). This finding suggests that animals injected with EPO have experienced a greater up-regulation in EPOR than those injected with C.E.R.A.. In a study analyzing the effect of EPO on regulation of its receptor expression in sheep, it was found that EPOR mRNA was up-regulated as a result of increased endogenous EPO levels after phlebotomy induced anemia [120]. An *in vitro* study using murine cell lines reported an increase in the number of EPOR per cell after 6 days of incubation with EPO, without altering EPOR

binding affinity [188]. In a different study, erythroleukemic cells cultured in presence of EPO had a higher number of EPOR than cytokines stimulated cells [189]. EPOR up-regulation was also reported in mice cerebral vascular endothelial cells after treatment with EPO [190].

4.4.3. EPOR binding with EPO and C.E.R.A.

The equilibrium dissociation constant (K_D, the ratio of the dissociation and association rate constants) was significantly higher for C.E.R.A. ($p < 0.01$, Table 4.1), indicating that it has a slower association rate and/or a faster dissociation rate than EPO. Analysis of equilibration curves in a comparative *in vitro* binding study for EPO and C.E.R.A. with soluble recombinant EPOR and EPOR expressing cultured human cells indicated that the difference in affinity is driven mainly by slower association [110].

The faster occupation of EPOR by EPO molecules suggests that, for a given time interval, production of the EPO/EPOR complex is higher than production of the C.E.R.A./EPOR complex. The faster binding between EPO and EPOR on the cell surface can explain the significantly higher k_{syn} / R_0 in the EPO treatment group, where rapid disappearance of free EPOR from the medium stimulates the synthesis of more receptors by a positive feedback control mechanism.

4.4.4. Disposition nonlinearity of EPO and C.E.R.A.

According to Equation (4.5), the degree of nonlinearity is determined by K_D and $C_{in}^{TM}(t)$, the input concentration to target-mediated tissues. When K_D and $C_{in}^{TM}(t)$ have comparable values, the drug metabolic rate depends nonlinearly on drug concentration. A very large K_D value or a very small $C_{in}^{TM}(t)$ results in linear, first-order kinetics. The maximum degree of nonlinearity is expected at the highest $C_{in}^{TM}(t)$ observed at the highest

observed plasma concentration. The nonlinearity index was much greater than 1 (Table 4.1), which indicates a significant degree of nonlinearity for both drugs. The nonlinearity of EPO was greater, in accordance with its larger nonlinearity index ($p < 0.01$).

4.4.5. Endocytosis and metabolism of surface-bound EPO and C.E.R.A.

Slow internalization of the drug/receptor complex to the intracellular space reduces drug elimination by increasing the probability of drug dissociation into the medium; slow degradation in lysosomes counteracts elimination by increasing the likelihood that the complex will be re-secreted, intact, to the cell surface. The parameter k_{int} lumps the processes of internalization and degradation together. Thus, the results of the current analysis cannot elucidate which process drives the smaller k_{int} value observed for C.E.R.A. (Table 4.1). Panchapakesan et.al. hypothesized that the very slow association but fast dissociation between C.E.R.A. and EPOR results in a brief binding period that is barely long enough to permit internalization [191]. Our finding that the difference between EPO and C.E.R.A. k_{int} values agree well with the differences in K_D values (10 *versus* 15-folds, respectively) supports the hypothesis of Panchapakesan et al. and suggests that internalization of surface-bound EPOR is the rate-limiting step in post-binding events.

Although EPOR expressed in cultured Ba/F and UT-7/EPO cells was bound approximately 5 times more quickly by EPO than by darbepoetin alpha, both drugs were internalized at the same rate and there were no differences in their fractions degraded or re-secreted after internalization [113]. Contrary to these patterns, we found that EPO and C.E.R.A. had different k_{int} values, which suggests that the metabolic fate of the C.E.R.A.-EPOR complex is unique.

4.4.6. In vivo erythropoiesis of EPO and C.E.R.A.

It has been proposed that ESAs function *via* the same mechanism [192]: they interact directly with EPOR on the cell surface and induce a conformational change in the receptor, which triggers the intracellular Janus kinase signal transduction required for the production of RBCs [182]. In this setup, the bound receptor concentration can serve as a PD marker of the pharmacological effect of ESAs with K_D and k_{int} values being considered as qualitative measures for receptor occupancy and receptor activation duration, respectively. The fact that C.E.R.A. has a higher K_D value (i.e., lower occupancy) suggests that the greater *in vivo* erythropoietic activity reported for C.E.R.A. compared with EPO [111] can be attributed to the slower internalization and/or degradation of C.E.R.A.-EPOR complex (i.e., smaller k_{int} value) which results in prolonged signaling *in vivo*. Increased EPOR occupancy increases the rate of erythropoiesis, not by increasing the rate of cell division, but by increasing the recruitment and differentiation of more erythroid progenitor cells. However, once all available progenitors are actively dividing, the occupation of further receptors becomes trivial [192]. This hypothesis is supported by the fact that maximum erythropoiesis is elicited even when only a minor fraction of EPORs is activated [109, 193]. Accordingly, it seems that the erythropoietic activity of ESAs depend on their ability to recruit more cells rather than their ability to occupy more receptors. In presence of equivalent receptor occupation efficiencies (i.e., equal K_D values), cell recruitment potential depends solely on the survival of ESA molecule after binding with EPOR or even after endocytosis that is increased by decreased k_{int} values. Therefore, long-acting EPO analogues such as

darbepoetin alpha receptors [194] and C.E.R.A. [111] demonstrate higher potency than EPO *in vivo* despite their lower affinity to EPOR.

4.5. Conclusion

The adopted receptor-based recirculation model accounts for: 1) drug-receptor binding, 2) receptor turnover, and 3) drug/receptor complex endocytosis and lysosomal degradation enabling an in-depth mechanistic analysis of the PK/PD of EPO and C.E.R.A. in adult sheep. As predicted by the model, the slower elimination of C.E.R.A. can be explained in terms of the following mechanisms: 1) less EPOR up-regulation induced by C.E.R.A. administration; 2) slower binding of C.E.R.A. to EPOR; and 3) reduced internalization and/or degradation rate of surface-bound C.E.R.A.. Slower C.E.R.A./EPOR complex elimination explains the greater *in vivo* erythropoiesis observed for C.E.R.A. [111] despite its lower affinity to its receptor.

Table 4.1. Receptor-related pharmacokinetic parameters of EPO and C.E.R.A. obtained by fitting a receptor-based recirculation model to TIM data from adult sheep.

Parameter (units)	Definition	EPO (n = 7)	C.E.R.A. (n = 5)	*p*-value
		Mean (CV%)	Mean (CV%)	
k_{syn} / R_0 (1/min)	Initial EPOR normalized synthesis rate constant	21.0 (17)	2.70 (31.3)	< 0.01
k_{deg} (1/min)	EPOR degradation rate constant	1.10 (19.6)	0.70 (32.4)	< 0.01
$t_{1/2}(k_{deg})$* (min)	EPOR degradation half-life	0.66 (19.9)	1.06 (29)	< 0.05
K_D (pmol)	Drug/EPOR equilibrium dissociation constant	6.00 (29.6)	88.4 (18.3)	< 0.01
NLI	Nonlinearity index	106 (31.1)	14.8 (20.2)	< 0.01
k_{int} (1/min)	Drug/EPOR internalization rate constant	0.40 (2.2)	0.04 (17.7)	< 0.01
$t_{1/2}(k_{int})$* (min)	Drug/EPOR internalization half-life	1.72 (2.2)	17.7 (16.1)	< 0.01

CV%, Coefficient of Variation. *half-lives were calculated as: ln(2)/corresponding rate constant.

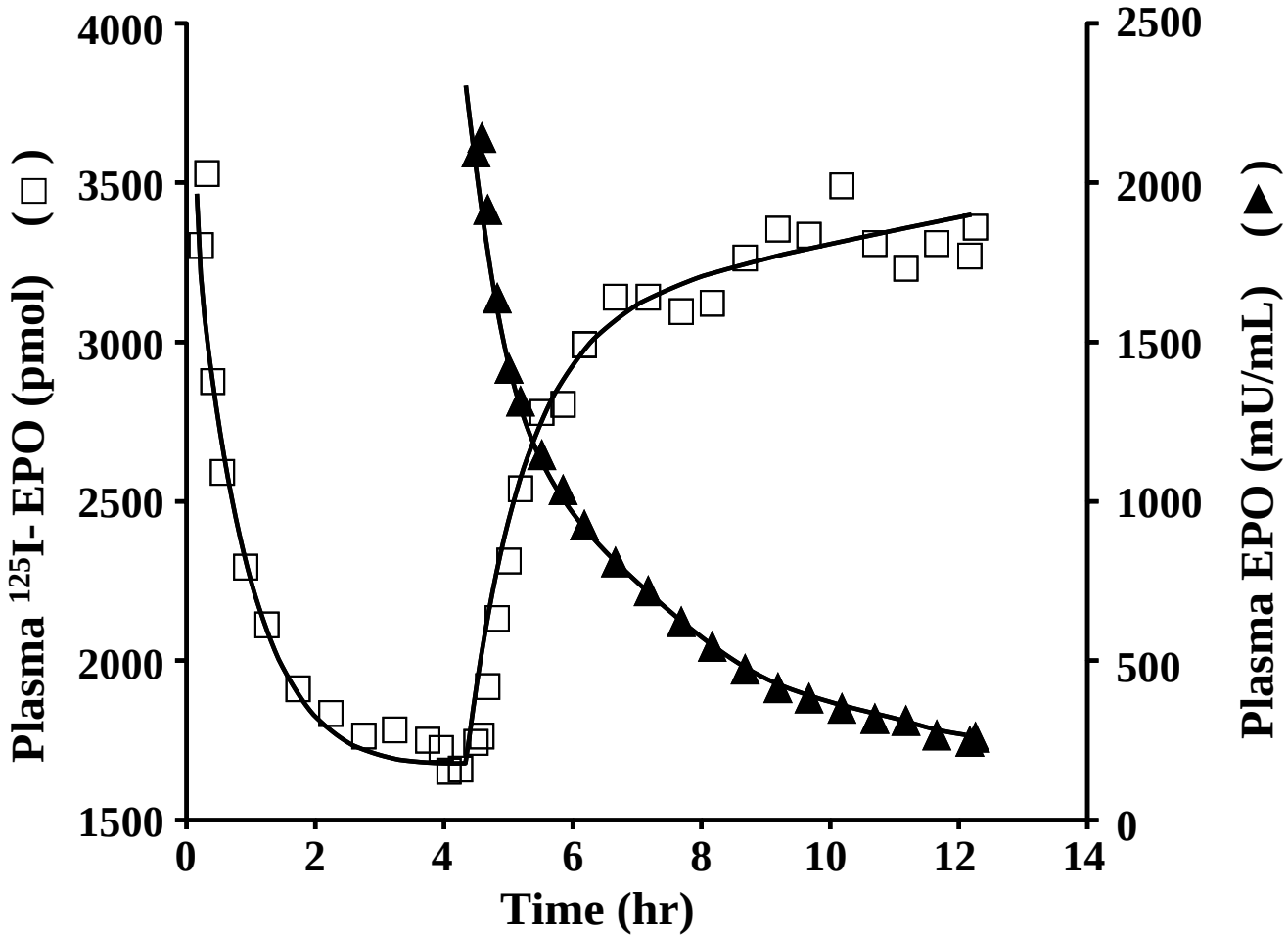

Figure 4.1. Representative fit of the receptor-based recirculation model to the ^{125}I-EPO TIM tracer data (squares) in adult sheep. The non-tracer EPO data (triangles) are fitted to a general cross validation cubic spline function.

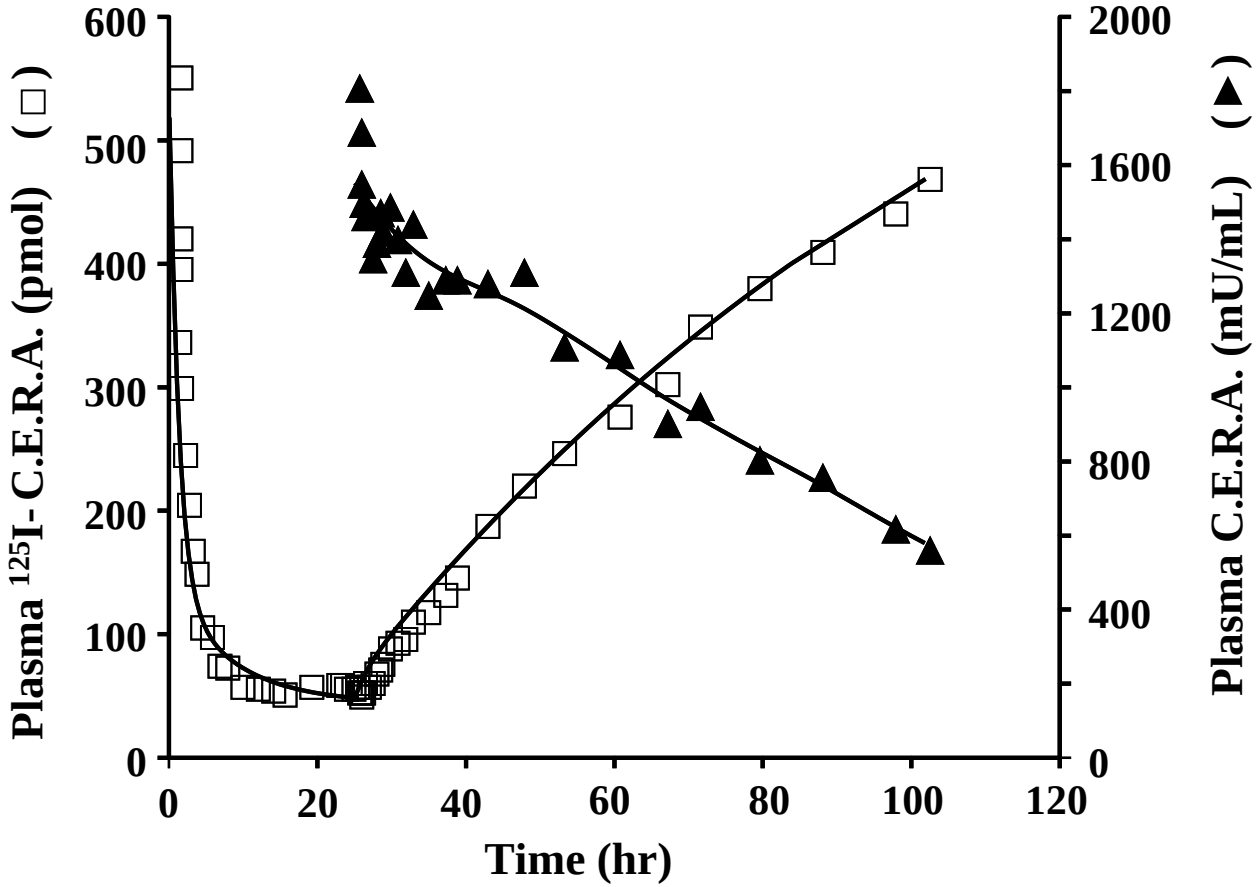

Figure 4.2. Representative fit of the receptor-based recirculation model to the ^{125}I-C.E.R.A. TIM tracer data (squares) in adult sheep. The non-tracer C.E.R.A. data (triangles) are fitted to a general cross validation cubic spline function.

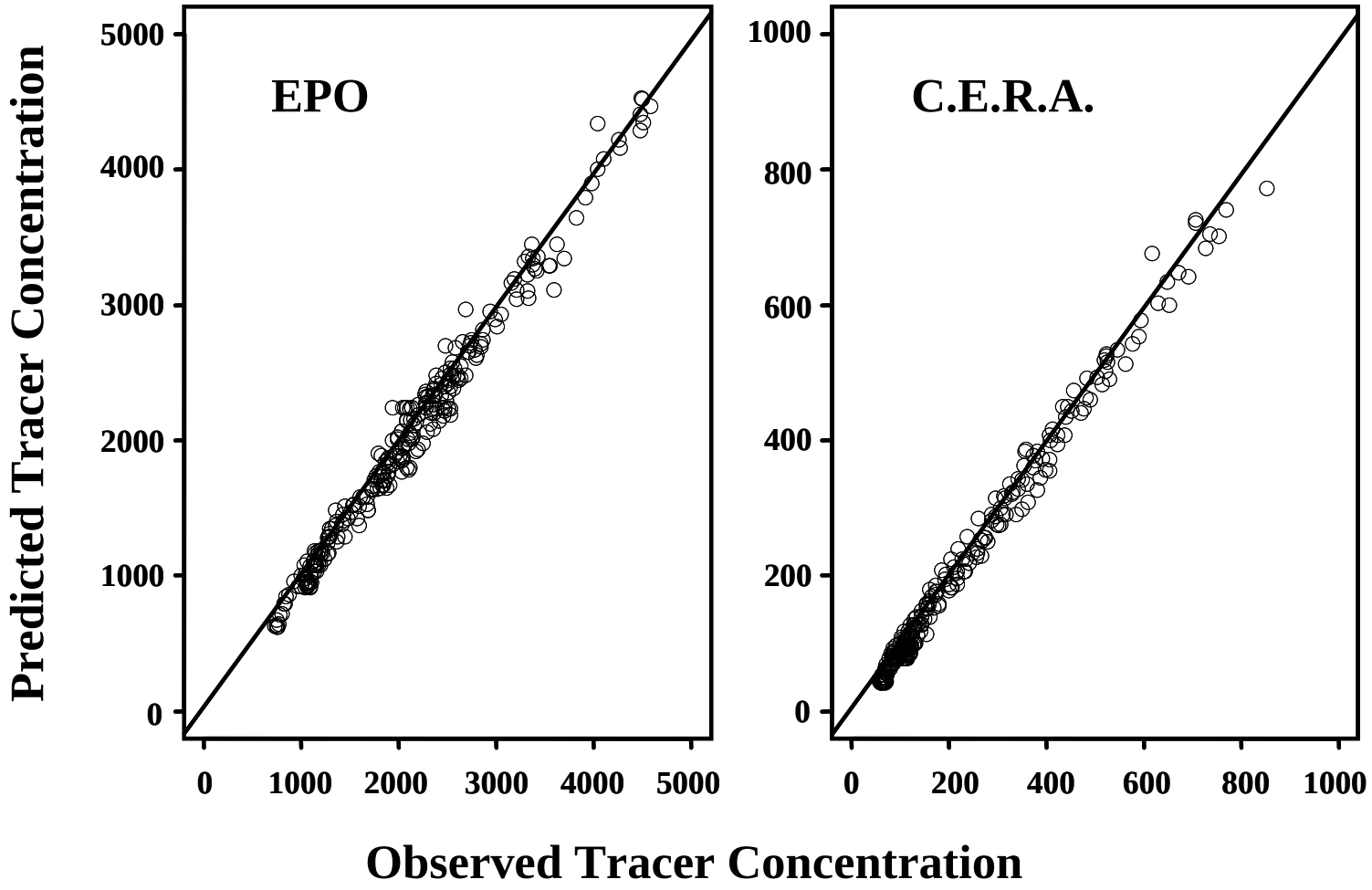

Figure 4.3. Predicted *versus* observed plasma tracer concentrations in EPO and C.E.R.A. treatment populations.

CHAPTER 5. SENSITIVITY ANALYSIS OF THE RECEPTOR-BASED RECIRCULATION MODEL

5.1. Introduction

Physiologically based pharmacokinetic (PBPK) models follow the anatomical scheme of mammalian species by connecting physiologically realistic compartments, representing kinetically important organs or tissues *via* arterial and venous blood pathways. The models comprise physiological parameters such as organ volumes, blood flow rates, etc., as well as drug-dependent parameters such as tissue-to-blood partition coefficients, tissue membrane permeabilities, metabolic rate parameters, and protein binding. A common feature for all these parameters is inherent variability, and hence a successful and complete PBPK model will describe the effect of variability and uncertainty of the underlying parameters on the model output(s). Sensitivity analysis is the appropriate mathematical tool for the later problem [195]. Recently, sensitivity analysis has drawn a lot of attention in PBPK modeling, especially in the field of risk assessment and toxicokinetics [196-199].

Sensitivity analysis in pharmacokinetics (PK) and pharmacodynamics (PD) is defined as the systematic investigation of the relationship between PK or PD model response(s) and perturbations occurring in the system structure and/or parameters [200]. Sensitivity analysis provides detailed information regarding the time course of the impact of each model parameter on model output(s) [196, 198, 199]. This information can be useful at the initial model specification stage in: (1) discriminating between which parameters that needs to be included and those that should be left out of the model [195]; and (2) deriving an optimal PK or PD experimental design (e.g., sampling times, input

doses, etc.) [196]. At the model assessment and validation stage, the sensitivity analysis allows to characterize the degree of confidence in the final parameter estimates [195].

Sensitivity analysis methods can be classified to “Local” and “Global”. The Local methods depend on computation of analytical sensitivities; the partial derivatives of model output(s) with respect to model parameters [94, 201]. The Global methods depend on Monte Carlo simulation techniques [197, 202-205]. Briefly, in the Monte Carlo method, a probability distribution for each of the model input parameters is randomly sampled, and the model is run using the chosen set of parameter values. This process is repeated a large number of times until the probability distributions for the desired model outputs have been created. This method allows assessment of parameter uncertainty effect on the variability in the model output. Despite the partial derivative methods don’t predict an overall model output variability, they allow ranking of model parameters according to their influence on the relative change in the model output. These methods don’t require large number of simulations that are needed for the Monte Carlo methods, so they take significantly less computation time. For the Monte Carlo methods to be adequate, the input parameter distributions should reflect the true parameter variability. However, this information is usually not available [94]. Thus, partial derivative methods offer a simpler way to investigate parameter sensitivities than Monte Carlo methods.

The tracer interaction method (TIM) is a sensitive and accurate methodology for analyzing non-linear, saturation kinetics under dynamic conditions, by monitoring perturbations in the level of a tracer form of the drug following the introduction of the parent drug [125]. In Chapters 3 and Chapter 4, the TIM was used to estimate parameters of a receptor-based recirculation model developed to analyze recombinant human

erythropoietin and Continuous Erythropoietin Receptor Activator (C.E.R.A.) disposition in adult sheep. The aim of this work was to evaluate the appropriateness of the TIM design in estimation of the model parameters using a partial derivative sensitivity method.

5.2. Methods

5.2.1. Pharmacokinetic model

The model studied in this work was previously introduced (Chapter 3, section 3.2.5). Briefly, the model consists of three tissues, heart-lung segment (HLS), non-target mediated disposition (NTM) and target mediated disposition (TM), interconnected by arteries and veins (Figure 3.2). Linear drug disposition through HLS, and NTM tissues was described by stochastic transport principles, namely, transit time density function and convolution relationship. Nonlinear drug disposition through TM tissues was considered by a receptor-based model (Figure 3.3) that assumes quasi-equilibrium condition and accounts for drug-receptor binding, receptor turnover, and drug/receptor complex endocytosis. The model equations used in the current analysis are:

$$d\,y_1/dt = -\alpha\, y_1 + \lambda \cdot \alpha \cdot (Inf(t) + f_{out}^{NTM}(t) + f_{out}^{TM}(t)) \quad , \quad y_1(0) = D_{iv} \cdot \lambda \cdot \alpha \tag{5.1}$$

$$d\,y_2/dt = -\beta \cdot y_2 + (1-\lambda) \cdot \beta \cdot (Inf(t) + f_{out}^{NTM}(t) + f_{out}^{TM}(t)) \quad , \quad y_2(0) = D_{iv} \cdot (1-\lambda) \cdot \beta \tag{5.2}$$

$$f_{out}^{HLS}(t) = y_1 + y_2 \tag{5.3}$$

$$d\,y_3/dt = -\alpha \cdot y_3 + P_{NTM} \cdot \lambda \cdot \alpha \cdot f_{out}^{HLS}(t) \quad , \quad y_3(0) = 0 \tag{5.4}$$

$$d\,y_4/dt = -\beta \cdot y_4 + P_{NTM} \cdot (1-\lambda) \cdot \beta \cdot f_{out}^{HLS}(t) \quad , \quad y_4(0) = 0 \tag{5.5}$$

$$f_{out}^{NTM}(t) = y_3 + y_4 \tag{5.6}$$

$$f_{out}^{TM}(t) = P_{TM} \cdot (1 - E_{TM}(t)) \cdot f_{out}^{HLS}(t) \tag{5.7}$$

$$E_{TM}(t) = \frac{R^{*}/R_0}{C_{in}^{TM}(t)} \quad , \quad 0 \le E_{TM}(t) \le 1 \tag{5.8}$$

$$C_{in}^{TM}(t) = \frac{P_{TM} \cdot f_{out}^{HLS}(t)}{P_{TM} \cdot Q} = \frac{f_{out}^{HLS}(t)}{Q} \tag{5.9}$$

$$\frac{d\,R_{tot}}{dt} \Big/ R_0 = k_{syn}/R_0 - k_{deg} \cdot R_{tot}/R_0 + (k_{deg} - k_{int}) \cdot R^{*}/R_0 \quad , \quad R_{tot}(0)/R_0 = 1 \tag{5.10}$$

$$C_{out}^{tot}(t) = (f_{out}^{NTM}(t) + f_{out}^{TM}(t))/Q \tag{5.11}$$

where Q is cardiac output, P_i is fraction of blood flow to i^{th} tissue for i=TM or NTM ($P_{TM} + P_{NTM} = 1$), $f_{out}^{i}(t)$ is the output rate from i^{th} tissue for i=HLS, TM or NTM, (*) denotes convolution, $D_{iv} \cdot \delta(t)$ is IV bolus dose of the tracer, $Inf(t)$ is constant rate infusion of the tracer, $UIR(t)$ is unit impulse response function, which reduces to a transit time density function ($g(t)$) under the assumption that the tissue is non-extracting, $E_{TM}(t)$ is receptor-dependent extraction function, R_{tot} is total EPOR (R_{tot} = free receptor, R + bound receptor, R*), R_0 is initial receptor concentration, $C_{in}^{TM}(t)$ is input drug concentration to TM tissues, $C_{out}^{TM}(t)$ is output drug concentration from TM tissues, K_D is drug/receptor equilibrium dissociation constant (K_D = dissociation rate constant, k_{off} / association rate constant, k_{on}), k_{syn} is receptor synthesis rate constant, k_{deg} is receptor degradation rate constant, k_{int} is drug/receptor internalization rate constant.

In case of a TIM experimental design:

$$R^*/R_0 = \begin{cases} \dfrac{R_{tot}/R_0 \cdot C_{in}^{TM}(t)}{K_D + C_{in}^{TM}(t)} & for \quad 0 < t \le t_{cold} \\ \dfrac{R_{tot}/R_0 \cdot C_{in}^{TM}(t)}{K_D + C_{cold}(t)} & for \quad t > t_{cold} \end{cases} \tag{5.12}$$

where $C_{cold}(t)$ is non-tracer plasma concentrations, t_{cold} is time of injection of the non-tracer, and $C_{out}^{tot}(t)$ is total output plasma concentration.

5.2.2. Sensitivity analysis

A sensitivity analysis was implemented to evaluate the influence of each model parameter on the predicted plasma concentration-time profile. The model parameters investigated included the transit time density function parameters; α, β, λ, and receptor-related parameters; k_{syn} / R_0, k_{deg}, K_D, and k_{int}.

Sensitivity function (*S(t)*) was obtained using the partial derivatives of predicted plasma concentration-time profile with respect to model parameters [94, 201]. The *S(t)* was calculated using the central difference method:

$$S(t) = \frac{\partial C_{out}^{tot}(\theta_i, t)}{\partial \theta_i} \cong \frac{C_{out}^{tot}(\theta_i + \Delta\theta_i, t) - C_{out}^{tot}(\theta_i - \Delta\theta_i, t)}{2\Delta\theta_i} \tag{5.13}$$

where $C_{out}^{tot}(\theta_i, t)$ is the total plasma tracer concentrations predicted at the i^{th} parameter θ_i and time *t*. $\Delta\theta_i$ is the change in parameter θ_i (5% was used for all parameters). While parameter θ_i was investigated, all other parameters were held constant. The log-normalized *S(t)*:

$$NS(t) = \frac{\partial \ln C_{out}^{tot}(\theta_i, t)}{\partial \ln \theta_i} \cong S(t) \cdot \frac{\theta_i}{C_{out}^{tot}(\theta_i, t)} \tag{5.14}$$

determines the relative change in $C_{out}^{tot}(\theta_i, t)$ caused by a small relative change in θ_i [94, 201]. A *NS(t)* that is near zero indicates that the corresponding θ_i has only little influence on the plasma concentration response. A θ_i that has *NS(t)* further away from zero, in the positive or the negative side, is associated with a greater influence on $C_{out}^{tot}(\theta_i, t)$. Clewell et al [94] has defined cut-off values for high, medium, and low normalized sensitivity values to be: >0.5, 0.2-0.5, and <0.2, respectively.

5.2.3. Simulations

Simulations of the total plasma tracer concentrations, $C_{out}^{tot}(t)$ (Eq. 5.11) according to the TIM experimental setting were performed using WINFUNFIT, an interactive Microsoft Windows program evolved from the general non-linear regression program FUNFIT [172]. A detailed description of the theory and principles of the TIM was previously published [125]. Briefly, a single IV bolus dose of a tracer form of the drug is initially administered, then immediately followed by a constant rate infusion of the tracer. An IV bolus injection of the parent drug is administered when the plasma level of the tracer approached steady state. Blood samples are collected subsequent to the tracer and the non-tracer administrations for determination of plasma drug levels. In the current study, the TIM experimental conditions used for C.E.R.A. in Chapter 4 were implemented. The tracer bolus dose was 50 mU/kg, the tracer infusion rate was 1.6 mU/h/kg, the time of non-tracer bolus input was 20 hours, the non-tracer bolus dose was 104 U/kg, and the tracer sampling time range was 0-85 hours. The nominal parameter values were the mean values of C.E.R.A. parameter estimates obtained by individual fittings of the physiologic model to TIM data from 5 adult sheep (see Chapter 4). The physiologic model parameter values used for the simulations are listed in Table 5.1. The

physiological parameters, Q and P_{TM}, were fixed to sheep values drawn from literature [51], with P_{TM} assumed to be equal to the fraction of blood flow to the bone marrow. The body weight was fixed to 28.4 kg.

5.3. Results and discussion

Table 5.2 shows the maximum absolute relative sensitivities of the model parameters. All parameters exhibited medium (0.2 to 0.5) to high (>0.5) maximum absolute relative sensitivities at the simulated TIM conditions, indicating that those parameters were reliably estimated with the implemented experimental design. Maximum absolute sensitivity of parameter β was larger than that of parameters α and λ (1 *versus* 0.3). Among receptor-related parameters, k_{int} showed the lowest sensitivity (maximum absolute sensitivity: 0.5 *versus* ~1.2 for k_{syn} / R_0, k_{deg} and K_D).

The time-dependent sensitivity of the venous blood tracer concentrations predicted by the model to the transit-time density function and receptor-related parameters are depicted in Figures 5.1 and 5.2, respectively. All absolute sensitivity values ranged from 0 to +1.3. Sensitivity values of the transit time density function parameters peaked prior to non-tracer administration with minor perturbations that occurred during or after the non-tracer input. Those perturbations fell rapidly to zero and remained there almost to the end of the experiment (Figure 5.1). On the other hand, sensitivities of receptor-related parameters increased gradually with time and peaked around the non-tracer input (Figure 5.2). After non-tracer perturbation, the overall model output was much more sensitive to changes in receptor-related parameters than to changes in density function parameters, indicating that the drug-receptor interaction was the most important factor determining the shape of the tracer concentration-time curve

after perturbation. This result is expected because after the non-tracer administration, the competition on the binding sites of the receptor is maximum, therefore, it can be assumed that the plasma concentration will be mainly affected by the receptor-related processes.

From Figure 5.1, maximum absolute sensitivity occurred at approximately zero hour for parameter β and at approximately 8 hour for parameter α. Thus, β indicates a fast initial distribution phase from highly perfused tissues, while α reflects a slow terminal distribution from poorly perfused tissues. Although K_D, k_{deg}, and k_{syn} / R_0 are important in determining system response between approximately zero and 10 hours after the non-tracer input, it seems that only k_{deg} and k_{syn} / R_0 can influence the response at later times (i.e., from 10 hours after non-tracer administration until the end of the experiment) (Figure 5.2). Unlike $K_{D,}$ the absolute sensitivity of which peaks at a non-tracer input time and vanishes afterwards, the absolute sensitivity of k_{int} peaks 40 hours after the non-tracer input (Figure 5.2).

5.4. Conclusion

A comprehensive, partial derivative sensitivity analysis showed that the TIM experimental setting is adequate for estimation of the physiologic model parameters. Although, the time course of tracer plasma concentrations in the TIM design is determined by both linear distribution and receptor-related parameters before the non-tracer injection, it is primarily determined by receptor-related parameters after the injection.

Table 5.1. Physiologic model input parameter values used for sensitivity analysis simulations.

Parameter	Definition	Units	Value
α	Transit time density function rate parameter	h^{-1}	0.14
β	Transit time density function rate parameter	h^{-1}	185
λ	Transit time density function mixing parameter	h^{-1}	0.001
k_{syn}/R_0	Initial receptor normalized zero-order receptor synthesis rate constant	h^{-1}	164
k_{deg}	First-order receptor degradation rate constant	h^{-1}	42.5
K_D	Drug–receptor equilibrium dissociation constant	pmole	88.4
k_{int}	First-order drug/receptor internalization rate constant	h^{-1}	2.41

Table 5.2. Maximum absolute relative sensitivities of the physiologic model parameters.

Parameter	Definition	Value
α	Transit time density function rate parameter	0.3
β	Transit time density function rate parameter	0.9
λ	Transit time density function mixing parameter	0.3
k_{syn}/R_0	Initial receptor normalized zero-order receptor synthesis rate constant	1.3
k_{deg}	First-order receptor degradation rate constant	1.2
K_D	Drug–receptor equilibrium dissociation constant	1.2
k_{int}	First-order drug/receptor internalization rate constant	0.5

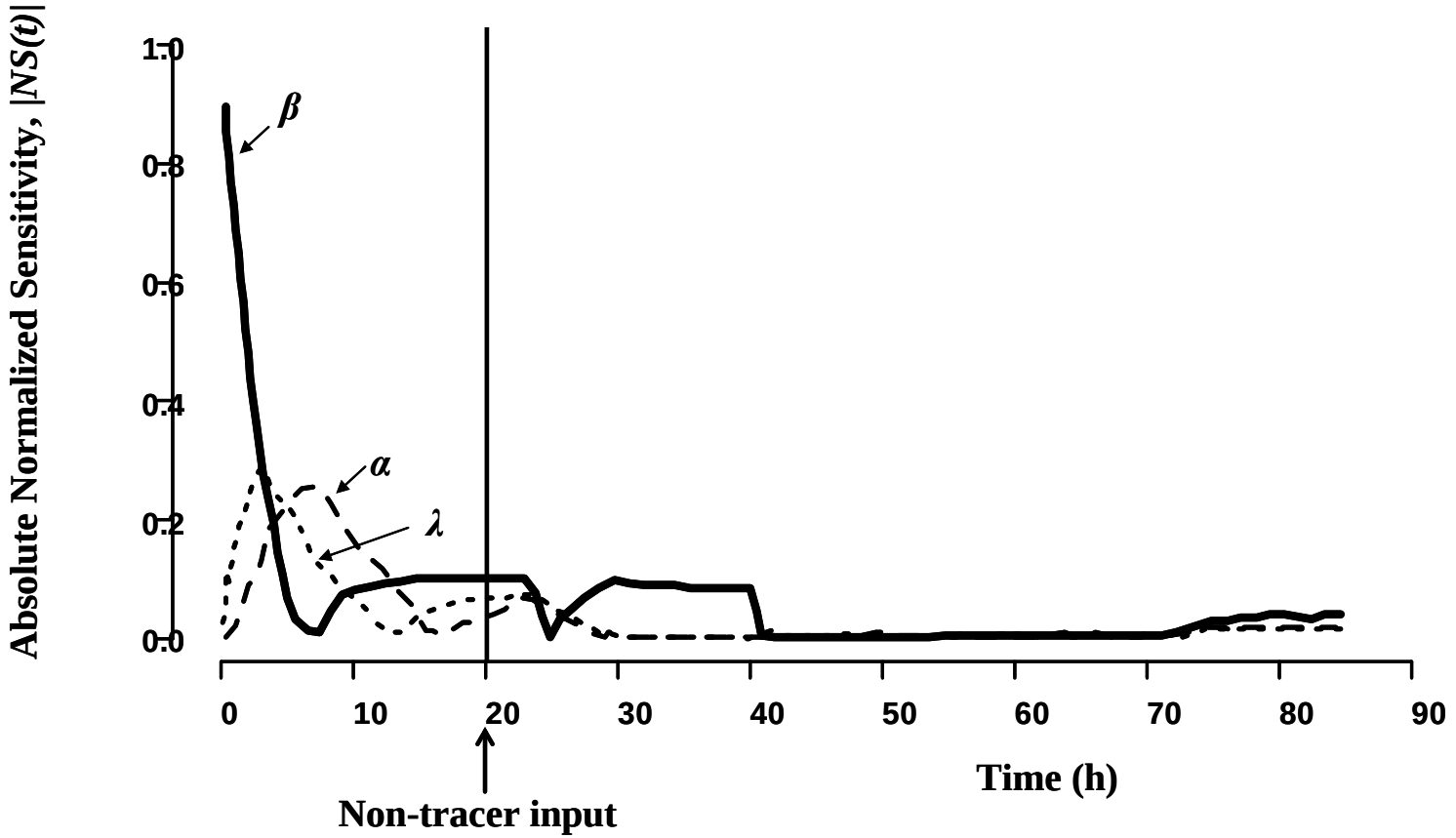

Figure 5.1. Absolute normalized sensitivity function for the physiologic model transit time density function parameters using TIM plasma tracer concentrations as the model output. Symbols are defined in the text.

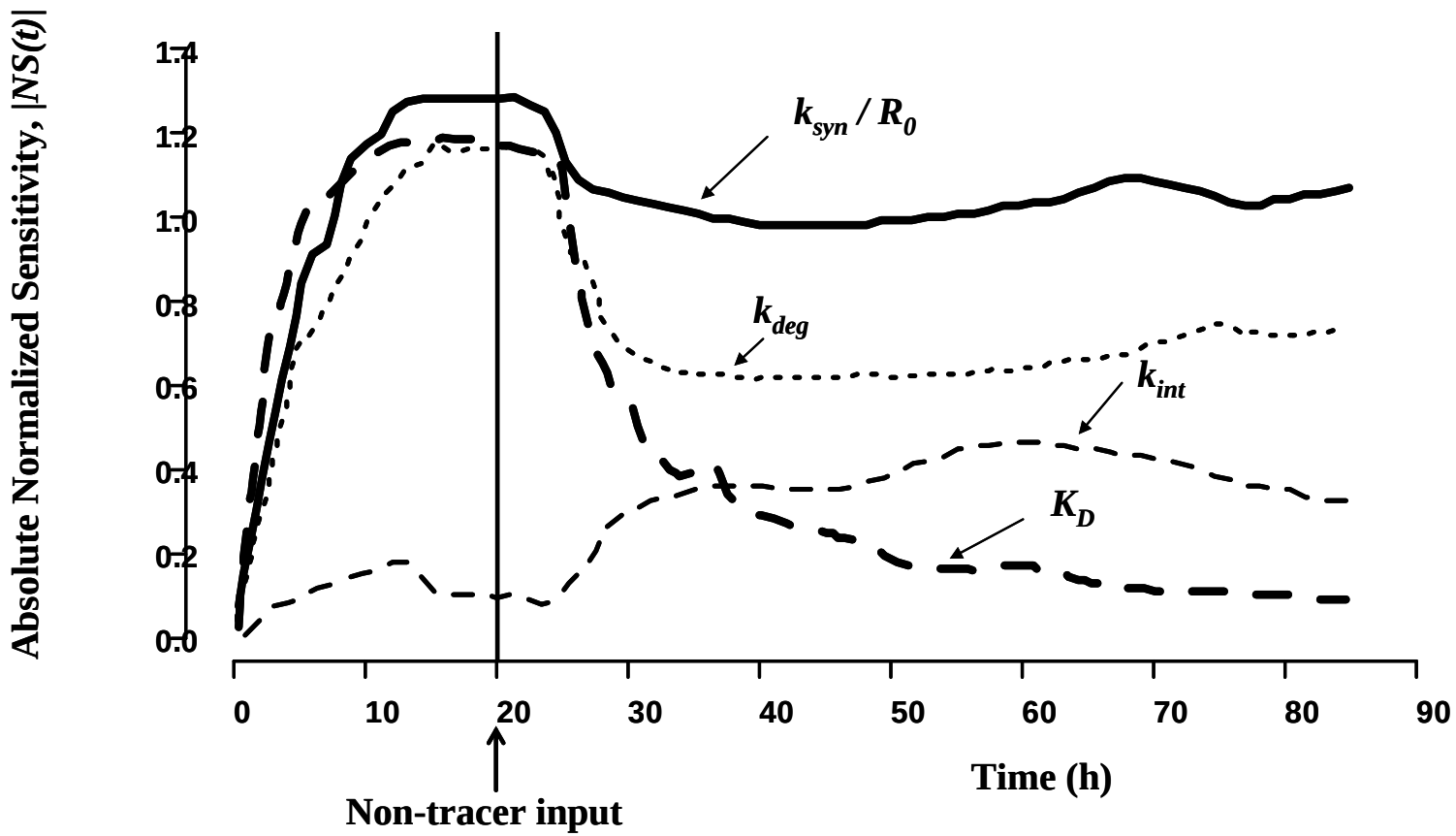

Figure 5.2. Absolute normalized sensitivity function for the physiologic model receptor-related parameters using TIM plasma tracer concentrations as the model output. Symbols are defined in the text.

CHAPTER 6. EQUIVALENCE OF COMPARTMENTAL AND RECIRCULATION TARGET-MEDIATED DISPOSITION PHARMACOKINETIC MODELS

6.1. Introduction

Target-mediated disposition (TMD) is a phenomenon where drug distribution and/or elimination are influenced by capacity-limited binding to a target (receptor or enzyme) [102]. This binding results in dose-dependent events, including a decrease in the volume of distribution at steady state and/or target-mediated clearance with increasing dose level [102, 103]. A general mechanism-based pharmacokinetic (PK) model of TMD was developed to describe the behavior of such systems [103]. The model comprises elements for target turnover, drug–target binding, and drug–target complex endocytosis. The TMD model in the framework of a two- or three-compartment model has been applied to analyze the disposition of various small molecules, peptides, proteins, hormones, and monoclonal antibodies, using plasma concentration–time data obtained from individual or population pharmacokinetic studies in different mammalian species [104-106].

Unlike the classical compartmental models which depend on series of kinetically similar compartments to describe the system's behavior, physiologically based pharmacokinetic (PBPK) models use well-defined tissues in a heterogenous structure that comprises parameters representing mammalian anatomy and physiology. In the classical approach, a first-order process describes the drug transfer between compartments, while a convection process *via* the vascular network characterizes the transfer between tissue blocks in the physiological approach. Conventional models assume instant and

homogenous distribution of drug molecules through a given kinetic space which is not the case for PBPK models that allow selection between one- and multi-compartment tissue structure, depending on the drug properties and the nature of a given tissue.

Although PBPK models offer significantly increased relevance over classical models for interpreting and predicting different physiological scenarios [21, 62], they require estimation of a large number of input parameters. Therefore, parametrization of a PBPK model cannot be based only on routine clinical pharmacokinetic data [63], but also requires extensive literature resources, separate *in vitro* and *in vivo* experiments, concentration measurements in several tissues (using invasive or destructive sampling), *in silico* predictions, and allometric scaling [21]. Thus, building a PBPK model is often times a complex process associated with uncertainty levels introduced into model parameters. Such uncertainty can influence the accuracy of predictions using a PBPK model and may lead to a final model that fails to reflect true *in vivo* drug concentrations [94, 95].

The drawbacks of traditional PBPK models necessitated the use of minimal models and the search for alternative means to mathematically represent the processes of drug transport within a physiological structure [25, 26]. Linear systems analysis (LSA) principles applied to physiological modeling, usually referred to as recirculation models, provide a scientifically attractive method of reducing the complexity of the traditional models. This approach views the organ/tissue as a general “building block” that is characterized by a unit impulse response (UIR) function in the framework of input-output convolution relationship, rather than assuming a flow rate- or permeability rate-limited structure defined using systems of ordinary differential equations [96, 101, 128-130,

143]. The UIR function, also known as the transfer function, encapsulates the essential two fundamental disposition components, namely distribution and elimination, and therefore can be reparametrized in terms of an extraction fraction which represents the probability that a drug molecule which enters the organ/tissue will be eliminated; and a transit time distribution function. The distribution function can be specified on an empirical basis [96, 134, 135, 137] or it can reflect rigorous, mechanism-based processes on the sub-organ or even the cellular level [143, 144].

Despite several reports published on PBPK models (about 360 research papers on MEDLINE since 2005), very few have compared the physiological and classical compartmental approaches. The aim of this work is two-fold: 1) to identify the physiological conditions at which a TMD-two compartment model approximates a minimal, LSA-based, TMD-recirculation model (i.e. the conditions at which estimates of receptor-related parameters using both models are expected to be the same); and 2) evaluate the influence of the host structure (compartmental or recirculation) on parameter estimation accuracy and precision.

6.2. Theoretical

6.2.1. Compartmental target-mediated disposition model (COMP-TMD)

The general compartmental pharmacokinetic model of TMD proposed by Mager and Jusko [103] is illustrated in Figure 6.1. The model assumes that drug upon reaching the central compartment (C) binds with a second order rate (k_{on}) to the free receptor (R) to form the drug–receptor complex (R^*), which in turn, dissociates by a first-order rate process (k_{off}). The internalization and degradation of the drug–receptor complex is represented as a first-order rate process (k_{int}). The receptor is synthesized at a zero-order

rate (k_{syn}) and degraded at a first-order rate (k_{deg}). The drug in the central compartment undergoes linear distribution to and from a nonspecific tissue compartment (A_T) by first-order rates (k_{pt}, k_{tp}), and can be directly eliminated by a first-order process (k_{el}). The full TMD PK model is described by:

$$dC/dt = -(k_{el} + k_{pt}) \cdot C + k_{tp} \cdot A_T/V - k_{on} \cdot R \cdot C + k_{off} \cdot R^* + In(t) \quad (6.1)$$

$$dA_T/dt = -k_{tp} \cdot A_T + k_{pt} \cdot C \cdot V \quad (6.2)$$

$$dR/dt = k_{syn} + k_{off} \cdot R^* - k_{on} \cdot R \cdot C - k_{\deg} R \quad (6.3)$$

$$dR^*/dt = -(k_{off} + k_{\text{int}}) \cdot R^* + k_{on} \cdot R \cdot C \quad (6.4)$$

where V denotes the volume of the central compartment and $In(t)$ is the external input rate function.

In this Chapter, it is assumed, for simplifying the analysis, that the free drug is not endogenously produced. Accordingly, for an exogenous input that involves an intravenous (IV) bolus dose (D_{iv}) at steady state, the initial conditions for Eqs. 6.1–6.4 after the input are defined as:

$$C(0) = D_{iv}/V \quad (6.5a)$$

$$A_T(0) = 0 \quad (6.5b)$$

$$R(0) = R_{ss} = k_{syn}/k_{\deg} \quad (6.5c)$$

$$R^*(0) = 0 \quad (6.5d)$$

where R_{ss} denotes the steady-state free receptor concentration.

6.2.2. Recirculation target-mediated disposition model (REC-TMD)

The model consists of 3 tissues: heart–lung segment (HLS), non-target-mediated disposition tissue (NTM), and target-mediated disposition tissue (TM), which are

interconnected by arteries and veins (Figure 6.2, Panel A). The cardiac output is given by Q, and P_i is the fraction of blood flow to ith tissue for i=TM or NTM ($P_{TM} + P_{NTM} = 1$). Drug disposition in the HLS and NTM tissues is assumed to be linear. Therefore, the output rates from both tissues ($f_{out}^{HLS}(t)$ and $f_{out}^{NTM}(t)$) are described by the following convolution equations (* denotes convolution) that relate the input and output rates for a given tissue to a unit impulse response function ($UIR(t)$):

$$f_{out}^{HLS}(t) = [\, D_{iv} \cdot \delta(t) + f_{out}^{NTM}(t) + f_{out}^{TM}(t)] * UIR_{HLS}(t) \tag{6.6}$$

$$f_{out}^{NTM}(t) = P_{NTM} \cdot f_{out}^{HLS}(t) * UIR_{NTM}(t) \tag{6.7}$$

and:

$$UIR_i(t) = (1 - E_i) \cdot g_i(t) \qquad for\ i = HLS, NTM \tag{6.8}$$

where D_{iv} is IV bolus input, $\delta(t)$ is Dirac-delta function, E is the extraction ratio and $g(t)$ is a transit time density function that is empirically described as an exponential distribution function:

$$g_{HLS}(t) = \alpha \cdot \exp(-\alpha \cdot t) \tag{6.9a}$$

$$g_{NTM}(t) = \beta \cdot \exp(-\beta \cdot t) \tag{6.9b}$$

where α and β are rate parameters.

Assuming both HLS is non-extracting, the $UIR_{HLS}(t)$ function reduces to the transit time density function ($g_{HLS}(t)$).

Equations 6.6–6.9 were conveniently converted to the equivalent first-order differential equations, which are simpler to manipulate numerically and computationally because they avoid the convolution operator. Introducing the dummy variables y_1 and y_2 where:

$$y_1 = [\, D_{iv} \cdot \delta(t) + f_{out}^{NTM}(t) + f_{out}^{TM}(t)] * \exp(-\alpha \cdot t) \tag{6.10}$$

$$y_2 = f_{out}^{HLS}(t) * \exp(-\beta \cdot t) \tag{6.11}$$

and:

$$f_{out}^{HLS}(t) = \alpha \cdot y_1 \tag{6.12}$$

$$f_{out}^{NTM}(t) = P_{NTM} \cdot (1 - E_{NTM}) \cdot \beta \cdot y_2 \tag{6.13}$$

Differentiating the convolution equations 6.10 and 6.11 with respect to time gives:

$$dy_1/dt = -\alpha \cdot y_1 + f_{out}^{NTM}(t) + f_{out}^{TM}(t) \qquad , y_1(0) = D_{iv} \tag{6.14}$$

$$dy_2/dt = -\beta \cdot y_2 + f_{out}^{HLS}(t) \qquad , y_2(0) = 0 \tag{6.15}$$

Nonlinear drug disposition through TM tissues is considered by a flow limited mass transfer model [39] integrated with receptor-mediated elimination (Figure 6.2, Panel B). The TM tissues are divided into extracellular (blood + interstitial) and intracellular spaces separated by cellular membrane (assuming lack of capillary membrane resistance). The binding of free drug in the extracellular space (C_{EC}) with R to form R^* is controlled by k_{on} and k_{off}. The endocytosis of R^* to the intracellular space is governed by k_{int}. The receptor turnover in the extracellular space is represented by k_{syn} and k_{deg}. The mass balance for the free drug in the extracellular space:

$$\begin{aligned} V_{EC} \cdot dC_{EC}/dt = {} & P_{TM} \cdot Q \cdot (C_{in}^{TM} - C_{out}^{TM}) \\ & - k_{on} \cdot V_{EC} \cdot R \cdot C_{EC} + k_{off} \cdot V_{EC} \cdot R^* \qquad , C_{EC}(0) = 0 \end{aligned} \tag{6.16}$$

where V_{EC} is the volume of the extracellular space, C_{in}^{TM} is the drug concentration in the arterial blood entering the TM tissues that is given by:

$$C_{in}^{TM}(t) = P_{TM} \cdot f_{out}^{HLS}(t) / (P_{TM} \cdot Q) = f_{out}^{HLS}(t) / Q \tag{6.17}$$

, C_{out}^{TM} is the drug concentration in the venous blood emerging from the TM tissues. $P_{TM} \cdot Q \cdot C_{in}^{TM}$ and $P_{TM} \cdot Q \cdot C_{out}^{TM}$ are the drug input rate, f_{in}^{TM}, and output rate, f_{out}^{TM}, respectively. The changes in *R* and *R** are as described by equations 6.3 and 6.4 in the COMP-TMD model.

Under the assumption that the TM tissues behave as a "well-stirred" structure [40], where the effluent blood is in equilibrium with the extracellular space (i.e., C_{out}^{TM} = C_{EV}), equation 6.16 becomes:

$$\begin{aligned} V_{EC} \cdot d\, C_{out}^{TM} / dt = {} & P_{TM} \cdot Q \cdot (C_{in}^{TM} - C_{out}^{TM}) \\ & - k_{on} \cdot V_{EC} \cdot R \cdot C_{out}^{TM} + k_{off} \cdot V_{EC} \cdot R^{*} \qquad , C_{out}^{TM}(0) = 0 \end{aligned} \tag{6.18}$$

Finally, the total plasma concentration that is measured in venous blood (C_{out}^{tot}) is given by:

$$C_{out}^{tot}(t) = (f_{out}^{NTM}(t) + f_{out}^{TM}(t)) / Q \tag{6.19}$$

6.2.3. Moment analysis of linearized COMP-TMD model

Equations 6.1 and 6.4 can be written as:

$$\begin{aligned} dC/dt = {} & -(k_{el} + k_{pt}) \cdot C + k_{tp} \cdot A_T / V - k_{on} \cdot (R_{tot} - R^{*}) \cdot C + k_{off} \cdot R^{*} \\ & , C(0) = D_{iv} / V \end{aligned} \tag{6.20}$$

$$dR^{*}/dt = -(k_{off} + k_{\text{int}}) \cdot R^{*} + k_{on} \cdot (R_{tot} - R^{*}) \cdot C \qquad , R^{*}(0) = 0 \tag{6.21}$$

where R_{tot} is the total receptor (*R*+*R**). Under linear, non-saturable binding conditions, when *C* <<< *R*, few occupancies happen resulting in *R** <<< R_{tot} and $R_{tot} \approx R_{ss}$. Accordingly, equations 6.20 and 6.21 reduce to:

$$dC/dt = -(k_{el} + k_{pt}) \cdot C + k_{tp} \cdot A_T / V - k_{on} \cdot R_{ss} \cdot C + k_{off} \cdot R^{*} \quad , C(0) = D_{iv} / V \tag{6.22}$$

$$dR^*/dt = -(k_{off} + k_{\text{int}}) \cdot R^* + k_{on} \cdot R_{ss} \cdot C \qquad , R^*(t=0) = 0 \tag{6.23}$$

Solving equations 6.22, 6.23, and 6.2 for the free drug plasma concentration using Laplace transform yields:

$$C(s) = \frac{D_{iv}}{V} \cdot \frac{1}{k_{el} + A + B} \tag{6.24a}$$

where:

$$A = \frac{k_{on} \cdot R_{ss} \cdot (s + k_{\text{int}})}{s + k_{\text{int}} + k_{off}} \tag{6.24b}$$

$$B = \frac{s \cdot (s + k_{pt} + k_{tp})}{s + k_{tp}} \tag{6.24c}$$

The AUC and AUMC/AUC for the linearized compartmental model are:

$$AUC = \lim_{s \to 0} C(s) = \frac{D_{iv}}{V} \cdot \frac{k_{\text{int}} + k_{off}}{k_{el} \cdot (k_{\text{int}} + k_{off}) + k_{\text{int}} \cdot k_{on} \cdot R_{ss}} \tag{6.25}$$

$$\frac{AUMC}{AUC} = \frac{-\lim_{s \to 0} (dC(s)/ds)}{\lim_{s \to 0} C(s)} = \frac{(k_{\text{int}} + k_{off})^2 \cdot (k_{pt} + k_{tp}) + k_{off} \cdot k_{on} \cdot R_{ss} \cdot k_{tp}}{k_{tp} \cdot (k_{\text{int}} + k_{off}) \cdot [k_{el} \cdot (k_{\text{int}} + k_{off}) + k_{\text{int}} \cdot k_{on} \cdot R_{ss}]} \tag{6.26}$$

When $k_{el} = 0$, equations 6.25 and 6.26 reduce to:

$$AUC = \frac{D_{iv}}{V} \cdot \frac{k_{\text{int}} + k_{off}}{k_{\text{int}} \cdot k_{on} \cdot R_{ss}} \tag{6.27}$$

$$\frac{AUMC}{AUC} = \frac{(k_{\text{int}} + k_{off})^2 \cdot (k_{pt} + k_{tp}) + k_{off} \cdot k_{on} \cdot R_{ss} \cdot k_{tp}}{k_{tp} \cdot (k_{\text{int}} + k_{off}) \cdot k_{\text{int}} \cdot k_{on} \cdot R_{ss}} \tag{6.28}$$

6.2.4. Moment analysis of linearized REC-TMD model

Under linear conditions, drug disposition through TM tissues can be described by:

$$\begin{aligned} V_{EC} \cdot d\,C_{out}^{TM}/dt = {} & P_{TM} \cdot Q \cdot (C_{in}^{TM} - C_{out}^{TM}) \\ & - k_{on} \cdot V_{EC} \cdot R_{ss} \cdot C_{out}^{TM} + k_{off} \cdot V_{EC} \cdot R^* \qquad , C_{out}^{TM}(0) = 0 \end{aligned} \tag{6.29}$$

$$dR^*/dt = -(k_{off} + k_{\text{int}}) \cdot R^* + k_{on} \cdot R_{ss} \cdot C_{out}^{TM} \tag{6.30}$$

The solution of equations 6.29 and 6.30 for the output drug concentration from the TM tissues in the Laplace domain is given by:

$$C_{out}^{TM}(s) = \frac{A}{s + A + B} \cdot C_{in}^{TM}(s) \tag{6.31}$$

where:

$$A = \frac{P_{TM} \cdot Q}{V_{EC}} \tag{6.31a}$$

$$B = k_{on} \cdot R_{ss} - \frac{k_{off} \cdot k_{on} \cdot R_{ss}}{s + k_{\text{int}} + k_{off}} \tag{6.31b}$$

Rearranging equation 6.31:

$$UIR_{TM}(s) = \frac{C_{out}^{TM}(s)}{C_{in}^{TM}(s)} = \frac{A}{s + A + B} \tag{6.32}$$

For a closed-loop recirculation model with same input and sampling sites, the response in the Laplace domain is described by [96]:

$$C_{out}^{tot}(s) = \frac{D_{iv}}{Q} \cdot \frac{UIR_{sp}(s)}{1 - UIR_{sp}(s)} \tag{6.33}$$

where $UIR_{sp}(s)$ is the laplace transform of the single-pass unit impulse response. For the recirculation model presented in Figure 6.2A:

$$UIR_{sp}(s) = UIR_{HLS}(s) \cdot [P_{NTM} \cdot UIR_{NTM}(s) + P_{TM} \cdot UIR_{TM}(s)] \tag{6.34}$$

The AUC and AUMC/AUC for the linearized recirculation model are:

$$AUC = \lim_{s \to 0} C_{out}^{tot}(s) = \frac{D_{iv}}{Q} \cdot \frac{1 - (P_{NTM} \cdot E_{NTM} + P_{TM} \cdot E_{TM})}{P_{NTM} \cdot E_{NTM} + P_{TM} \cdot E_{TM}} \tag{6.35}$$

$$\frac{AUMC}{AUC} = \frac{-\lim_{s \to 0} (d\, C_{out}^{tot}(s) / ds)}{\lim_{s \to 0} C_{out}^{tot}(s)} = \frac{MTT_{HLS} + P_{NTM} \cdot MTT_{NTM} + P_{TM} \cdot MTT_{TM}}{P_{NTM} \cdot E_{NTM} + P_{TM} \cdot E_{TM}} \tag{6.36}$$

where E_{TM} is the extraction ratio from the TM tissues:

$$E_{TM} = 1 - \lim_{s \to 0} UIR_{TM}(s) = \frac{k_{\text{int}} \cdot k_{on} \cdot R_{ss} \cdot V_{EC}}{P_{TM} \cdot Q \cdot (k_{\text{int}} + k_{off}) + k_{\text{int}} \cdot k_{on} \cdot R_{ss} \cdot V_{EC}} \tag{6.37}$$

, and *MTT* denotes the mean transit time:

$$MTT_{HLS} = -\lim_{s \to 0} (d\, g_{HLS}(s)/ds) = \frac{1}{\alpha} \tag{6.38}$$

$$MTT_{NTM} = -\lim_{s \to 0} (d\, g_{NTM}(s)/ds) = \frac{1}{\beta} \tag{6.39}$$

$$\begin{aligned} MTT_{TM} &= \frac{-\lim_{s \to 0} (d\, UIR_{TM}(s)/ds)}{\lim_{s \to 0} UIR_{TM}(s)} \\ &= \frac{[(k_{\text{int}} + k_{off})^2 + k_{off} \cdot k_{on} \cdot R_{ss}] \cdot V_{EC}}{(k_{\text{int}} + k_{off}) \cdot [P_{TM} \cdot Q \cdot (k_{\text{int}} + k_{off}) + k_{\text{int}} \cdot k_{on} \cdot R_{ss} \cdot V_{EC}]} \end{aligned} \tag{6.40}$$

When P_{TM} = 1, equations 6.35 and 6.36 reduce to:

$$AUC = \frac{D_{iv}}{V_{EC}} \cdot \frac{k_{\text{int}} + k_{off}}{k_{\text{int}} \cdot k_{on} \cdot R_{ss}} \tag{6.41}$$

$$\frac{AUMC}{AUC} = \frac{(k_{\text{int}} + k_{off})^2 \cdot (Q/V_{EC} + \alpha) + k_{off} \cdot k_{on} \cdot R_{ss} \cdot \alpha}{\alpha \cdot (k_{\text{int}} + k_{off}) \cdot k_{\text{int}} \cdot k_{on} \cdot R_{ss}} + \frac{1}{\alpha} \tag{6.42}$$

6.3. Methods

6.3.1. Simulations

The effect of the host structure (compartmental or recirculation) on drug and receptor kinetics was studied at different $C_{input}(0)/K_D$ ratios (1,5,10,50, and 100), where $K_D = k_{off}/k_{on}$, $C_{input}(0) = C(0)$ in the COMP-TMD model and $C_{input}(0) = C_{in}^{TM}(0)$ in the REC-TMD model. $C_{in}^{TM}(0)$ was calculated for an IV bolus external input (D_{iv}) from Eqs. 6.6, 6.8, 6.9a, and 6.17 to be:

$$C_{in}^{TM}(0) = D_{iv} \cdot \alpha / Q \tag{6.43}$$

The values of drug–receptor binding as well as drug–receptor complex internalization parameters were set to recombinant human erythropoietin (EPO)-EPOR parameter values previously reported from an *in vitro* trafficking study in cultured Ba/F3 and UT-7/EPO cells [113]. The EPOR turnover parameter values were obtained from a previous intravenous PK study in humans [206]. The receptor-related parameter values were: EPOR production rate constant (k_{syn}), 9.141 pmole·h^{-1}; EPOR degradation rate constant (k_{deg}), 0.079 h^{-1}; EPO/EPOR association rate constant (k_{on}), 0.03 pmole^{-1}· h^{-1}; EPO/EPOR dissociation rate constant (k_{off}), 1.74 h^{-1}; and EPO/EPOR complex internalization rate constant (k_{int}), 3.6 h^{-1}.

In the COMP-TMD model, the receptor-independent parameter values were set to EPO values in humans [206]. The parameter values were: first-order elimination rate constant (k_{el}), 0.106 h^{-1}; plasma-to-tissue distribution rate constant (k_{pt}), 0.064 h^{-1}; tissue-to-plasma distribution rate constant (k_{tp}), 0.123 h^{-1}; and central volume of distribution (V), 0.032 L· kg^{-1}. In the REC-TMD model, parameters Q and P_{TM} were fixed to human cardiac output and fraction of blood flow to bone marrow previously reported in the literature (Q, 4.5 L· h^{-1}·kg^{-1}; and P_{TM}, 0.092) [48, 207]. The volume of the extracellular space in the TM tissues, V_{EC}, was set to 0.257 L which is equivalent to 43% of red marrow water in a human weighting 70 kg [208]. The percentage was based on the fraction of the extracellular fluid to total body water [208]. The HLS transit time density function parameter, α, was fixed to 140.6 h^{-1} in order to equate $C(0)$ in the COMP-TMD model with $C_{in}^{TM}(0)$ in the REC-TMD model. The NTM tissues transit time density function parameter, β, was set to an arbitrary value of 2.4 h^{-1}. Selection of β to be much smaller than α mimics the physiology, where it seems logical to expect that drug

distribution through the systemic circulation is slower than that through the pulmonary circulation. The NTM tissues extraction ratio, E_{NTM}, was fixed to 0.001.This value was selected to equate the non-receptor mediated elimination clearance in both the COMP-TMD and REC-TMD models (i.e., $k_{el} \cdot V = P_{TM} \cdot Q \cdot E_{NTM}$). The average human body weight in the simulations was taken to be 70 kg.

Simulations were also performed at perturbed values for k_{el}, k_{pt}, and k_{tp} in COMP-TMD model; and P_{TM}, V_{EC}, and α in REC-TMD model. Dependence of the maximal plasma concentration, C_{max}, predicted by REC-TMD on Q, V_{EC}, α, R_{ss}, K_D, and k_{int} was also simulated at $Cinput(0)/K_D$ ratio of 10.

All simulations were performed using WINFUNFIT, an interactive Microsoft Windows program evolved from the general nonlinear regression program FUNFIT [172].

6.3.2. Parameter estimation analysis

The approach of Dutta and Ebling [209], with modifications, was used to investigate the estimation accuracy and precision of COMP-TMD and REC-TMD model parameters. For each model, noisy individual datasets were generated using $SIMULATION block in NONMEM (version VI, level 2) [210]. The models were numerically solved using the stiff differential equation solver ADVAN8. The parameter true values were V = 2.24 L; k_{el} = 0.106 h^{-1}; k_{pt} = 0.064 h^{-1}; k_{tp} = 0.123 h^{-1}; Q = 312 L/h; P_{TM} = 0.9; VEC = 2.24 L; E_{NTM} = 0.007; α = 140 h^{-1}; β = 14 h^{-1}; k_{syn} = 9.141 pmol/h; k_{deg} = 0.079 h^{-1}; k_{on} = 0.03 1/pmol/h; k_{off} = 1.74 h^{-1}; and k_{int} = 3.6 h^{-1}. The pharmacokinetic design used was a dose-escalation study with the administered doses in each model set to achieve $C_{input}(0)/K_D$ ratios of 1, 5, 10, 50, and 100. A proportional variance model with

10% error was used in data construction. For each structural model (COMP-TMD or REC-TMD), a total of 1,000 datasets were generated. Simulations of COMP-TMD and REC-TMD models were performed at 9, and 8 time points, respectively, between 0 and 100 hours. The number of time points in each model is equivalent to the number of parameters to be estimated (see next paragraph). For a given structural model, the sampling times were selected by maximization of D-criterion (determinant of Fisher information matrix) using PROC MODEL and PROC OPTEX in SAS® (version 9.2, SAS Institute Inc., Cary, NC, USA) according to the implementation of Atkinson et al [211]. The sampling times for both models at each dosing level are listed in Table 6.1. Optimization of sampling times was performed to reduce unintentional bias introduced by selecting times that increase sensitivity to parameters of one of the models at expense of the other.

All individual datasets simulated from a given structural model were fitted by the corresponding model to give estimates of the model parameters (COMP-TMD: k_{el}, k_{pt}, k_{tp}, V, k_{syn}, k_{deg}, k_{on}, k_{off}, and k_{int}; and REC-TMD: α, β, E_{NTM}, k_{syn}, k_{deg}, k_{on}, k_{off}, and k_{int}). All fittings and parameter estimations were performed using the extended least squares method in NONMEM VI [212]. The initial estimates for the parameters were chosen at random from a uniform distribution of ±25% of the true parameter value.

The parameter estimates of the successful runs for the COMP-TMD and REC-TMD models were analyzed for accuracy and precision. The percentage bias (inaccuracy) was assessed by:

$$\%Bias = \frac{MEAN(estimate) - true}{true} \cdot 100 \qquad (6.44)$$

with 95% asymptotic confidence interval:

$$95\%\,C.I. = \%Bias \pm 1.96 \cdot SE_{bias} \tag{6.45}$$

where SE_{bias} is the standard error of the bias:

$$SE_{bias} = \frac{SD(estimate)}{\sqrt{N} \cdot true} \cdot 100 \tag{6.46}$$

where N is the number of converging runs. The percentage relative standard error of the estimate $(\%RSE_{est})$,

$$\%RSE_{est} = \frac{SD(estimate)}{\sqrt{N} \cdot MEAN(estimate)} \cdot 100 \tag{6.47}$$

was used as a measure for estimation imprecision.

6.4. Results and discussion

Although COMP-TMD and REC-TMD models host the same receptor-based model, they adopt different structural assumptions: 1) The COMP-TMD model is an open-system, while the REC-TMD model is a closed-system, 2) The COMP-TMD model assumes inter-compartmental transport that is mediated by a first-order process (represented by the parameters k_{pt}, and k_{tp}), while the REC-TMD model assumes convective inter-tissue transfer that is mediated via the vascular network (represented by the parameters Q, P_{TM}, and P_{NTM}), 3) The COMP-TMD model assumes that drug molecules distribute instantly and homogenously upon entering the compartment, while the REC-TMD model uses transit time distribution function to reflect delayed and heterogeneous distribution through HLS and NTM tissues, 4) Non-receptor mediated elimination in COMP-TMD model is represented by a first-order process through the parameter k_{el}, while in the REC-TMD model it is based on the extraction ratio E_{NTM} and blood flow-dependent clearance, $P_{NTM} \cdot Q \cdot E_{NTM}$, 5) Although receptor-mediated elimination in both models is dependent on processes representing drug-receptor

association, k_{on}, dissociation, k_{off}, and endocytosis, k_{int}; free receptor synthesis, k_{syn}, and degradation, k_{deg}; as well as on interaction site volume, V and V_{EC} in COMP-TMD and REC-TMD models, respectively, it also depends on blood flow in case of the recirculation model (as it is evident from the derivation of the extraction ratio of the TM tissues, E_{TM}, for the linearized form of the REC-TMD model, equation 37). Our analysis aims at investigating the influence of the different hosting structures on receptor and drug concentration-time profiles; deriving the conditions at which such profiles coincide between the two models; and assessing the quality of parameter estimations in both structures.

6.4.1. Simulations

The TMD model allows prediction of the time courses of free (R) and bound (R^*) receptor concentrations as shown in Figures 6.3 and 6.4. Both the COMP-TMD and REC-TMD models showed an initial rapid drop in R levels followed by gradual recovery to the initial steady-state condition (Figure 6.3). The concentration–time profiles of R^* demonstrated an initial rapid rise followed by a secondary sharp then slow decline to very small value (Figure 6.4).

Both the compartmental and recirculation models exhibited dose-dependent events, with the extent of the R level drop (correspondingly, the rise in R^* level), and the duration of the R level recovery (correspondingly, the decline in R^* level) were increased in accordance with increased dosing levels. In general, the recovery and decline periods of R and R^* levels, respectively, were significantly longer in the recirculation model than in the compartmental model (~ 5, 10, 11,14, and 15 times for $C_{input}(0)/K_D$ ratios of 1,5,10,50, and 100, respectively).

The initial drop in the free receptor (R) level (Figure 6.3) that correlates with the initial rise in the bound receptor (R^*) level (Figure 6.4) is dictated by the second-order binding process which takes place with a rate $k_{on} \cdot C$ in the COMP-TMD, and $k_{on} \cdot C_{out}^{TM}$ in the REC-TMD model. The binding process is balanced by the first-order dissociation process, $k_{off} \cdot R^*$, that result in the recovery for R (Figure 6.3) and the decline for R^* (Figure 6.4). The duration of this equilibrium process is controlled by the time the free receptors are converted to their bound form (i.e. the time required for the free receptors to become saturated), which depends on the drug level relative to its equilibrium dissociation constant.

Subsequent to the equilibrium process, the R level is restored to the initial baseline steady state (Figure 6.3) as a result of the constant receptor production process, k_{syn}, at a rate that is determined by the receptor elimination constant k_{deg}. The decline in R^* level to 0 following equilibrium (Figure 6.4) is predominated by an internalization process, $k_{int} \cdot R^*$.

Figure 6.5 shows the free drug plasma time-concentration profiles as predicted by the COMP-TMD and REC-TMD models. In the compartmental model, a biphasic decline can be seen, while a rapid increase from 0 to maximum concentration followed by a slow decline can be observed for the recirculation model. Corresponding to the longer R recovery and R^* decline periods for the recirculatory model compared to the compartmental model, the drug residence time in the former was ~ 250, 50, 40,34, and 36 folds larger for $C_{input}(0)/K_D$ ratios of 1,5,10,50, and 100, respectively. However, this increase in the residence time was accompanied by ~ 50 folds smaller maximal

concentration for the REC-TMD versus the COMP-TMD model at the corresponding doses.

To understand the reason(s) behind the prolonged receptor activity period and drug residence time observed upon simulation of REC-TMD components using physiologically plausible values for Q, P_{TM}, V_{EC}, α, and β; values obtained from *in vitro* experiments for k_{on}, k_{off}, and k_{int}; and values obtained from COMP-TMD model for E_{NTM}, k_{syn} and k_{deg}, the statistical moments of the linearized forms of both models were derived. Comparison of the COMP-TMD model zero-moment (equations 6.25 and 6.27) with that of the REC-TMD model (equations 6.35, 6.37, and 6.41) suggests equal clearance if: 1) Elimination rate constant in the compartmental model, k_{el}, is equal to zero, 2) Fraction of blood flow to TM tissues in the recirculation model, P_{TM}, is equal to 1, and 3) Volume of central compartment in the COMP-TMD model, V, is equal to volume of the TM extracellular space in the REC-TMD model, V_{EC}. These findings indicate that a well-perfused target tissues, negligible non-receptor mediated clearance ($k_{el} \cdot V$ and $P_{NTM} \cdot Q \cdot E_{NTM}$ in COMP-TMD and REC-TMD models, respectively), and extracellular volume of distribution that approximates drug initial volume of distribution are essential for comparable drug and receptor profiles. Besides the fore mentioned conditions, 1) Equal plasma-to-tissue distribution constant, k_{pt}, and cardiac output (Q)/V_{EC}, 2) Equal tissue-to-plasma distribution constant, k_{tp}, and HLS distribution constant, α, in COMP-TMD and REC-TMD models, respectively, and 3) $\alpha \rightarrow \infty$ (which implies that drug distribution through the HLS is very rapid and equilibrium between venous and arterial blood is fast) are required for the mean residence times calculated according to the compartmental

(equations 6.26 and 6.28) and recirculation (equations 6.36, 6.37-6.40, and 6.42) models to become identical.

To determine if the linearly derived conditions apply to the non-linear case, the drug and receptor time-concentration profiles were simulated using the conditions identified by the moment analysis (Figure 6.6, Lower Panel). The identical R and R^* and the almost identical C and C_{out}^{tot} concentrations between the COMP-TMD and REC-TMD models following administration of a large bolus dose indicate the validity of these conditions when drug-receptor binding is saturable and suggests that the difference in receptor activity period and drug residence time between the two models (Figure 6.6, Upper Panel) is impacted by values of non-receptor related parameters, namely, k_{el}, k_{pt}, k_{tp}, P_{TM}, Q, α, β, E_{NTM}, and V_{EC} rather than dose- or time-dependent events. However, using parameter values that force linear clearance and mean residence time to be equal between the two models, the only difference that can be observed between drug plasma concentrations is during the first few minutes where maximal concentrations (C_{max}) predicted by the compartmental model is still larger than that of the recirculation model (Figure 6.6, Lower Panel).

Figure 6.7, Upper Panel shows the dependence of C_{max} in the REC-TMD model on Q, V_{EC}, and α. Increasing Q decreases C_{max} suggesting better agreement between the compartmental and recirculation models in lower mammals such as rodents than in humans. Since C_{max} decreases by increasing V_{EC}, closer C_{max} values are expected when solid mass of the target tissue is much larger than its water content. Rapid equilibrium between venous and arterial blood drug concentrations is not only needed for close mean

residence time between the two models, but also for higher REC-TMD C_{max} values as suggested by the increase in C_{max} with increased α.

Unlike the compartmental model where C_{max} is independent of receptor-related parameters, C_{max} in the recirculation model is affected by receptor-mediated processes since it is reached after the drug's first passage through the system. Free receptor concentration determines the capacity of receptor-mediated elimination process, the larger the R, the greater the rate of elimination. The uptake rate of the drug by receptors is determined by the equilibrium dissociation constant where a high K_D value indicates either slow association rate with and/or fast dissociation rate from the receptors, and hence leads to reduced receptor-mediated elimination rate. The parameter k_{int} lumps the processes of internalization and degradation together. Slow internalization of the drug/receptor complex to the intracellular space reduces drug elimination by increasing the probability of drug dissociation into the medium; slow degradation in lysosomes overcomes elimination by increasing the chances of the complex to be re-secreted, intact, to the cell surface. The previous facts explain the increase in the recirculation model C_{max} with decreased R_{ss}, increased K_D, and reduced k_{int} values (Figure 6.7, Lower Panel). However, the REC-TMD model parameters can be ranked according to the relative change in C_{max} value caused by a 5% relative change in parameter value as follows: $V_{EC} > Q > \alpha > R_{ss} > K_D > k_{int}$, and the influence of k_{int} was minute (< 0.01%).

Erythropoietin (EPO) promotes the proliferation and differentiation of Bone marrow (BM) erythroid progenitor cells (burst-forming unit-erythroids and colony-forming unit-erythroids) by binding to EPO receptors (EPOR) on cell surface [108]. Simultaneously, degradation of the formed complex *via* internalization followed by

targeting to lysosomes is promoted by activation of EPOR [109]. In this study, using EPO/EPOR system to illustrate the differences between COMP-TMD and REC-TMD models was because of several evidences provided by previous studies that EPO exhibits TMD. Higher EPO concentrations was observed in patients with aplastic anemia (anemia due to damage of BM stem cells) than in patients with beta-thalassemia (anemia caused by reduced synthesis of hemoglobin beta chains) at the same hemoglobin concentration [112]. EPO clearance decreases with increased dosing level in rats [121] and humans [122]. In adult sheep, EPO clearance was significantly reduced by BM ablation [114], while it was not affected by hepatectomy or nephrectomy [116]. The disappearance of EPO non-linear disposition by BM ablation [123] provides strong evidence that EPO TMD is due to its saturable interaction with EPOR in the BM. Recently, EPOR mRNA level in the BM was correlated with EPO clearance [120].

6.4.2. Parameter estimation analysis

The influence of the host structure, compartmental or recirculation, on estimation accuracy and precision of receptor turnover parameters, k_{syn} and k_{deg}, drug–receptor binding parameters, k_{on} and k_{off}, and drug–receptor complex internalization parameter, k_{int}, is shown in Figure 6.8. The relative bias and imprecision of all receptor-related parameters were less than 7 and 6%, respectively, indicating good estimation efficiency using the pharmacokinetic design implemented in this study that involves simultaneous fitting to small and large IV bolus doses at D-optimized sampling times.

In the compartmental model, the true values of all receptor-related parameters were under predicted, while in the recirculation model, only k_{syn}, k_{deg}, and k_{off} were under estimated (Figure 6.8, Left Panel). Ranking of receptor parameters in the COMP-TMD

and REC-TMD models according to the farthest relative bias values is: $k_{syn} < k_{deg} < k_{on} < k_{int} < k_{off}$ (Figure 6.8, Left Panel). Overlapping relative bias intervals can be observed for the parameters k_{syn}, k_{deg}, k_{off}, and k_{int} when estimated within a compartmental or a recirculatory structure (Figure 6.8, Left Panel). Although k_{on} estimate was less than the true value in the COMP-TMD model, but greater than the true value in the REC-TMD model, the distance of the relative bias value from the zero line and the length of the bias confidence interval were almost identical between the two models (Figure 6.8, Left Panel). These findings suggest that the nature of the hosting structure does not significantly affect the estimation accuracy of the receptor-related parameters.

TMD model parameters were estimated with high precision as indicated by a maximum relative standard error, %RSE, less than 6% in both models (Figure 6.8, Right Panel). The order of receptor-related parameters in the COMP-TMD and REC-TMD models according to the %RSE values is: $k_{syn} < k_{deg} < k_{on} < k_{int} < k_{off}$ (Figure 6.8, Right Panel). Similar to estimation accuracy, precision of k_{syn}, k_{deg}, and k_{on} was comparable between both models. The difference between the two models can be observed in the %RSE of k_{off} (~1.3 folds larger for COMP-TMD) and k_{int} (~2 folds larger for REC-TMD) (Figure 6.8, Right Panel).

Figure 6.9 illustrates the estimation accuracy and precision of the compartmental model distribution parameters (k_{pt} and k_{tp}), the non-receptor-mediated elimination parameter (k_{el}), and volume of distribution (V); and that of the recirculation model transit time distribution parameters (α and β), and non-receptor-mediated extraction ratio (E_{NTM}). The estimation accuracy of V, k_{el}, α, and E_{NTM} was high (relative bias was very close to zero) (Figure 6.9, Upper Panel). The parameters k_{pt}, k_{tp}, and α were reasonably estimated

with bias percentage ranging from 1 to 4% (Figure 6.9, Upper Panel). All non-receptor related parameters were estimated with high precision as evident by a %RSE of less than 0.5% (Figure 6.9, Lower Panel).

In this analysis setting REC-TMD model E_{NTM} to be equal to 0.007 was to equate the non-receptor mediated elimination clearance in both the COMP-TMD and REC-TMD models (i.e., $k_{el} \cdot V = P_{TM} \cdot Q \cdot E_{NTM}$). Selection of the fraction of blood flow to the TM tissues, P_{TM}, to be equal to 0.9 and the volume of the extracellular space, V_{EC}, to be equal to the compartmental model volume of distribution, V, was to achieve close clearance and mean residence time between the two models (as discussed in the previous section) which provides an equal basis for comparison of the different structures.

6.5. Conclusion

Target-mediated disposition (TMD)-compartmental models can provide a suitable approximation for TMD-recirculation models under conditions of well-perfused target tissue, comparable drug initial distribution volume and target tissue extracellular volume, negligible non-receptor mediated clearance, rapid equilibrium between venous and arterial blood drug concentrations, small extracellular volume, reduced cardiac output, low receptor pool concentration, and high drug-receptor equilibrium dissociation constant. Incorporation of a TMD model in a recirculatory structure does not significantly affect the estimation accuracy and precision of receptor-related parameters. Selection between receptor-based compartmental and recirculation models shouldn't be based only on goodness-of-fit criteria but also on available information about target tissue composition and blood supply, as well as drug biochemical (e.g., *in vitro* binding

properties) and pharmacokinetic (e.g., initial volume of distribution, non-receptor mediated clearance, etc.) properties.

Table 6.1. D-optimal sampling times for COMP-TMD and REC-TMD models at different doses.

Dose (pmole/kg)	Sampling times (hours)	
	COMP-TMD	REC-TMD
2	0, 0.049, 0.179, 0.426, 0.858, 1.59, 2.81, 5.16, 12.7	0.005, 0.035, 0.121, 0.299, 0.671, 1.50, 3.27, 6.61
9	0, 0.061, 0.255, 0.693, 1.62, 3.43, 6.39, 10.3, 15.3	0.005, 0.038, 0.146, 0.433, 1.21, 3.39, 8.99, 17.5
18.6	0, 0.042, 0.181, 0.542, 1.52, 4.34, 10.2, 17.6, 25.3	0.005, 0.037, 0.136, 0.368, 0.927, 2.71, 12.5, 28.4
93	0, 0.011, 0.057, 0.463, 3.19, 10.31, 23.0, 38.5, 49.0	0.004, 0.018, 0.064, 0.178, 0.658, 20.3, 56.8, 75.6
185.6	0, 0.006, 0.033, 0.439, 3.34, 11.2, 26.3, 47.6, 60.5	0.003, 0.013, 0.043, 0.141, 0.583, 23.0, 71.5, 95.3

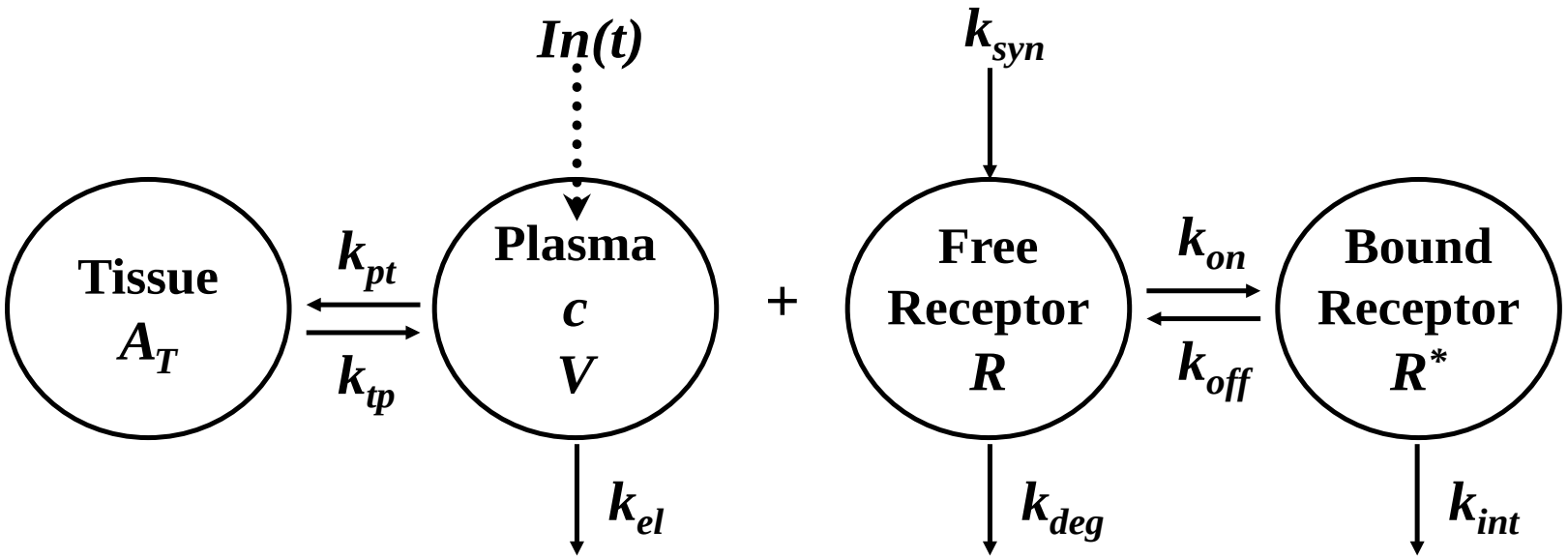

Figure 6.1. Target-mediated disposition model incorporated in a two-compartment model as proposed by Mager and Jusko. Symbols are defined in the text.

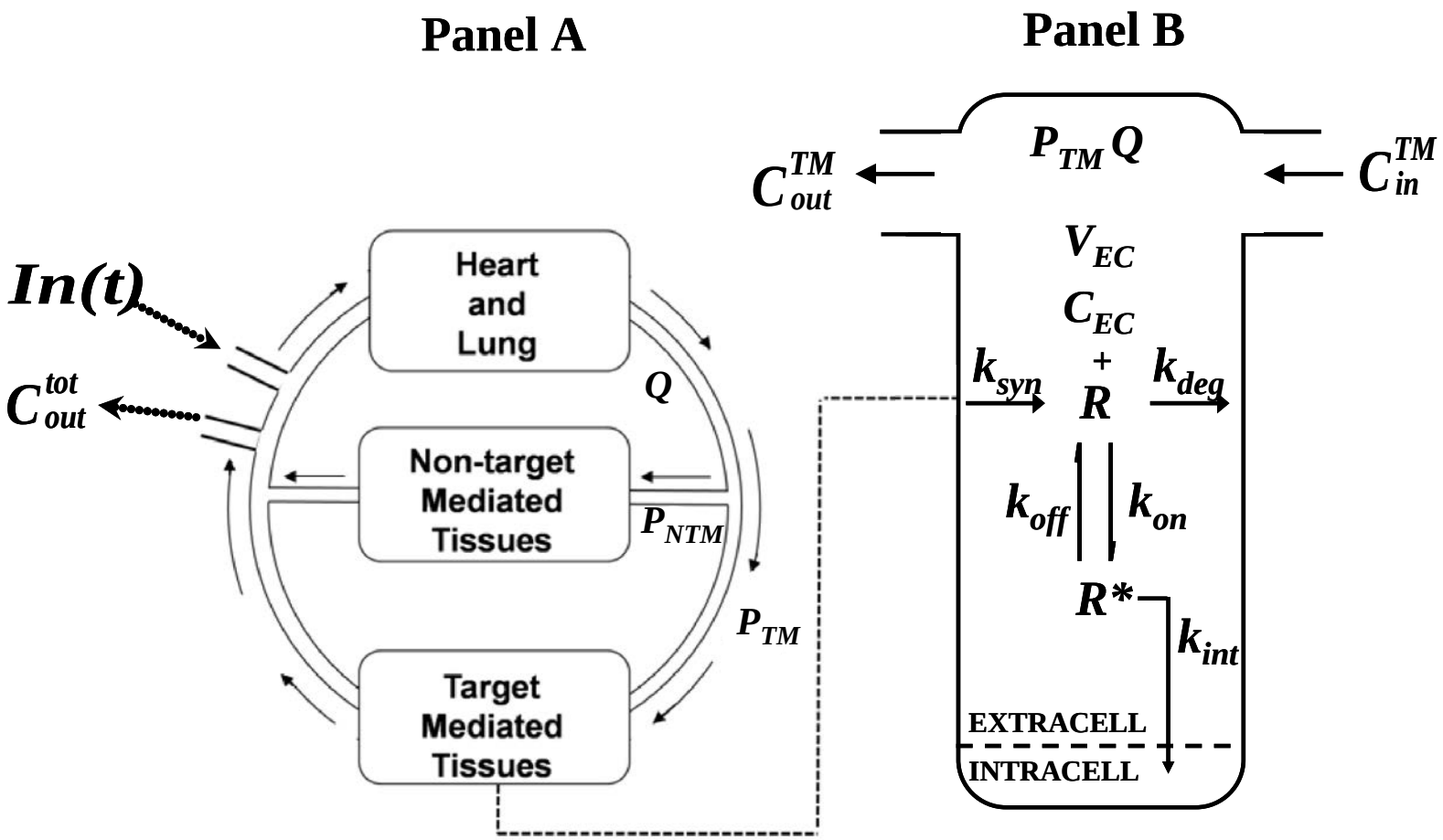

Figure 6.2. Target-mediated disposition model (Panel B) incorporated in a recirculation model (Panel A). Symbols are defined in the text.

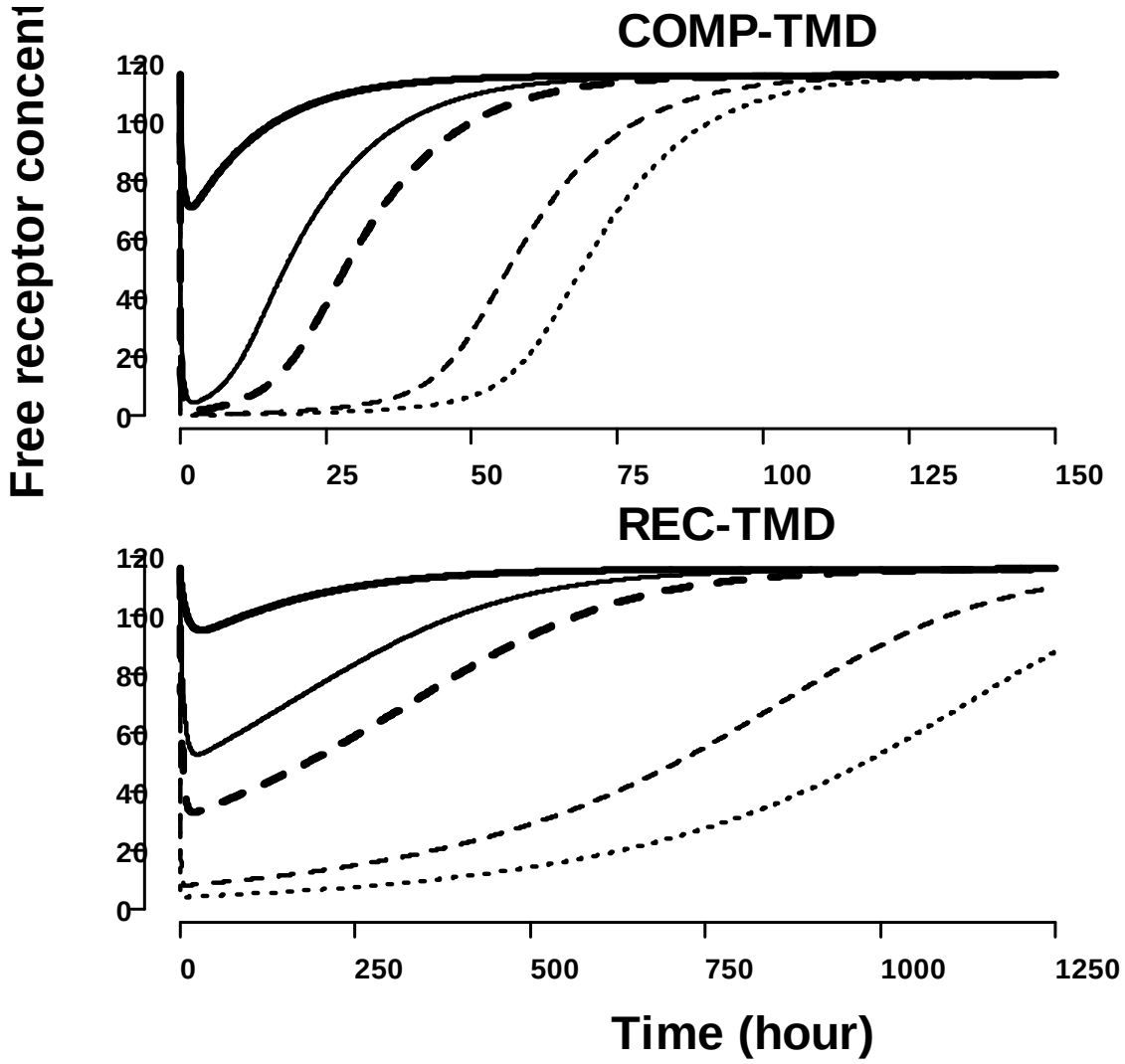

Figure 6.3. Simulated free receptor time–concentration profiles for COMP-TMD and REC-TMD models at increasing $C_{input}(0)/K_D$ ratios (bold solid: 1, regular solid: 5, bold dashed: 10, regular dashed: 50, and dotted: 100). The parameter values are V = 2.24 L; k_{el} = 0.106 h^{-1}; k_{pt} = 0.064 h^{-1}; k_{tp} = 0.123 h^{-1}; Q = 312 L/h; P_{TM} = 0.092; V_{EC} = 0.26 L; E_{NTM} = 0.001; α = 140.6 h^{-1}; β = 2.4 h^{-1}; k_{syn} = 9.141 pmol/h; k_{deg} = 0.079 h^{-1}; k_{on} = 0.03 1/pmol/h; k_{off} = 1.74 h^{-1}; and k_{int} = 3.6 h^{-1}.

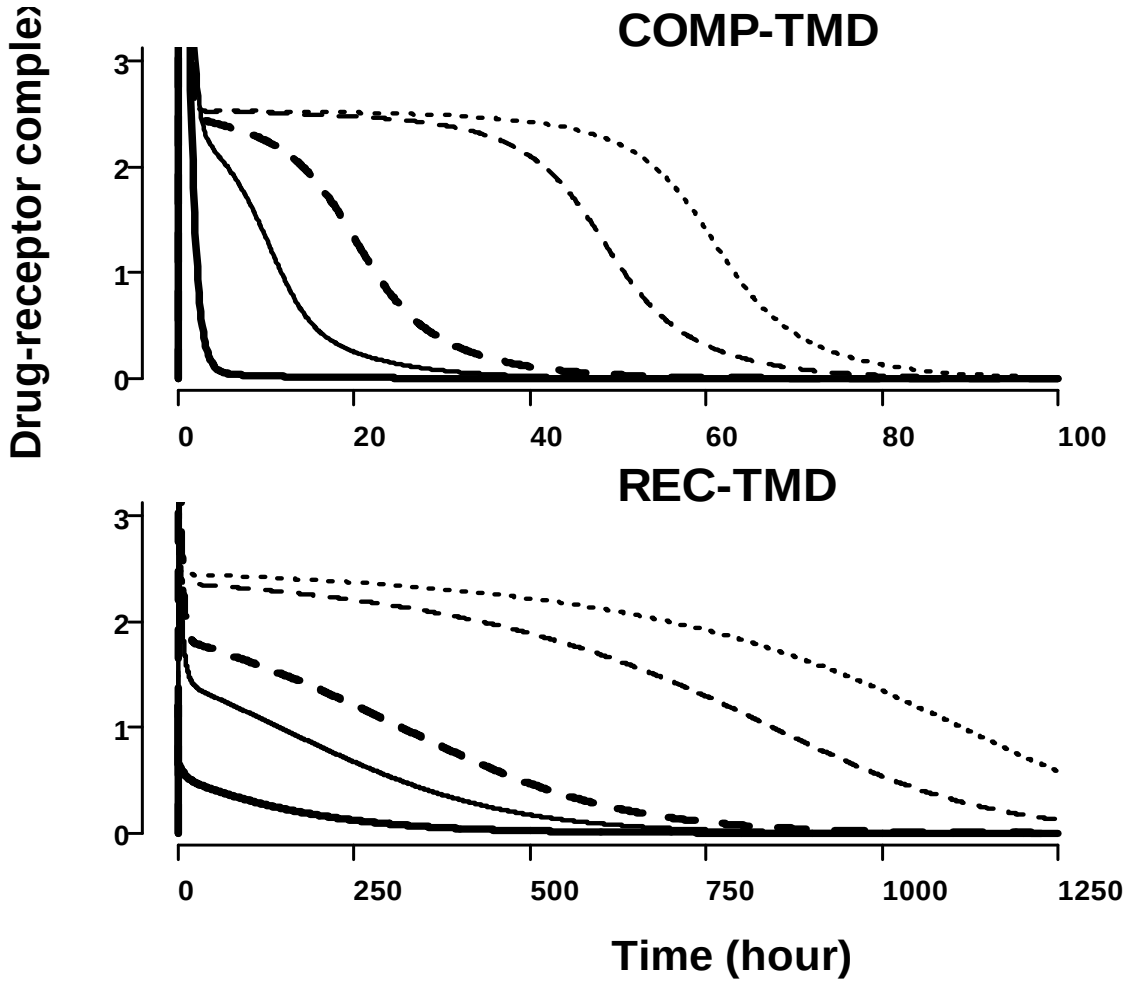

Figure 6.4. Simulated drug/receptor complex time–concentration profiles for COMP-TMD and REC-TMD models at increasing $C_{input}(0)/K_D$ ratios (bold solid: 1, regular solid: 5, bold dashed: 10, regular dashed: 50, and dotted: 100). The parameter values are V = 2.24 L; k_{el} = 0.106 h^{-1}; k_{pt} = 0.064 h^{-1}; k_{tp} = 0.123 h^{-1}; Q = 312 L/h; P_{TM} = 0.092; V_{EC} = 0.26 L; E_{NTM} = 0.001; α = 140.6 h^{-1}; β = 2.4 h^{-1}; k_{syn} = 9.141 pmol/h; k_{deg} = 0.079 h^{-1}; k_{on} = 0.03 1/pmol/h; k_{off} = 1.74 h^{-1}; and k_{int} = 3.6 h^{-1}.

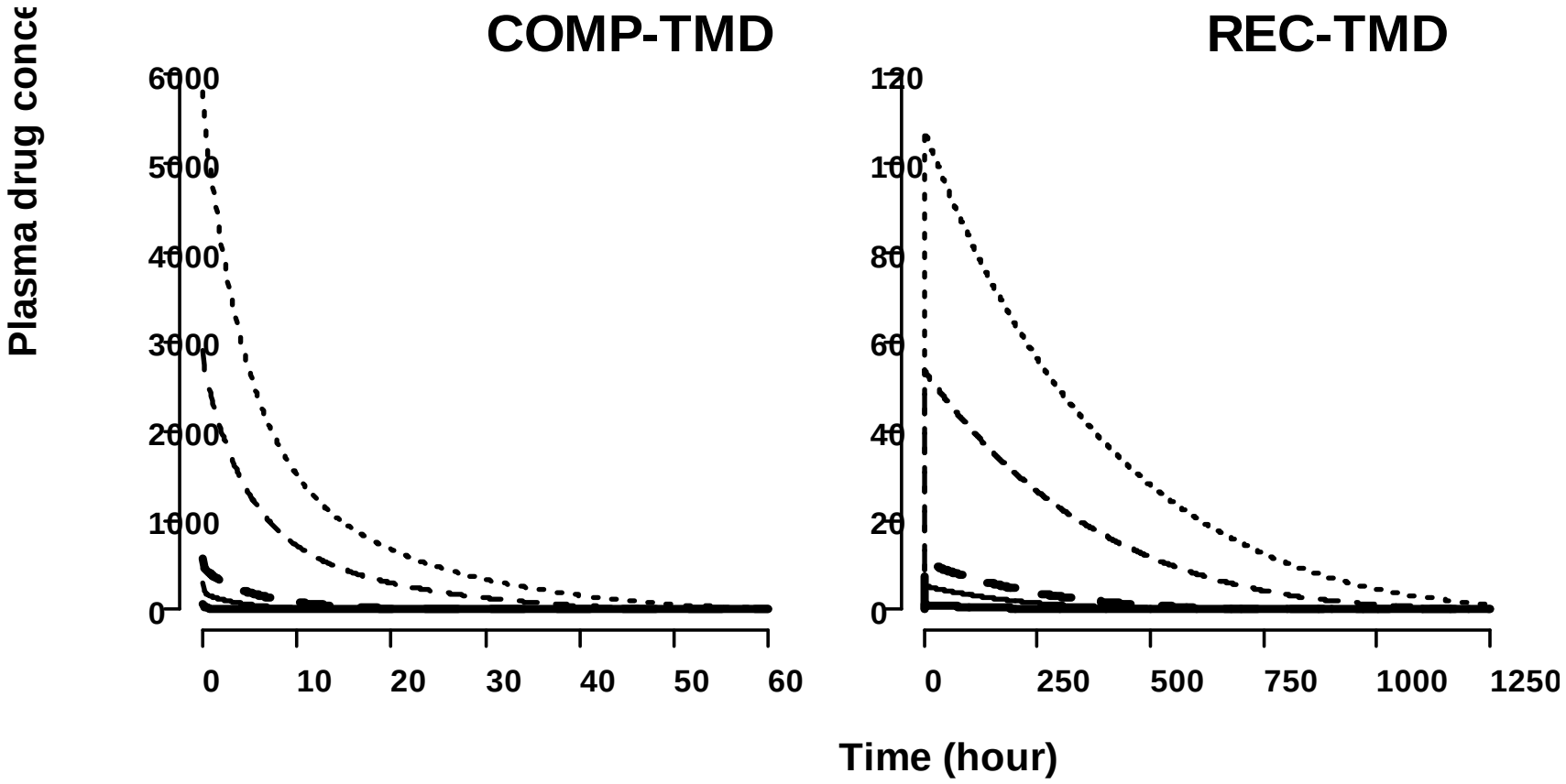

Figure 6.5. Simulated plasma drug time–concentration profiles for COMP-TMD and REC-TMD models at increasing $C_{input}(0)/K_D$ ratios (bold solid: 1, regular solid: 5, bold dashed: 10, regular dashed: 50, and dotted: 100). The parameter values are V = 2.24 L; k_{el} = 0.106 h^{-1}; k_{pt} = 0.064 h^{-1}; k_{tp} = 0.123 h^{-1}; Q = 312 L/h; P_{TM} = 0.092; V_{EC} = 0.26 L; E_{NTM} = 0.001; α = 140.6 h^{-1}; β = 2.4 h^{-1}; k_{syn} = 9.141 pmol/h; k_{deg} = 0.079 h^{-1}; k_{on} = 0.03 1/pmol/h; k_{off} = 1.74 h^{-1}; and k_{int} = 3.6 h^{-1}.

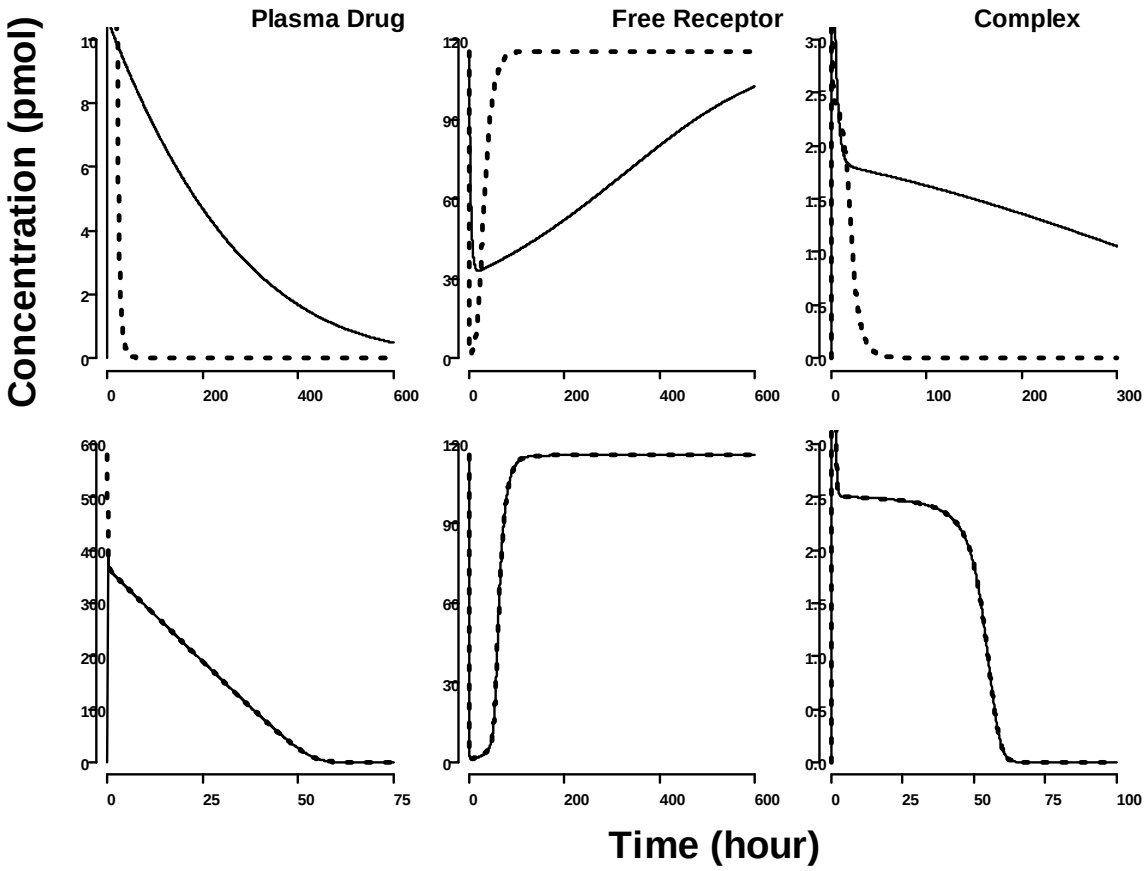

Figure 6.6. Simulated plasma drug, free receptor, and drug/receptor complex time–concentration profiles for COMP-TMD (dotted line) and REC-TMD (solid line) models at $C_{input}(0)/K_D$ ratio of 10 using two different sets of parameter values (Upper Panel: k_{el} = 0.106 h^{-1}, k_{pt} = 0.064 h^{-1}, k_{tp} = 0.123 h^{-1}, P_{TM} = 0.092, V_{EC} = 0.26 L, α = 140.6 h^{-1}; and Lower Panel: k_{el} = 0 h^{-1}, k_{pt} = 139 h^{-1}, k_{tp} = α = 500 h^{-1}, P_{TM} = 1, V_{EC} = 2.24 L). Values of other parameters are V = 2.24 L; Q = 312 L/h; E_{NTM} = 0.001; β = 2.4 h^{-1}; k_{syn} = 9.141 pmol/h; k_{deg} = 0.079 h^{-1}; k_{on} = 0.03 1/pmol/h; k_{off} = 1.74 h^{-1}; and k_{int} = 3.6 h^{-1}.

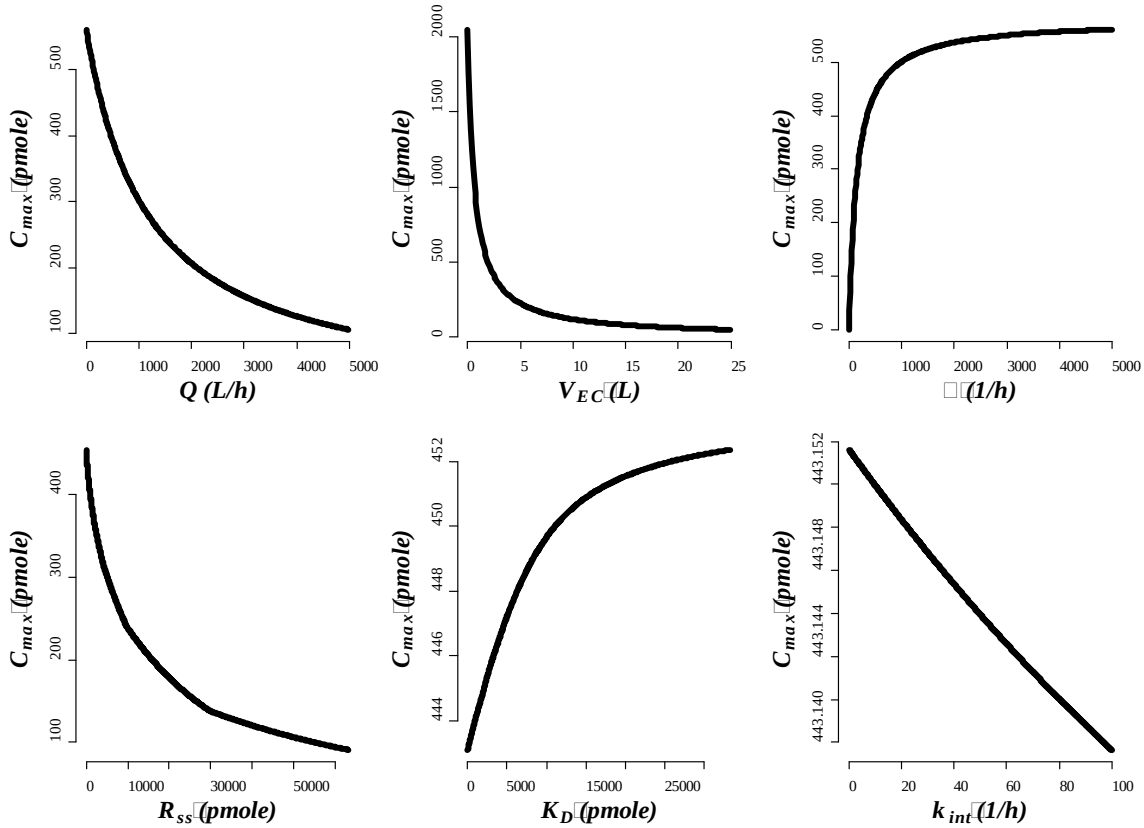

Figure 6.7. Dependence of Cmax in the REC-TMD model on Q, V_{EC}, α, Rss, K_D, and k_{int} at $C_{input}(0)/K_D$ ratio of 10. Parameter values used while investigating the parameter of interest are V_{EC} = 2.24 L; Q = 312 L/h; P_{TM} = 1; E_{NTM} = 0.001; β = 2.4 h^{-1}; k_{syn} = 9.141 pmol/h; k_{deg} = 0.079 h^{-1}; k_{on} = 0.03 1/pmol/h; k_{off} = 1.74 h^{-1}; and k_{int} = 3.6 h^{-1}.

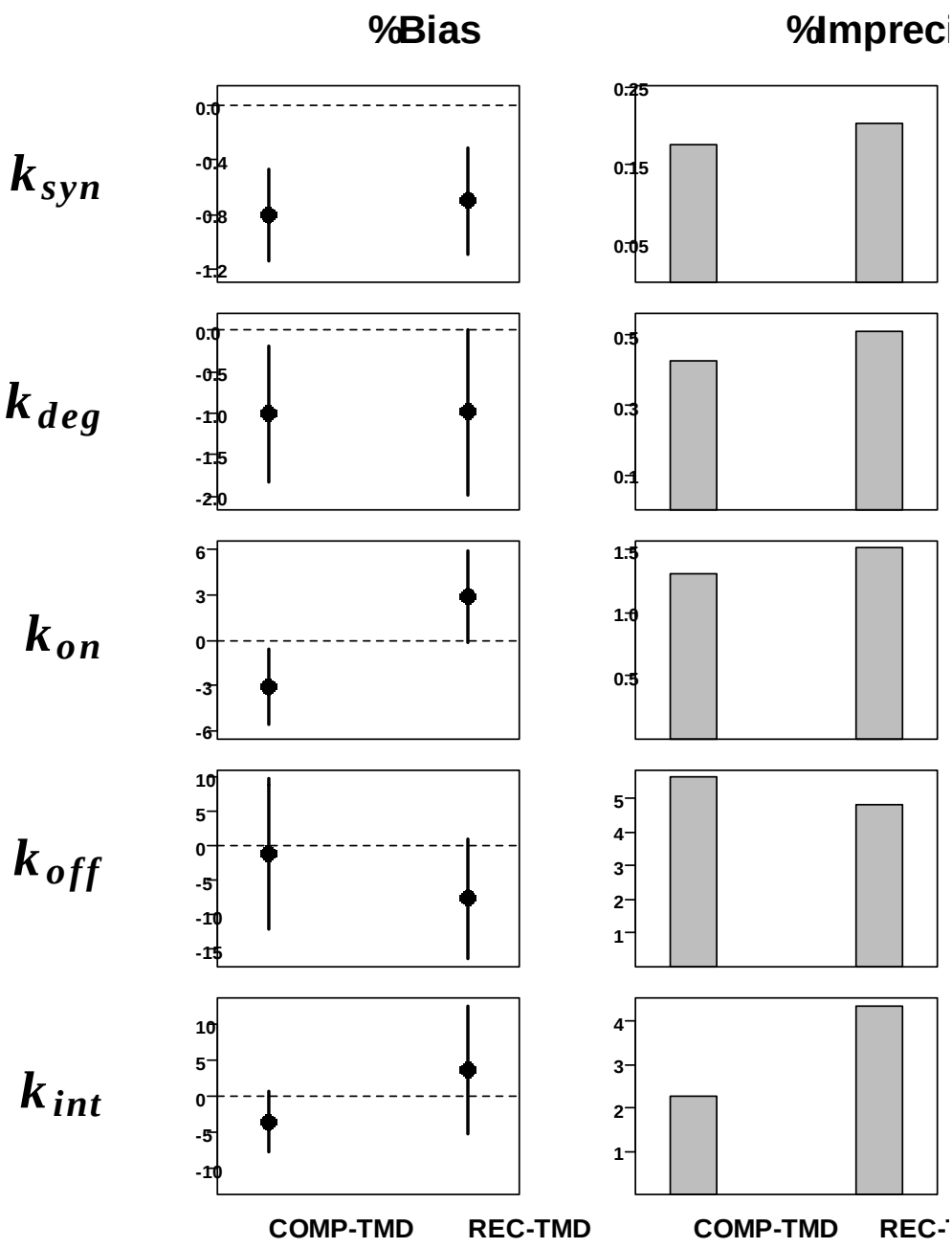

Figure 6.8. Relative estimation bias (mean and asymptotic 95% confidence interval) and imprecision of receptor-related parameters, k_{syn}, k_{deg}, k_{on}, k_{off}, and k_{int}, when incorporated in COMP-TMD and REC-TMD models. % Bias was calculated as the deviation of the mean parameter estimate from the true parameter value expressed as a percentage from the true value. % Imprecision was calculated as the relative standard error of the parameter estimate.

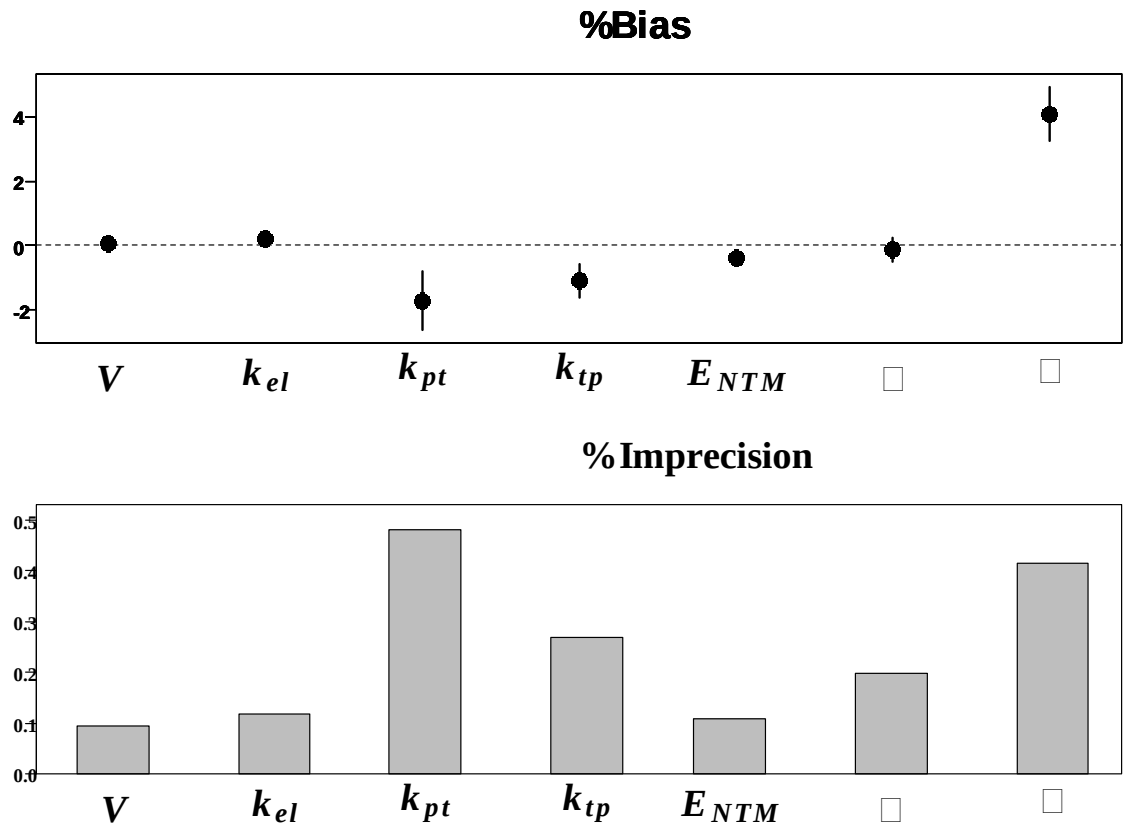

Figure 6.9. Relative estimation bias (mean and asymptotic 95% confidence interval) and imprecision of receptor-independent parameters in COMP-TMD model, V, k_{el}, k_{pt}, and k_{tp}; and in REC-TMD model, E_{NTM} , α, and β. % Bias was calculated as the deviation of the mean parameter estimate from the true parameter value expressed as a percentage from the true value. % Imprecision was calculated as the relative standard error of the parameter estimate.

CHAPTER 7. SUMMARY AND CONCLUSIONS

The overall hypothesis of this work is that physiologically based pharmacokinetic modeling is a more appropriate approach to characterize the pharmacokinetics (PK) of target mediated disposition (TMD) drugs than the abstract classical compartmental approach and can extend the applications of the receptor-based models. Based on this hypothesis, the primary objective was to develop a mechanistic modeling platform that integrates a minimal, linear system analysis based recirculation model and a receptor based model to characterize the PK properties of drugs experiencing TMD.

The research presented in this dissertation explored three main stages of model development: 1) Model formulation (Chapter 3); 2) Model application (Chapters 3 and 4); and 3) Model evaluation (Chapters 5 and 6). In Chapter 3, a receptor-based recirculation model that accounts for drug-receptor binding, receptor turnover, and drug/receptor complex endocytosis and lysosomal degradation was mathematically formulated.

In the same chapter, pharmacokinetics (PK) of Continuous Erythropoietin Receptor Activator (C.E.R.A.), a long acting recombinant human erythropoietin (EPO) analogue, was studied in adult sheep with normal and ablated bone marrow (BM) using a sensitive and specific technique, the tracer interaction method (TIM). To quantitatively assess the interaction of C.E.R.A. with EPO receptor (EPOR) populations located inside and outside the BM in adult sheep, the developed model was fitted to the tracer component of the TIM with the non-tracer component being represented as a forcing function. The developed model, together with the TIM, was able to quantitatively assess the interaction of C.E.R.A. with hematopoietic and non-hematopoietic EPOR population

in adult sheep. As predicted by the model, the hematopoietic EPOR has higher production and degradation rates, similar affinity to C.E.R.A., and it is more involved in C.E.R.A's *in vivo* elimination, compared to the non-hematopoietic population. The TIM detected a saturable interaction between C.E.R.A. and non-hematopoietic EPOR, which contradicts the known behavior of EPO.

Besides the model-based analysis of the TIM data presented in Chapter 3, a non-compartmental analysis was conducted using the non-tracer component of the TIM. The information obtained from this analysis enabled direct assessment of the effect of BM ablation on C.E.R.A. macro-parameters (e.g., clearance, half-life, volume of distribution at steady state, etc.). In agreement with the physiologic model, the non-compartmental analysis provided clear evidence that BM plays a major role in the *in vivo* elimination of C.E.R.A.

In Chapter 4, the model developed in Chapter 3 was further applied to provide a mechanism based explanation for C.E.R.A.'s slower elimination and greater erythropoietic activity *in vivo* compared to EPO. This was achieved by analyzing EPO and C.E.R.A. TIM data collected in adult sheep. As predicted by the model, the slower elimination of C.E.R.A. can be explained in terms of the following mechanisms: 1) less EPOR up-regulation induced by C.E.R.A. administration; 2) slower binding of C.E.R.A. to EPOR; and 3) reduced internalization and/or degradation rate of surface-bound C.E.R.A.. Slower C.E.R.A./EPOR complex elimination explains the greater *in vivo* erythropoiesis observed for C.E.R.A. despite its lower affinity to its receptor.

To investigate the suitability of the TIM experimental design used in Chapters 3 and 4 for estimation of the developed model parameters, a comprehensive, partial-

derivative sensitivity analysis was performed in Chapter 5. It was found that the TIM experimental setting is adequate for estimation of the physiologic model parameters. The analysis also showed that the time course of tracer plasma concentrations in the TIM design is determined by both linear distribution and receptor-related parameters before the non-tracer injection, but it is primarily determined by receptor-related parameters after the injection.

In Chapter 6, the physiological conditions at which a TMD-two compartment model approximates a minimal, linear systems analysis, TMD-recirculation model were identified by: 1) Comparing statistical moments of linearized forms of both models; and 2) Simulation of drug and receptor profiles at different IV bolus doses based on EPO/EPOR parameter values reported in literature for humans and perturbing these parameter values. It was found that conditions of well-perfused target tissue, comparable drug initial distribution volume and target tissue extracellular volume, negligible non-receptor mediated clearance, rapid equilibrium between venous and arterial blood drug concentrations, small extracellular volume, reduced cardiac output, low receptor pool concentration, and high drug-receptor equilibrium dissociation constant are necessary for equivalent compartmental and recirculation models.

In the same chapter, the influence of the host structure on parameter estimation efficiency was evaluated by simulation of 1,000 datasets for each model at D-optimized sampling times in a dose-escalation design followed by re-estimation of the parameters and calculation of estimation metrics. It was showed that incorporation of a TMD model in a recirculatory structure does not significantly affect the estimation accuracy and precision of receptor-related parameters. The main conclusion of the chapter is that

selection between receptor-based compartmental and recirculation models shouldn't be based only on goodness-of-fit criteria but also on available information about target tissue composition and blood supply, as well as drug biochemical (e.g., *in vitro* binding properties) and pharmacokinetic (e.g., initial volume of distribution, non-receptor mediated clearance properties.

APPENDIX A. WINFUNFIT CODES FOR CHAPTERS 3-5

A.1. Fortran subroutines for fitting the recirculation model to TIM

data

```
! THESE SUBROUTINES TO DEFINE THE MODEL TO BE FITTED BY
WINFUNFIT
! PROGRAMMED BY MHE IN FEBRUARY 2010

SUBROUTINE USERMODEL_ODE(T,Y,YPRIME,P,NP,IFUN)
! THIS SUBROUTINE DEFINES THE MODEL DIFFERENTIAL EQUATIONS

IMPLICIT NONE
REAL*8 :: Y(*), YPRIME(*), P(*) ,T
INTEGER  :: NP,IFUN
REAL*8 ::
Z,TD,CEST,ALPHA,BETA,GAMMA,LAMDA,R,D,Q,Ksyn,Kdeg,Kint,KD,P1,TCOLD,
X,ONE,TWO,FOUT1,FOUT2,FOUT3,ONE = 1D0, Z=0D0

ALPHA=P(1)
BETA=P(2)
LAMDA=P(3)
Ksyn=P(4)
KD=P(5)
Kdeg=P(6)
Kint=P(7)
P1=P(8)
R=P(9)
D=P(10)
Q=P(11)
TCOLD=P(12)

FOUT1=Y(1)+Y(2)
FOUT3=Y(3)+Y(4)

    IF (T .GT. TCOLD) THEN
        CALL CUBIC_GCV(TD,CEST)
        Z=DEXP(CEST)
    ELSE IF (T .LE. TCOLD) THEN
        Z= FOUT1/Q
    END IF

X=Y(5)/(KD+Z)
FOUT2=P1*(ONE-X)*FOUT1
```

```
    IF(IFUN.EQ.1)THEN
        YPRIME(1) = -ALPHA*Y(1)+ LAMDA*ALPHA*(R + FOUT2+FOUT3)
        YPRIME(2) = -BETA*Y(2)+(ONE-LAMDA)*BETA*(R + FOUT2+FOUT3)
        YPRIME(3) = -ALPHA*Y(3)+(ONE-P1)*LAMDA*ALPHA*FOUT1
        YPRIME(4) = -BETA*Y(4)+(ONE-P1)*(ONE-LAMDA)*BETA*FOUT1
        YPRIME(5) = Ksyn-Kdeg*Y(5)+(Kdeg-Kint)*X*FOUT1/Q
    ENDIF
    RETURN
    END


SUBROUTINE USERMODEL_ODE_JACOBIAN (T,Y,DFDT,DFDY,N,P,NP,IFUN)
! THIS SUBROUTINE IS NECESSARY FOR SOLVING STIFF DIFFERENTIAL
EQUATIONS
! THIS SUBROUTINE DEFINES THE PARTIAL DERIVATIVE OF EACH
DIFFERENTIAL EQUATION WITH RESPECT TO TIME AND EACH Y VARIABLE

 IMPLICIT NONE
 INTEGER, INTENT(IN)::N,NP,IFUN
 DOUBLE PRECISION, INTENT(IN)::T
 DOUBLE PRECISION,DIMENSION(N), INTENT (IN)::Y
 DOUBLE PRECISION,DIMENSION(N),INTENT(OUT)::DFDT
 DOUBLE PRECISION,DIMENSION(N,N),INTENT(OUT)::DFDY
 DOUBLE PRECISION,DIMENSION(NP),INTENT(IN)::P
 DOUBLE PRECISION,PARAMETER::ZERO=0D0,ONE=1D0
 DOUBLE PRECISION ::
Z,TD,CEST,ALPHA,BETA,GAMMA,LAMDA,R,D,Q,Ksyn,Kdeg,Kint,KD,P1,TCOLD,
X

ALPHA=P(1)
BETA=P(2)
LAMDA=P(3)
Ksyn=P(4)
KD=P(5)
Kdeg=P(6)
Kint=P(7)
P1=P(8)
R=P(9)
D=P(10)
Q=P(11)
TCOLD=P(12)

 IF(IFUN.EQ.1)THEN
        DFDT(1)=ZERO
        DFDT(2)=ZERO
        DFDT(3)=ZERO
```

```
        DFDT(4)=ZERO
        DFDT(5)=ZERO

IF (T .GT. TCOLD) THEN
                CALL CUBIC_GCV(TD,CEST)
                Z=DEXP(CEST)
                X= ONE/(KD+Z)

                DFDY(1,1)=-ALPHA+LAMDA*ALPHA*P1-
LAMDA*ALPHA*P1*Y(5)*X
                DFDY(1,2)=LAMDA*ALPHA*P1-LAMDA*ALPHA*P1*Y(5)*X
                DFDY(1,5)=-LAMDA*ALPHA*P1*(Y(1)+Y(2))*X
                DFDY(2,1)=(ONE-LAMDA)*BETA*P1-(ONE-
LAMDA)*BETA*P1*Y(5)*X
                DFDY(2,2)=-BETA+(ONE-LAMDA)*BETA*P1-(ONE-
LAMDA)*BETA*P1*Y(5)*X
                DFDY(2,5)=-(ONE-LAMDA)*BETA*P1*(Y(1)+Y(2))*X
                DFDY(5,1)=(Kdeg-Kint)*X*Y(5)/Q
                DFDY(5,2)=(Kdeg-Kint)*X*Y(5)/Q
                DFDY(5,5)=-Kdeg+(Kdeg-Kint)*X*(Y(1)+Y(2))/Q

ELSE IF (T .LE. TCOLD) THEN
                Z= ZERO
                X=ONE/(KD+((Y(1)+Y(2))/Q))

                DFDY(1,1)=-ALPHA+LAMDA*ALPHA*P1-
LAMDA*ALPHA*P1*KD*Y(5)*X*X
                DFDY(1,2)=LAMDA*ALPHA*P1-
LAMDA*ALPHA*P1*KD*Y(5)*X*X
                DFDY(1,5)=-LAMDA*ALPHA*P1*(Y(1)+Y(2))*X
                DFDY(2,1)=(ONE-LAMDA)*BETA*P1-(ONE-
LAMDA)*BETA*P1*KD*Y(5)*X*X
                DFDY(2,2)=-BETA +(ONE-LAMDA)*BETA*P1-(ONE-
LAMDA)*BETA*P1*KD*Y(5)*X*X
                DFDY(2,5)=-(ONE-LAMDA)*BETA*P1*(Y(1)+Y(2))*X
                DFDY(5,1)=(Kdeg-Kint)*KD*Y(5)*X*X/Q
                DFDY(5,2)=(Kdeg-Kint)*KD*Y(5)*X*X/Q
                DFDY(5,5)=-Kdeg+(Kdeg-Kint)*X*(Y(1)+Y(2))/Q
        END IF

        DFDY(1,3)=LAMDA*ALPHA
        DFDY(1,4)=LAMDA*ALPHA
        DFDY(2,3)=(ONE-LAMDA)*BETA
        DFDY(2,4)=(ONE-LAMDA)*BETA
        DFDY(5,3)=ZERO
        DFDY(5,4)=ZERO
```

```
        DFDY(3,1)=LAMDA*ALPHA*(ONE-P1)
        DFDY(3,2)=LAMDA*ALPHA*(ONE-P1)
        DFDY(3,5)=ZERO
        DFDY(3,3)=-ALPHA
        DFDY(3,4)=ZERO
        DFDY(4,1)=(ONE-LAMDA)*BETA*(ONE-P1)
        DFDY(4,2)=(ONE-LAMDA)*BETA*(ONE-P1)
        DFDY(4,5)=ZERO
        DFDY(4,3)=ZERO
        DFDY(4,4)=-BETA
ENDIF
END SUBROUTINE USERMODEL_ODE_JACOBIAN


SUBROUTINE USERMODEL(T,Y,P,NP,IFUN)
! THIS SUBROUTINE:
! (1) DEFINES THE EQUATIONS TO BE FITTED
! (2) ASSIGNS NAMES TO THE PARAMETERS (IFUN=-1000 CALL)
! (3) ALLOWS THE USER TO DEFINE AND REGISTER EVENT (IFUN =-1000
CALL)
! (4) INTERACTIVELY ALLOWS THE USER TO SELECT THE ALGORITHM TO
BE
! USED BY WINFUNFIT FOR THE INTEGRATION OF THE DIFFERENTIAL
EQUATIONS SPECIFIED IN THE SUBROUTINE "USERMODEL_ODE" GIVEN
ABOVE.
! (5) ALLOWS FITTING SPLINES TO EXTERNAL DATA
! (6) PROVIDES THE USER THE OPPORTUNITY TO MAKE SPECIAL
CALCULATIONS AND PLOTS AFTER WINFUNFIT HAS COMPLETED A
FITTING TO A DATA SET (IFUN=0 CALL)

IMPLICIT  NONE
INTEGER                    :: NP, IFUN, JFUN, J,JY,I,JOB1,JOB2
INTEGER,PARAMETER          :: NEQN=5
REAL*8                     :: FX1,FX2,RT_SS,FOUT1_SS,A,B,C,AA,BB
REAL*8                     :: T, Y,
P(*),ALPHA,BETA,GAMMA,LAMDA,R,D,Q,Ksyn,Kdeg,Kint,KD,P1,FSS,RT_0,TCO
LD,X,FOUT1,FOUT2,FOUT3,Y1,Y2,Y3,Y4,Y5
INTEGER                    :: NOBSB, NOBSP, LUN, NSIGDIGITS,NPS=200,NOBS
REAL*8                     :: FACTOR, ZERO = 0D0, TZERO = 0D0 , ONE = 1D0
,TWO = 2D0 , THREE = 3D0
REAL*8                     ::  TOBS(50),COBS(50),CLN(50), TC(200), CC(200) ,DT
LOGICAL, SAVE              :: SHOWIT, PLOTSAVED,FIRSTCALL=.TRUE.
CHARACTER (LEN=256)        :: ID, DATAFILENAME,COLDNAME
CHARACTER (LEN=20)         :: PNAME
REAL*8                     :: YZERO(NEQN)
```

```
ALPHA=P(1)
BETA=P(2)
LAMDA=P(3)
Ksyn=P(4)
KD=P(5)
Kdeg=P(6)
Kint=P(7)
P1=P(8)
R=P(9)
D=P(10)
Q=P(11)
TCOLD=P(12)
FSS=P(13)
RT_0=P(14)

    IF(IFUN.EQ.-1000)THEN
        IF (FIRSTCALL.EQ..TRUE.) THEN
                PRINT*, "ENTER THE NAME OF FILE FOR COLD :"
                READ*, COLDNAME
                OPEN(UNIT=8, FILE=COLDNAME, STATUS='OLD')
                READ (8,*) NOBS
                        DO I= 1, NOBS
                                READ (8,*) TOBS(I),COBS(I)
                                PRINT*, TOBS(I), COBS(I)
                                CLN(I)=LOG(COBS(I))
                        END DO
                CALL CUBIC_GCV_FIT(TOBS,CLN,NOBS)
                CLOSE (8,STATUS='SAVE')
                FIRSTCALL = .FALSE.
        ENDIF

        CALL SetFunfitParameterName(1,"ALPHA")
        CALL SetFunfitParameterName(2,"BETA")
        CALL SetFunfitParameterName(3,"LAMDA")
        CALL SetFunfitParameterName(4,"Ksyn")
        CALL SetFunfitParameterName(5,"KD")
        CALL SetFunfitParameterName(6,"Kdeg")
        CALL SetFunfitParameterName(7,"Kint")
        CALL SetFunfitParameterName(8,"P1")
        CALL SetFunfitParameterName(9,"R")
        CALL SetFunfitParameterName(10,"D")
        CALL SetFunfitParameterName(11,"Q")
        CALL SetFunfitParameterName(12,"TCOLD")
        CALL SetFunfitParameterName(13,"FSS")
        CALL SetFunfitParameterName(14,"RT_0")
```

```
        CALL SET_INTEGRATOR(6)
ENDIF

IF(IFUN.EQ.1) THEN          !FIND SS SOLUTIONS FOR INITIAL CONDITIONS
   JOB1 = 0
   RT_SS = 0.1D0
   A=Kdeg*KD*Q*Q*P1
   B=(Kint-Kdeg)*Q*FSS*KD
   C=-Ksyn*Q*FSS*KD

    DO
          FX1 = A*RT_SS*RT_SS+B*RT_SS+C
           ! NOTE THE FUNCTION IS EVALUATED BEFORE THE CALL
          CALL SINGLE_POSETIVE_ROOT_FINDER (RT_SS, FX1, JOB1)
          ! THE INITIAL SEARCH FOR A BRACKET ASSUMES THAT FX
          ! IS MONOTONIC
          IF (JOB1 /= 1) EXIT
   ENDDO

   JOB2 = 0
   FOUT1_SS= 0.1D0
   AA=Q*P1*RT_SS-FSS
   BB=-Q*KD*FSS

   DO
   FX2 = AA*FOUT1_SS+BB
   CALL SINGLE_POSETIVE_ROOT_FINDER (FOUT1_SS, FX2, JOB2)
   IF (JOB2 /= 1) EXIT
   ENDDO

   YZERO(1) = LAMDA*ALPHA*D+LAMDA*FOUT1_SS
   YZERO(2)=(ONE-LAMDA)*BETA*D+(ONE-LAMDA)*FOUT1_SS
   YZERO(3)= LAMDA*(ONE-P1)*FOUT1_SS
   YZERO(4) = (ONE-LAMDA)*(ONE-P1)*FOUT1_SS
   YZERO(5)= RT_0

        JY = 1
        CALL
INTEGRATE_USERMODEL_ODE(T,Y1,P,NP,IFUN,TZERO,YZERO,NEQN,JY)
         JY=2
         CALL
INTEGRATE_USERMODEL_ODE(T,Y2,P,NP,IFUN,TZERO,YZERO,NEQN,JY)
         JY=3
         CALL
INTEGRATE_USERMODEL_ODE(T,Y3,P,NP,IFUN,TZERO,YZERO,NEQN,JY)
         JY=4
```

```
          CALL
INTEGRATE_USERMODEL_ODE(T,Y4,P,NP,IFUN,TZERO,YZERO,NEQN,JY)
          JY=5
          CALL
INTEGRATE_USERMODEL_ODE(T,Y5,P,NP,IFUN,TZERO,YZERO,NEQN,JY)

          FOUT1=Y1+Y2
          FOUT3=Y3+Y4
          X=Y5/(KD+FOUT1/Q)
          FOUT2=P1*(ONE-X)*FOUT1
          Y=(FOUT2+FOUT3)/Q
ENDIF

IF(IFUN.EQ.0)THEN  ! SPECIAL USER OUTPUT SECTION
         CALL PROMT(SHOWIT) ! WANT TO SEE USER PLOT(S)?
          IF(SHOWIT) THEN
                IF(TOBS(1).GT.0.0) THEN
                      DT = (TOBS(NOBS) - TOBS(1))/FLOAT(NPS-1)
                      DO J=1, NPS
                            TC(J) = P(12) + DT*FLOAT(J-1)
                            CALL CUBIC_GCV(TC(J), CC(J))
                            CC(J) = DEXP(CC(J))
                      ENDDO
                ENDIF          !TCOLD > 0

         CALL ADDOBSERVATIONSLEFT(1)
         CALL ADDFITTEDCURVELEFT(1)
         CALL LEFTLABEL('PLASMA 125I-CERA (CPM/ML)')
         IF(TCOLD.GT.0.0) THEN
                      CALL RIGHTLABEL('COLD CERA CONC. (MU/ML) ')
                      CALL ADD_POINTS_RIGHT(TOBS, COBS, NOBS)
                      CALL ADD_CURVE_RIGHT(TC,CC,NPS)
         ENDIF
         CALL TITLE('CERA TIM (SUBJECT 50082)')
         CALL XLABEL('TIME (HR)')
         CALL DISPLAYPLOT
         ! RECORD PLOT ID IF PLOT IS SAVED
         CALL RECORDPLOTIFSAVED(3)
    ENDIF      ! SHOWIT
ENDIF          ! IFUN = 0
RETURN
!*********  N O N  OPTIONAL DEFINITION SECTION **************
!
! THIS IS FOR RECORDING OF THE MODEL USED IN THE FITTING :
!
    ENTRY MODELID(ID)
```

```
      ID = 'INF TIM MODEL V1.0'
      RETURN
      END
```

A.2. Fortran subroutines for generalized cross validated cubic spline fitting

```
SUBROUTINE CUBIC_GCV_FIT (T,F,N)
!THIS SUBROUTINE FITS A GCV CUBIC SPLINE TO DATA POINTS
! COPYRIGHT PV-P
! INPUT:
!     T,F        ARRAYS OF LENGTH N TO BE FITTED BY CUBIC
!              GENERALIZED CROSS VAIDATION (F=F(T))
!
! R E S T R I C T I O N S :  N MUST NOT EXCEED 2000

      SAVE C,Y,TSAVE,NSAVE
      PARAMETER (NMAX=2000,NWK=7*(NMAX+2),IC=NMAX-1)
      DOUBLE PRECISION FF(NMAX),X(NMAX),Y(NMAX),DF(NMAX),ONE,
      C(IC,3),SE(NMAX),WK(NWK),VAR,D,ZERO,Z2,SSSE,SSRES
      REAL T(*), F(*), TSAVE(NMAX)
      DATA  ONE, ZERO / 1D0 , 0D0 /

    IF(N.GT.NMAX)STOP '** ERROR  (CUBIC_GCV_FIT) : TOO LARGE ARRAY'
    IF(N.LT.2) STOP   '** ERROR  (CUBIC_GCV_FIT) : TOO SMALL ARRAY'

     DO J =   1,N
          FF(J) = DBLE(F(J))
          DF(J) = ONE
          X(J) = DBLE(T(J))
          TSAVE(J) = T(J)
      ENDDO

      NSAVE = N
      VAR = - ONE

      CALL CUBGCV (X,FF,DF,N,Y,C,IC,VAR,1,SE,WK,IER)

      IF(IER.NE.0) THEN
          PRINT*,'** ERROR (CUBIC_GCV_FIT): IER =',IER
          READ*
          STOP
      ENDIF
      RETURN
!*****
      ENTRY CUBIC_GCV(TCALC,FCALC) ! INPUT: TCALC, OUTPUT: FCALC
```

```
      TT = MAX(TSAVE(1),TCALC)
      TT = MIN(TT,TSAVE(NSAVE))

      DO J = 1,NSAVE-1
         IF(TT.LE.TSAVE(J+1)) THEN
                  D = DBLE(TT-TSAVE(J))
                  FCALC = SNGL(((C(J,3)*D+C(J,2))*D+C(J,1))*D+Y(J))
                  EXIT
         ENDIF
      ENDDO
      RETURN
      END
!******

!    ALGORITHM 642 COLLECTED ALGORITHMS FROM ACM.
!    ALGORITHM APPEARED IN ACM-TRANS. MATH. SOFTWARE, VOL.12, NO.
!    2, JUN., 1986, P. 150.
!   SUBROUTINE NAME     - CUBGCV
!
!-----------------------------------------------------------------------
!
!   COMPUTER           - VAX/DOUBLE
!
!   AUTHOR             - M.F.HUTCHINSON
!                        CSIRO DIVISION OF MATHEMATICS AND STATISTICS
!                        P.O. BOX 1965
!                        CANBERRA, ACT 2601
!                        AUSTRALIA
!
!   LATEST REVISION     - 15 AUGUST 1985
!
!   PURPOSE            - CUBIC SPLINE DATA SMOOTHER
!
!   USAGE              - CALL CUBGCV (X,F,DF,N,Y,C,IC,VAR,JOB,SE,WK,IER)
!
!   ARGUMENTS    X      - VECTOR OF LENGTH N CONTAINING THE
!                         ABSCISSAE OF THE N DATA POINTS
!                         (X(I),F(I)) I=1..N. (INPUT) X
!                         MUST BE ORDERED SO THAT
!                         X(I) .LT. X(I+1).
!                F      - VECTOR OF LENGTH N CONTAINING THE
!                         ORDINATES (OR FUNCTION VALUES)
!                         OF THE N DATA POINTS (INPUT).
!                DF     - VECTOR OF LENGTH N. (INPUT/OUTPUT)
!                         DF(I) IS THE RELATIVE STANDARD DEVIATION
```

```
!                 OF THE ERROR ASSOCIATED WITH DATA POINT I.
!                 EACH DF(I) MUST BE POSITIVE.  THE VALUES IN
!                 DF ARE SCALED BY THE SUBROUTINE SO THAT
!                 THEIR MEAN SQUARE VALUE IS 1, AND UNSCALED
!                 AGAIN ON NORMAL EXIT.
!                 THE MEAN SQUARE VALUE OF THE DF(I) IS RETURNED
!                 IN WK(7) ON NORMAL EXIT.
!                 IF THE ABSOLUTE STANDARD DEVIATIONS ARE KNOWN,
!                 THESE SHOULD BE PROVIDED IN DF AND THE ERROR
!                 VARIANCE PARAMETER VAR (SEE BELOW) SHOULD THEN
!                 BE SET TO 1.
!                 IF THE RELATIVE STANDARD DEVIATIONS ARE UNKNOWN,
!                 SET EACH DF(I)=1.
!           N     - NUMBER OF DATA POINTS (INPUT).
!                 N MUST BE .GE. 3.
!           Y,C   - SPLINE COEFFICIENTS. (OUTPUT) Y
!                 IS A VECTOR OF LENGTH N. C IS
!                 AN N-1 BY 3 MATRIX. THE VALUE
!                 OF THE SPLINE APPROXIMATION AT T IS
!                 S(T)=((C(I,3)*D+C(I,2))*D+C(I,1))*D+Y(I)
!                 WHERE X(I).LE.T.LT.X(I+1) AND
!                 D = T-X(I).
!           IC    - ROW DIMENSION OF MATRIX C EXACTLY
!                 AS SPECIFIED IN THE DIMENSION
!                 STATEMENT IN THE CALLING PROGRAM. (INPUT)
!           VAR    - ERROR VARIANCE. (INPUT/OUTPUT)
!                 IF VAR IS NEGATIVE (I.E. UNKNOWN) THEN
!                 THE SMOOTHING PARAMETER IS DETERMINED
!                 BY MINIMIZING THE GENERALIZED CROSS VALIDATION
!                 AND AN ESTIMATE OF THE ERROR VARIANCE IS
!                 RETURNED IN VAR.
!                 IF VAR IS NON-NEGATIVE (I.E. KNOWN) THEN THE
!                 SMOOTHING PARAMETER IS DETERMINED TO MINIMIZE
!                 AN ESTIMATE, WHICH DEPENDS ON VAR, OF THE TRUE
!                 MEAN SQUARE ERROR, AND VAR IS UNCHANGED.
!                 IN PARTICULAR, IF VAR IS ZERO, THEN AN
!                 INTERPOLATING NATURAL CUBIC SPLINE IS CALCULATED.
!                 VAR SHOULD BE SET TO 1 IF ABSOLUTE STANDARD
!                 DEVIATIONS HAVE BEEN PROVIDED IN DF (SEE ABOVE).
!           JOB   - JOB SELECTION PARAMETER. (INPUT)
!                JOB = 0 SHOULD BE SELECTED IF POINT STANDARD ERROR
!                 ESTIMATES ARE NOT REQUIRED IN SE.
!                JOB = 1 SHOULD BE SELECTED IF POINT STANDARD ERROR
!                 ESTIMATES ARE REQUIRED IN SE.
!           SE    - VECTOR OF LENGTH N CONTAINING BAYESIAN STANDARD
!                 ERROR ESTIMATES OF THE FITTED SPLINE VALUES IN Y.
```

```
!                SE IS NOT REFERENCED IF JOB=0. (OUTPUT)
!          WK    - WORK VECTOR OF LENGTH 7*(N + 2). ON NORMAL EXIT
!                THE FIRST 7 VALUES OF WK ARE ASSIGNED AS FOLLOWS:-
!
!                WK(1) = SMOOTHING PARAMETER (= RHO/(RHO + 1))
!                WK(2) = ESTIMATE OF THE NUMBER OF DEGREES OF
!                     FREEDOM OF THE RESIDUAL SUM OF SQUARES
!                WK(3) = GENERALIZED CROSS VALIDATION
!                WK(4) = MEAN SQUARE RESIDUAL
!                WK(5) = ESTIMATE OF THE TRUE MEAN SQUARE ERROR
!                     AT THE DATA POINTS
!                WK(6) = ESTIMATE OF THE ERROR VARIANCE
!                WK(7) = MEAN SQUARE VALUE OF THE DF(I)
!
!                IF WK(1)=0 (RHO=0) AN INTERPOLATING NATURAL CUBIC
!                SPLINE HAS BEEN CALCULATED.
!                IF WK(1)=1 (RHO=INFINITE) A LEAST SQUARES
!                REGRESSION LINE HAS BEEN CALCULATED.
!                WK(2) IS AN ESTIMATE OF THE NUMBER OF DEGREES OF
!                FREEDOM OF THE RESIDUAL WHICH REDUCES TO THE
!                USUAL VALUE OF N-2 WHEN A LEAST SQUARES
!                REGRESSION LINE IS CALCULATED.
!                WK(3),WK(4),WK(5) ARE CALCULATED WITH THE DF(I)
!                SCALED TO HAVE MEAN SQUARE VALUE 1.  THE
!                UNSCALED VALUES OF WK(3),WK(4),WK(5) MAY BE
!                CALCULATED BY DIVIDING BY WK(7).
!                WK(6) COINCIDES WITH THE OUTPUT VALUE OF VAR IF
!                VAR IS NEGATIVE ON INPUT.  IT IS CALCULATED WITH
!                THE UNSCALED VALUES OF THE DF(I) TO FACILITATE
!                COMPARISONS WITH A PRIORI VARIANCE ESTIMATES.
!
!          IER   - ERROR PARAMETER. (OUTPUT)
!                TERMINAL ERROR
!                 IER = 129, IC IS LESS THAN N-1.
!                 IER = 130, N IS LESS THAN 3.
!                 IER = 131, INPUT ABSCISSAE ARE NOT
!                   ORDERED SO THAT X(I).LT.X(I+1).
!                 IER = 132, DF(I) IS NOT POSITIVE FOR SOME I.
!                 IER = 133, JOB IS NOT 0 OR 1.
!
!  PRECISION/HARDWARE  - DOUBLE
!
!  REQUIRED ROUTINES   - SPINT1,SPFIT1,SPCOF1,SPERR1
!
!  REMARKS     THE NUMBER OF ARITHMETIC OPERATIONS REQUIRED BY
!          SUBROUTINE IS PROPORTIONAL TO N.
```

```
!             THE SUBROUTINE USES AN ALGORITHM DEVELOPED BY M.F.
!              HUTCHINSON AND F.R. DE HOOG, 'SMOOTHING NOISY DATA WITH
!              SPLINE FUNCTIONS', NUMER. MATH. (IN PRESS)
!
!-----------------------------------------------------------------------
!
      SUBROUTINE CUBGCV(X,F,DF,N,Y,C,IC,VAR,JOB,SE,WK,IER)
!
!---SPECIFICATIONS FOR ARGUMENTS---
      INTEGER N,IC,JOB,IER
      DOUBLE PRECISION X(N),F(N),DF(N),Y(N),C(IC,3),SE(N),VAR,WK(0:N+1,7)
!
!---SPECIFICATIONS FOR LOCAL VARIABLES---
      DOUBLE PRECISION
      DELTA,ERR,GF1,GF2,GF3,GF4,R1,R2,R3,R4,TAU,RATIO,AVH,AVDF,AVAR,Z
      ERO,ONE,STAT(6),P,Q
!
      DATA RATIO/2.0D0/
      DATA TAU/1.618033989D0/
      DATA ZERO,ONE/0.0D0,1.0D0/
!
!---INITIALIZE---
      IER = 133
      IF (JOB.LT.0 .OR. JOB.GT.1) GO TO 140
      CALL SPINT1(X,AVH,F,DF,AVDF,N,Y,C,IC,WK,WK(0,4),IER)
      IF (IER.NE.0) GO TO 140
      AVAR = VAR
      IF (VAR.GT.ZERO) AVAR = VAR*AVDF*AVDF
!
!---CHECK FOR ZERO VARIANCE---
      IF (VAR.NE.ZERO) GO TO 10
      R1 = ZERO
      GO TO 90
!
!---FIND LOCAL MINIMUM OF GCV OR THE EXPECTED MEAN SQUARE
!    ERROR
   10 R1 = ONE
      R2 = RATIO*R1
      CALL
SPFIT1(X,AVH,DF,N,R2,P,Q,GF2,AVAR,STAT,Y,C,IC,WK,WK(0,4),WK(0,6),WK(0,
7))
   20 CALL
SPFIT1(X,AVH,DF,N,R1,P,Q,GF1,AVAR,STAT,Y,C,IC,WK,WK(0,4),WK(0,6),WK(0,
7))
      IF (GF1.GT.GF2) GO TO 30
!
```

```
!---EXIT IF P ZERO---
      IF (P.LE.ZERO) GO TO 100
      R2 = R1
      GF2 = GF1
      R1 = R1/RATIO
      GO TO 20

   30 R3 = RATIO*R2
   40 CALL
SPFIT1(X,AVH,DF,N,R3,P,Q,GF3,AVAR,STAT,Y,C,IC,WK,WK(0,4),WK(0,6),WK(0,
7))
      IF (GF3.GT.GF2) GO TO 50
!
!---EXIT IF Q ZERO---
      IF (Q.LE.ZERO) GO TO 100
      R2 = R3
      GF2 = GF3
      R3 = RATIO*R3
      GO TO 40

   50 R2 = R3
      GF2 = GF3
      DELTA = (R2-R1)/TAU
      R4 = R1 + DELTA
      R3 = R2 - DELTA
      CALL
SPFIT1(X,AVH,DF,N,R3,P,Q,GF3,AVAR,STAT,Y,C,IC,WK,WK(0,4),WK(0,6),WK(0,
7))
      CALL
SPFIT1(X,AVH,DF,N,R4,P,Q,GF4,AVAR,STAT,Y,C,IC,WK,WK(0,4),WK(0,6),WK(0,
7))
!
!---GOLDEN SECTION SEARCH FOR LOCAL MINIMUM---
   60 IF (GF3.GT.GF4) GO TO 70
      R2 = R4
      GF2 = GF4
      R4 = R3
      GF4 = GF3
      DELTA = DELTA/TAU
      R3 = R2 - DELTA
      CALL
SPFIT1(X,AVH,DF,N,R3,P,Q,GF3,AVAR,STAT,Y,C,IC,WK,WK(0,4),WK(0,6),WK(0,
7))
      GO TO 80

   70 R1 = R3
```

```
      GF1 = GF3
      R3 = R4
      GF3 = GF4
      DELTA = DELTA/TAU
      R4 = R1 + DELTA
      CALL
SPFIT1(X,AVH,DF,N,R4,P,Q,GF4,AVAR,STAT,Y,C,IC,WK,WK(0,4),WK(0,6),WK(0,
7))
   80 ERR = (R2-R1)/ (R1+R2)
      IF (ERR*ERR+ONE.GT.ONE .AND. ERR.GT.1.0D-6) GO TO 60
      R1 = (R1+R2)*0.5D0
!
!---CALCULATE SPLINE COEFFICIENTS---
   90 CALL
SPFIT1(X,AVH,DF,N,R1,P,Q,GF1,AVAR,STAT,Y,C,IC,WK,WK(0,4),WK(0,6),WK(0,
7))
  100 CALL SPCOF1(X,AVH,F,DF,N,P,Q,Y,C,IC,WK(0,6),WK(0,7))
!
!---OPTIONALLY CALCULATE STANDARD ERROR ESTIMATES---
      IF (VAR.GE.ZERO) GO TO 110
      AVAR = STAT(6)
      VAR = AVAR/ (AVDF*AVDF)
  110 IF (JOB.EQ.1) CALL SPERR1(X,AVH,DF,N,WK,P,AVAR,SE)
!
!---UNSCALE DF---
      DO 120 I = 1,N
        DF(I) = DF(I)*AVDF
  120 CONTINUE
!
!--PUT STATISTICS IN WK---
      DO 130 I = 0,5
        WK(I,1) = STAT(I+1)
  130 CONTINUE
      WK(5,1) = STAT(6)/ (AVDF*AVDF)
      WK(6,1) = AVDF*AVDF
      GO TO 150
!
!---CHECK FOR ERROR CONDITION---
  140 CONTINUE
!     IF (IER.NE.0) CONTINUE
  150 RETURN
      END

      SUBROUTINE SPINT1(X,AVH,Y,DY,AVDY,N,A,C,IC,R,T,IER)
!
! INITIALIZES THE ARRAYS C, R AND T FOR ONE DIMENSIONAL CUBIC
```

```
! SMOOTHING SPLINE FITTING BY SUBROUTINE SPFIT1.  THE VALUES
! DF(I) ARE SCALED SO THAT THE SUM OF THEIR SQUARES IS N
! AND THE AVERAGE OF THE DIFFERENCES X(I+1) - X(I) IS CALCULATED
! IN AVH IN ORDER TO AVOID UNDERFLOW AND OVERFLOW PROBLEMS IN
! SPFIT1.
!
! SUBROUTINE SETS IER IF ELEMENTS OF X ARE NON-INCREASING,
! IF N IS LESS THAN 3, IF IC IS LESS THAN N-1 OR IF DY(I) IS
! NOT POSITIVE FOR SOME I.
!
!---SPECIFICATIONS FOR ARGUMENTS---
      INTEGER N,IC,IER
      DOUBLE PRECISION
X(N),Y(N),DY(N),A(N),C(IC,3),R(0:N+1,3),T(0:N+1,2),AVH,AVDY
!
!---SPECIFICATIONS FOR LOCAL VARIABLES---
      INTEGER I
      DOUBLE PRECISION E,F,G,H,ZERO
      DATA ZERO/0.0D0/
!
!---INITIALIZATION AND INPUT CHECKING---
      IER = 0
      IF (N.LT.3) GO TO 60
      IF (IC.LT.N-1) GO TO 70
!
!---GET AVERAGE X SPACING IN AVH---
      G = ZERO
      DO 10 I = 1,N - 1
        H = X(I+1) - X(I)
        IF (H.LE.ZERO) GO TO 80
        G = G + H
   10 CONTINUE
      AVH = G/ (N-1)
!
!---SCALE RELATIVE WEIGHTS---
      G = ZERO
      DO 20 I = 1,N
        IF (DY(I).LE.ZERO) GO TO 90
        G = G + DY(I)*DY(I)
   20 CONTINUE
      AVDY = DSQRT(G/N)
!
      DO 30 I = 1,N
        DY(I) = DY(I)/AVDY
   30 CONTINUE
!
```

```
!---INITIALIZE H,F---
      H = (X(2)-X(1))/AVH
      F = (Y(2)-Y(1))/H
!
!---CALCULATE A,T,R---
      DO 40 I = 2,N - 1
        G = H
        H = (X(I+1)-X(I))/AVH
        E = F
        F = (Y(I+1)-Y(I))/H
        A(I) = F - E
        T(I,1) = 2.0D0* (G+H)/3.0D0
        T(I,2) = H/3.0D0
        R(I,3) = DY(I-1)/G
        R(I,1) = DY(I+1)/H
        R(I,2) = -DY(I)/G - DY(I)/H
   40 CONTINUE
!
!---CALCULATE C = R'*R---
      R(N,2) = ZERO
      R(N,3) = ZERO
      R(N+1,3) = ZERO
      DO 50 I = 2,N - 1
        C(I,1) = R(I,1)*R(I,1) + R(I,2)*R(I,2) + R(I,3)*R(I,3)
        C(I,2) = R(I,1)*R(I+1,2) + R(I,2)*R(I+1,3)
        C(I,3) = R(I,1)*R(I+2,3)
   50 CONTINUE
      RETURN
!
!---ERROR CONDITIONS---
   60 IER = 130
      RETURN

   70 IER = 129
      RETURN

   80 IER = 131
      RETURN

   90 IER = 132
      RETURN
      END
      SUBROUTINE

 SPFIT1(X,AVH,DY,N,RHO,P,Q,FUN,VAR,STAT,A,C,IC,R,T,U,V)
!
```

```
! FITS A CUBIC SMOOTHING SPLINE TO DATA WITH RELATIVE
! WEIGHTING DY FOR A GIVEN VALUE OF THE SMOOTHING PARAMETER
! RHO USING AN ALGORITHM BASED ON THAT OF C.H. REINSCH (1967),
! NUMER. MATH. 10, 177-183.
!
! THE TRACE OF THE INFLUENCE MATRIX IS CALCULATED USING AN
! ALGORITHM DEVELOPED BY M.F.HUTCHINSON AND F.R.DE HOOG
(NUMER.
! MATH., IN PRESS), ENABLING THE GENERALIZED CROSS VALIDATION
! AND RELATED STATISTICS TO BE CALCULATED IN ORDER N
OPERATIONS.
!
! THE ARRAYS A, C, R AND T ARE ASSUMED TO HAVE BEEN INITIALIZED
! BY THE SUBROUTINE SPINT1.  OVERFLOW AND UNDERFLOW PROBLEMS
ARE
! AVOIDED BY USING P=RHO/(1 + RHO) AND Q=1/(1 + RHO) INSTEAD OF
! RHO AND BY SCALING THE DIFFERENCES X(I+1) - X(I) BY AVH.
!
! THE VALUES IN DF ARE ASSUMED TO HAVE BEEN SCALED SO THAT THE
! SUM OF THEIR SQUARED VALUES IS N.  THE VALUE IN VAR, WHEN IT IS
! NON-NEGATIVE, IS ASSUMED TO HAVE BEEN SCALED TO COMPENSATE
FOR
! THE SCALING OF THE VALUES IN DF.
!
! THE VALUE RETURNED IN FUN IS AN ESTIMATE OF THE TRUE MEAN
SQUARE
! WHEN VAR IS NON-NEGATIVE, AND IS THE GENERALIZED CROSS
VALIDATION
! WHEN VAR IS NEGATIVE.
!
!---SPECIFICATIONS FOR ARGUMENTS---
      INTEGER IC,N
      DOUBLE PRECISION
X(N),DY(N),RHO,STAT(6),A(N),C(IC,3),R(0:N+1,3),T(0:N+1,2),U(0:N+1),V(0:N+1),
FUN,VAR,AVH,P,Q
!
!---LOCAL VARIABLES---
      INTEGER I
      DOUBLE PRECISION E,F,G,H,ZERO,ONE,TWO,RHO1
      DATA ZERO,ONE,TWO/0.0D0,1.0D0,2.0D0/
!
!---USE P AND Q INSTEAD OF RHO TO PREVENT OVERFLOW OR
UNDERFLOW---
      RHO1 = ONE + RHO
      P = RHO/RHO1
      Q = ONE/RHO1
```

```
      IF (RHO1.EQ.ONE) P = ZERO
      IF (RHO1.EQ.RHO) Q = ZERO
!
!---RATIONAL CHOLESKY DECOMPOSITION OF P*C + Q*T---
      F = ZERO
      G = ZERO
      H = ZERO
      DO 10 I = 0,1
        R(I,1) = ZERO
   10 CONTINUE
      DO 20 I = 2,N - 1
        R(I-2,3) = G*R(I-2,1)
        R(I-1,2) = F*R(I-1,1)
        R(I,1) = ONE/ (P*C(I,1)+Q*T(I,1)-F*R(I-1,2)-G*R(I-2,3))
        F = P*C(I,2) + Q*T(I,2) - H*R(I-1,2)
        G = H
        H = P*C(I,3)
   20 CONTINUE
!
!---SOLVE FOR U---
      U(0) = ZERO
      U(1) = ZERO
      DO 30 I = 2,N - 1
        U(I) = A(I) - R(I-1,2)*U(I-1) - R(I-2,3)*U(I-2)
   30 CONTINUE
      U(N) = ZERO
      U(N+1) = ZERO
      DO 40 I = N - 1,2,-1
        U(I) = R(I,1)*U(I) - R(I,2)*U(I+1) - R(I,3)*U(I+2)
   40 CONTINUE
!
!---CALCULATE RESIDUAL VECTOR V---
      E = ZERO
      H = ZERO
      DO 50 I = 1,N - 1
        G = H
        H = (U(I+1)-U(I))/ ((X(I+1)-X(I))/AVH)
        V(I) = DY(I)* (H-G)
        E = E + V(I)*V(I)
   50 CONTINUE
      V(N) = DY(N)* (-H)
      E = E + V(N)*V(N)
!
!---CALCULATE UPPER THREE BANDS OF INVERSE MATRIX---
      R(N,1) = ZERO
      R(N,2) = ZERO
```

```
      R(N+1,1) = ZERO
      DO 60 I = N - 1,2,-1
        G = R(I,2)
        H = R(I,3)
        R(I,2) = -G*R(I+1,1) - H*R(I+1,2)
        R(I,3) = -G*R(I+1,2) - H*R(I+2,1)
        R(I,1) = R(I,1) - G*R(I,2) - H*R(I,3)
   60 CONTINUE
!
!---CALCULATE TRACE---
      F = ZERO
      G = ZERO
      H = ZERO
      DO 70 I = 2,N - 1
        F = F + R(I,1)*C(I,1)
        G = G + R(I,2)*C(I,2)
        H = H + R(I,3)*C(I,3)
   70 CONTINUE
      F = F + TWO* (G+H)
!
!---CALCULATE STATISTICS---
      STAT(1) = P
      STAT(2) = F*P
      STAT(3) = N*E/ (F*F)
      STAT(4) = E*P*P/N
      STAT(6) = E*P/F
      IF (VAR.GE.ZERO) GO TO 80
      STAT(5) = STAT(6) - STAT(4)
      FUN = STAT(3)
      GO TO 90

   80 STAT(5) = DMAX1(STAT(4)-TWO*VAR*STAT(2)/N+VAR,ZERO)
      FUN = STAT(5)
   90 RETURN
      END
      SUBROUTINE SPERR1(X,AVH,DY,N,R,P,VAR,SE)
!
! CALCULATES BAYESIAN ESTIMATES OF THE STANDARD ERRORS OF THE
FITTED
! VALUES OF A CUBIC SMOOTHING SPLINE BY CALCULATING THE
DIAGONAL ELEMENTS
! OF THE INFLUENCE MATRIX.
!
!---SPECIFICATIONS FOR ARGUMENTS---
      INTEGER N
      DOUBLE PRECISION X(N),DY(N),R(0:N+1,3),SE(N),AVH,P,VAR
```

```
!
!---SPECIFICATIONS FOR LOCAL VARIABLES---
      INTEGER I
      DOUBLE PRECISION F,G,H,F1,G1,H1,ZERO,ONE
      DATA ZERO,ONE/0.0D0,1.0D0/
!
!---INITIALIZE---
      H = AVH/ (X(2)-X(1))
      SE(1) = ONE - P*DY(1)*DY(1)*H*H*R(2,1)
      R(1,1) = ZERO
      R(1,2) = ZERO
      R(1,3) = ZERO
!
!---CALCULATE DIAGONAL ELEMENTS---
      DO 10 I = 2,N - 1
        F = H
        H = AVH/ (X(I+1)-X(I))
        G = -F - H
        F1 = F*R(I-1,1) + G*R(I-1,2) + H*R(I-1,3)
        G1 = F*R(I-1,2) + G*R(I,1) + H*R(I,2)
        H1 = F*R(I-1,3) + G*R(I,2) + H*R(I+1,1)
        SE(I) = ONE - P*DY(I)*DY(I)* (F*F1+G*G1+H*H1)
   10 CONTINUE
      SE(N) = ONE - P*DY(N)*DY(N)*H*H*R(N-1,1)
!
!---CALCULATE STANDARD ERROR ESTIMATES---
      DO 20 I = 1,N
        SE(I) = DSQRT(DMAX1(SE(I)*VAR,ZERO))*DY(I)
   20 CONTINUE
      RETURN
      END
      SUBROUTINE SPCOF1(X,AVH,Y,DY,N,P,Q,A,C,IC,U,V)
!
! CALCULATES COEFFICIENTS OF A CUBIC SMOOTHING SPLINE FROM
! PARAMETERS CALCULATED BY SUBROUTINE SPFIT1.
!
!---SPECIFICATIONS FOR ARGUMENTS---
      INTEGER IC,N
      DOUBLE PRECISION
X(N),Y(N),DY(N),P,Q,A(N),C(IC,3),U(0:N+1),V(0:N+1),AVH
!
!---SPECIFICATIONS FOR LOCAL VARIABLES---
      INTEGER I
      DOUBLE PRECISION H,QH
!
!---CALCULATE A---
```

```
      QH = Q/ (AVH*AVH)
      DO 10 I = 1,N
        A(I) = Y(I) - P*DY(I)*V(I)
        U(I) = QH*U(I)
   10 CONTINUE
!
!---CALCULATE C---
      DO 20 I = 1,N - 1
        H = X(I+1) - X(I)
        C(I,3) = (U(I+1)-U(I))/ (3.0D0*H)
        C(I,1) = (A(I+1)-A(I))/H - (H*C(I,3)+U(I))*H
        C(I,2) = U(I)
   20 CONTINUE
      RETURN
      END
!
!UT HERE.....END OF CUBGCV.FOR
```

A.3. Fortran subroutines for positive root finding

```
SUBROUTINE SINGLE_POSETIVE_ROOT_FINDER (X, FX, JOB)
! THIS SUBROUTINE FINDS SINGLE POSETIVE ROOT
! THE INITIAL SEARCH FOR A BRACKET ASSUMES THAT FX IS MONOTONIC
! COPYRIGHT PV-P
! INPUT:
!   X        THE VARIABLE TO WHICH THE ROOT IS WANTED TO BE FOUND
!   FX       THE FUNCTION THAT IS SOLVED FOR X
!   JOB      INDICATOR FOR MISSION COMPLETION

  IMPLICIT NONE
  SAVE
  INTEGER,               INTENT (INOUT) :: JOB
  DOUBLE PRECISION,      INTENT (INOUT) :: X
  DOUBLE PRECISION,      INTENT (IN)    :: FX
  ! LOCALS
  INTEGER                           :: NEVAL, NEXT
  INTEGER, PARAMETER                    :: MAX_NEVAL = 50
  DOUBLE PRECISION                  :: XA, FXA, XB, FXB, XTRY, TOL, ZERO =
0D0, HALF = 0.5D0, FACTOR = 10D0, BIG
  DOUBLE PRECISION                  :: A,B,C,D,E,FA,FB,FC,P,Q,R,S,TOL1, XM,
TWO = 2D0, THREE = 3D0, ONE = 1D0
  DOUBLE PRECISION, PARAMETER           :: EPS=EPSILON(XA)
  LOGICAL                           :: BRACKETING_DONE, FXA_NEXT
  !
  !
  IF(X <= ZERO) STOP ' SINGLE_POSETIVE_ROOT_FINDER: IMPRPOPER
USAGE'
```

```
  IF(JOB == 0) THEN
    BRACKETING_DONE = .FALSE.
    XA  = X
    FXA = FX
    X = FACTOR*X
    FXA_NEXT = .FALSE.
    BIG = HUGE(ZERO)/(FACTOR*FACTOR)
    TOL = DSQRT(EPS)                          ! PENDING TOL SUITABLE VALUE
    NEVAL = 1
    JOB = 1
    GOTO 1000
  ENDIF

  NEVAL = NEVAL + 1
  IF(NEVAL > MAX_NEVAL) STOP ' SINGLE_POSETIVE_ROOT_FINDER:
COULD NOT FIND ROOT'


  IF(.NOT. BRACKETING_DONE) THEN

    IF(FXA_NEXT)THEN
       XA = X
       FXA = FX
    ELSE
       XB = X
       FXB = FX
    ENDIF


    IF(FXA*FXB < ZERO)THEN
      BRACKETING_DONE = .TRUE.
!                           PRINT*, 'X, XA, XB, FXA, FXB',X, XA, XB, FXA, FXB
!                           READ*
      A = XA
      B = XB
      FA = FXA
      FB = FXB
      C = B
      FC = FB
      NEXT = 1

    ELSE

      IF(FXA_NEXT) THEN
        IF(X < BIG) X = FACTOR*XB
```

```
      ELSE
        XTRY = X/FACTOR
        IF(XTRY > ZERO) X = XA/FACTOR
      ENDIF
      FXA_NEXT = .NOT. FXA_NEXT
      GO TO 1000
    ENDIF

  ENDIF

     GOTO (5,10) NEXT   ! WE HAVE BRACKETED THE ROOT SO LET US NOW
FIND IT
5 CONTINUE
                IF ((FB > ZERO .AND. FC > ZERO) .OR. (FB < ZERO .AND. FC <
ZERO)) THEN
                        C=A
                        FC=FA
                        D=B-A
                        E=D
                END IF
                IF (ABS(FC) < ABS(FB)) THEN
                        A=B
                        B=C
                        C=A
                        FA=FB
                        FB=FC
                        FC=FA
                END IF
                TOL1=TWO*EPS*ABS(B)+HALF*TOL
                XM=HALF*(C-B)
                IF (ABS(XM) <= TOL1 .OR. FB == ZERO) THEN
                        X=B
                        JOB = 2
       GOTO 1000
                END IF
                IF (ABS(E) >= TOL1 .AND. ABS(FA) > ABS(FB)) THEN
                        S=FB/FA
                        IF (A == C) THEN
                                P=TWO*XM*S
                                Q=ONE-S
                        ELSE
                                Q=FA/FC
                                R=FB/FC
                                P=S*(TWO*XM*Q*(Q-R)-(B-A)*(R-ONE))
                                Q=(Q-ONE)*(R-ONE)*(S-ONE)
                        END IF
```

```
                        IF (P > ZERO) Q = -Q
                        P=ABS(P)
                        IF (TWO*P  <  MIN(THREE*XM*Q-
ABS(TOL1*Q),ABS(E*Q))) THEN
                                E=D
                                D=P/Q
                        ELSE
                                D=XM
                                E=D
                        END IF
                ELSE
                        D=XM
                        E=D
                END IF
                A=B
                FA=FB
                B=B+MERGE(D,SIGN(TOL1,XM), ABS(D) > TOL1 )
     NEXT = 2
     X = B
     GOTO 1000
 10    CONTINUE
                FB = FX
   GO TO 5
          X=B
          JOB = 2
1000 CONTINUE  ! ONLY RETURN POINT
    RETURN
END SUBROUTINE SINGLE_POSETIVE_ROOT_FINDER
```

APPENDIX B. WINFUNFIT CODES FOR CHAPTER 6

B.1. Fortran subroutines for simulation of the compartmental model

```
! THESE SUBROUTINES TO DEFINE THE MODEL TO BE SIMULATED BY
WINFUNFIT
! PROGRAMMED BY MHE IN FEBRUARY 2011

SUBROUTINE USERMODEL_ODE(T,Y,YPRIME,P,NP,IFUN)
! THIS SUBROUTINE DEFINES THE MODEL DIFFERENTIAL EQUATIONS

IMPLICIT NONE
REAL*8 :: Y(*), YPRIME(*), P(*) ,T
INTEGER  :: NP,IFUN
REAL*8 :: V,KEL,KPT,KTP,D,KSYN,KDEG,KON,KOFF,KINT

V=P(1)
KEL=P(2)
KPT=P(3)
KTP=P(4)
KSYN=P(5)
KDEG=P(6)
KON=P(7)
KOFF=P(8)
KINT=P(9)
D=P(10)

IF(IFUN.EQ.1)THEN
    YPRIME(1) = -KON*Y(1)*Y(3)+KOFF*Y(4)-(KEL+KPT)*Y(1)+KTP*Y(2)/V
    YPRIME(2) = -KTP*Y(2)+KPT*Y(1)*V
    YPRIME(3) = KSYN-KON*Y(1)*Y(3)+KOFF*Y(4)-KDEG*Y(3)
    YPRIME(4) = KON*Y(1)*Y(3)-(KOFF+KINT)*Y(4)
ENDIF
RETURN
END

SUBROUTINE USERMODEL_ODE_JACOBIAN (T,Y,DFDT,DFDY,N,P,NP,IFUN)
! THIS SUBROUTINE IS NECESSARY FOR SOLVING STIFF DIFFERENTIAL
EQUATIONS
! THIS SUBROUTINE DEFINES THE PARTIAL DERIVATIVE OF EACH
DIFFERENTIAL EQUATION WITH RESPECT TO TIME AND EACH Y VARIABLE

 IMPLICIT NONE

 INTEGER, INTENT(IN)::N,NP,IFUN
 DOUBLE PRECISION, INTENT(IN)::T
```

```
 DOUBLE PRECISION,DIMENSION(N), INTENT (IN)::Y
 DOUBLE PRECISION,DIMENSION(N),INTENT(OUT)::DFDT
 DOUBLE PRECISION,DIMENSION(N,N),INTENT(OUT)::DFDY
 DOUBLE PRECISION,DIMENSION(NP),INTENT(IN)::P
 DOUBLE PRECISION,PARAMETER::ZERO=0D0
 DOUBLE PRECISION :: V,KEL,KPT,KTP,D,KSYN,KDEG,KON,KOFF,KINT

V=P(1)
KEL=P(2)
KPT=P(3)
KTP=P(4)
KSYN=P(5)
KDEG=P(6)
KON=P(7)
KOFF=P(8)
KINT=P(9)
D=P(10)

 IF(IFUN.EQ.1)THEN
        DFDT(1)=ZERO
        DFDT(2)=ZERO
        DFDT(3)=ZERO
        DFDT(4)=ZERO

        DFDY(1,1)=-KON*Y(3)-(KEL+KPT)
        DFDY(1,2)=KTP/V
        DFDY(1,3)=-KON*Y(1)
        DFDY(1,4)=KOFF

        DFDY(2,1)=KPT/V
        DFDY(2,2)=-KTP
        DFDY(2,3)=ZERO
        DFDY(2,4)=ZERO

        DFDY(3,1)=-KON*Y(3)
        DFDY(3,2)=ZERO
        DFDY(3,3)=-KON*Y(1)-KDEG
        DFDY(3,4)=KOFF

        DFDY(4,1)=KON*Y(3)
        DFDY(4,2)=ZERO
        DFDY(4,3)=KON*Y(1)
        DFDY(4,4)=-(KOFF+KINT)
ENDIF
END SUBROUTINE USERMODEL_ODE_JACOBIAN
```

```
SUBROUTINE USERMODEL(T,Y,P,NP,IFUN)
! THIS SUBROUTINE:
! (1) DEFINES THE EQUATIONS TO BE FITTED
! (2) ASSIGNS NAMES TO THE PARAMETERS (IFUN=-1000 CALL)
! (3) ALLOWS THE USER TO DEFINE AND REGISTER EVENT (IFUN =-1000
CALL)
! (4) INTERACTIVELY ALLOWS THE USER TO SELECT THE ALGORITHM TO
BE
! USED BY WINFUNFIT FOR THE INTEGRATION OF THE DIFFERENTIAL
EQUATIONS SPECIFIED IN THE SUBROUTINE "USERMODEL_ODE" GIVEN
ABOVE.
! (5) ALLOWS FITTING SPLINES TO EXTERNAL DATA
! (6) PROVIDES THE USER THE OPPORTUNITY TO MAKE SPECIAL
CALCULATIONS AND PLOTS AFTER WINFUNFIT HAS COMPLETED A
FITTING TO A DATA SET (IFUN=0 CALL)

IMPLICIT  NONE
INTEGER                    :: NP, IFUN, JFUN, J,JY,I
INTEGER,PARAMETER          :: NEQN=4
REAL*8                     :: T, Y, P(*)
REAL*8                     ::
V,KEL,KPT,KTP,D,KSYN,KDEG,KON,KOFF,KINT,Y1,Y2,Y3,Y4
INTEGER                    :: NOBSB, NOBSP, LUN, NSIGDIGITS
REAL*8                     :: FACTOR, ZERO = 0D0, TZERO = 0D0
LOGICAL, SAVE              :: SHOWIT, PLOTSAVED
CHARACTER (LEN=256)        :: ID, DATAFILENAME
CHARACTER (LEN=20)         :: PNAME
REAL*8                     :: YZERO(NEQN)

V=P(1)
KEL=P(2)
KPT=P(3)
KTP=P(4)
KSYN=P(5)
KDEG=P(6)
KON=P(7)
KOFF=P(8)
KINT=P(9)
D=P(10)

    IF(IFUN.EQ.-1000)THEN
        CALL SetFunfitParameterName(1,"V")
        CALL SetFunfitParameterName(2,"KEL")
        CALL SetFunfitParameterName(3,"KPT")
        CALL SetFunfitParameterName(4,"KTP")
```

```
            CALL SetFunfitParameterName(5,"KSYN")
            CALL SetFunfitParameterName(6,"KDEG")
            CALL SetFunfitParameterName(7,"KON")
            CALL SetFunfitParameterName(8,"KOFF")
            CALL SetFunfitParameterName(9,"KINT")
            CALL SetFunfitParameterName(10,"D")

            CALL SET_INTEGRATOR(6)
      ENDIF

IF(IFUN.EQ.1) THEN

          YZERO(1) = D/V
          YZERO(2)=ZERO
          YZERO(3)= KSYN/KDEG
          YZERO(4) = ZERO

          JY = 1
          CALL
INTEGRATE_USERMODEL_ODE(T,Y1,P,NP,IFUN,TZERO,YZERO,NEQN,JY)
           JY=2
           CALL
INTEGRATE_USERMODEL_ODE(T,Y2,P,NP,IFUN,TZERO,YZERO,NEQN,JY)
           JY=3
           CALL
INTEGRATE_USERMODEL_ODE(T,Y3,P,NP,IFUN,TZERO,YZERO,NEQN,JY)
           JY=4
           CALL
INTEGRATE_USERMODEL_ODE(T,Y4,P,NP,IFUN,TZERO,YZERO,NEQN,JY)

          Y=Y1          ! Simulate Plasma Concentration
          !Y=Y3         ! Simulate Free Receptor Concentration
          !Y=Y4         ! Simulate Bound Receptor Concentration
ENDIF

IF(IFUN.EQ.0)THEN  ! SPECIAL USER OUTPUT SECTION
          CALL PROMT(SHOWIT) ! WANT TO SEE USER PLOT(S)?
           IF(SHOWIT) THEN
             CALL ADDOBSERVATIONSLEFT(1)
             CALL ADDFITTEDCURVELEFT(1)
             CALL LEFTLABEL('PLASMA CONC. (PMOLE)')
             CALL TITLE('SIMULATED COMP-TMD PLASMA CONCENTRATION')
             CALL XLABEL('TIME (HR)')
             CALL DISPLAYPLOT
             ! RECORD PLOT ID IF PLOT IS SAVED
             CALL RECORDPLOTIFSAVED(3)
```

```
        ENDIF           ! SHOWIT
ENDIF           ! IFUN = 0
RETURN
!*********  N O N  OPTIONAL DEFINITION SECTION **************
!
! THIS IS FOR RECORDING OF THE MODEL USED IN THE FITTING :
!
    ENTRY MODELID(ID)
    ID = 'INF TIM MODEL V1.0'
    RETURN
    END
```

B.2. Fortran subroutines for simulation of the recirculation model

```
! THESE SUBROUTINES TO DEFINE THE MODEL TO BE SIMULATED BY
WINFUNFIT
! PROGRAMMED BY MHE IN FEBRUARY 2011

SUBROUTINE USERMODEL_ODE(T,Y,YPRIME,P,NP,IFUN)
! THIS SUBROUTINE DEFINES THE MODEL DIFFERENTIAL EQUATIONS

IMPLICIT NONE
REAL*8 :: Y(*), YPRIME(*), P(*) ,T
INTEGER  :: NP,IFUN
REAL*8 ::
ALPHA,BETA,ENTM,KSYN,KDEG,KON,KOFF,KINT,P1,Q,VEC,D,FOUT1,FOUT2,
FOUT3,CIN,ONE = 1D0

ALPHA=P(1)
BETA=P(2)
ENTM=P(3)
KSYN=P(4)
KDEG=P(5)
KON=P(6)
KOFF=P(7)
KINT=P(8)
P1=P(9)
Q=P(10)
VEC=P(11)
D=P(12)

FOUT1= ALPHA*Y(1)
FOUT3=(ONE-P1)*(ONE-ENTM)*BETA*Y(2)
FOUT2=P1*Q*Y(3)
CIN=FOUT1/Q

IF(IFUN.EQ.1)THEN
```

```
        YPRIME(1) = -ALPHA*Y(1)+(FOUT2+FOUT3)
        YPRIME(2) = -BETA*Y(2)+FOUT1
        YPRIME(3) = -KON*Y(4)*Y(3)+KOFF*Y(5)+((P1*Q)/VEC)*(CIN-Y(3))
        YPRIME(4) = KSYN-KDEG*Y(4)-KON*Y(4)*Y(3)+KOFF*Y(5)
        YPRIME(5) = -KINT*Y(5)-KOFF*Y(5)+KON*Y(4)*Y(3)
ENDIF
RETURN
END


SUBROUTINE USERMODEL_ODE_JACOBIAN (T,Y,DFDT,DFDY,N,P,NP,IFUN)

! THIS SUBROUTINE IS NECESSARY FOR SOLVING STIFF DIFFERENTIAL
EQUATIONS
! THIS SUBROUTINE DEFINES THE PARTIAL DERIVATIVE OF EACH
DIFFERENTIAL EQUATION WITH RESPECT TO TIME AND EACH Y VARIABLE

 IMPLICIT NONE
 INTEGER, INTENT(IN)::N,NP,IFUN
 DOUBLE PRECISION, INTENT(IN)::T
 DOUBLE PRECISION,DIMENSION(N), INTENT (IN)::Y
 DOUBLE PRECISION,DIMENSION(N),INTENT(OUT)::DFDT
 DOUBLE PRECISION,DIMENSION(N,N),INTENT(OUT)::DFDY
 DOUBLE PRECISION,DIMENSION(NP),INTENT(IN)::P
 DOUBLE PRECISION,PARAMETER::ZERO=0D0,ONE=1D0
 DOUBLE PRECISION ::
ALPHA,BETA,ENTM,KSYN,KDEG,KON,KOFF,KINT,P1,Q,VEC,D

ALPHA=P(1)
BETA=P(2)
ENTM=P(3)
KSYN=P(4)
KDEG=P(5)
KON=P(6)
KOFF=P(7)
KINT=P(8)
P1=P(9)
Q=P(10)
VEC=P(11)
D=P(12)

 IF(IFUN.EQ.1)THEN
        DFDT(1)=ZERO
        DFDT(2)=ZERO
        DFDT(3)=ZERO
        DFDT(4)=ZERO
```

```
        DFDT(5)=ZERO

        DFDY(1,1)=-ALPHA
        DFDY(1,2)=(ONE-P1)*(ONE-ENTM)*BETA
        DFDY(1,3)=P1*Q
        DFDY(1,4)=ZERO
        DFDY(1,5)=ZERO

        DFDY(2,1)=ALPHA
        DFDY(2,2)=-BETA
        DFDY(2,3)=ZERO
        DFDY(2,4)=ZERO
        DFDY(2,5)=ZERO

        DFDY(3,1)=P1*ALPHA/VEC
        DFDY(3,2)=ZERO
        DFDY(3,3)=-KON*Y(4)-P1*Q/VEC
        DFDY(3,4)=-KON*Y(3)
        DFDY(3,5)=KOFF

        DFDY(4,1)=ZERO
        DFDY(4,2)=ZERO
        DFDY(4,3)=-KON*Y(4)
        DFDY(4,4)=-KDEG-KON*Y(3)
        DFDY(4,5)=KOFF

        DFDY(5,1)=ZERO
        DFDY(5,2)=ZERO
        DFDY(5,3)=KON*Y(4)
        DFDY(5,4)=KON*Y(3)
        DFDY(5,5)=-KINT-KOFF
ENDIF
END SUBROUTINE USERMODEL_ODE_JACOBIAN


SUBROUTINE USERMODEL(T,Y,P,NP,IFUN)
! THIS SUBROUTINE:
! (1) DEFINES THE EQUATIONS TO BE FITTED
! (2) ASSIGNS NAMES TO THE PARAMETERS (IFUN=-1000 CALL)
! (3) ALLOWS THE USER TO DEFINE AND REGISTER EVENT (IFUN =-1000
CALL)
! (4) INTERACTIVELY ALLOWS THE USER TO SELECT THE ALGORITHM TO
BE
! USED BY WINFUNFIT FOR THE INTEGRATION OF THE DIFFERENTIAL
EQUATIONS SPECIFIED IN THE SUBROUTINE "USERMODEL_ODE" GIVEN
ABOVE.
```

```
! (5) ALLOWS FITTING SPLINES TO EXTERNAL DATA
! (6) PROVIDES THE USER THE OPPORTUNITY TO MAKE SPECIAL
CALCULATIONS AND PLOTS AFTER WINFUNFIT HAS COMPLETED A
FITTING TO A DATA SET (IFUN=0 CALL)

IMPLICIT  NONE
INTEGER                    :: NP, IFUN, JFUN, J,JY,I
INTEGER,PARAMETER          :: NEQN=5
REAL*8                     :: T, Y, P(*)
REAL*8                     ::
ALPHA,BETA,ENTM,KSYN,KDEG,KON,KOFF,KINT,P1,Q,VEC,D,FOUT1,FOUT2,
FOUT3,Y1,Y2,Y3,Y4,Y5
INTEGER                    :: NOBSB, NOBSP, LUN, NSIGDIGITS
REAL*8                     :: FACTOR, ZERO = 0D0, TZERO = 0D0 , ONE = 1D0
LOGICAL, SAVE              :: SHOWIT, PLOTSAVED
CHARACTER (LEN=256)        :: ID, DATAFILENAME
CHARACTER (LEN=20)         :: PNAME
REAL*8                     :: YZERO(NEQN)

ALPHA=P(1)
BETA=P(2)
ENTM=P(3)
KSYN=P(4)
KDEG=P(5)
KON=P(6)
KOFF=P(7)
KINT=P(8)
P1=P(9)
Q=P(10)
VEC=P(11)
D=P(12)

IF(IFUN.EQ.-1000)THEN
        CALL SetFunfitParameterName(1,"ALPHA")
        CALL SetFunfitParameterName(2,"BETA")
        CALL SetFunfitParameterName(3,"ENTM")
        CALL SetFunfitParameterName(4,"KSYN")
        CALL SetFunfitParameterName(5,"KDEG")
        CALL SetFunfitParameterName(6,"KON")
        CALL SetFunfitParameterName(7,"KOFF")
        CALL SetFunfitParameterName(8,"KINT")
        CALL SetFunfitParameterName(9,"P1")
        CALL SetFunfitParameterName(10,"Q")
        CALL SetFunfitParameterName(11,"VEC")
        CALL SetFunfitParameterName(12,"D")
```

```
        CALL SET_INTEGRATOR(6)
ENDIF

IF(IFUN.EQ.1) THEN

        YZERO(1) = D
        YZERO(2)=ZERO
        YZERO(3)= ZERO
        YZERO(4) = KSYN/KDEG
        YZERO(5)= ZERO

        JY = 1
        CALL
INTEGRATE_USERMODEL_ODE(T,Y1,P,NP,IFUN,TZERO,YZERO,NEQN,JY)
         JY=2
         CALL
INTEGRATE_USERMODEL_ODE(T,Y2,P,NP,IFUN,TZERO,YZERO,NEQN,JY)
         JY=3
         CALL
INTEGRATE_USERMODEL_ODE(T,Y3,P,NP,IFUN,TZERO,YZERO,NEQN,JY)
         JY=4
         CALL
INTEGRATE_USERMODEL_ODE(T,Y4,P,NP,IFUN,TZERO,YZERO,NEQN,JY)
         JY=5
         CALL
INTEGRATE_USERMODEL_ODE(T,Y5,P,NP,IFUN,TZERO,YZERO,NEQN,JY)

        FOUT1=ALPHA*Y1
        FOUT3=(ONE-P1)*(ONE-ENTM)*BETA*Y2
        FOUT2=P1*Q*Y3
        Y=(FOUT2+FOUT3)/Q        ! Simulate Plasma Concentration
        !Y=Y4          ! Simulate Free Receptor Concentration
        !Y=Y5          ! Simulate Bound Receptor Concentration
ENDIF

IF(IFUN.EQ.0)THEN  ! SPECIAL USER OUTPUT SECTION
        CALL PROMT(SHOWIT) ! WANT TO SEE USER PLOT(S)?
         IF(SHOWIT) THEN
           CALL ADDOBSERVATIONSLEFT(1)
           CALL ADDFITTEDCURVELEFT(1)
           CALL LEFTLABEL('PLASMA CONC. (PMOLE)')
           CALL TITLE('SIMULATED REC-TMD PLASMA CONCENTRATION')
           CALL XLABEL('TIME (HR)')
           CALL DISPLAYPLOT
           ! RECORD PLOT ID IF PLOT IS SAVED
           CALL RECORDPLOTIFSAVED(3)
```

```
          ENDIF          ! SHOWIT
ENDIF           ! IFUN = 0
RETURN
!*********  N O N  OPTIONAL DEFINITION SECTION **************
!
! THIS IS FOR RECORDING OF THE MODEL USED IN THE FITTING :
!
    ENTRY MODELID(ID)
    ID = 'INF TIM MODEL V1.0'
    RETURN
    END
```

APPENDIX C. NONMEM CODES FOR CHAPTER 6

C.1. Control stream file for simulation/fitting of the compartmental model

```
$PROB SIMULATION/FITTING OF COMPARTMENTAL TMD MODEL
$DATA comp.csv IGNORE=C
$INPUT TIME DV EVID CMT AMT
$SUBROUTINE ADVAN = 8 TOL =4
$MODEL NCOMP = 4
        COMP=(BLOOD)
        COMP=(PERIPH)
        COMP=(FREEREC)
        COMP=(BOUNDREC)
$PK
        IF(ICALL.EQ.4) THEN
                KEL=THETA(1)
                KPT=THETA(2)
                KTP=THETA(3)
                KSYN=THETA(4)
                KDEG=THETA(5)
                KON=THETA(6)
                KOFF=THETA(7)
                KINT=THETA(8)
                V=THETA(9)
        ELSE
                KEL=THETA(10)
                KPT=THETA(11)
                KTP=THETA(12)
                KSYN=THETA(13)
                KDEG=THETA(14)
                KON=THETA(15)
                KOFF=THETA(16)
                KINT=THETA(17)
                V=THETA(18)
        ENDIF
        KELA=THETA(10)
        KPTA=THETA(11)
        KTPA=THETA(12)
        KSYNA=THETA(13)
        KDEGA=THETA(14)
        KONA=THETA(15)
        KOFFA=THETA(16)
        KINTA=THETA(17)
        VA=THETA(18)
```

```
        F1=1/V
        A_0(3)=KSYN/KDEG
$DES
        DADT(1)= -KON*A(1)*A(3)+KOFF*A(4)-(KEL+KPT)*A(1)+KTP*A(2)/V
        DADT(2)= -KTP*A(2)+KPT*A(1)*V
        DADT(3)= KSYN-KON*A(1)*A(3)+KOFF*A(4)-KDEG*A(3)
        DADT(4)= KON*A(1)*A(3)-(KOFF+KINT)*A(4)
$ERROR
        sol=A(1)
        IF(ICALL.EQ.4) THEN
                Y = sol*(1+ETA(1))
        ELSE
                Y = sol*(1+ETA(2))
        ENDIF
$THETA
        0.106  FIX
        0.064  FIX
        0.123  FIX
        9.141 FIX
        0.079 FIX
        0.03 FIX
        1.74 FIX
        3.6 FIX
        2.24 FIX
        (0,0.1306)
        (0,0.069)
        (0,0.116)
        (0,9.59)
        (0,0.066)
        (0,0.0324)
        (0,1.6)
        (0,3.329)
        (0,2.37)
$OMEGA
        0.01 FIX  ; 10% proportional error model
        0.011
$SIM (12345) SUBPROB=1000 (2000 NORMAL)
$ESTIMATION   MAXEVALS=9999999   PRINT=0 NOABORT NSIG=2
$TABLE KELA KPTA KTPA VA KSYNA KDEGA KONA KOFFA KINTA
NOAPPEND NOHEADER NOPRINT FILE=comptab.txt
```

C.2. Control stream file for simulation/fitting of the recirculation model

```
$PROB SIMULATION/FITTING OF RECIRCULATION TMD MODEL
$DATA rec.csv IGNORE=C
```

```
$INPUT TIME DV EVID CMT AMT
$SUBROUTINE ADVAN = 8 TOL =4
$MODEL NCOMP = 5
        COMP=(HEART)
        COMP=(NTM)
        COMP=(TM)
        COMP=(FREEREC)
        COMP=(BOUNDREC)
$PK
        IF(ICALL.EQ.4) THEN
                ALPHA=THETA(1)
                BETA=THETA(2)
                ENTM=THETA(3)
                KSYN=THETA(4)
                KDEG=THETA(5)
                KON=THETA(6)
                KOFF=THETA(7)
                KINT=THETA(8)
        ELSE
                ALPHA=THETA(9)
                BETA=THETA(10)
                ENTM=THETA(11)
                KSYN=THETA(12)
                KDEG=THETA(13)
                KON=THETA(14)
                KOFF=THETA(15)
                KINT=THETA(16)
        ENDIF
        ALPHAA = THETA(9)
        BETAA = THETA(10)
        ENTMA = THETA(11)
        KSYNA = THETA(12)
        KDEGA = THETA(13)
        KONA = THETA(14)
        KOFFA = THETA(15)
        KINTA = THETA(16)
        QQ=312
        P1=0.9
        VEC=2.24
        A_0(4)=KSYN/KDEG
$DES
        FOUT1=ALPHA*A(1)
        FOUT3=(1-P1)*(1-ENTM)*BETA*A(2)
        FOUT2=P1*QQ*A(3)
        CIN=FOUT1/QQ
```

```
        DADT(1)= -ALPHA*A(1)+(FOUT2+FOUT3)
        DADT(2)= -BETA*A(2)+FOUT1
        DADT(3) = -KON*A(4)*A(3)+KOFF*A(5)+((P1*QQ)/VEC)*(CIN-A(3))
        DADT(4)= KSYN-KDEG*A(4)-KON*A(4)*A(3)+KOFF*A(5)
        DADT(5)= -KINT*A(5)-KOFF*A(5)+KON*A(4)*A(3)
$ERROR
        FOUTT1=ALPHA*A(1)
        FOUTT3=(1-P1)*(1-ENTM)*BETA*A(2)
        FOUTT2=P1*QQ*A(3)
        sol=(FOUTT2+FOUTT3)/QQ
        IF(ICALL.EQ.4) THEN
                Y = sol*(1+ETA(1))
        ELSE
                Y = sol*(1+ETA(2))
        ENDIF
$THETA
        140 FIX
        14 FIX
        0.007 FIX
        9.141 FIX
        0.079 FIX
        0.03 FIX
        1.74 FIX
        3.6 FIX
        (0,107.55)
        (0,13.1)
        (0,0.009,1)
        (0,9.59)
        (0,0.066)
        (0,0.0324)
        (0,1.6)
        (0,3.329)
$OMEGA
        0.01 FIX  ; 10% proportional error model
        0.011
$SIM (12345) SUBPROB=1000 (2000 NORMAL)
$ESTIMATION   MAXEVALS=9999999   PRINT=0 NOABORT NSIG=2
$TABLE ALPHAA BETAA ENTMA KSYNA KDEGA KONA KOFFA KINTA
NOAPPEND NOHEADER NOPRINT FILE=rectab.txt
```

APPENDIX D. SAS CODES FOR CHAPTER 6

D.1. Compartmental model D-optimal sampling times

```
data Candidates;
do Time = 0 to 100 by 0.001;
output;
end;

proc model data=Candidates noprint;
dependent C1 C2 C3 C4;
parm KSYN 9.141 KDEG 0.079 KON 0.03 KOFF 1.74 KINT 3.6 KPT 0.064 KTP
0.123 V 2.24 KEL 0.106;
dose=129.92;
if ( time=0 ) then
        do;
                C1=dose/V;
                C2=0;
                C3=KSYN/KDEG;
                C4=0;
        end;
 else
        do;
            dert.C1= -KON*C1*C3+KOFF*C4-(KEL+KPT)*C1+KTP*C2/V;
            dert.C2= -KTP*C2+KPT*C1*V;
            dert.C3= KSYN-KON*C1*C3+KOFF*C4-KDEG*C3;
            dert.C4= KON*C1*C3-(KOFF+KINT)*C4;
        end;
solve C1 C2 C3 C4/ out=Solution time=Time;

proc model data=Solution noprint;
dependent C1 C2 C3 C4;
parm KSYN 9.141 KDEG 0.079 KON 0.03 KOFF 1.74 KINT 3.6 KPT 0.064 KTP
0.123 V 2.24 KEL 0.106;
dose=129.92;
if ( time=0 ) then
        do;
            C1=dose/V;
            C2=0;
            C3=KSYN/KDEG;
            C4=0;
        end;
else
        do;
            dert.C1= -KON*C1*C3+KOFF*C4-(KEL+KPT)*C1+KTP*C2/V;
            dert.C2= -KTP*C2+KPT*C1*V;
```

```
            dert.C3= KSYN-KON*C1*C3+KOFF*C4-KDEG*C3;
            dert.C4= KON*C1*C3-(KOFF+KINT)*C4;
        end;
f1 = getder( C1, KSYN );
f2 = getder( C1, KDEG );
f3 = getder( C1, KON );
f4 = getder( C1, KOFF );
f5 = getder( C1, KINT );
f6 = getder( C1, KPT );
f7 = getder( C1, KTP );
f8 = getder( C1, V );
f9 = getder( C1, KEL );
outvar f1 f2 f3 f4 f5 f6 f7 f8 f9;
restrict KSYN=9.141,  KDEG=0.079,  KON=0.03,  KOFF=1.74,  KINT=3.6,
KPT=0.064, KTP=0.123, V=2.24, KEL=0.106;
fit C1 / out=Jacobian dynamic;
run;

proc optex data=Jacobian coding=NONE;
model f1 f2 f3 f4 f5 f6 f7 f8 f9/ noint;
generate n=9 method=m_fedorov niter=100 keep=1 CRITERION=D;
output out=Design;
id Time;
proc print data=Design;
run;
```

D.2. Recirculation model D-optimal sampling times

```
data Candidates;
do Time = 0 to 100 by 0.001;
output;
end;

proc model data=Candidates noprint;
dependent C1 C2 C3 C4 C5 C6;
parm KSYN  9.141  KDEG  0.079  KON  0.03  KOFF  1.74  KINT  3.6 ALPHA 140
BETA 14 ENTM 0.007;
dose=129.92;
QQ=312;
P1=0.9;
VEC=2.24;
if ( time=0 ) then
        do;
            C1=dose;
            C2=0;
            C3=0;
            C4=KSYN/KDEG;
```

```
            C5=0;
            C6=0;
        end;
else
        do;
          dert.C1= -ALPHA*C1+C6*QQ;
          dert.C2= -BETA*C2+ALPHA*C1;
          dert.C3 = -KON*C4*C3+KOFF*C5+((P1*QQ)/VEC)*((ALPHA*C1/QQ)-C3);
         dert.C4= KSYN-KDEG*C4-KON*C4*C3+KOFF*C5;
         dert.C5= -KINT*C5-KOFF*C5+KON*C4*C3;
         dert.C6=(P1*QQ*dert.C3+(1-P1)*(1-ENTM)*BETA*dert.C2)/QQ;
        end;
solve C1 C2 C3 C4 C5 C6/ out=Solution time=Time;

proc model data=Solution noprint;
dependent C1 C2 C3 C4 C5 C6;
parm KSYN 9.141 KDEG 0.079 KON 0.03 KOFF 1.74 KINT 3.6 ALPHA 140
BETA 14 ENTM 0.007;
dose=129.92;
QQ=312;
P1=0.9;
VEC=2.24;
if ( time=0 ) then
        do;
            C1=dose;
            C2=0;
            C3=0;
            C4=KSYN/KDEG;
            C5=0;
            C6=0;
        end;
else
        do;
          dert.C1= -ALPHA*C1+C6*QQ;
          dert.C2= -BETA*C2+ALPHA*C1;
          dert.C3 = -KON*C4*C3+KOFF*C5+((P1*QQ)/VEC)*((ALPHA*C1/QQ)-C3);
          dert.C4= KSYN-KDEG*C4-KON*C4*C3+KOFF*C5;
          dert.C5= -KINT*C5-KOFF*C5+KON*C4*C3;
          dert.C6=(P1*QQ*dert.C3+(1-P1)*(1-ENTM)*BETA*dert.C2)/QQ;
        end;
f1 = getder( C6, KSYN );
f2 = getder( C6, KDEG );
f3 = getder( C6, KON );
f4 = getder( C6, KOFF );
f5 = getder( C6, KINT );
f6 = getder( C6, ALPHA );
```

```
f7 = getder( C6, BETA );
f8 = getder( C6, ENTM );
outvar f1 f2 f3 f4 f5 f6 f7 f8;
restrict KSYN=9.141,  KDEG=0.079,  KON=0.03,  KOFF=1.74,  KINT=3.6,
ALPHA=140, BETA=14, ENTM=0.007;
fit C6 / out=Jacobian dynamic;
run;

proc optex data=Jacobian coding=NONE;
model f1 f2 f3 f4 f5 f6 f7 f8/ noint;
generate n=8 method=m_fedorov niter=100 keep=1 CRITERION=D;
output out=Design;
id Time;
proc print data=Design;
run;
```

APPENDIX E. R CODES FOR CHAPTER 6

E.1. Compartmental model parameters bias and precision calculation

```
#################################################################
##Data manipulation-extraction-cleaning
#1) In nonmem summary output delete the model specifications till the part (problem no. 1---).
#2) Copy the summary into excel sheet as separate columns.
#3) Copy the (TERMINATED or SUCCESSFUL) column and the (ERROR=) and the (Subproblem number) column to #another excel #sheet.
#4) Add cells to the (Subproblem number) column till it matches the (TERMINATED or SUCCESSFUL) words.
#5) Name the (TERMINATED or SUCCESSFUL) column as (xx1) and the (Subproblem number) column as (xx2).
#6) SaVe the excel sheet as (nmsummary.csV).
#7) Copy the nonmem table into excel sheet and add the names of the parameters as lower cases (eg. #alpha,KSYN,--etc.).
#8) SaVe excel sheet as (nmparam.csV).
#################################################################
data=read.csv("C://Documents and Settings/melkomy/Desktop/NMcomp/nmsummary1a.csv")
data2<-data[data$XX1=="SUCCESSFUL",]
XX4<-as.vector(data2$XX2)
XX5<-as.numeric(XX4)
XX5<-as.numeric(XX4)
XX6<-XX5[XX5<=1000]
succ<-XX6
index<-(succ*50)-5
nn<-length(succ)
data.man=read.csv("C://Documents and Settings/melkomy/Desktop/NMcomp/nmparam1a.csv")
data.fin<-data.man[index,]
write.csv(data.fin,file="C://Documents and Settings/melkomy/Desktop/NMcomp/extrparam1a.csv")
###################################
#####################################################################
##calculation of bias and precision
#####################################################################
param<-read.csv("C://Documents and Settings/melkomy/Desktop/NMcomp/extrparam1a.csv")
KEL.true=0.106
KPT.true=0.064
KTP.true=0.123
V.true=2.24
KSYN.true=9.141
```

```
KDEG.true=0.079
KON.true=0.03
KOFF.true=1.74
KINT.true=3.6

KEL.bias<-((mean(param$KEL)-KEL.true)/KEL.true)*100
KPT.bias<-((mean(param$KPT)-KPT.true)/KPT.true)*100
KTP.bias<-((mean(param$KTP)-KTP.true)/KTP.true)*100
V.bias<-((mean(param$V)-V.true)/V.true)*100
KSYN.bias<-((mean(param$KSYN)-KSYN.true)/KSYN.true)*100
KDEG.bias<-((mean(param$KDEG)-KDEG.true)/KDEG.true)*100
KON.bias<-((mean(param$KON)-KON.true)/KON.true)*100
KOFF.bias<-((mean(param$KOFF)-KOFF.true)/KOFF.true)*100
KINT.bias<-((mean(param$KINT)-KINT.true)/KINT.true)*100

KEL.bias.rse<-(sd(param$KEL)/(KEL.true*sqrt(nn)))*100
KEL.bias.upp<-KEL.bias+1.96*KEL.bias.rse
KEL.bias.low<-KEL.bias-1.96*KEL.bias.rse

KPT.bias.rse<-(sd(param$KPT)/(KPT.true*sqrt(nn)))*100
KPT.bias.upp<-KPT.bias+1.96*KPT.bias.rse
KPT.bias.low<-KPT.bias-1.96*KPT.bias.rse

KTP.bias.rse<-(sd(param$KTP)/(KTP.true*sqrt(nn)))*100
KTP.bias.upp<-KTP.bias+1.96*KTP.bias.rse
KTP.bias.low<-KTP.bias-1.96*KTP.bias.rse

V.bias.rse<-(sd(param$V)/(V.true*sqrt(nn)))*100
V.bias.upp<-V.bias+1.96*V.bias.rse
V.bias.low<-V.bias-1.96*V.bias.rse

KSYN.bias.rse<-(sd(param$KSYN)/(KSYN.true*sqrt(nn)))*100
KSYN.bias.upp<-KSYN.bias+1.96*KSYN.bias.rse
KSYN.bias.low<-KSYN.bias-1.96*KSYN.bias.rse

KDEG.bias.rse<-(sd(param$KDEG)/(KDEG.true*sqrt(nn)))*100
KDEG.bias.upp<-KDEG.bias+1.96*KDEG.bias.rse
KDEG.bias.low<-KDEG.bias-1.96*KDEG.bias.rse

KON.bias.rse<-(sd(param$KON)/(KON.true*sqrt(nn)))*100
KON.bias.upp<-KON.bias+1.96*KON.bias.rse
KON.bias.low<-KON.bias-1.96*KON.bias.rse

KOFF.bias.rse<-(sd(param$KOFF)/(KOFF.true*sqrt(nn)))*100
KOFF.bias.upp<-KOFF.bias+1.96*KOFF.bias.rse
KOFF.bias.low<-KOFF.bias-1.96*KOFF.bias.rse
```

```
KINT.bias.rse<-(sd(param$KINT)/(KINT.true*sqrt(nn)))*100
KINT.bias.upp<-KINT.bias+1.96*KINT.bias.rse
KINT.bias.low<-KINT.bias-1.96*KINT.bias.rse

KEL.prec<-(sd(param$KEL)/(sqrt(nn)*mean(param$KEL)))*100
KPT.prec<-(sd(param$KPT)/(sqrt(nn)*mean(param$KPT)))*100
KTP.prec<-(sd(param$KTP)/(sqrt(nn)*mean(param$KTP)))*100
V.prec<-(sd(param$V)/(sqrt(nn)*mean(param$V)))*100
KSYN.prec<-(sd(param$KSYN)/(sqrt(nn)*mean(param$KSYN)))*100
KDEG.prec<-(sd(param$KDEG)/(sqrt(nn)*mean(param$KDEG)))*100
KON.prec<-(sd(param$KON)/(sqrt(nn)*mean(param$KON)))*100
KOFF.prec<-(sd(param$KOFF)/(sqrt(nn)*mean(param$KOFF)))*100
KINT.prec<-(sd(param$KINT)/(sqrt(nn)*mean(param$KINT)))*100
#####################################
##output results
#####################################
KEL<-c(KEL.bias,KEL.bias.low,KEL.bias.upp,KEL.prec)
KPT<-c(KPT.bias,KPT.bias.low,KPT.bias.upp,KPT.prec)
KTP<-c(KTP.bias,KTP.bias.low,KTP.bias.upp,KTP.prec)
V<-c(V.bias,V.bias.low,V.bias.upp,V.prec)
KSYN<-c(KSYN.bias,KSYN.bias.low,KSYN.bias.upp,KSYN.prec)
KDEG<-c(KDEG.bias,KDEG.bias.low,KDEG.bias.upp,KDEG.prec)
KON<-c(KON.bias,KON.bias.low,KON.bias.upp,KON.prec)
KOFF<-c(KOFF.bias,KOFF.bias.low,KOFF.bias.upp,KOFF.prec)
KINT<-c(KINT.bias,KINT.bias.low,KINT.bias.upp,KINT.prec)
NRUN<-c(nn,nn,nn,nn)

summary<-
matrix(data=c(KEL,KPT,KTP,V,KSYN,KDEG,KON,KOFF,KINT,NRUN),nrow=4,ncol
=10,byrow=F,dimnames=list(c("Bias","Bias.Low","Bias.UPP","Precision"),c("KEL","K
PT","KTP","V","KSYN","KDEG","KON","KOFF","KINT","NRUN")))
write.csv(summary,file="C://Documents and
Settings/melkomy/Desktop/NMcomp/rsummary1a.csv")
```

E.2. Recirculation model parameters bias and precision calculation

```
#############################################################
##Data manipulation-extraction-cleaning
#1) In nonmem summary output delete the model specifications till the part (problem no.
1---).
#2) Copy the summary into excel sheet as separate columns.
#3) Copy the (TERMINATED or SUCCESSFUL) column and the (ERROR=) and the
(Subproblem number) column to #another excel #sheet.
#4) Add cells to the (Subproblem number) column till it matches the (TERMINATED or
SUCCESSFUL) words.
```

```
#5) Name the (TERMINATED or SUCCESSFUL) column as (xx1) and the (Subproblem
number) column as (xx2).
#6) SaVe the excel sheet as (nmsummary.csV).
#7) Copy the nonmem table into excel sheet and add the names of the parameters as
lower cases (eg. #alpha,KSYN,--etc.).
#8) SaVe excel sheet as (nmparam.csV).
#################################################################
data=read.csv("C://Documents and
Settings/melkomy/Desktop/NMrec/nmsummary1a.csv")
data2<-data[data$XX1=="SUCCESSFUL",]
XX4<-as.vector(data2$XX2)
XX5<-as.numeric(XX4)
XX6<-XX5[XX5<=1000]
succ<-XX6
index<-(succ*45)-5
nn<-length(succ)
data.man=read.csv("C://Documents and
Settings/melkomy/Desktop/NMrec/nmparam1a.csv")
data.fin<-data.man[index,]
write.csv(data.fin,file="C://Documents and
Settings/melkomy/Desktop/NMrec/extrparam1a.csv")
###################################
#####################################################################
##calculation of bias and precision
#####################################################################
param<-read.csv("C://Documents and
Settings/melkomy/Desktop/NMrec/extrparam1a.csv")
ALPHA.true=140
BETA.true=14
ENTM.true=0.007
KSYN.true=9.141
KDEG.true=0.079
KON.true=0.03
KOFF.true=1.74
KINT.true=3.6

ALPHA.bias<-((mean(param$ALPHA)-ALPHA.true)/ALPHA.true)*100
BETA.bias<-((mean(param$BETA)-BETA.true)/BETA.true)*100
ENTM.bias<-((mean(param$ENTM)-ENTM.true)/ENTM.true)*100
KSYN.bias<-((mean(param$KSYN)-KSYN.true)/KSYN.true)*100
KDEG.bias<-((mean(param$KDEG)-KDEG.true)/KDEG.true)*100
KON.bias<-((mean(param$KON)-KON.true)/KON.true)*100
KOFF.bias<-((mean(param$KOFF)-KOFF.true)/KOFF.true)*100
KINT.bias<-((mean(param$KINT)-KINT.true)/KINT.true)*100

ALPHA.bias.rse<-(sd(param$ALPHA)/(ALPHA.true*sqrt(nn)))*100
```

```
ALPHA.bias.upp<-ALPHA.bias+1.96*ALPHA.bias.rse
ALPHA.bias.low<-ALPHA.bias-1.96*ALPHA.bias.rse

BETA.bias.rse<-(sd(param$BETA)/(BETA.true*sqrt(nn)))*100
BETA.bias.upp<-BETA.bias+1.96*BETA.bias.rse
BETA.bias.low<-BETA.bias-1.96*BETA.bias.rse

ENTM.bias.rse<-(sd(param$ENTM)/(ENTM.true*sqrt(nn)))*100
ENTM.bias.upp<-ENTM.bias+1.96*ENTM.bias.rse
ENTM.bias.low<-ENTM.bias-1.96*ENTM.bias.rse

KSYN.bias.rse<-(sd(param$KSYN)/(KSYN.true*sqrt(nn)))*100
KSYN.bias.upp<-KSYN.bias+1.96*KSYN.bias.rse
KSYN.bias.low<-KSYN.bias-1.96*KSYN.bias.rse

KDEG.bias.rse<-(sd(param$KDEG)/(KDEG.true*sqrt(nn)))*100
KDEG.bias.upp<-KDEG.bias+1.96*KDEG.bias.rse
KDEG.bias.low<-KDEG.bias-1.96*KDEG.bias.rse

KON.bias.rse<-(sd(param$KON)/(KON.true*sqrt(nn)))*100
KON.bias.upp<-KON.bias+1.96*KON.bias.rse
KON.bias.low<-KON.bias-1.96*KON.bias.rse

KOFF.bias.rse<-(sd(param$KOFF)/(KOFF.true*sqrt(nn)))*100
KOFF.bias.upp<-KOFF.bias+1.96*KOFF.bias.rse
KOFF.bias.low<-KOFF.bias-1.96*KOFF.bias.rse

KINT.bias.rse<-(sd(param$KINT)/(KINT.true*sqrt(nn)))*100
KINT.bias.upp<-KINT.bias+1.96*KINT.bias.rse
KINT.bias.low<-KINT.bias-1.96*KINT.bias.rse

ALPHA.prec<-(sd(param$ALPHA)/(sqrt(nn)*mean(param$ALPHA)))*100
BETA.prec<-(sd(param$BETA)/(sqrt(nn)*mean(param$BETA)))*100
ENTM.prec<-(sd(param$ENTM)/(sqrt(nn)*mean(param$ENTM)))*100
KSYN.prec<-(sd(param$KSYN)/(sqrt(nn)*mean(param$KSYN)))*100
KDEG.prec<-(sd(param$KDEG)/(sqrt(nn)*mean(param$KDEG)))*100
KON.prec<-(sd(param$KON)/(sqrt(nn)*mean(param$KON)))*100
KOFF.prec<-(sd(param$KOFF)/(sqrt(nn)*mean(param$KOFF)))*100
KINT.prec<-(sd(param$KINT)/(sqrt(nn)*mean(param$KINT)))*100
#####################################
##output results
#####################################
ALPHA<-c(ALPHA.bias,ALPHA.bias.low,ALPHA.bias.upp,ALPHA.prec)
BETA<-c(BETA.bias,BETA.bias.low,BETA.bias.upp,BETA.prec)
ENTM<-c(ENTM.bias,ENTM.bias.low,ENTM.bias.upp,ENTM.prec)
KSYN<-c(KSYN.bias,KSYN.bias.low,KSYN.bias.upp,KSYN.prec)
```

```
KDEG<-c(KDEG.bias,KDEG.bias.low,KDEG.bias.upp,KDEG.prec)
KON<-c(KON.bias,KON.bias.low,KON.bias.upp,KON.prec)
KOFF<-c(KOFF.bias,KOFF.bias.low,KOFF.bias.upp,KOFF.prec)
KINT<-c(KINT.bias,KINT.bias.low,KINT.bias.upp,KINT.prec)
NRUN<-c(nn,nn,nn,nn)

summary<-
matrix(data=c(ALPHA,BETA,ENTM,KSYN,KDEG,KON,KOFF,KINT,NRUN),nrow=4
,ncol=9,byrow=F,dimnames=list(c("Bias","Bias.Low","Bias.UPP","Precision"),c("ALPH
A","BETA","ENTM","KSYN","KDEG","KON","KOFF","KINT","NRUN")))
write.csv(summary,file="C://Documents and
Settings/melkomy/Desktop/NMrec/rsummary1a.csv")
```

E.3. Plotting of Figure 6.8

```
 ##############################################################
equiv.data=read.csv("F://Simulations_new/recept.csv")
dev.new(width=7.5, height=10)
par(mfrow=c(5,2),oma=c(2.5,5.5,3.5,0.5),mar=c(0.5,5.5,1,0))
par<-unique(equiv.data$param)

for(i in 1:length(par)){
data<-equiv.data[equiv.data$param==par[i],]
#Bias plot
bias.comp0<-data$bias[data$model=="COMP-TMD"]
bias.comp.up<-data$bias.up[data$model=="COMP-TMD"]
bias.comp.low<-data$bias.low[data$model=="COMP-TMD"]
bias.rec0<-data$bias[data$model=="REC-TMD"]
bias.rec.up<-data$bias.up[data$model=="REC-TMD"]
bias.rec.low<-data$bias.low[data$model=="REC-TMD"]
x.lim<-c(0.8,2.2)
if((bias.comp0*bias.rec0)<0){
y.up<-max(abs(c(bias.comp.low,bias.comp.up,bias.rec.low,bias.rec.up)))+0.1
y.low<--y.up
}else{
y.up<-max(bias.comp.up,bias.rec.up,0)+0.1
y.low<-min(bias.comp.low,bias.rec.low,0)-0.1
}
y.dat.comp.up<-
seq(min(bias.comp0,bias.comp.up),max(bias.comp0,bias.comp.up),by=0.01)
x.dat.comp.up<-rep(1,length(y.dat.comp.up))
y.dat.comp.low<-
seq(min(bias.comp0,bias.comp.low),max(bias.comp0,bias.comp.low),by=0.01)
x.dat.comp.low<-rep(1,length(y.dat.comp.low))
y.dat.rec.up<-seq(min(bias.rec0,bias.rec.up),max(bias.rec0,bias.rec.up),by=0.01)
x.dat.rec.up<-rep(2,length(y.dat.rec.up))
y.dat.rec.low<-seq(min(bias.rec0,bias.rec.low),max(bias.rec0,bias.rec.low),by=0.01)
```

```
x.dat.rec.low<-rep(2,length(y.dat.rec.low))
plot(data$bias, data$prec,
type="n",xlim=x.lim,ylim=c(y.low,y.up),xlab="",ylab="",las=1,xaxt="n",yaxt="n",main=
"",font=2)
points(1,bias.comp0,col ="black",pch=16,cex=2)
points(2,bias.rec0,col ="black",pch=16,cex=2)
lines(x.dat.comp.up,y.dat.comp.up, col = "black", lwd = 2)
lines(x.dat.comp.low,y.dat.comp.low, col = "black", lwd = 2)
lines(x.dat.rec.up,y.dat.rec.up, col = "black", lwd = 2)
lines(x.dat.rec.low,y.dat.rec.low, col = "black", lwd = 2)
abline(h=0,lty=2,cex=2)
if(i==5){
axis(side=1, at=c(1,2),las=1,labels=c("COMP-TMD","REC-
TMD"),font=2,cex.axis=1.5,tick=F)
}
if(i==1) POS.Bias<-c(0,-0.4,-0.8,-1.2)
if(i==2) POS.Bias<-c(0,-0.5,-1,-1.5,-2)
if(i==3) POS.Bias<-c(6,3,0,-3,-6)
if(i==4) POS.Bias<-c(10,5,0,-5,-10,-15)
if(i==5) POS.Bias<-c(10,5,0,-5,-10)
axis(side=2,las=1,font=2,cex=1.2,at=POS.Bias)

#plot precision
prec.comp<-data$prec[data$model=="COMP-TMD"]
prec.rec<-data$prec[data$model=="REC-TMD"]
if(i<5){
put.names=F
}else{
put.names=T
}
excess<-c(0.05,0.05,0.05,0.2,0.2)
if(i==1) POS.Prec<-c(0.05,0.15,0.25)
if(i==2) POS.Prec<-c(0.1,0.3,0.5)
if(i==3) POS.Prec<-c(0.5,1,1.5)
if(i==4) POS.Prec<-c(1,2,3,4,5)
if(i==5) POS.Prec<-c(1,2,3,4)
barplot(height=data$prec,width=0.5,space=c(3,0.5),legend.text=F,beside=T,xlim=c(0,3),
ylim=c(0,max(prec.comp,prec.rec)+excess[i]),yaxt="n",axisnames=put.names,cex.names
=1.5,names.arg=c("COMP-TMD","REC-TMD"),las=1,main="",font=2)
axis(side=2,las=1,font=2,cex=1.2,at=POS.Prec)
box()
}
#################################
#Put text
mtext(text="%Bias", side=3, line=1, outer=T,col="black",cex=1.5,font=2,at=0.32)
```

```
mtext(text="%Imprecision", side=3, line=1,
outer=T,col="black",cex=1.5,font=2,at=0.82)
##########################################################
mtext(text=expression(bolditalic("k"[int])), side=2,
line=0.1,outer=T,las=2,col="black",cex=2,font=4,at=0.1,family="serif")
mtext(text=expression(bolditalic("k"[off])), side=2,
line=0.1,outer=T,las=2,col="black",cex=2,font=4,at=0.3,family="serif")
mtext(text=expression(bolditalic("k"[on])), side=2,
line=0.1,outer=T,las=2,col="black",cex=2,font=4,at=0.5,family="serif")
mtext(text=expression(bolditalic("k"[deg])), side=2,
line=0.1,outer=T,las=2,col="black",cex=2,font=4,at=0.7,family="serif")
mtext(text=expression(bolditalic("k"[syn])), side=2,
line=0.1,outer=T,las=2,col="black",cex=2,font=4,at=0.9,family="serif")
```

E.4 Plotting of Figure 6.9

```
##############################################################
equiv.data=read.csv("F://Simulations_new/nonrecept.csv")
par.names<-
c(expression(bolditalic("V")),expression(bolditalic("k"[el])),expression(bolditalic("k"[pt]
)),expression(bolditalic("k"[tp])),expression(bolditalic("E"[NTM])),expression(bolditalic(
alpha)),expression(bolditalic(beta)))
dev.new(width=10, height=7.5)
par(mfrow=c(2,1),oma=c(0,0,0,0),mar=c(2.5,2.5,4.5,0.5))
#Bias plot
y.up<-max(equiv.data$bias.up,0)+0.1
y.low<-min(equiv.data$bias.low,0)-0.1
par<-unique(equiv.data$param)
for(i in 1:length(par)){
data<-equiv.data[equiv.data$param==par[i],]
bias0<-data$bias
biasup<-data$bias.up
biaslow<-data$bias.low
x.lim<-c(0.8,7.2)
y.dat.up<-seq(min(bias0,biasup),max(bias0,biasup),by=0.01)
x.dat.up<-rep(i,length(y.dat.up))
y.dat.low<-seq(min(bias0,biaslow),max(bias0,biaslow),by=0.01)
x.dat.low<-rep(i,length(y.dat.low))
plot(data$bias, data$prec,
type="n",xlim=x.lim,ylim=c(y.low,y.up),xlab="",ylab="",las=1,main="%Bias",cex.main
=2,font=2,xaxt="n")
points(i,bias0,col ="black",pch=16,cex=2)
lines(x.dat.up,y.dat.up, col = "black", lwd = 2)
lines(x.dat.low,y.dat.low, col = "black", lwd = 2)
par(new=T)
}
axis(side=1,las=1,font=2,cex.axis=2,at=1:7,labels=par.names,family="serif",tick=F)
```

```
abline(h=0,lty=2,cex=2)

#Precision plot
barplot(height=equiv.data$prec,width=0.5,space=c(0,1.25,1.1,1.25,1,1.25,1.25),legend.te
xt=F,beside=T,xlim=c(0,7),ylim=c(0,max(equiv.data$prec)+0.05),axisnames=T,cex.nam
es=2,names.arg=par.names,las=1,main="%Imprecision",cex.main=2,font=2,family="seri
f")
box()
```

APPENDIX F. PUBLICATIONS AND SUBMITTED MANSUSCRIPTS

1. El-Komy MH, and Veng-Pedersen P, Equivalence of compartmental and recirculation target-mediated disposition pharmacokinetic models. Submitted to J Pharmacokinet Pharmacodyn.
2. Kania-Korwel I, Barnhart CD, Stamou M, Truong KM, El-Komy MH, Lein PJ, Veng-Pedersen P, and Lehmler HJ, 2,2',3,5',6-Pentachlorobiphenyl (PCB 95) and its hydroxylated metabolites are enantiomerically enriched in female mice. Accepted in Environ Sci Technol.
3. El-Komy MH, Schmidt RL, Widness JA, Veng-Pedersen P, Differential pharmacokinetic analysis of in vivo erythropoietin receptor interaction with erythropoietin and continuous erythropoietin receptor activator in sheep. Biopharm Drug Dispos 32: 276-288
4. El-Komy MH, Widness JA, Veng-Pedersen P (2011) Pharmacokinetic analysis of continuous erythropoietin receptor activator disposition using a target-mediated, physiologic recirculation model and a tracer interaction methodology. Drug Metab Dispos 39: 603-609
5. Kania-Korwel I, El-Komy MH, Veng-Pedersen P, Lehmler HJ (2010) Clearance of polychlorinated biphenyl atropisomers is enantioselective in female C57Bl/6 mice. Environ Sci Technol 44: 2828-35

REFERENCES

1. Teorell T (1937) Kinetics of distribution of substances administered to the body I The extravascular modes of administration. Archives Internationales De Pharmacodynamie Et De Therapie 57: 205-225

2. Bellman R, Jacquez J, Kalaba R (1960) Some Mathematical Aspects of Chemotherapy: I. One-Organ Models. Bulletin of Mathematical Biology 22: 181-198

3. Jacquez J, Bellman R, Kalaba R (1960) Some Mathematical Aspects of Chemotherapy—II: The Distribution of a Drug in the Body. Bulletin of Mathematical Biology 22: 309-322

4. Bischoff KB, Brown RG (1967) Drug Distribution in Mammals. Chemical Engineering Progress Symposium Series 62: 32-45

5. Baxter LT, Zhu H, Mackensen DG, Jain RK (1994) Physiologically based pharmacokinetic model for specific and nonspecific monoclonal antibodies and fragments in normal tissues and human tumor xenografts in nude mice. Cancer Res 54: 1517-1528

6. Chen HS, Gross JF (1979) Physiologically based pharmacokinetic models for anticancer drugs. Cancer Chemother Pharmacol 2: 85-94

7. Dedrick RL, Myers CE, Bungay PM, DeVita VT, Jr. (1978) Pharmacokinetic rationale for peritoneal drug administration in the treatment of ovarian cancer. Cancer Treat Rep 62: 1-11

8. Gallo JM, Vicini P, Orlansky A, Li S, Zhou F, Ma J, Pulfer S, Bookman MA, Guo P (2004) Pharmacokinetic model-predicted anticancer drug concentrations in human tumors. Clin Cancer Res 10: 8048-8058

9. Kirman CR, Hays SM, Kedderis GL, Gargas ML, Strother DE (2000) Improving cancer dose-response characterization by using physiologically based pharmacokinetic modeling: an analysis of pooled data for acrylonitrile-induced brain tumors to assess cancer potency in the rat. Risk Anal 20: 135-151

10. Tsukamoto Y, Kato Y, Ura M, Horii I, Ishikawa T, Ishitsuka H, Sugiyama Y (2001) Investigation of 5-FU disposition after oral administration of capecitabine, a triple-prodrug of 5-FU, using a physiologically based pharmacokinetic model in a human cancer xenograft model: comparison of the simulated 5-FU exposures in the tumour tissue between human and xenograft model. Biopharm Drug Dispos 22: 1-14

11. Tsukamoto Y, Kato Y, Ura M, Horii I, Ishitsuka H, Kusuhara H, Sugiyama Y (2001) A physiologically based pharmacokinetic analysis of capecitabine, a triple prodrug of 5-FU, in humans: the mechanism for tumor-selective accumulation of 5-FU. Pharm Res 18: 1190-1202

12. Gentry PR, Covington TR, Andersen ME, Clewell HJ, 3rd (2002) Application of a physiologically based pharmacokinetic model for isopropanol in the derivation of a reference dose and reference concentration. Regul Toxicol Pharmacol 36: 51-68

13. Gentry PR, Covington TR, Clewell H, Anderson ME (2003) Application of a physiologically based pharmacokinetic model for reference dose and reference concentration estimation for acetone. Journal of Toxicology and Environmental Health-Part A 66: 2209-2225

14. Haddad S, Beliveau M, Tardif R, Krishnan K (2001) A PBPK modeling-based approach to account for interactions in the health risk assessment of chemical mixtures. Toxicological Sciences 63: 125-131

15. Leavens TL, Bond JA (1996) Pharmacokinetic model describing the disposition of butadiene and styrene in mice. Toxicology 113: 310-313

16. Bailer AJ, Dankovic DA (1997) An introduction to the use of physiologically based pharmacokinetic models in risk assessment. Stat Methods Med Res 6: 341-358

17. Clewell HJ, 3rd, Andersen ME (1996) Use of physiologically based pharmacokinetic modeling to investigate individual versus population risk. Toxicology 111: 315-329

18. Clewell HJ, 3rd, Gentry PR, Gearhart JM (1997) Investigation of the potential impact of benchmark dose and pharmacokinetic modeling in noncancer risk assessment. J Toxicol Environ Health 52: 475-515

19. el-Masri HA, Thomas RS, Benjamin SA, Yang RS (1995) Physiologically based pharmacokinetic/pharmacodynamic modeling of chemical mixtures and possible applications in risk assessment. Toxicology 105: 275-282

20. Bischoff KB (1986) Physiological pharmacokinetics. Bull Math Biol 48: 309-322

21. Nestorov I (2003) Whole body pharmacokinetic models. Clin Pharmacokinet 42: 883-908

22. Henthorn TK, Avram MJ, Krejcie TC, Shanks CA, Asada A, Kaczynski DA (1992) Minimal compartmental model of circulatory mixing of indocyanine green. Am J Physiol 262: H903-910

23. Upton RN (2004) The two-compartment recirculatory pharmacokinetic model--an introduction to recirculatory pharmacokinetic concepts. Br J Anaesth 92: 475-484

24. Upton RN, Zheng DA, Grant C, Martinez AM (2000) Development and validation of a recirculatory physiological model of the myocardial concentrations of lignocaine after intravenous administration in sheep. J Pharm Pharmacol 52: 181-189

25. Weiss M, Krejcie TC, Avram MJ (2007) A minimal physiological model of thiopental distribution kinetics based on a multiple indicator approach. Drug Metab Dispos 35: 1525-1532

26. Weiss M, Roelsgaard K, Bender D, Keiding S (2002) Determinants of [13N]ammonia kinetics in hepatic PET experiments: a minimal recirculatory model. Eur J Nucl Med Mol Imaging 29: 1648-1656

27. Nestorov IA, Aarons LJ, Arundel PA, Rowland M (1998) Lumping of whole-body physiologically based pharmacokinetic models. J Pharmacokinet Biopharm 26: 21-46

28. Filser JG, Csanady GA, Kreuzer PE, Kessler W (1995) Toxicokinetic models for volatile industrial chemicals and reactive metabolites. Toxicol Lett 82-83: 357-366

29. Kaneko T, Horiuchi J, Sato A (2000) Development of a physiologically based pharmacokinetic model of organic solvent in rats. Pharmacol Res 42: 465-470

30. Krewski D, Withey JR, Ku LF, Andersen ME (1994) Applications of physiologic pharmacokinetic modeling in carcinogenic risk assessment. Environ Health Perspect 102 Suppl 11: 37-50

31. O'Flaherty EJ (1998) A physiologically based kinetic model for lead in children and adults. Environ Health Perspect 106 Suppl 6: 1495-1503

32. Gibaldi M, Perrier D (1982) Pharmacokinetics. Marcel Dekker, Inc. New York, NY

33. Blakey GE, Nestorov IA, Arundel PA, Aarons LJ, Rowland M (1997) Quantitative structure-pharmacokinetics relationships: I. Development of a whole-body physiologically based model to characterize changes in pharmacokinetics across a homologous series of barbiturates in the rat. J Pharmacokinet Biopharm 25: 277-312

34. Igari Y, Sugiyama Y, Awazu S, Hanano M (1982) Comparative physiologically based pharmacokinetics of hexobarbital, phenobarbital and thiopental in the rat. J Pharmacokinet Biopharm 10: 53-75

35. Ritschel WA, Banerjee PS (1986) Physiological pharmacokinetic models: principles, applications, limitations and outlook. Methods Find Exp Clin Pharmacol 8: 603-614

36. Bjorkman S, Stanski DR, Harashima H, Dowrie R, Harapat SR, Wada DR, Ebling WF (1993) Tissue distribution of fentanyl and alfentanil in the rat cannot be described by a blood flow limited model. J Pharmacokinet Biopharm 21: 255-279

37. Gerlowski LE, Jain RK (1983) Physiologically based pharmacokinetic modeling: principles and applications. J Pharm Sci 72: 1103-1127

38. Peng B, Andrews J, Nestorov I, Brennan B, Nicklin P, Rowland M (2001) Tissue distribution and physiologically based pharmacokinetics of antisense phosphorothioate oligonucleotide ISIS 1082 in rat. Antisense Nucleic Acid Drug Dev 11: 15-27

39. Weiss M (1982) Moments of Physiological Transit-Time Distributions and the Time Course of Drug Disposition in the Body. Journal of Mathematical Biology 15: 305-318

40. Pang KS, Rowland M (1977) Hepatic clearance of drugs. I. Theoretical considerations of a "well-stirred" model and a "parallel tube" model. Influence of hepatic blood flow, plasma and blood cell binding, and the hepatocellular enzymatic activity on hepatic drug clearance. J Pharmacokinet Biopharm 5: 625-653

41. Obach RS (1999) Prediction of human clearance of twenty-nine drugs from hepatic microsomal intrinsic clearance data: An examination of in vitro half-life approach and nonspecific binding to microsomes. Drug Metab Dispos 27: 1350-1359

42. Rowland M (1984) Protein binding and drug clearance. Clin Pharmacokinet 9 Suppl 1: 10-17

43. Bischoff KB, Dedrick RL (1968) Thiopental pharmacokinetics. J Pharm Sci 57: 1346-1351

44. Carpenter RL (1999) Aerosol deposition modeling using ACSL. Drug Chem Toxicol 22: 73-90

45. Thomas RS, Lytle WE, Keefe TJ, Constan AA, Yang RS (1996) Incorporating Monte Carlo simulation into physiologically based pharmacokinetic models using advanced continuous simulation language (ACSL): a computational method. Fundam Appl Toxicol 31: 19-28

46. Ball R, Schwartz SL (1994) CMATRIX: software for physiologically based pharmacokinetic modeling using a symbolic matrix representation system. Comput Biol Med 24: 269-276

47. Levitt DG (2009) PKQuest_Java: free, interactive physiologically based pharmacokinetic software package and tutorial. BMC Res Notes 2: 158

48. Brown RP, Delp MD, Lindstedt SL, Rhomberg LR, Beliles RP (1997) Physiological parameter values for physiologically based pharmacokinetic models. Toxicol Ind Health 13: 407-484

49. Davies B, Morris T (1993) Physiological parameters in laboratory animals and humans. Pharm Res 10: 1093-1095

50. Leggett RW, Williams LR (1991) Suggested reference values for regional blood volumes in humans. Health Phys 60: 139-154

51. Upton RN (2008) Organ weights and blood flows of sheep and pig for physiological pharmacokinetic modelling. J Pharmacol Toxicol Methods 58: 198-205

52. Igari Y, Sugiyama Y, Sawada Y, Iga T, Hanano M (1983) Prediction of diazepam disposition in the rat and man by a physiologically based pharmacokinetic model. J Pharmacokinet Biopharm 11: 577-593

53. De Buck SS, Mackie CE (2007) Physiologically based approaches towards the prediction of pharmacokinetics: in vitro-in vivo extrapolation. Expert Opin Drug Metab Toxicol 3: 865-878

54. Ito K, Houston JB (2005) Prediction of human drug clearance from in vitro and preclinical data using physiologically based and empirical approaches. Pharm Res 22: 103-112

55. Shiran MR, Proctor NJ, Howgate EM, Rowland-Yeo K, Tucker GT, Rostami-Hodjegan A (2006) Prediction of metabolic drug clearance in humans: in vitro-in vivo extrapolation vs allometric scaling. Xenobiotica 36: 567-580

56. Zuegge J, Schneider G, Coassolo P, Lave T (2001) Prediction of hepatic metabolic clearance: comparison and assessment of prediction models. Clin Pharmacokinet 40: 553-563

57. Lave T, Coassolo P, Reigner B (1999) Prediction of hepatic metabolic clearance based on interspecies allometric scaling techniques and in vitro-in vivo correlations. Clin Pharmacokinet 36: 211-231

58. Poulin P, Schoenlein K, Theil FP (2001) Prediction of adipose tissue: plasma partition coefficients for structurally unrelated drugs. J Pharm Sci 90: 436-447

59. Rodgers T, Leahy D, Rowland M (2005) Physiologically based pharmacokinetic modeling 1: predicting the tissue distribution of moderate-to-strong bases. J Pharm Sci 94: 1259-1276

60. Rodgers T, Rowland M (2006) Physiologically based pharmacokinetic modelling 2: predicting the tissue distribution of acids, very weak bases, neutrals and zwitterions. J Pharm Sci 95: 1238-1257

61. Schmitt W (2008) General approach for the calculation of tissue to plasma partition coefficients. Toxicol In Vitro 22: 457-467

62. Thygesen P, Macheras P, Van Peer A (2009) Physiologically-based PK/PD modelling of therapeutic macromolecules. Pharm Res 26: 2543-2550

63. Weiss M (2000) Physiological Modelling and The Effect Site. In: Vuyk J, Engbers F, Groen-Mulder S (eds) On the Study and Practice of Intravenous Anaesthesia Kluver Academic Publishers, Dordrecht – Boston – London, pp 3-16

64. Bjorkman S, Wada DR, Stanski DR (1998) Application of physiologic models to predict the influence of changes in body composition and blood flows on the pharmacokinetics of fentanyl and alfentanil in patients. Anesthesiology 88: 657-667

65. Wada DR, Bjorkman S, Ebling WF, Harashima H, Harapat SR, Stanski DR (1997) Computer simulation of the effects of alterations in blood flows and body composition on thiopental pharmacokinetics in humans. Anesthesiology 87: 884-899

66. Weiss M, Hubner GH, Hubner IG, Teichmann W (1996) Effects of cardiac output on disposition kinetics of sorbitol: Recirculatory modelling. British Journal of Clinical Pharmacology 41: 261-268

67. Dennison JE, Bigelow PL, Mumtaz MM, Andersen ME, Dobrev ID, Yang RS (2005) Evaluation of potential toxicity from co-exposure to three CNS depressants (toluene, ethylbenzene, and xylene) under resting and working conditions using PBPK modeling. J Occup Environ Hyg 2: 127-135

68. Hamelin G, Charest-Tardif G, Truchon G, Tardif R (2005) Physiologically based modeling of n-hexane kinetics in humans following inhalation exposure at rest and under physical exertion: impact on free 2,5-hexanedione in urine and on n-hexane in alveolar air. J Occup Environ Hyg 2: 86-97; quiz D86-87

69. Reddy MB, Andersen ME, Morrow PE, Dobrev ID, Varaprath S, Plotzke KP, Utell MJ (2003) Physiological modeling of inhalation kinetics of octamethylcyclotetrasiloxane in humans during rest and exercise. Toxicol Sci 72: 3-18

70. Bjorkman S (2005) Prediction of drug disposition in infants and children by means of physiologically based pharmacokinetic (PBPK) modelling: theophylline and midazolam as model drugs. Br J Clin Pharmacol 59: 691-704

71. Bouzom F, Walther B (2008) Pharmacokinetic predictions in children by using the physiologically based pharmacokinetic modelling. Fundam Clin Pharmacol 22: 579-587

72. Clewell HJ, Gentry PR, Covington TR, Sarangapani R, Teeguarden JG (2004) Evaluation of the potential impact of age- and gender-specific pharmacokinetic differences on tissue dosimetry. Toxicol Sci 79: 381-393

73. Ginsberg G, Hattis D, Russ A, Sonawane B (2004) Physiologically based pharmacokinetic (PBPK) modeling of caffeine and theophylline in neonates and adults: implications for assessing children's risks from environmental agents. J Toxicol Environ Health A 67: 297-329

74. Johnson TN, Rostami-Hodjegan A (2011) Resurgence in the use of physiologically based pharmacokinetic models in pediatric clinical pharmacology: parallel shift in incorporating the knowledge of biological elements and increased applicability to drug development and clinical practice. Paediatr Anaesth 21: 291-301

75. Price K, Haddad S, Krishnan K (2003) Physiological modeling of age-specific changes in the pharmacokinetics of organic chemicals in children. J Toxicol Environ Health A 66: 417-433

76. Thompson CM, Johns DO, Sonawane B, Barton HA, Hattis D, Tardif R, Krishnan K (2009) Database for physiologically based pharmacokinetic (PBPK) modeling: physiological data for healthy and health-impaired elderly. J Toxicol Environ Health B Crit Rev 12: 1-24

77. Willmann S, Hohn K, Edginton A, Sevestre M, Solodenko J, Weiss W, Lippert J, Schmitt W (2007) Development of a physiology-based whole-body population model for assessing the influence of individual variability on the pharmacokinetics of drugs. J Pharmacokinet Pharmacodyn 34: 401-431

78. Yang F, Tong X, McCarver DG, Hines RN, Beard DA (2006) Population-based analysis of methadone distribution and metabolism using an age-dependent physiologically based pharmacokinetic model. J Pharmacokinet Pharmacodyn 33: 485-518

79. Edginton AN, Schmitt W, Willmann S (2006) Development and evaluation of a generic physiologically based pharmacokinetic model for children. Clin Pharmacokinet 45: 1013-1034

80. Li J, Gwilt PR (2003) The effect of age on the early disposition of doxorubicin. Cancer Chemother Pharmacol 51: 395-402

81. Corley RA, Grant DM, Farris E, Weitz KK, Soelberg JJ, Thrall KD, Poet TS (2005) Determination of age and gender differences in biochemical processes affecting the disposition of 2-butoxyethanol and its metabolites in mice and rats to improve PBPK modeling. Toxicol Lett 156: 127-161

82. Hays SM, Elswick BA, Blumenthal GM, Welsch F, Conolly RB, Gargas ML (2000) Development of a physiologically based pharmacokinetic model of 2-methoxyethanol and 2-methoxyacetic acid disposition in pregnant rats. Toxicol Appl Pharmacol 163: 67-74

83. Emond C, Raymer JH, Studabaker WB, Garner CE, Birnbaum LS (2010) A physiologically based pharmacokinetic model for developmental exposure to BDE-47 in rats. Toxicol Appl Pharmacol 242: 290-298

84. Edginton AN, Willmann S (2008) Physiology-based simulations of a pathological condition: prediction of pharmacokinetics in patients with liver cirrhosis. Clin Pharmacokinet 47: 743-752

85. Johnson TN, Boussery K, Rowland-Yeo K, Tucker GT, Rostami-Hodjegan A (2010) A semi-mechanistic model to predict the effects of liver cirrhosis on drug clearance. Clin Pharmacokinet 49: 189-206

86. Zhao P, Vieira Mde L, Grillo JA, Song P, Wu TC, Zheng JH, Arya V, Berglund EG, Atkinson AJ, Jr., Sugiyama Y, Pang KS, Reynolds KS, Abernethy DR, Zhang L, Lesko LJ, Huang SM (2012) Evaluation of exposure change of nonrenally eliminated drugs in patients with chronic kidney disease using physiologically based pharmacokinetic modeling and simulation. J Clin Pharmacol 52: 91S-108S

87. Bjorkman S, Wada DR, Berling BM, Benoni G (2001) Prediction of the disposition of midazolam in surgical patients by a physiologically based pharmacokinetic model. J Pharm Sci 90: 1226-1241

88. Vossen M, Sevestre M, Niederalt C, Jang IJ, Willmann S, Edginton AN (2007) Dynamically simulating the interaction of midazolam and the CYP3A4 inhibitor itraconazole using individual coupled whole-body physiologically-based pharmacokinetic (WB-PBPK) models. Theor Biol Med Model 4: 13

89. Zhang X, Quinney SK, Gorski JC, Jones DR, Hall SD (2009) Semiphysiologically based pharmacokinetic models for the inhibition of midazolam clearance by diltiazem and its major metabolite. Drug Metab Dispos 37: 1587-1597

90. Rowland Yeo K, Jamei M, Yang J, Tucker GT, Rostami-Hodjegan A (2010) Physiologically based mechanistic modelling to predict complex drug-drug interactions involving simultaneous competitive and time-dependent enzyme inhibition by parent compound and its metabolite in both liver and gut - the effect of diltiazem on the time-course of exposure to triazolam. Eur J Pharm Sci 39: 298-309

91. Kato M, Shitara Y, Sato H, Yoshisue K, Hirano M, Ikeda T, Sugiyama Y (2008) The quantitative prediction of CYP-mediated drug interaction by physiologically based pharmacokinetic modeling. Pharm Res 25: 1891-1901

92. Rekic D, Roshammar D, Mukonzo J, Ashton M (2011) In silico prediction of efavirenz and rifampicin drug-drug interaction considering weight and CYP2B6 phenotype. Br J Clin Pharmacol 71: 536-543

93. Mahmood I (1999) Allometric issues in drug development. J Pharm Sci 88: 1101-1106

94. Clewell HJ, 3rd, Lee TS, Carpenter RL (1994) Sensitivity of physiologically based pharmacokinetic models to variation in model parameters: methylene chloride. Risk Anal 14: 521-531

95. Nestorov I (2001) Modelling and simulation of variability and uncertainty in toxicokinetics and pharmacokinetics. Toxicol Lett 120: 411-420

96. Veng-Pedersen P, Freise KJ, Schmidt RL, Widness JA (2008) Pharmacokinetic differentiation of drug candidates using system analysis and physiological-based modelling. Comparison of C.E.R.A. and erythropoietin. J Pharm Pharmacol 60: 1321-1334

97. Weiss M (2007) Mechanistic modeling of digoxin distribution kinetics incorporating slow tissue binding. Eur J Pharm Sci 30: 256-263

98. Weiss M, Krejcie TC, Avram MJ (2007) Circulatory transport and capillary-tissue exchange as determinants of the distribution kinetics of inulin and antipyrine in dog. J Pharm Sci 96: 913-926

99. Weiss M, Reekers M, Vuyk J, Boer F (2011) Circulatory model of vascular and interstitial distribution kinetics of rocuronium: a population analysis in patients. J Pharmacokinet Pharmacodyn 38: 165-178

100. Weiss M (1999) The anomalous pharmacokinetics of amiodarone explained by nonexponential tissue trapping. J Pharmacokinet Biopharm 27: 383-396

101. Cutler DJ (1979) Linear Recirculation Model for Drug Disposition. Journal of Pharmacokinetics and Biopharmaceutics 7: 101-116

102. Levy G (1994) Pharmacologic target-mediated drug disposition. Clin Pharmacol Ther 56: 248-252

103. Mager DE, Jusko WJ (2001) General pharmacokinetic model for drugs exhibiting target-mediated drug disposition. J Pharmacokinet Pharmacodyn 28: 507-532

104. Jonsson EN, Macintyre F, James I, Krams M, Marshall S (2005) Bridging the pharmacokinetics and pharmacodynamics of UK-279,276 across healthy volunteers and stroke patients using a mechanistically based model for target-mediated disposition. Pharm Res 22: 1236-1246

105. Mager DE (2006) Target-mediated drug disposition and dynamics. Biochem Pharmacol 72: 1-10

106. Ng CM, Stefanich E, Anand BS, Fielder PJ, Vaickus L (2006) Pharmacokinetics/pharmacodynamics of nondepleting anti-CD4 monoclonal antibody (TRX1) in healthy human volunteers. Pharm Res 23: 95-103

107. Kinoshita H, Ohishi N, Kato M, Tokura S, Okazaki A (1992) Pharmacokinetics and distribution of recombinant erythropoietin in rats. Arzneimittelforschung 42: 174-178

108. Lacombe C, Mayeux P (1999) The molecular biology of erythropoietin. Nephrol Dial Transplant 14 Suppl 2: 22-28

109. Sawyer ST, Krantz SB, Goldwasser E (1987) Binding and Receptor-Mediated Endocytosis of Erythropoietin in Friend Virus-Infected Erythroid-Cells. Journal of Biological Chemistry 262: 5554-5562

110. Jarsch M, Brandt M, Lanzendorfer M, Haselbeck A (2008) Comparative erythropoietin receptor binding kinetics of CERA and epoetin-beta determined by surface plasmon resonance and competition binding assay. Pharmacology 81: 63-69

111. Haselbeck A, Tare N, Pill J (2002) Pre-clinical pharmacokinetics and pharmacodynamics of CERA (Continuous Erythropoiesis Receptor Activator) indicate a superior new therapy for anemia. Blood 100: 228a-228a

112. Stohlman F, Jr., Brecher G (1959) Humoral regulation of erythropoiesis. V. Relationship of plasma erythropoietine level to bone marrow activity. Proc Soc Exp Biol Med 100: 40-43

113. Gross AW, Lodish HF (2006) Cellular trafficking and degradation of erythropoietin and novel erythropoiesis stimulating protein (NESP). Journal of Biological Chemistry 281: 2024-2032

114. Chapel S, Veng-Pedersen P, Hohl RJ, Schmidt RL, McGuire EM, Widness JA (2001) Changes in erythropoietin pharmacokinetics following busulfan-induced bone marrow ablation in sheep: evidence for bone marrow as a major erythropoietin elimination pathway. J Pharmacol Exp Ther 298: 820-824

115. Veng-Pedersen P, Chapel S, Al-Huniti NH, Schmidt RL, Sedars EM, Hohl RJ, Widness JA (2004) Pharmacokinetic tracer kinetics analysis of changes in erythropoietin receptor population in phlebotomy-induced anemia and bone marrow ablation. Biopharm Drug Dispos 25: 149-156

116. Widness JA, Veng-Pedersen P, Schmidt RL, Lowe LS, Kisthard JA, Peters C (1996) In vivo 125I-erythropoietin pharmacokinetics are unchanged after anesthesia, nephrectomy and hepatectomy in sheep. J Pharmacol Exp Ther 279: 1205-1210

117. Macdougall IC, Robson R, Opatrna S, Liogier X, Pannier A, Jordan P, Dougherty FC, Reigner B (2006) Pharmacokinetics and pharmacodynamics of intravenous and subcutaneous continuous erythropoietin receptor activator (C.E.R.A.) in patients with chronic kidney disease. Clin J Am Soc Nephrol 1: 1211-1215

118. Fishbane S, Pannier A, Liogier X, Jordan P, Dougherty FC, Reigner B (2007) Pharmacokinetic and pharmacodynamic properties of methoxy polyethylene glycol-epoetin beta are unaffected by the site of subcutaneous administration. Journal of Clinical Pharmacology 47: 1390-1397

119. Kupcova V, Sperl J, Pannier A, Jordan P, Dougherty FC, Reigner B (2008) The effect of severe hepatic impairment on the pharmacokinetics and haematological response of CERA. Current Medical Research and Opinion 24: 1943-1950

120. Nalbant D, Saleh M, Goldman FD, Widness JA, Veng-Pedersen P (2010) Evidence of receptor-mediated elimination of erythropoietin by analysis of erythropoietin receptor mRNA expression in bone marrow and erythropoietin clearance during anemia. J Pharmacol Exp Ther 333: 528-532

121. Kato M, Kamiyama H, Okazaki A, Kumaki K, Kato Y, Sugiyama Y (1997) Mechanism for the nonlinear pharmacokinetics of erythropoietin in rats. J Pharmacol Exp Ther 283: 520-527

122. Veng-Pedersen P, Widness JA, Pereira LM, Peters C, Schmidt RL, Lowe LS (1995) Kinetic evaluation of nonlinear drug elimination by a disposition decomposition analysis. Application to the analysis of the nonlinear elimination kinetics of erythropoietin in adult humans. J Pharm Sci 84: 760-767

123. Veng-Pedersen P, Chapel S, Al-Huniti NH, Schmidt RL, Sedars EM, Hohl RJ, Widness JA (2003) A differential pharmacokinetic analysis of the erythropoietin receptor population in newborn and adult sheep. J Pharmacol Exp Ther 306: 532-537

124. Woo S, Krzyzanski W, Jusko WJ (2007) Target-mediated pharmacokinetic and pharmacodynamic model of recombinant human erythropoietin (rHuEPO). J Pharmacokinet Pharmacodyn 34: 849-868

125. Veng-Pedersen P, Widness JA, Wang J, Schmidt RL (1997) A tracer interaction method for nonlinear pharmacokinetics analysis: application to evaluation of nonlinear elimination. J Pharmacokinet Biopharm 25: 569-593

126. Veng-Pedersen P (1991) Stochastic interpretation of linear pharmacokinetics: a linear system analysis approach. J Pharm Sci 80: 621-631

127. Veng-Pedersen P (2001) Noncompartmentally-based pharmacokinetic modeling. Adv Drug Deliv Rev 48: 265-300

128. Vaughan DP, Hope I (1979) Applications of a Recirculatory Stochastic Pharmacokinetic Model - Limitations of Compartmental Models. Journal of Pharmacokinetics and Biopharmaceutics 7: 207-225

129. Verotta D, Sheiner LB, Ebling WF, Stanski DR (1989) A Semiparametric Approach to Physiological Flow Models. Journal of Pharmacokinetics and Biopharmaceutics 17: 463-491

130. Weiss M, Forster W (1979) Pharmacokinetic Model Based on Circulatory Transport. European Journal of Clinical Pharmacology 16: 287-293

131. Yano Y, Yamaoka K, Tanaka H (1989) A nonlinear least squares program, MULTI(FILT), based on fast inverse Laplace transform for microcomputers. Chem Pharm Bull (Tokyo) 37: 1035-1038

132. Purves RD (1994) MINIM 3.0 Manual: A Macintosh Application for Non-Linear Parameter Estimation. Department of Pharmacology, University of Otargo Medical School, PO Box 913, Dunedin, New Zealand.

133. Schalla M, Weiss M (1999) Pharmacokinetic curve fitting using numerical inverse Laplace transformation. Eur J Pharm Sci 7: 305-309

134. Krejcie TC, Jacquez JA, Avram MJ, Niemann CU, Shanks CA, Henthorn TK (1996) Use of parallel Erlang density functions to analyze first-pass pulmonary uptake of multiple indicators in dogs. J Pharmacokinet Biopharm 24: 569-588

135. Kuipers JA, Boer F, Olofsen E, Bovill JG, Burm AG (2001) Recirculatory pharmacokinetics and pharmacodynamics of rocuronium in patients: the influence of cardiac output. Anesthesiology 94: 47-55

136. Roberts MS, Donaldson JD, Rowland M (1988) Models of hepatic elimination: comparison of stochastic models to describe residence time distributions and to predict the influence of drug distribution, enzyme heterogeneity, and systemic recycling on hepatic elimination. J Pharmacokinet Biopharm 16: 41-83

137. Weiss M (1984) A note on the role of generalized inverse Gaussian distributions of circulatory transit times in pharmacokinetics. J Math Biol 20: 95-102

138. Lapidus L, Amundson NR (1952) Mathematics of Adsorption in Beds .6. The Effect of Longitudinal Diffusion in Ion Exchange and Chromatographic Columns. Journal of Physical Chemistry 56: 984-988

139. Yamaoka K, Nakagawa T (1976) Moment Analysis for Reaction Chromatography. Journal of Chromatography 117: 1-10

140. Roberts MS, Rowland M (1985) Hepatic Elimination - Dispersion Model. Journal of Pharmaceutical Sciences 74: 585-587

141. Roberts MS, Rowland M (1986) A Dispersion Model of Hepatic Elimination .1. Formulation of the Model and Bolus Considerations. Journal of Pharmacokinetics and Biopharmaceutics 14: 227-260

142. Yano Y, Yamaoka K, Aoyama Y, Tanaka H (1989) 2-Compartment Dispersion Model for Analysis of Organ Perfusion System of Drugs by Fast Inverse Laplace Transform (Filt). Journal of Pharmacokinetics and Biopharmaceutics 17: 179-202

143. Weiss M, Roberts MS (1996) Tissue distribution kinetics as determinant of transit time dispersion of drugs in organs: application of a stochastic model to the rat hindlimb. J Pharmacokinet Biopharm 24: 173-196

144. Weiss M (1999) Cellular pharmacokinetics: effects of cytoplasmic diffusion and binding on organ transit time distribution. J Pharmacokinet Biopharm 27: 233-256

145. Roberts MS, Rowland M (1986) Correlation between in-vitro microsomal enzyme activity and whole organ hepatic elimination kinetics: analysis with a dispersion model. J Pharm Pharmacol 38: 177-181

146. Chou CH, Evans AM, Fornasini G, Rowland M (1993) Relationship between lipophilicity and hepatic dispersion and distribution for a homologous series of barbiturates in the isolated perfused in situ rat liver. Drug Metab Dispos 21: 933-938

147. Chou CH, Rowland M (1997) Effect of altered tissue binding on the disposition of barbital in the isolated perfused rat liver: application of the axial dispersion model. J Pharm Sci 86: 1310-1314

148. Diaz-Garcia JM, Evans AM, Rowland M (1992) Application of the axial dispersion model of hepatic drug elimination to the kinetics of diazepam in the isolated perfused rat liver. J Pharmacokinet Biopharm 20: 171-193

149. Hussein Z, McLachlan AJ, Rowland M (1994) Distribution kinetics of salicylic acid in the isolated perfused rat liver assessed using moment analysis and the two-compartment axial dispersion model. Pharm Res 11: 1337-1345

150. Oliver RE, Heatherington AC, Jones AF, Rowland M (1997) A physiologically based pharmacokinetic model incorporating dispersion principles to describe solute distribution in the perfused rat hindlimb preparation. J Pharmacokinet Biopharm 25: 389-412

151. Roberts MS, Fraser S, Wagner A, McLeod L (1990) Residence time distributions of solutes in the perfused rat liver using a dispersion model of hepatic elimination: 2. Effect of pharmacological agents, retrograde perfusions, and enzyme inhibition on evans blue, sucrose, water, and taurocholate. J Pharmacokinet Biopharm 18: 235-258

152. Roberts MS, Fraser S, Wagner A, McLeod L (1990) Residence time distributions of solutes in the perfused rat liver using a dispersion model of hepatic elimination: 1. Effect of changes in perfusate flow and albumin concentration on sucrose and taurocholate. J Pharmacokinet Biopharm 18: 209-234

153. Schwab AJ, Geng W, Pang KS (1998) Application of the dispersion model for description of the outflow dilution profiles of noneliminated reference indicators in rat liver perfusion studies. J Pharmacokinet Biopharm 26: 163-181

154. Fanning KJ, Anissimov YG, Roberts MS (2009) Sulphonylurea physicochemical-pharmacokinetic relationships in the pancreas and liver. J Pharm Sci 98: 2807-2821

155. Fanning KJ, Roberts MS (2007) Characterization of the physiological spaces and distribution of tolbutamide in the perfused rat pancreas. Pharm Res 24: 512-520

156. Hung DY, Chang P, Cheung K, McWhinney B, Masci PP, Weiss M, Roberts MS (2002) Cationic drug pharmacokinetics in diseased livers determined by fibrosis index, hepatic protein content, microsomal activity, and nature of drug. J Pharmacol Exp Ther 301: 1079-1087

157. Hung DY, Siebert GA, Chang P, Roberts MS (2005) Hepatic pharmacokinetics of taurocholate in the normal and cholestatic rat liver. Br J Pharmacol 145: 57-65

158. Li P, Robertson TA, Thorling CA, Zhang Q, Fletcher LM, Crawford DH, Roberts MS (2011) Hepatic pharmacokinetics of cationic drugs in a high-fat emulsion-induced rat model of nonalcoholic steatohepatitis. Drug Metab Dispos 39: 571-579

159. Weiss M, Krejcie TC, Avram MJ (2006) Transit time dispersion in pulmonary and systemic circulation: effects of cardiac output and solute diffusivity. Am J Physiol Heart Circ Physiol 291: H861-870

160. Weiss M, Kuhlmann O, Hung DY, Roberts MS (2000) Cytoplasmic binding and disposition kinetics of diclofenac in the isolated perfused rat liver. Br J Pharmacol 130: 1331-1338

161. Hung DY, Chang P, Weiss M, Roberts MS (2001) Structure-hepatic disposition relationships for cationic drugs in isolated perfused rat livers: transmembrane exchange and cytoplasmic binding process. J Pharmacol Exp Ther 297: 780-789

162. Brandt M, Lanzendorfer M, Frische J, Haselbeck A, Jarsch M (2006) Different receptor binding activity of CERA (continuous erythropoietin receptor activator) compared with epoetin beta determined by surface plasmon resonance and competition assay on UT-7 cells. Nephrology Dialysis Transplantation 21: 9-9

163. Locatelli F, Del Vecchio L (2008) Optimizing the management of renal anemia: challenges and new opportunities. Kidney International 74: S33-S37

164. Sulowicz W, Locatelli F, Ryckelynck JP, Balla J, Csiky B, Harris K, Ehrhard P, Beyer U, Investigators PS (2007) Once-monthly subcutaneous CERA maintains stable hemoglobin control in patients with chronic kidney disease on dialysis and converted directly from epoetin one to three times weekly. Clinical Journal of the American Society of Nephrology 2: 637-646

165. Mager DE, Krzyzanski W (2005) Quasi-equilibrium pharmacokinetic model for drugs exhibiting target-mediated drug disposition. Pharm Res 22: 1589-1596

166. Gibiansky L, Gibiansky E, Kakkar T, Ma P (2008) Approximations of the target-mediated drug disposition model and identifiability of model parameters. J Pharmacokinet Pharmacodyn 35: 573-591

167. Mager DE, Neuteboom B, Efthymiopoulos C, Munafo A, Jusko WJ (2003) Receptor-mediated pharmacokinetics and pharmacodynamics of interferon-beta1a in monkeys. J Pharmacol Exp Ther 306: 262-270

168. Jin F, Krzyzanski W (2004) Pharmacokinetic model of target-mediated disposition of thrombopoietin. AAPS PharmSci 6: E9

169. Widness JA, Schmidt RL, Veng-Pedersen P, Modi NB, Sawyer ST (1992) A sensitive and specific erythropoietin immunoprecipitation assay: application to pharmacokinetic studies. J Lab Clin Med 119: 285-294

170. Chapel SH, Veng-Pedersen P, Schmidt RL, Widness JA (2000) A pharmacodynamic analysis of erythropoietin-stimulated reticulocyte response in phlebotomized sheep. J Pharmacol Exp Ther 295: 346-351

171. Al-Huniti NH, Widness JA, Schmidt RL, Veng-Pedersen P (2005) Pharmacodynamic analysis of changes in reticulocyte subtype distribution in phlebotomy-induced stress erythropoiesis. J Pharmacokinet Pharmacodyn 32: 359-376

172. Veng-Pedersen P (1977) Curve Fitting and Modeling in Pharmacokinetics and Some Practical Experiences with Nonlin and a New Program Funfit. Journal of Pharmacokinetics and Biopharmaceutics 5: 513-531

173. Hutchinson MF, de Hoog FR (1985) Smoothing Noisy Data with Spline Functions. Numerische Mathematik 47: 99-106

174. Jelkmann W, Bohlius J, Hallek M, Sytkowski AJ (2008) The erythropoietin receptor in normal and cancer tissues. Crit Rev Oncol Hematol 67: 39-61

175. Anagnostou A, Liu ZY, Steiner M, Chin K, Lee ES, Kessimian N, Noguchi CT (1994) Erythropoietin Receptor Messenger-Rna Expression in Human Endothelial-Cells. Proceedings of the National Academy of Sciences of the United States of America 91: 3974-3978

176. Juul SE, Yachnis AT, Christensen RD (1998) Tissue distribution of erythropoietin and erythropoietin receptor in the developing human fetus. Early Human Development 52: 235-249

177. Nagai A, Nakagawa E, Choi HB, Hatori K, Kobayashi S, Kim SU (2001) Erythropoietin and erythropoietin receptors in human CNS neurons, astrocytes, microglia, and oligodendrocytes grown in culture. Journal of Neuropathology and Experimental Neurology 60: 386-392

178. Ogilvie M, Yu XB, Nicolas-Metral V, Pulido SM, Liu C, Ruegg UT, Noguchi CT (2000) Erythropoietin stimulates proliferation and interferes with differentiation of myoblasts. Journal of Biological Chemistry 275: 39754-39761

179. Peters WP, Henner WD, Grochow LB, Olsen G, Edwards S, Stanbuck H, Stuart A, Gockerman J, Moore J, Bast RC, Jr., et al. (1987) Clinical and pharmacologic effects of high dose single agent busulfan with autologous bone marrow support in the treatment of solid tumors. Cancer Res 47: 6402-6406

180. Walrafen P, Verdier F, Kadri Z, Chretien S, Lacombe C, Mayeux P (2005) Both proteasomes and lysosomes degrade the activated erythropoietin receptor. Blood 105: 600-608

181. Koury MJ, Bondurant MC (1988) Maintenance by erythropoietin of viability and maturation of murine erythroid precursor cells. J Cell Physiol 137: 65-74

182. Remy I, Wilson IA, Michnick SW (1999) Erythropoietin receptor activation by a ligand-induced conformation change. Science 283: 990-993

183. Kato M, Miura K, Kamiyama H, Okazaki A, Kumaki K, Kato Y, Sugiyama Y (1998) Pharmacokinetics of erythropoietin in genetically anemic mice. Drug Metab Dispos 26: 126-131

184. Veng-Pedersen P, Widness JA, Pereira LM, Schmidt RL, Lowe LS (1999) A comparison of nonlinear pharmacokinetics of erythropoietin in sheep and humans. Biopharm Drug Dispos 20: 217-223

185. Yoon WH, Park SJ, Kim IC, Lee MG (1997) Pharmacokinetics of recombinant human erythropoietin in rabbits and 3/4 nephrectomized rats. Res Commun Mol Pathol Pharmacol 96: 227-240

186. Klinger M, Arias M, Vargemezis V, Besarab A, Sulowicz W, Gerntholtz T, Ciechanowski K, Dougherty FC, Beyer U (2007) Efficacy of intravenous methoxy polyethylene glycol-epoetin beta administered every 2 weeks compared with epoetin administered 3 times weekly in patients treated by hemodialysis or peritoneal dialysis: a randomized trial. Am J Kidney Dis 50: 989-1000

187. Kendall RG, Chapman C, Hartley AE, Norfolk DR (1991) Storage and preparation of samples for erythropoietin radioimmunoassay. Clin Lab Haematol 13: 189-196

188. Broudy VC, Nakamoto B, Lin N, Papayannopoulou T (1990) Dynamics of erythropoietin receptor expression on erythropoietin-responsive murine cell lines. Blood 75: 1622-1626

189. Grossi A, Vannucchi AM, Bacci P, Caporale R, Cappelli G, Visconti G, Pagliai G, Ferrini PR (1998) Erythropoietin upregulates the expression of its own receptor in TF-1 cell line. Leuk Res 22: 145-151

190. Li Y, Lu Z, Keogh CL, Yu SP, Wei L (2007) Erythropoietin-induced neurovascular protection, angiogenesis, and cerebral blood flow restoration after focal ischemia in mice. J Cereb Blood Flow Metab 27: 1043-1054

191. Panchapakesan U, Sumual S, Pollock C (2007) Nanomedicines in the treatment of anemia in renal disease: focus on CERA (Continuous Erythropoietin Receptor Activator). Int J Nanomedicine 2: 33-38

192. Elliott S, Pham E, Macdougall IC (2008) Erythropoietins: a common mechanism of action. Exp Hematol 36: 1573-1584

193. Fraser JK, Lin FK, Berridge MV (1988) Expression of high affinity receptors for erythropoietin on human bone marrow cells and on the human erythroleukemic cell line, HEL. Exp Hematol 16: 836-842

194. Egrie JC, Dwyer E, Browne JK, Hitz A, Lykos MA (2003) Darbepoetin alfa has a longer circulating half-life and greater in vivo potency than recombinant human erythropoietin. Exp Hematol 31: 290-299

195. Nestorov IA, Aarons LJ, Rowland M (1997) Physiologically based pharmacokinetic modeling of a homologous series of barbiturates in the rat: a sensitivity analysis. J Pharmacokinet Biopharm 25: 413-447

196. Evans MV, Crank WD, Yang HM, Simmons JE (1994) Applications of sensitivity analysis to a physiologically based pharmacokinetic model for carbon tetrachloride in rats. Toxicol Appl Pharmacol 128: 36-44

197. Hetrick DM, Jarabek AM, Travis CC (1991) Sensitivity analysis for physiologically based pharmacokinetic models. J Pharmacokinet Biopharm 19: 1-20

198. Varkonyi P, Bruckner JV, Gallo JM (1995) Effect of parameter variability on physiologically-based pharmacokinetic model predicted drug concentrations. J Pharm Sci 84: 381-384

199. Spear RC, Bois FY, Woodruff T, Auslander D, Parker J, Selvin S (1991) Modeling benzene pharmacokinetics across three sets of animal data: parametric sensitivity and risk implications. Risk Anal 11: 641-654

200. Nestorov IA (1999) Sensitivity analysis of pharmacokinetic and pharmacodynamic systems: I. A structural approach to sensitivity analysis of physiologically based pharmacokinetic models. Journal of Pharmacokinetics and Biopharmaceutics 27: 577-596

201. Licata AC, Dekant W, Smith CE, Borghoff SJ (2001) A physiologically based pharmacokinetic model for methyl tert-butyl ether in humans: implementing sensitivity and variability analyses. Toxicol Sci 62: 191-204

202. Farrar D, Allen B, Crump K, Shipp A (1989) Evaluation of uncertainty in input parameters to pharmacokinetic models and the resulting uncertainty in output. Toxicol Lett 49: 371-385

203. Portier CJ, Kaplan NL (1989) Variability of Safe Dose Estimates When Using Complicated Models of the Carcinogenic Process - a Case-Study - Methylene-Chloride. Fundamental and Applied Toxicology 13: 533-544

204. Bois FY, Zeise L, Tozer TN (1990) Precision and sensitivity of pharmacokinetic models for cancer risk assessment: tetrachloroethylene in mice, rats, and humans. Toxicol Appl Pharmacol 102: 300-315

205. Krewski D, Wang Y, Bartlett S, Krishnan K (1995) Uncertainty, variability, and sensitivity analysis in physiological pharmacokinetic models. J Biopharm Stat 5: 245-271

206. Krzyzanski W, Wyska E (2008) Pharmacokinetics and pharmacodynamics of erythropoietin receptor in healthy volunteers. Naunyn Schmiedebergs Arch Pharmacol 377: 637-645

207. Kahn D, Weiner GJ, Ben-Haim S, Ponto LL, Madsen MT, Bushnell DL, Watkins GL, Argenyi EA, Hichwa RD (1994) Positron emission tomographic measurement of bone marrow blood flow to the pelvis and lumbar vertebrae in young normal adults. Blood 83: 958-963

208. International Commission on Radiological Protection. Report of the task group on refrrence man. ICRP Publication 23, New York: Pergamon Press, 1975.

209. Dutta S, Ebling WF (1997) Parameter estimability of biphasic response models. J Pharm Sci 86: 44-51

210. Beal SL, Sheiner LB, Boeckmann AJ (2008) NONMEM Users Guides, Parts I–VIII. Icon Development Solutions, Ellicott City, MD

211. Atkinson AC, Donev AN, Tobias RD (2007) Non-linear Models. In: Atkinson AC, Donev AN, Tobias RD (eds) Optimum Experimental Designs, with SAS. Oxford University Press, USA pp 248-288

212. Peck CC, Beal SL, Sheiner LB, Nichols AI (1984) Extended least squares nonlinear regression: a possible solution to the "choice of weights" problem in analysis of individual pharmacokinetic data. J Pharmacokinet Biopharm 12: 545-558